



Dissertation

Design, synthesis and biophysical evaluation of small molecules targeting the K-Ras- PDE δ interaction

vorgelegt von

Diplom-Chemiker Gunther Zimmermann

aus Usingen, Hessen

der Fakultät Chemie und Chemische Biologie

der Technischen Universität Dortmund

zur Erlangung des akademischen Grades eines

Doktors der Naturwissenschaften (Dr. rer. nat.)

Dekan: Prof. Dr. Roland Winter

1. Prof. Dr. Herbert Waldmann

2. Prof. Dr. Daniel Rauh

Datum der Einreichung:

Datum der mündlichen Prüfung:

Die vorliegende Arbeit entstand in der Zeit von März 2010 bis Juni 2014 unter der Anleitung von Prof. Herbert Waldmann an der Fakultät Chemie und Chemische Biologie der Technischen Universität Dortmund und am Max-Planck-Institut für molekulare Physiologie.

Teile dieser Arbeit wurden in den folgenden Beiträgen veröffentlicht:

Weise, K.; Kapoor, S.; Werkmüller, A.; Möbitz, S.; Zimmermann, G.; Triola, G.; Waldmann, H.; Winter, R., Dissociation of the K-Ras4B/PDE δ complex upon contact with lipid membranes. *J Am Chem Soc* **2012**, *134* (28), 11503-10.

Zimmermann, G.*; Papke, B.*; Ismail, S.*; Vartak, N.; Chandra, A.; Hoffmann, M.; Hahn, S. A.; Triola, G.; Wittinghofer, A.; Bastiaens, P. I.; Waldmann, H., Small molecule inhibition of the K-Ras4B/PDE δ interaction impairs oncogenic K-Ras signaling. *Nature* **2013**, *497* (7451), 638-42.* equal contribution.

Spiegel, S.; Cromm, P.; Zimmermann, G.; Grossmann, T.; Waldmann H., Small molecule modulation of Ras Signaling - The Holy Grail in Anti-Cancer Drug Discovery. *Nat Chem Biol* (review), accepted.

Zimmermann, G.; Schultz-Fademrecht C.; Kuechler, P; Murarka, S.; Ismail, S.; Triola G.; Nussbaumer P.; Wittinghofer A.; Waldmann H., Structure-guided design and kinetic analysis of highly potent benzimidazole inhibitors targeting the prenyl binding site of PDE *J Med Chem*, Just Accepted Manuscript, DOI: 10.1021/jm500632s.

Dedicated to Aljona,
my family and friends
for their continuous support

TABLE OF CONTENTS

1 PREFACE	1
Cancer research targeting Ras	1
2 INTRODUCTION	2
2.1 Ras-GTPases	2
2.2 PDE δ : a prenyl-binding molecular chaperone	6
2.3 Small molecule binders of PDE δ	16
3 AIMS	17
4 RESULTS AND DISCUSSION	19
4.1 High-throughput screening for inhibitors of the K-Ras4B-PDE δ interaction	19
4.2 Thermodynamic and structural analysis of small molecule-PDE δ interactions	25
4.3 A fluorescence polarization assay to evaluate small molecule-PDE δ interactions	32
4.4 Synthesis and biophysical evaluation of a <i>bis</i> -benzimidazole library	37
4.5 Displacement titrations of TAMRA-Deltarasin with small molecules	69
4.6 Displacement titrations of biotinylated Atorvastatin with small molecules	70
4.7 Kinetic analysis of small molecule-PDE δ interactions	73
4.8 Effect of GppNHp-loaded Arl2/3 on the small molecule-PDE δ interaction	77
4.9 Effect of GppNHp-Arl2 on the kinetics of cargo displacement from PDE δ	82
4.10 Synthesis of benzimidazole-pyrrole hybrid inhibitors	87
4.11 Evaluation of <i>bis</i> -sulfonamides as PDE δ inhibitors	90
4.12 Cellular experiments with PDE δ inhibitors	94
4.13 Evaluation of the prenyl-specificity of PDE δ <i>in vitro</i>	103
4.14 Rational design of UNC119a/b inhibitors	104
5 SUMMARY	109
6 EXPERIMENTAL SECTION	114
7 APPENDIX	192
8 ZUSAMMENFASSUNG	211
9 LIST OF ABBREVIATIONS	216
10 REFERENCES	220
11 ACKNOWLEDGEMENTS (DANKSAGUNG)	229

1 PREFACE

Cancer research targeting Ras

The oncogenic protein Ras is a key cancer promoting molecule in many tumours. 20-30% of all human cancers display mutations in the Ras encoding genes resulting in uncontrolled cellular growth. Therefore, the Ras protein has been a central target for pharmaceutical research within the last decades. Unfortunately, none of these research efforts has resulted in effective medication directly targeting Ras.

Only recently it was realized how the cancer promoting effect of Ras is connected to the localization of Ras in the cell. The protein PDE δ has emerged as the central transporting agent for Ras. PDE δ regulates the cellular localization of Ras and Ras-dependent signal transduction. PDE δ has therefore been proposed as a novel target for suppressing oncogenic Ras signaling.

Due to their favourable pharmacological properties, small organic molecules are often required for the treatment of deadly diseases like cancer. Decades of research on small molecule inhibitors of Ras have not lead to success, therefore novel approaches for targeting Ras are of particular value. In this thesis, targeting the Ras-PDE δ interaction will be explored as a novel means of suppressing oncogenic Ras signaling. The rational development of small molecule inhibitors blocking this interaction and their impact on Ras signaling will be described in detail.

2 INTRODUCTION

2.1 Ras-GTPases

GTPases are proteins that bind and hydrolyze guanosine triphosphate (GTP). The Ras (rat sarcoma) GTPases regulate important cellular processes such as growth, differentiation and apoptosis.¹ Ras proteins bind GDP and GTP with very high affinity and display low intrinsic GTPase activity and nucleotide exchange rates.²⁻⁴ By cycling between an inactive GDP- and an active GTP-bound state, Ras proteins act as molecular switches (Figure 1, a). The nucleotide binding state of Ras proteins is controlled by guanosine nucleotide exchange factors (GEFs) and GTPase activating proteins (GAPs).

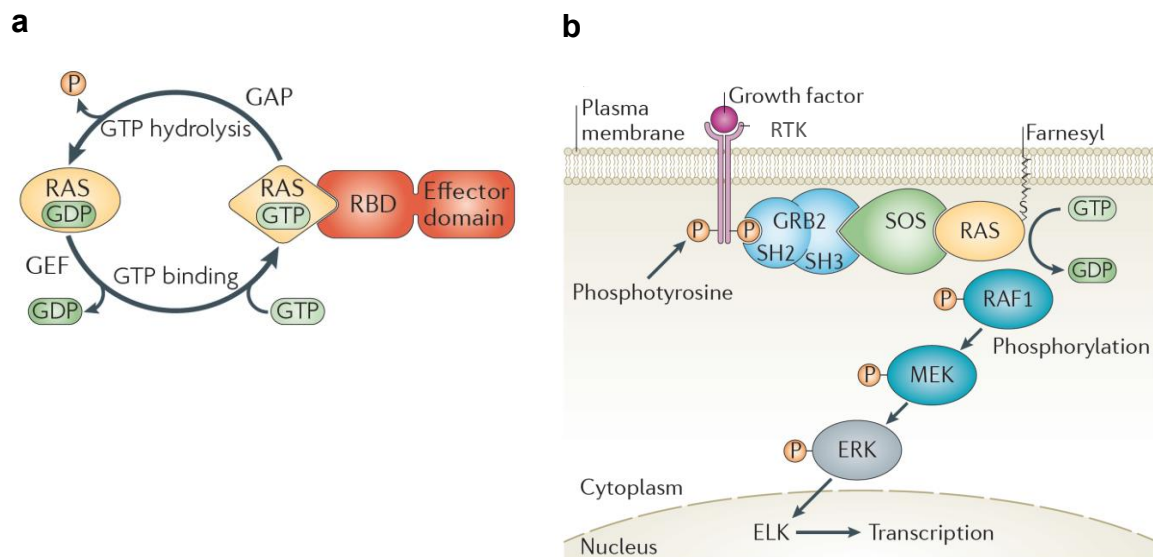


Figure 1: Biological switch function of Ras proteins.² a) Ras acts as molecular switch by cycling between the GDP- and GTP bound state, which is regulated by GAPs and GEFs. Inactive, GDP-bound Ras is activated by guanine nucleotide exchange factors (GEF), which induce GDP/GTP exchange. GTP loading changes the Ras protein conformation which results in binding to effectors via their Ras-binding domains (RBDs). The active state of Ras is regulated by its very slow intrinsic GTPase activity, which can be accelerated strongly by the interaction with a GTPase-activating protein (GAP); b) Mechanism of the Ras/Raf-1/Erk pathway which is frequently dysregulated in Ras dependent cancer. The adaptor protein GRB2 binds to active receptor tyrosine kinases (RTK) and to the GEF son of sevenless (SOS). SOS is therefore recruited to the plasma membrane where it can activate Ras. Ras binds RAF1 and stimulates its kinase activity, which results in downstream signaling cascades ending in activation of transcription factors like ELK.^{2,5}

The binding of GTP to Ras induces a conformational change, which allows Ras proteins to interact with effector proteins triggering different downstream signaling cascades. Ras proteins regulate cellular growth for example via the Ras/Raf/Mek/Erk pathway (Figure 1, b). In this signal transduction pathway binding of a growth factor to the extracellular part of a receptor tyrosine kinase (RTK) activates the cytoplasmic kinase activity. The adaptor protein GRB2 binds to active, phosphorylated RTK and recruits the GEF (SOS) to the plasma membrane. Upon activation by SOS, Ras binds RAF1 and stimulates its kinase activity, leading to the activation of phosphorylation cascades. Ultimately, transcription factors are activated which results for example in stimulation of cellular growth.

Due to this crucial role in the regulation of growth and proliferation, mutations in Ras-encoding genes are strongly associated with cancer development. Mutations can lock the Ras proteins in a GTP-bound active state, mainly by preventing the hydrolysis GTP catalyzed by GAPs.¹ As a result, the cycling of Ras between the active and the inactive state is impaired and Ras signaling pathways are permanently active, which may result in uncontrolled cellular growth.

Owing to the eminent role of Ras proteins in cancer development, oncogenic Ras signal transduction has been a major target in anti-cancer therapy for the last thirty years. However, despite intense efforts not a single therapeutic has reached the market.⁶ This failure in generating anti-Ras drugs can be at least partially attributed to the lack of a hydrophobic, druggable cavity, that allows efficient binding of small molecules. Only recently fragment based approaches have generated low affinity binders of Ras that may lead to biologically useful, high affinity compounds in the long run.^{7,8} Furthermore, selective inactivation of a particular Ras mutant (G12C) with covalent inhibitors has stirred novel interest in the modulation of Ras signaling by direct small molecule modulators of the GTPase.^{9,10}

2.1.1 Ras GTPases localization and spatiotemporal signaling

All Ras isoforms (K-Ras4A, K-Ras4B, N-Ras, H-Ras) feature a highly conserved G-domain and a lipidated C-terminal hypervariable region (HVR, Figure 2a). The biological function of Ras proteins is strictly linked to their dynamic, subcellular localization.¹¹⁻¹³ Correct Ras localization is mediated by posttranslational modifications at the HVR, which is different for all four Ras isoforms. All Ras isoforms are modified through a series of processing reactions including cysteine *S*-farnesylation (farnesyltransferase, FTase), proteolysis (RCE1) and C-

terminal carboxymethylation (ICMT, Figure 2a). These modifications, however, are not sufficient for ensuring stable binding to lipid double layers. H-Ras and N-Ras undergo additional, reversible *S*-palmitoylation at one or two cysteine residues (Figure 2b). A re/depalmitoylation cycle of N-Ras and H-Ras allows for reversible binding to endomembranes and regulates the dynamic cellular localization of these isoforms.^{11,14,15} K-Ras on the other hand is expressed as two isoforms K-Ras4A and K-Ras4B which are results of alternative splicing. K-Ras4A features a palmitoylation site, K-Ras4B on the other hand displays a poly lysine stretch in the HVR which facilitates membrane binding. Due to the positive charge of the polylysine sequence and the *C*-terminal farnesylation, K-Ras4B localizes primarily to the negatively charged plasma membrane (Figure 2a).

K-Ras4B is arguably the most important isoform for anti-cancer research. Mutations of the K-Ras gene occur frequently in lung, colorectal and pancreatic cancer. Impressively, in the very deadly pancreatic cancer more than 90% of all patients feature K-Ras mutations. Since K-Ras4B is more widely expressed than K-Ras4A, this splice variant is generally believed to be the key oncogenic protein in K-Ras driven tumours.¹⁶

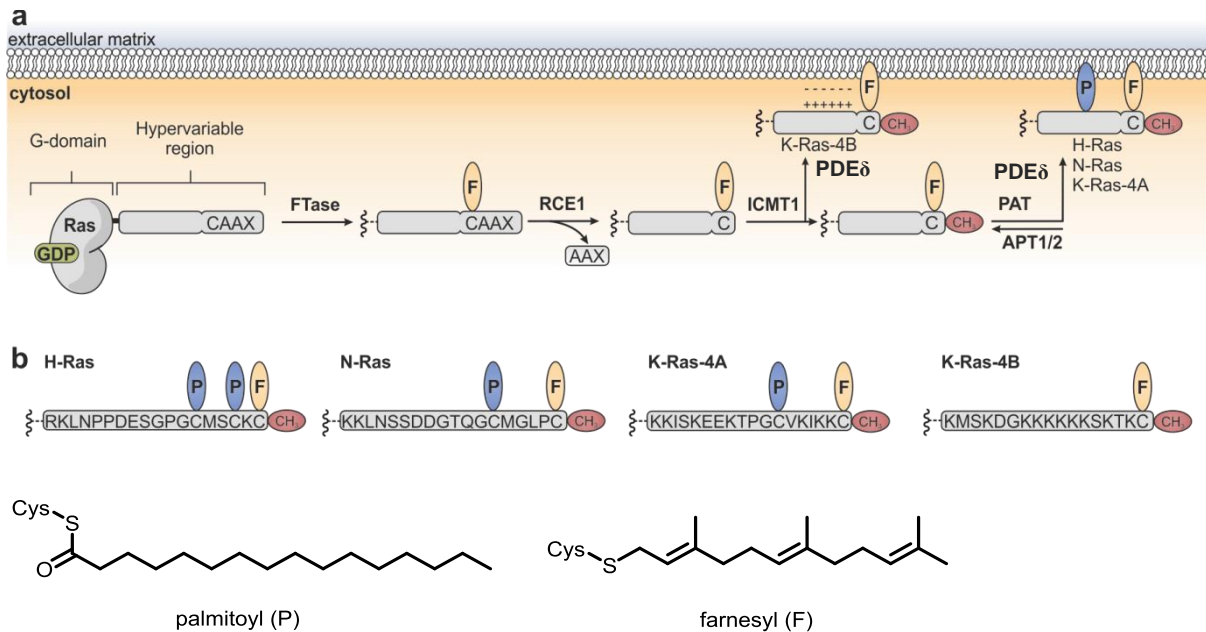


Figure 2 Posttranslational processing of Ras isoforms.¹⁷ H-Ras, N-Ras, K-Ras-4A/B all possess a highly homologous G-domain and a C-terminal hypervariable region (HVR). While the conserved G-domain is involved in nucleotide binding and effector interactions, the HVR undergoes a series of posttranslational modifications to enable stable membrane binding. (a) All Ras proteins are farnesylated (F, orange) by farnesyltransferase (FTase) at the C-terminal cysteine, Ras-converting enzyme1 (RCE1) cleaves the three C-terminal AAX residues of the CAAX box (C = cysteine, A = aliphatic amino acid and X = variable amino acid) and isoprenylcysteine carboxylmethyltransferase1 (ICMT1) transforms the C-terminal carboxylate into a methyl ester (red). In the case of K-Ras4B, electrostatic interactions of a poly lysine stretch with the negatively charged plasma membrane enable stable binding to the target membrane. The other isoforms are additionally modified by protein acyltransferases (PATs) with one or two palmitoyl groups (P, blue) at their C-terminal cysteines to enable stable binding to the target membrane. Palmitoylation is reversible and acylprotein thioesterases (APT1/2) release the Ras protein from the target membrane. The prenyl binding protein PDE δ additionally controls association of all Ras isoforms with lipid bilayers; (b) Posttranslational modifications for the four different Ras isoforms and chemical structures of the products of S-palmitoylation (left) and S-farnesylation (right).

2.1.2 Impairment of Ras spatiotemporal signaling with small molecules

The postranslational modifications of Ras proteins regulate localization of Ras in the cell and thereby control Ras dependent signaling.^{11,13,18,19} Initially interference with Ras localization, and signaling seemed to be readily possible by targeting processing enzymes like farnesyltransferase. Farnesyltransferase inhibitors suppress *S*-farnesylation of GTPases,^{5,20} and treatment of cells results in a cytosolic enrichment of non-functional Ras. A number of farnesyl transferase inhibitors have been tested in clinical trials, but ultimately failed to affect oncogenic Ras signaling mostly due to alternative prenylation pathways.²¹ Hence, if farnesyltransferase is inhibited, Ras becomes a substrate for geranylgeranyl transferase (GGTase) which results in retained membrane affinity. Treatment of cells with a combination of FTase and GGTase inhibitors to avoid alternative geranylgeranylation or dual prenylation inhibitors lead to toxicity and lacked the desired efficacy in clinical trials.^{22,23} Additionally, it is unclear whether a significant portion of the *in vitro* anti-cancer effect of farnesyl transferase inhibitors is due to inhibition of Ras signaling or due to relocalization of other GTPases. Targeting of the protease RCE1^{61,62} and the methyltransferase ICMT1⁶³ by small molecules has also been explored, but the overall anti-proliferative effect of these inhibitors was less pronounced compared to farnesyl transferase inhibitors.

In addition to targeting processing enzymes, farnesyl cysteine mimetics have been designed to compete with the interaction of Ras and prenyl-binding proteins. Unfortunately, these molecules were largely ineffective in clinical trials.²⁴⁻²⁶ Phenotypic screening approaches have revealed compounds which interfere with Ras localization, but the targets of the identified compounds remain unclear to date and therefore rational compound optimization is not possible.^{27,28} In summary, no clinically effective approach for impairment of oncogenic Ras signaling by means of subcellular relocalization of Ras has been developed. In particular, no approach that targets the most oncogenic isoform K-Ras4B has been reported and is available for the treatment of cancer patients.

2.2 PDE δ a prenyl-binding molecular chaperone

The *Pde6d* gene encodes a 17 kDa protein (PDE δ , PDE6D or PrBP/ δ) which was originally identified as the soluble δ -subunit of phosphodiesterase 6 (PDE6) in photoreceptor cells, where it detaches PDE6 from the membrane and thereby desensitizes the phototransduction

cascade.^{29,30} In subsequent studies PDE δ was found to function as a ubiquitously expressed, molecular chaperone for the transport of prenylated proteins.³¹ PDE δ is part of the UNC119/PDE δ /RhoGDI protein family, which share a common lipid binding motif. Each of the proteins features a beta-barrel fold that contains a large hydrophobic cavity which can accommodate lipid groups. While PDE δ and RhoGDI both preferentially interact with prenyl groups, UNC119a and UNC119b shuttle myristoylated proteins in the cell.³²⁻³⁶

In virtually all animals including the nematode *C. elegans*, orthologs of PDE δ were identified.^{29,37} Sequence identities of over 97% were observed between mouse, bovine, and human PDE δ by sequence similarity search. The amino acid sequence of PDE δ shows at least 70% sequence identity within vertebrates and around 50% sequence identity among invertebrates.³⁰ The conserved primary sequence suggests an eminent role of PDE δ in the trafficking of prenylated proteins like K-Ras4B inside the cell.

2.2.1 The prenyl-dependent interaction between Ras-GTPases and PDE δ

Biochemical and cellular studies have revealed crucial interactions between farnesylated GTPases, most notably K-Ras4B, and PDE δ .³⁸ PDE δ binds Ras family proteins and sequesters them from membranes thereby regulating specific localization of these proteins in the cell. K-Ras4B is enriched at the plasma membrane, however, until recently it was unclear how K-Ras4B is transported to the plasma membrane after synthesis and posttranslational modification at the endoplasmic reticulum. The prenyl-binding protein PDE δ was shown to mediate this transport of K-Ras4B to the plasma membrane (Figure 3).¹⁸

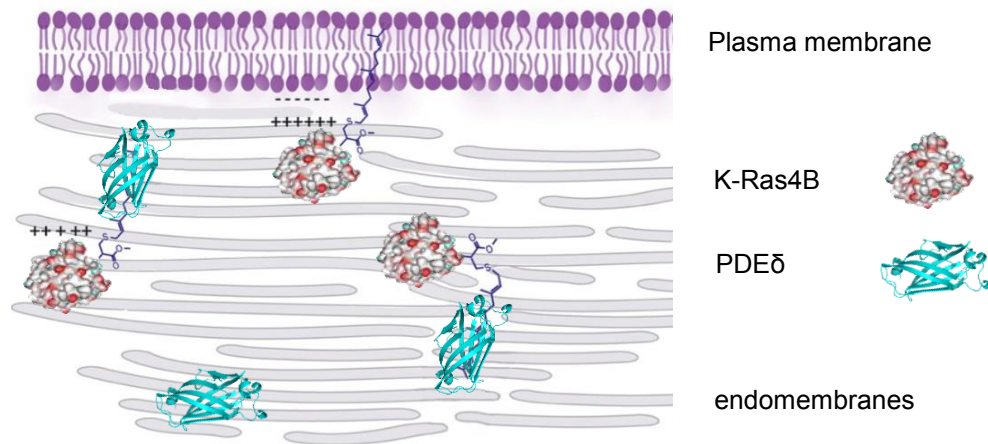


Figure 3 PDE δ (cyan) functions as a shuttle protein for Ras family proteins (shown here for K-Ras4B). Ras proteins are posttranslationally processed at the endoplasmic reticulum, and PDE δ transports for example K-Ras4B to the plasma membrane where it can exert its biological function.

The effect of PDE δ on Ras signal transduction has been investigated by siRNA. Knockdown of the *Pde6d* gene led to a significant decrease in Erk phosphorylation.^{18,39} This finding was attributed to an unspecific relocalization of Ras proteins in the cell in the absence of PDE δ .

The interaction between Ras proteins and PDE δ was also recently investigated at a molecular level. A biophysical investigation into the binding of PDE δ to several farnesylated peptides and semisynthetic Ras proteins revealed that the carboxymethylated, farnesylated C-terminal K-Ras4B-dodecapeptide binds to PDE δ with a higher affinity than a simple farnesylated cysteine methyl ester.⁴⁰ A semisynthetic K-Ras4B-protein does not display higher affinity for PDE δ than the C-terminal K-Ras4B-dodecapeptide, thus suggesting that PDE δ recognizes mainly the C-terminus of the lipidated protein.⁴⁰ Subsequently, the cocrystal structure of the Ras family protein Rheb in complex with PDE δ showed that the two proteins interact exclusively via the S-farnesylated C-terminus and the following 5-10 amino acids of Rheb (Figure 4, a). The crystal structure revealed a large, hydrophobic cavity of PDE δ which is occupied by the farnesyl group (Figure 4, b). The binding between Rheb and PDE δ is mediated by a few, key polar interactions. Arg61 of PDE δ shows a cation π interaction with a farnesyl double bond and Tyr149 forms a hydrogen bond with a backbone amide group of the Rheb C-terminus.

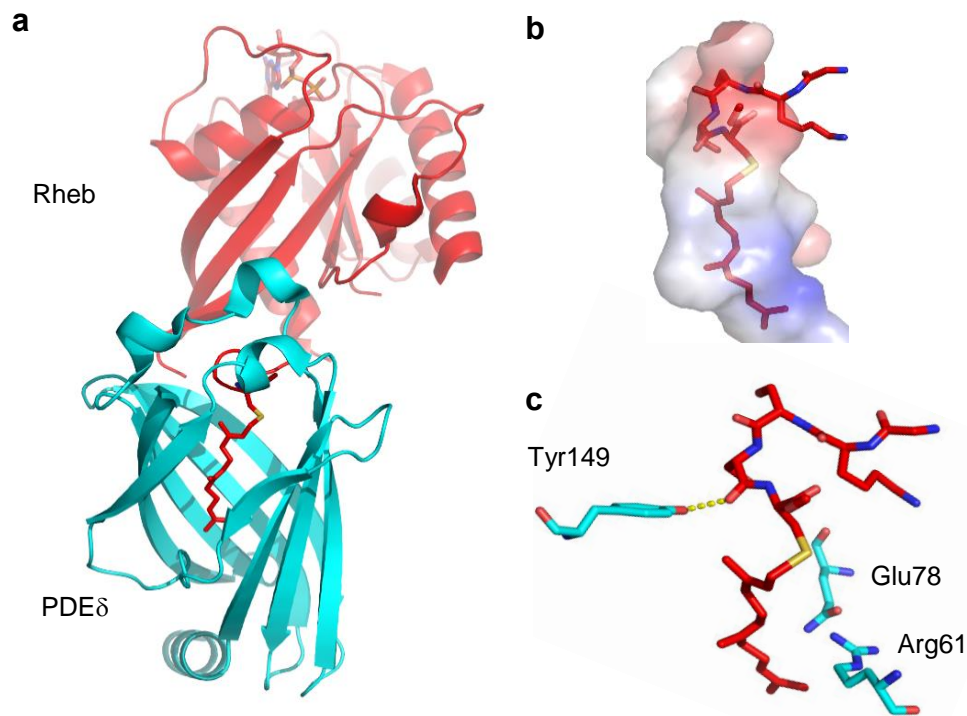


Figure 4 Interactions of farnesylated GDP-bound Rheb (red) in complex with PDEδ (cyan). a) PDEδ/Rheb overall structure, showing no protein backbone interactions; b) surface representation of hydrophobic cavity surrounding the farnesyl group; c) key hydrogen bond of Rheb C-terminus backbone amide with Tyr149.

2.2.2 Arl2/3-GTP and PDEδ regulate a transport system for prenylated cargo which controls the localization of Ras family proteins

The binding of farnesylated proteins to PDEδ is regulated by Arl2 and Arl3, which belong to the Arl (ADP-ribosylation factor-like) family of GTPases.⁴¹⁻⁴³ PDEδ is an effector of Arl2/3, which interacts exclusively with the GTP bound form. The crystal structure of the PDEδ/Arl2 complex revealed that the interaction is mediated by a series of parallel inter-protein β-sheet contacts (Figure 5).⁴¹

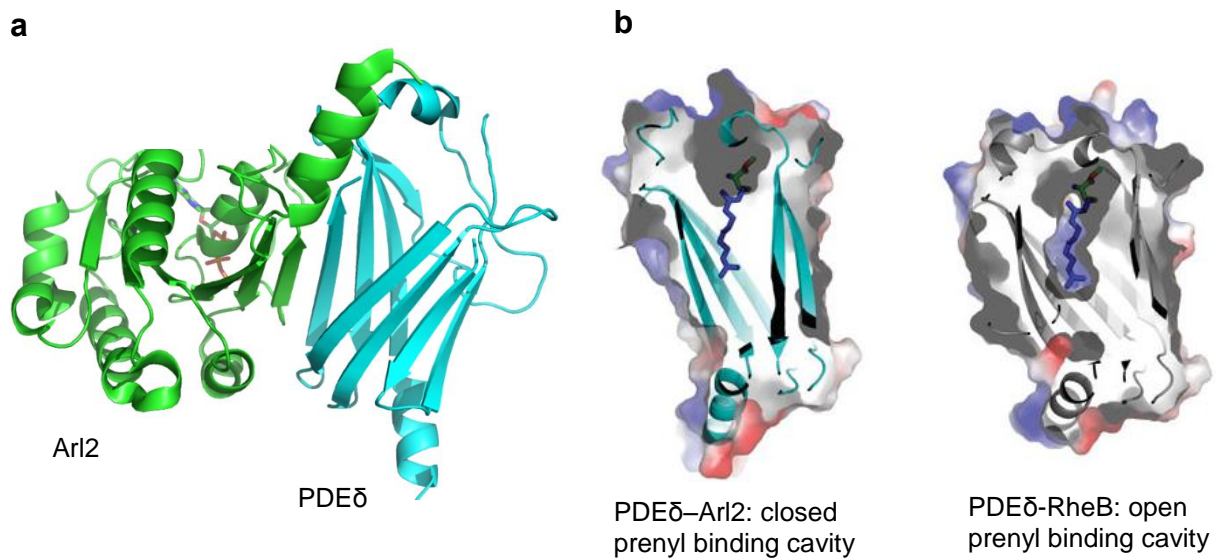


Figure 5 Structural analysis of the Arl2-PDE δ interaction a) Cocystal structure of Arl2-GppNHp (green) with PDE δ (cyan) (PDB: 1KSG). GTP-bound Arl can be biochemically mimicked by using the non-hydrolysable GTP analog GppNHp. GppNHp is shown as ball and sticks; b) Surface representation of PDE δ : The farnesyl binding pocket is closed in the presence of Arl2-GppNHp (left, farnesyl is modeled into the structure) and open in the presence of farnesylated proteins (right).⁴⁴

The binding site of Arl2/3 on PDE δ is therefore distinct from the binding site of farnesylated proteins like Rheb, and suggests a mechanism of allosteric control. It was demonstrated by Wittinghofer and coworkers that Arl proteins actively displace farnesylated protein cargo from PDE δ .⁴⁴ A short-lived, ternary complex between farnesylated proteins like Rheb, PDE δ and Arl2 thus mediates the release of farnesylated cargo at a specific location in the cell. The cargo system is reminiscent of the RhoGDI/Rho transport mechanism because RhoGDI preferentially binds the GDP bound form of Rho and acts as a solubilizing factor that sequesters and buries the lipid moiety.^{33,45} In the case of Rheb, PDE δ and Arl2, however, the nucleotide dependent interaction is observed between Arl2 and PDE δ and not between the Rho homologue Rheb and PDE δ . PDE δ has therefore been described as a GDI-like solubilizing factor (GSF).¹⁸

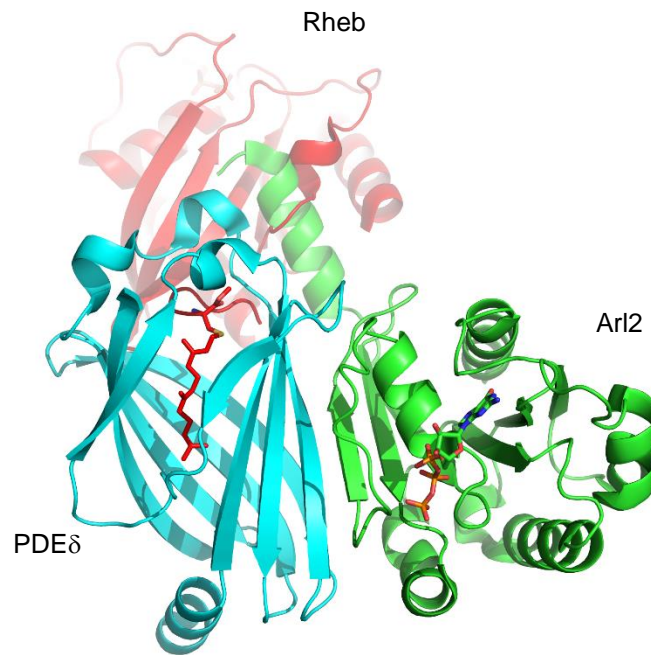


Figure 6 Ternary structure model of PDE δ /Arl2/Ras homologue (Rheb) generated from the PDB entries 1KSH and 3T5G. For Rheb (red) the farnesyl group is shown in ball and sticks. GppNHp bound to Arl2 is also shown in ball and sticks.

Recently, cellular experiments demonstrated how K-Ras localization and thus signaling is controlled by both PDE δ and the release factor Arl2 (Figure 7).¹³ Interestingly, electrostatic interactions alone cannot account for enrichment of K-Ras at the plasma membrane (compare Figure 3), due to the very large relative surface area of endomembranes in the cell. Instead K-Ras is sequestered continuously from endomembranes by PDE δ and delivered to perinuclear membranes where it is unloaded by Arl2. Electrostatic interactions transfer K-Ras to the negatively charged surface of the recycling endosome. Vesicular transport is then responsible for the observed enrichment of K-Ras at the plasma membrane.

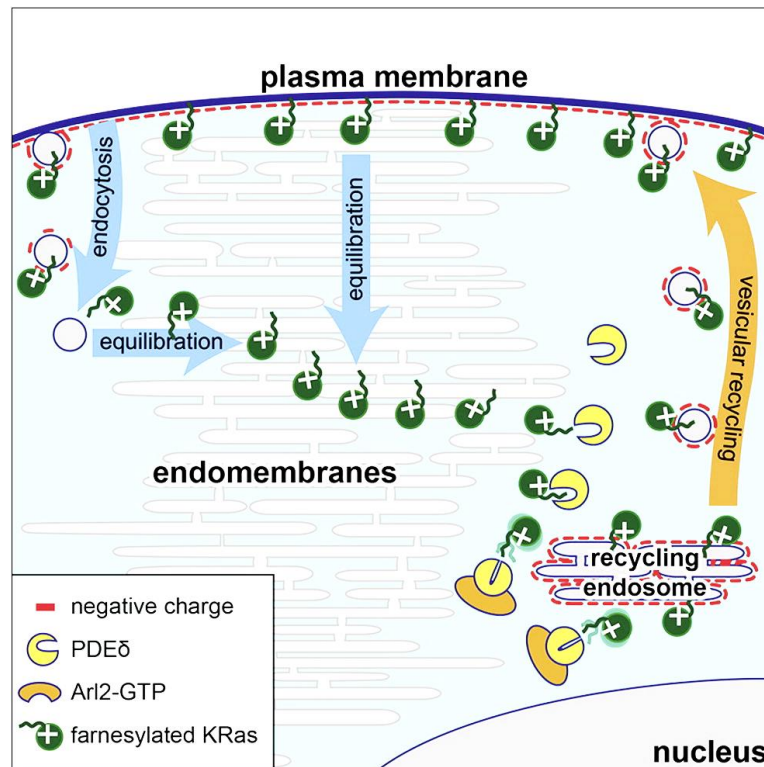


Figure 7 K-Ras localizes to the plasma membrane by spatial cycles of solubilization, trapping and vesicular transport.¹³ K-Ras is sequestered continuously from endomembranes by PDEδ and delivered to perinuclear membranes where it is unloaded by Arl2. Electrostatic interactions transfer K-Ras to the negatively charged surface of the recycling endosome. Vesicular transport leads to the observed enrichment of K-Ras at the plasma membrane.

2.2.3. Interactions between PDEδ and other prenylated proteins

In addition to the Ras GTPases, also other prenylated GTPases were identified as targets of PDEδ in yeast-two hybrid screens and proteomics experiments (Figure 8, left).³⁸ Due to its high expression levels in the retina, PDEδ plays an essential role in maintaining the spatial organization of prenylated proteins in photoreceptor cells.³⁷ PDEδ interacts with prenylated PDE6 subunits, farnesylated rhodopsin kinase (GRK1) and geranylgeranylated GRK7 in these cells (Figure 8, right).⁴⁶

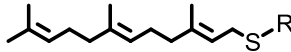
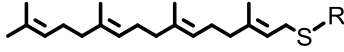
Target (GTPase)	prenyl	Target	prenyl
K-Ras	f	PDE α	f
N-Ras	f	PDE β	gg
H-Ras	f	GRK1	f
Rap1a	gg	GRK7	gg
Rap1b	gg	cTy	f
Rap2a	f	Ty	f
Rap2b	gg	DmPDE5/6	gg
RhoA	gg	Prostacyclin-R	f
RhoB	gg	RPGR-RCC1	-
Rho6 (Rnd1)	f	INPP5E	f
Rheb	f		
Rab8a	gg		
Rab13	f	farnesyl (f)	
Rab28	f		
GTP-Arl2	-		
GTP-Arl3	-	geranylgeranyl (gg)	

Figure 8 Interaction map of PDE δ with prenylated (farnesyl, f or geranylgeranyl, gg) and non prenylated proteins. Small GTPases are shown in the left column, other proteins on the right.

PDE δ binds to the GTPases Arl2/3 and the Retinitis Pigmentosa GTPase regulator (RPGR, RCC1 domain) via protein backbone interactions in a non-prenyl dependent fashion.^{47,48} It is of note that a number of the validated PDE δ interaction partners (RPGR, Arl3, INPP5E, Rab8a, Rab28, PDE α , PDE β , GRK1) are involved in diseases which involve the dysfunction of the primary cilium, a small organelle that protrudes from the cell body.

2.2.4 PDE δ , cilia and signaling

Cilia are specialized organelles which protrude from the cell surface of almost all mammalian cells.⁴⁹ Proteins that localize to cilia are often prenylated. Prenylated, ciliary proteins include the phosphoinositide phosphatase INPP5E, Phosphodiesterase 6 α and β subunits and the rhodopsin kinase GRK1. Mutations in the corresponding genes can lead to photoreceptor degeneration, MORM and Joubert syndrome in humans.⁵⁰⁻⁵³ Due to the involvement of the primary cilium in these diseases, they are often called ciliopathies. PDE δ controls the ciliary

targeting of prenylated proteins like the inositol phosphatase INPP5E.^{54,55} A homozygous mutation of PDE δ in Joubert syndrome impairs targeting of farnesylated INPP5E to the cilium.⁵⁶ Interestingly, the homozygous mutation blocks the binding of lipidated proteins and Arl2/3 to PDE δ and thus inactivates its function as a shuttle protein. While a PDE δ knockout mouse phenotypically only displays retinal degeneration and weight reduction, multi organ dysfunction is observed in humans with Joubert syndrome carrying mutant PDE δ .³⁷ Strikingly, the highest expression levels of PDE δ in human embryos were observed in the nervous system, kidney tubules and epithelial cells of the respiratory tract (Figure 9).

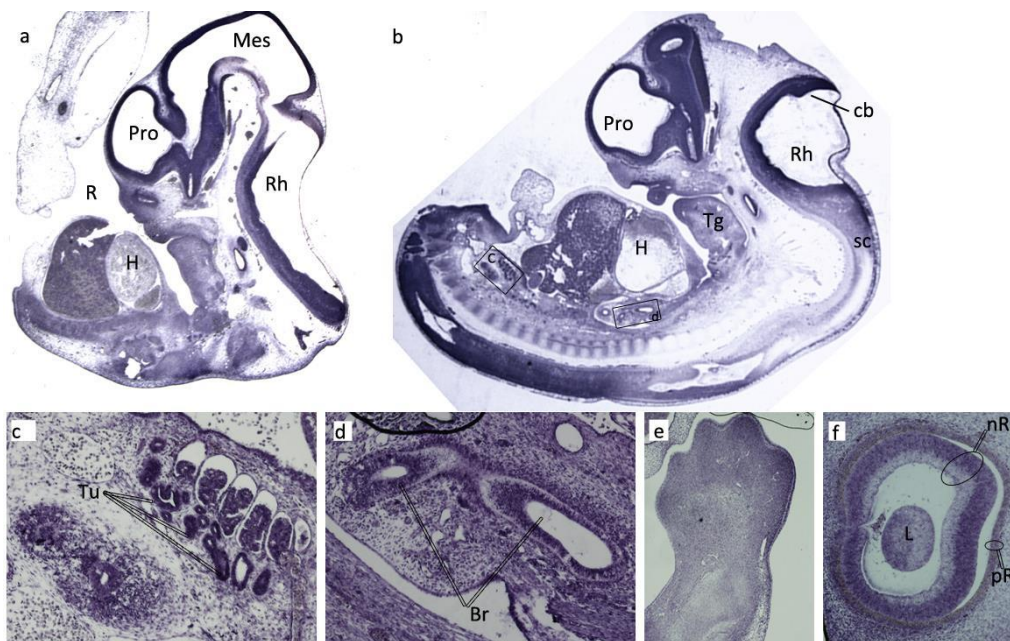


Figure 9 PDE δ expression in human embryos.⁵⁶ The protein is ubiquitously expressed within human tissues. PDE δ is most abundant in the entire central nervous system (prosencephalon (Pro), mesencephalon (Mes) and rhombencephalon (Rh) (a,b), in renal tubules (c) and in epithelial cells of the bronchus (d). PDE δ also localizes to the limb bud mesenchyme (e) and to the neural layer of the optic cup (future neural retina) (f). Br, bronchus; Cb, cerebellum; H, heart; L, lens; nR, neural retina; pR, pigment layer of retina; R, Rathke's pouch; sc, spinal cord; tg, tongue; Tu, renal tubules.⁵⁶

These organs are commonly affected by ciliopathies.⁵⁶ Within ciliated cells PDE δ localizes primarily to the basal body of the primary cilium.⁵⁶ The transport of prenylated proteins like INPP5E to primary cilia is largely not understood, however the involvement of PDE δ in this interaction network suggests the possibility to use small molecule binders of PDE δ to understand the underlying mechanisms.⁵⁴

2.2.5 Hedgehog signaling pathway

The Hedgehog signaling pathway is critically involved in the development of embryonic cells, but also plays a vital role in adult cells for example in cancers like basal cell carcinoma.⁵⁷ Briefly, Sonic Hedgehog (SHH) is a secreted, lipidated protein that binds to the patched receptor (PTC), which localizes in and around the primary cilium.⁵⁷ Upon binding of SHH to PTC, the smoothed receptor (SMO) relocates to the primary cilium and transcription factors (GLI) are activated which leads to transcription of the target genes (Figure 10).

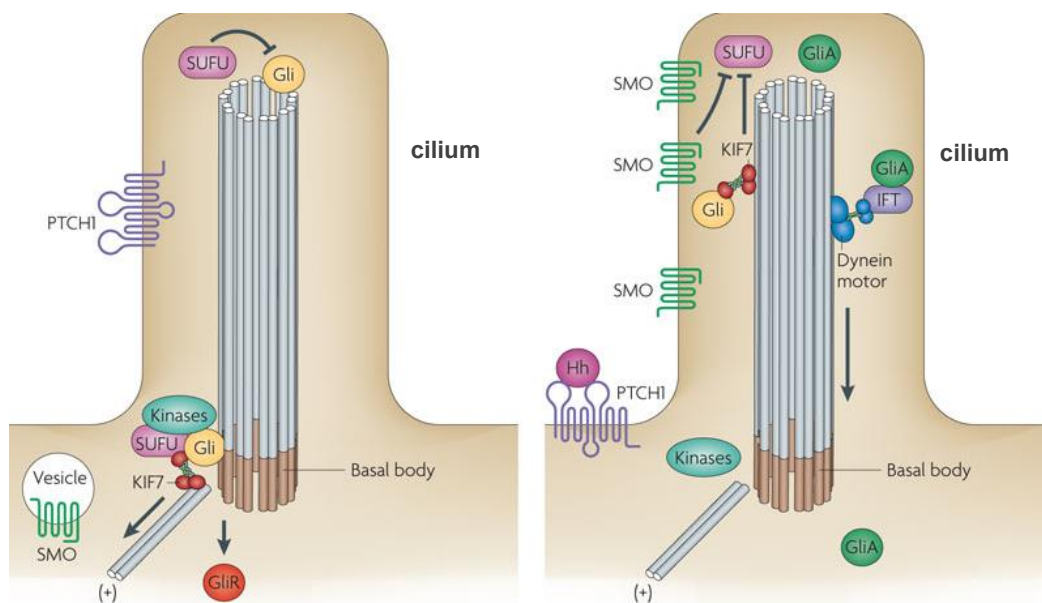


Figure 10 Hedgehog signaling pathway in vertebrates around the cilium.⁵⁷ a) off state: in the absence of ligand, PTCH1 localizes to the cilium and is thought to block the entry of Smoothed (SMO) to the cilium; b) on state: upon binding of Hedgehog protein (Hh) to PTCH1, SMO relocates to the ciliary membrane and activates GLI transcription factors like GliA which leads to activation of the target genes in the nucleus.⁵⁷

Since Hedgehog signaling in vertebrates requires the primary cilium,⁵⁷ and PDE δ plays a vital role in ciliopathies like Joubert syndrome, it can be reasoned that PDE δ has a general role in Hedgehog signaling. Additionally, the PDE δ interaction partner K-Ras has been shown to activate Hedgehog signaling in pancreatic tumor cells.^{58,59}

2.3 Small molecule binders of PDE δ

So far, no rational design strategy has been employed to find small molecules that target the prenyl binding cavity of PDE δ . Proteomics and phage display experiments, however, accidentally revealed small molecules binder of PDE δ .

In an effort to identify unknown binding partners of marketed drugs, the company Ambit Biosciences found that the clinically used HMG-CoA reductase inhibitor Atorvastatin (**1**) binds to PDE δ (Figure 11).⁶⁰ The penta-substituted pyrrole core structure of Atorvastatin was identified as the pharmacophore for PDE δ binding, and a library based on this core structure was synthesized. However, none of the synthesized molecules showed significantly better binding affinities than Atorvastatin. In addition to the originally reported pyrrole compounds, thiophenes, furans and imidazoles were patented for the use as PDE δ binders and the treatment of stroke.⁶⁰ By an elegant combination of yeast-three hybrid screening and affinity chromatography, Johnsson and coworkers could clearly show that Atorvastatin indeed targets PDE δ and that among the statin drug class only Atorvastatin interacts with PDE δ .⁶¹

In a different study proteomics experiments by Heck and coworkers revealed that the nanomolar PDE5 inhibitor PF-4540124 (**2**) also shows off-target binding to PDE δ with an approximate affinity of 1-10 μ M (Figure 11).^{62,63} Subsequently, four derivatives of PF-4540124 were synthesized and two of them showed stronger binding to PDE δ than to PDE5, as judged by quantitative proteomics experiments with immobilized compounds.⁶⁴ However, no absolute affinities for these compounds were reported.

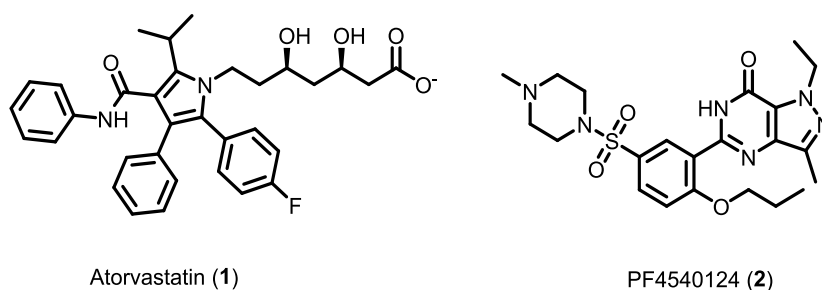


Figure 11 Structures of previously reported binders of PDE δ .

3 AIMS

Due to its eminent role in cancer, the Ras proteins have been a major target of pharmaceutical research. While numerous attempts have been made to find direct binders of Ras proteins that impair oncogenic signaling, not a single drug has emerged from these efforts. Oncogenic Ras signaling is tightly linked to the subcellular location of the Ras proteins. The spatial organization of Ras family proteins, and in particular of K-Ras, is maintained by the prenyl binding protein PDE δ . siRNA mediated knockdown of the *Pde6d* gene results in mislocalization of K-Ras and a decrease in the phosphorylation of downstream ERK-kinase. Knockdown of *Pde6d* impairs oncogenic K-Ras signaling, thus validating the K-Ras- PDE δ interaction as an interesting target for the development of novel anti-cancer therapeutics.

Since PDE δ features a large hydrophobic and therefore potentially druggable prenyl binding cavity, it seems feasible to find small molecules that interfere with the K-Ras-PDE δ interaction and thus impair oncogenic K-Ras signaling. Hence, the main aim of this work is the validation of the PDE δ -K-Ras interaction as a target for drug discovery aimed at cancers with mutations in K-Ras and the development of small molecules which are able to block this interaction.

For the identification of these inhibitors a biochemical assay that is amenable to high-throughput screening has to be designed and potential hit molecules have to be validated with other biophysical methods like isothermal titration calorimetry (ITC) and thermal shift assays. Hit compounds should be cocrystallized with PDE δ and then rationally improved by structure-guided design. Selected compounds shall be tested for their ability to break the K-Ras-PDE δ interaction in the living cell and for their impact on oncogenic Ras signaling. Since K-Ras mutations are observed in >90% of pancreatic cancers, the most promising molecule shall be evaluated in mice bearing K-Ras-dependent, human pancreatic cancer cell lines.

Although siRNA mediated knockdown of PDE δ yielded clear evidence that Ras signaling is dependent on PDE δ , the overall biological role of the prenyl binding protein is still debated. It is, for example, still unclear whether PDE δ only shuttles farnesylated proteins like Ras in the cell, or whether it can also transport geranylgeranylated proteins. Therefore biochemical model studies using differently prenylated peptides with the same sequence could reveal whether there is a prenyl specificity of PDE δ .

Previously, it was shown that the Arl2/3 GTPases allosterically regulate binding of prenylated proteins to PDE δ by interaction with a binding site distinct from the hydrophobic prenyl binding cavity. Arl2/3 GTPases can actively release cargo proteins from the prenyl binding cavity of PDE δ . Since prospective small molecule inhibitors of the K-Ras-PDE δ interaction are expected to bind into this hydrophobic cavity, it is of interest whether the mode of action of these molecules can be reversed by binding of Arl2/3.

Arl2/3 do not only regulate binding of prenylated cargo to PDE δ they also control cargo release from the closely related myristoyl binding proteins UNC119a and UNC119b. Similar to PDE δ , UNC119a/b feature large lipid binding cavities. Therefore, rational design of UNC119a/b inhibitors targeting this binding site seems feasible and selected compounds/peptides should be evaluated in biochemical assays for their ability to interact with UNC119a/b.

4 RESULTS AND DISCUSSION

A two-pronged strategy was employed for the identification of small molecule K-Ras-PDE δ inhibitors (Figure 12). The major focus was to develop a high throughput screening assay to identify novel scaffolds that bind to PDE δ . In a parallel approach it was also attempted to synthesize Sildenafil and Atorvastatin derivatives and evaluate them for their ability to break the K-Ras-PDE δ interaction.

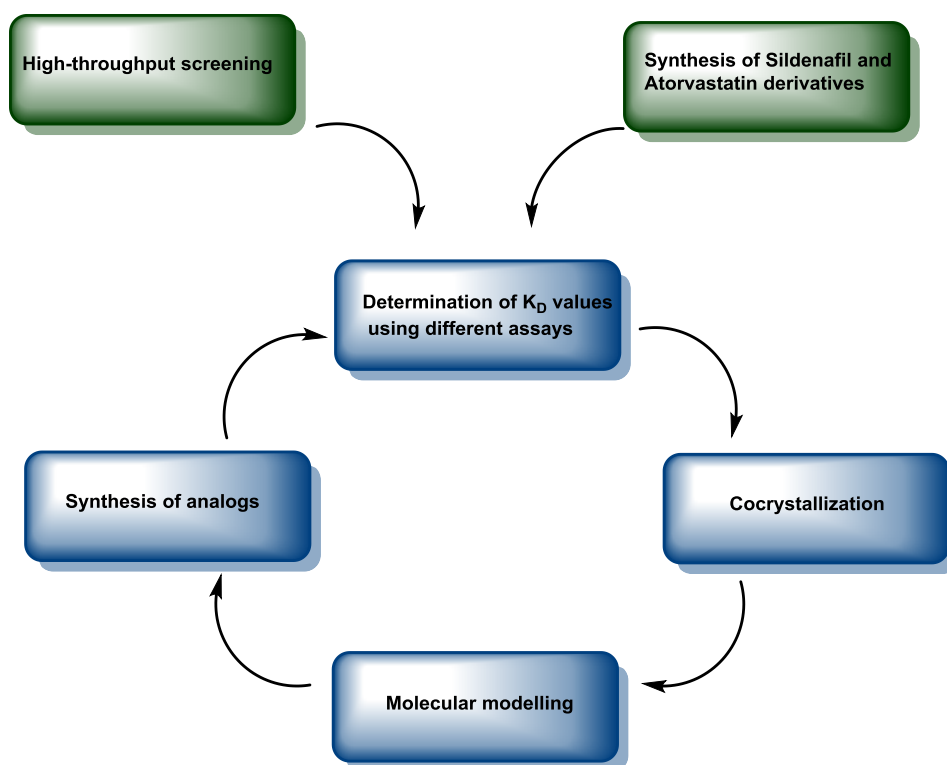


Figure 12 Approach for the identification PDE δ inhibitors. A two-pronged approach for entering the cycle of structure-guided design (blue) was followed: High-throughput screening was accompanied by the synthesis of Sildenafil and Atorvastatin derivatives.

4.1 Development of a high-throughput screening assay of the K-Ras4B-PDE δ interaction

Due to the size of the MPI Dortmund in-house library (ca. 200000 compounds), a high-throughput screening assay was needed to test these compounds for their ability to break the K-Ras4B-PDE δ interaction. Alpha technology has emerged as a powerful tool for studying biological interactions and for screening large compound libraries. As a bead-employing proximity assay, this technology is based on the generation of singlet oxygen upon excitation with visible light and its subsequent transfer from a donor to an acceptor bead, when both beads

are within 200 nm distance (Figure 13). As a result, the singlet oxygen causes a chemoluminescent ring opening reaction on the acceptor bead. For screening purposes Alpha technology has two advantages: a) There is a delay between excitation and detection of the emitted light and b) the emitted light has a shorter wavelength than the excitation source. Therefore, the intrinsic, short lived fluorescence of many compounds in the screening collection does not interfere with the assay.

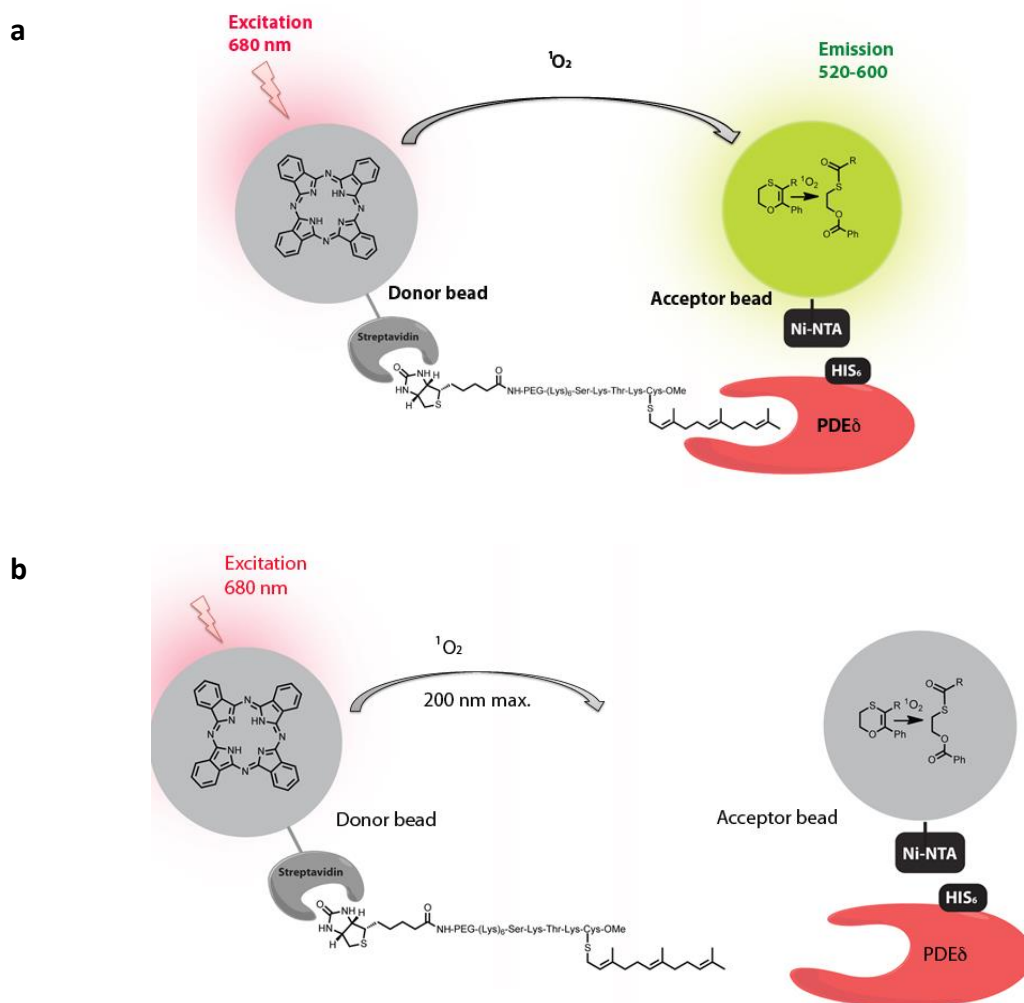
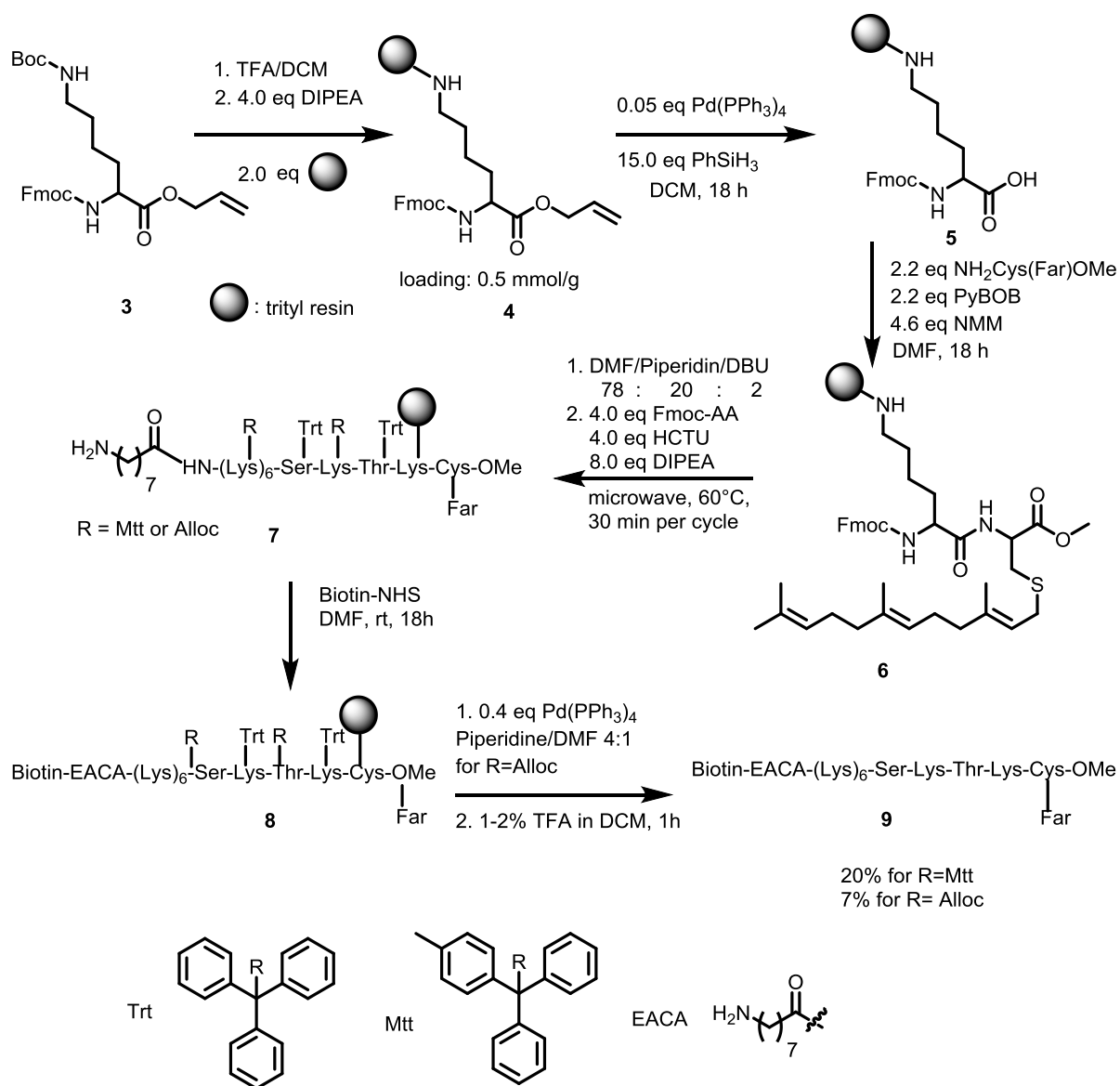


Figure 13 Alpha screening assay for the detection of small molecule inhibitors of the K-Ras4B-PDE δ interaction. a) The proximity based assay relies on a chemiluminescent reaction triggered by singlet oxygen. A donor bead recognizes the biotinylated K-Ras4B-peptide and an acceptor bead binds to the His-tagged protein. Upon excitation with visible light, singlet oxygen is produced at the donor bead. Due its limited lifetime the singlet oxygen can only reach the acceptor bead if the K-Ras4B peptide and PDE δ interact. b) In the presence of an inhibitor no emission between 520-600 nm is observed.

The K-Ras4B-PDE δ interaction is restricted to the last 5-10 C-terminal amino acids of K-Ras4B, therefore it is not necessary to work with full length, farnesylated K-Ras4B protein (K_D C-terminal K-Ras4B peptide 227 nM, K_D full-length K-Ras protein 302 nM).⁴⁴ In contrast to the full length protein, farnesylated K-Ras4B-peptides are readily available in milligram amounts by solid phase peptide synthesis. Owing to the bead-based assay setup both interaction partners, K-Ras4B and PDE δ , have to be affinity tagged. It was thus envisaged to synthesize a biotinylated, C-terminal K-Ras4B peptide and in parallel express His₆-tagged PDE δ in *E.coli*.

4.1.1 Synthesis of a C-terminal, biotinylated K-Ras4B peptide

The Waldmann group has established an elegant solid-phase synthesis approach for K-Ras4B peptides which employs the highly acid sensitive (chloro)-trityl linker.^{40,65} For the synthesis of a biotinylated K-Ras4B peptide an orthogonally protected lysine building block was Boc-deprotected and coupled to the solid support via the ϵ -amino group. The immobilized building block was C-terminally deprotected using Pd(PPh₃)₄ and phenylsilane (Scheme 1)⁶⁵ and the free acid was coupled to farnesylated cysteine methyl ester (PyBop, NMM). The N-terminus was elongated using cycles of Fmoc-deprotections and coupling to suitably protected amino acids.



Scheme 1 Synthesis of a biotinylated and farnesylated K-Ras4B peptide by solid phase synthesis.

After introduction of an eight-carbon linker, the free amino group on the *N*-terminus was reacted with Biotin-NHS-ester. Subsequent deprotection and cleavage from the solid support with 1% TFA in dichloromethane yielded the final peptide. For the synthesis of the biotinylated peptide two different lysine protecting group regimes were evaluated. Initially, the lysines were side chain-protected with the Alloc group as previously described.^{40,65} In an attempt to simplify the synthesis and increase the yield, the Alloc protecting group was replaced by the highly acid sensitive 4-methyltrityl (Mtt) group (Scheme 1). This change in the protecting group regime not only reduced the number of synthetic steps but also significantly improved the yield from 7% to 20%.

4.1.2. Expression of His₆-PDE δ in *E. Coli*

His₆-PDE δ was expressed in *E.-coli*-Rosetta cells following a slightly modified expression protocol from the group of Prof. Wittinghofer. After purification by affinity- and size exclusion chromatography, His₆-PDE δ was obtained in a high yield of 20 mg protein per liter expression culture (Figure 14)

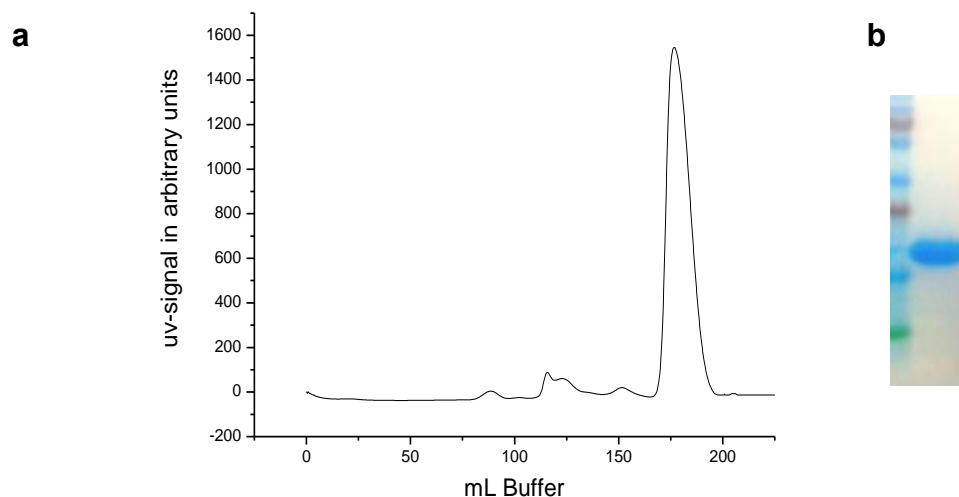


Figure 14 Expression and purification of His₆-PDE δ a) UV trace of preparative gel filtration chromatography; b) SDS-PAGE of pooled fractions (165-190 mL elution buffer) from gel filtration chromatography.

4.1.3 Implementation of an Alpha screen with His₆-PDE δ and biotinylated K-Ras4B peptide

The interaction between His₆-PDE δ and the biotinylated K-Ras4B peptide was initially evaluated using a serial dilution of the two components in a 1:1 ratio. Different additives were screened for their ability to suppress unspecific binding and thus to increase the signal to background ratio. Polyether based detergents (Tween 20, Triton-100), however decreased the signal, presumably by binding into the farnesyl binding cavity. Bovine serum albumin (BSA) completely abrogated the PDE δ /K-Ras4B interaction even when used at concentrations as low as 0.1%. This observation can be attributed to the binding of the farnesyl group to the fatty acid binding patches on the surface of BSA. The addition of the zwitterionic, steroid based detergent Chaps on the other hand was tolerated. After optimization of the incubation time the assay performed with a signal to background ratio of more than 500:1 and a z' of 0.8, where z' is a statistical quality assessment parameter for assays.⁶⁶ The apparent K_D of the interaction proved to be 600 nM, which is consistent with previous fluorescence polarization (FP) measurements (Figure 15).⁴⁰

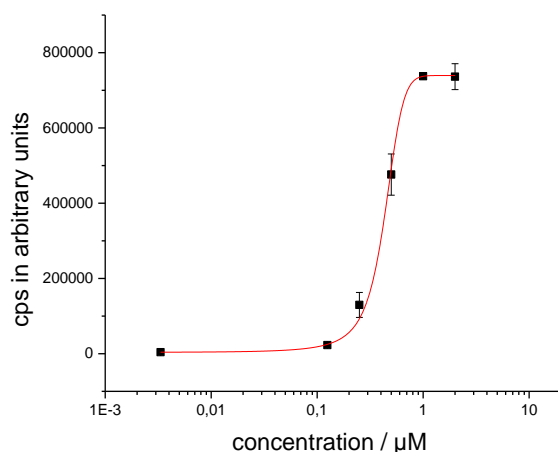


Figure 15 Representative serial dilutions of a 1:1 complex of His₆-PDE δ with a C-terminal, biotinylated K-Ras4B peptide measured by assay employing Alpha technology

For the displacement titrations with small molecules, Sildenafil and Atorvastatin were used as controls. Both compounds were able to break the PDE δ -K-Ras4B interaction (Figure 16). Atorvastatin proved to be the stronger binder, with an apparent $K_{D,app}$ below 3 μ M, whereas Sildenafil displayed an affinity $K_{D,app}$ of 4.3 μ M.

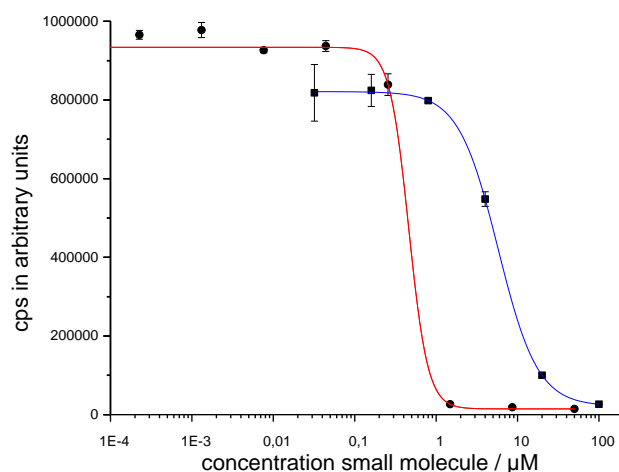


Figure 16 Displacement titrations of PDE δ /K-Ras4B complex with different concentrations of small molecule Atorvastatin (Fit: red), Sildenafil (Fit: blue) (concentration PDE δ 3 μ M, K-Ras4B 3 μ M) observed by chemiluminescent Alpha assay. Data were fit by an empirical dose response model and are derived from two independent sets of experiments.

With a working assay system in hand, a library of 40000 molecules was initially screened in a semi automatic fashion (PDE δ 600 nM, K-Ras4B 900 nM, 0.005% Chaps). Clustered hits of

this screening campaign were analysed in terms of their binding energy per atom (ligand efficiency),⁶⁷ and a series of *N*-substituted benzimidazoles emerged as the compounds with the highest per atom binding efficiency. These compounds were therefore further analysed by crystallography and orthogonal biophysical techniques.

4.2. Thermodynamic and structural analysis of small molecule-PDE δ interaction

In order to get insight into the binding mode of the highly ligand efficient benzimidazole fragments, compound **10** was cocrystallized with PDE δ by Dr. Shehab Ismail and it was found that two benzimidazole moieties are located within the prenyl binding pocket of PDE δ (Figure 17). The cocrystal structure of benzimidazole **10** with PDE δ revealed a virtually complete overlap of the two benzimidazole units with the farnesylated *C*-terminus in the Rheb-PDE δ crystal structure (Figure 17, a). Merely the position of Trp90 is slightly different in the cocrystal structure of **10** with PDE δ when compared to the Rheb-PDE δ structure (Figure 17, b). The movement of Trp90 can be attributed to the larger size and the rigidity of the two benzimidazole units compared to the farnesyl moiety.

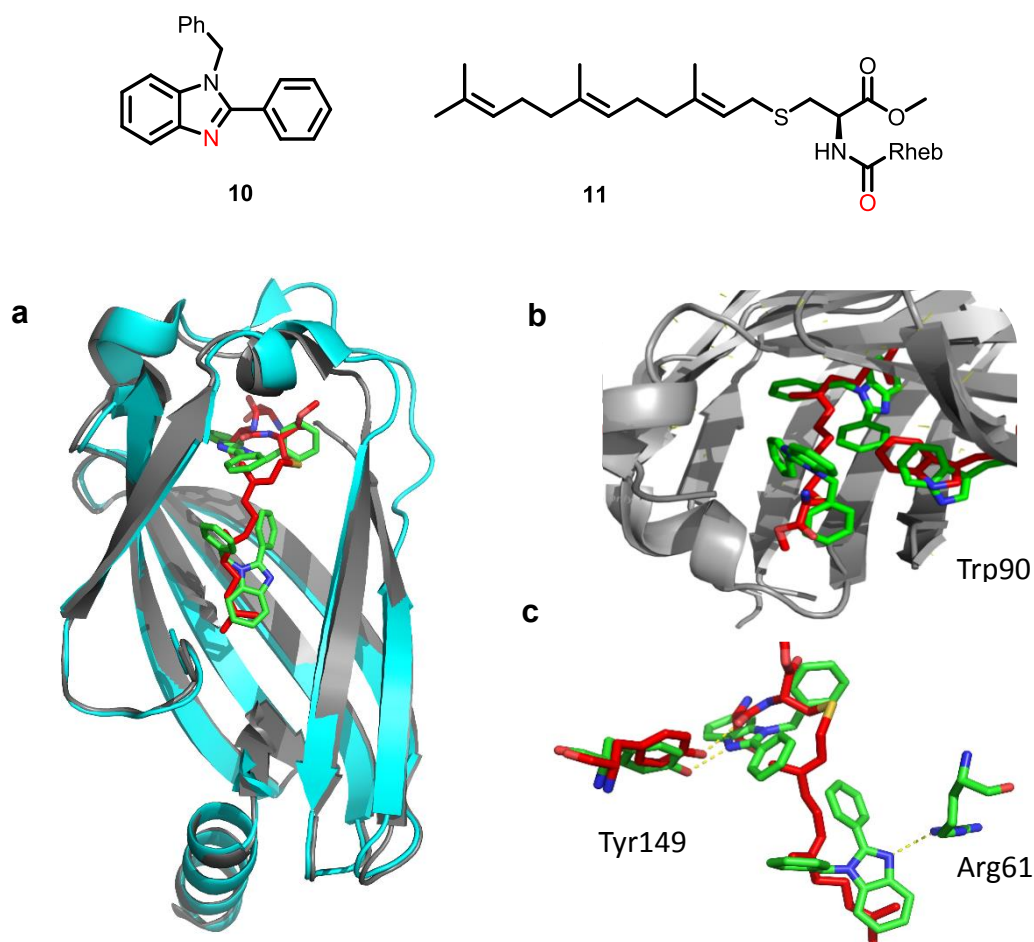


Figure 17 Crystal structure of farnesylated Rheb peptide (Farnesyl : red) with PDE δ in comparison with crystal structure of benzimidazole **10** (green) with PDE δ . In the chemical structure key hydrogen bond acceptors are highlighted in red. a) overlay of the two crystal structures; b) flip of Trp90 to accommodate the more bulky inhibitor. c) Key hydrogen bonding interactions (yellow) between Rheb-PDE δ and benzimidazole **10**-PDE δ . The crystal structure was solved by Dr. Shehab Ismail.

Hydrogen bonds to Tyr149 could be identified in both structures. In the Rheb-PDE δ complex Tyr149 interacts with the backbone carbonyl of Ser180, whereas in the benzimidazole **10**-PDE δ structure a key hydrogen bond to the benzimidazole unit is formed (Figure 17, c). Importantly, the **10**-PDE δ structure features an additional hydrogen bond between Arg61 and the other benzimidazole unit (Figure 17, c).

In order to validate the binding of two benzimidazole units to the prenyl binding cavity of PDE δ , cocrystallization with other benzimidazole fragments was attempted. The 1.4 Å crystal structure of benzimidazol fragment **12** confirmed that indeed two benzimidazole units can bind to PDE δ (Figure 18, a). An overlay with the cocrystal structure of benzimidazole **10** revealed

hydrogen bonds to the same amino acids, although the position of the individual benzimidazole units is slightly altered (Figure 18, b)).

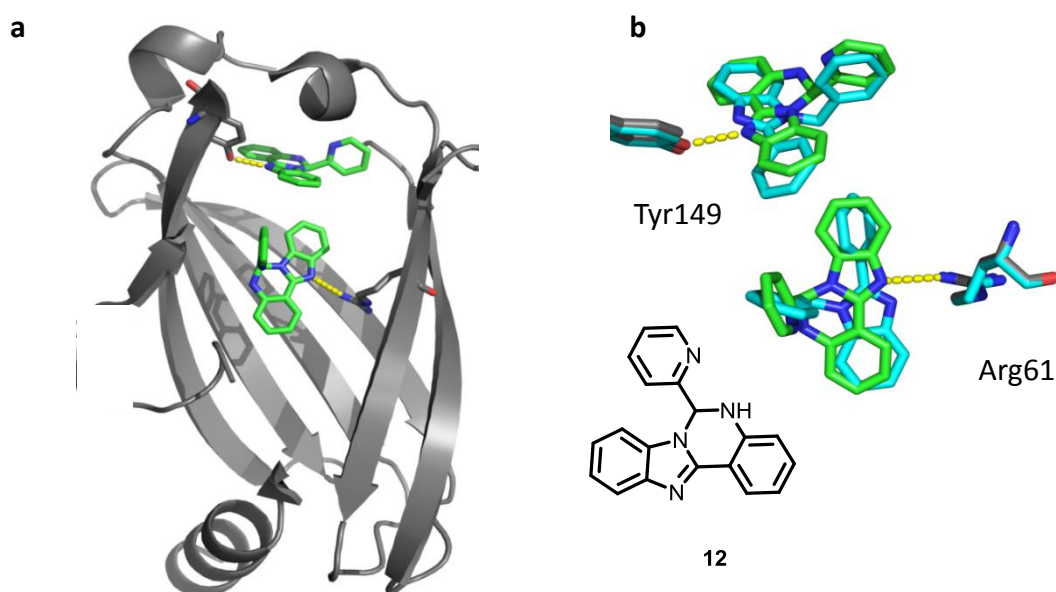


Figure 18 Cocystal structure of benzimidazole **12** (green sticks) with PDEδ. a) Key hydrogen bonds are highlighted in yellow. b) Overlay with cocystal structure of benzimidazole **10** (cyan sticks), key hydrogen bonds to Arg61 and Tyr149 are highlighted. The crystal structure was solved by Dr. Shehab Ismail.

With the structural data in hand, isothermal titration calorimetry (ITC) was performed to show that at physiologically relevant, low micromolar concentrations two benzimidazole fragments are bound to PDEδ. In ITC the change in heat upon interaction of two binding partners is measured. In a single experiment the stoichiometry, the equilibrium constant K_D and the thermodynamic profile of the interaction can be determined.⁶⁸⁻⁷²

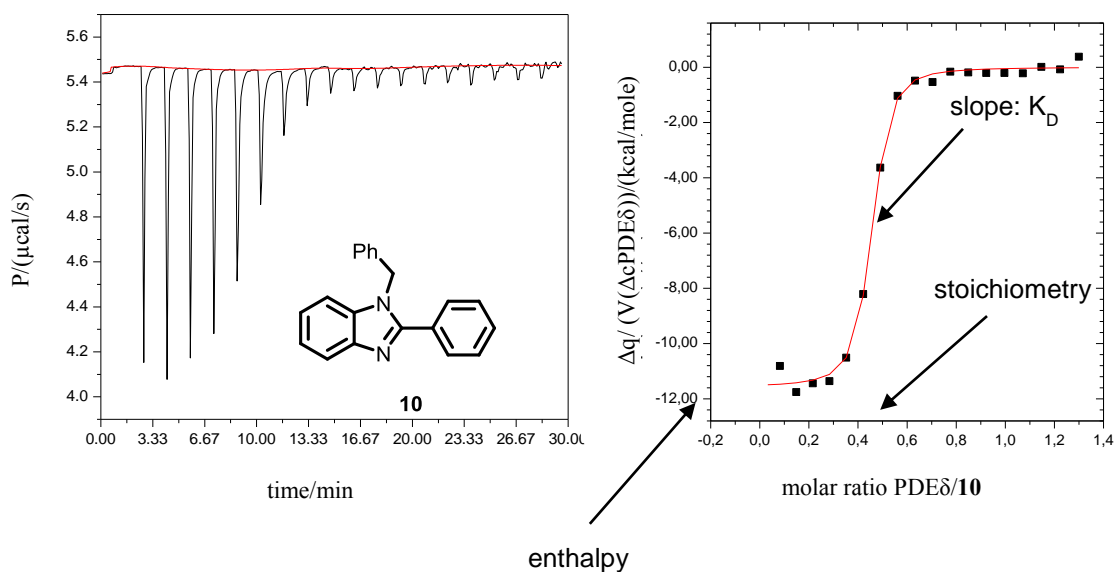


Figure 19 Raw injection trace (left) and total heat per injection (right) derived from a representative ITC experiment of compound **10**. P =power, V = volume, q =heat.

From the raw injection trace of the protein to ligand titration (Figure 19, left), it is apparent that binding of benzimidazole **10** is highly exothermic. The binding isotherm derived from the area under the curves (Figure 19, right) yielded a K_D value of 217 ± 12 nM and a stoichiometry of 1:2 PDE δ :benzimidazole. The stoichiometry is thus consistent with the X-ray data, underlining that even at low micromolar concentrations two molecules bind into the farnesyl binding pocket. The affinity constant K_D of the interaction can be translated into the overall free binding energy ΔG° . ΔG° consists of an entropic $-T\Delta S^\circ$ and an enthalpic contribution ΔH° , with a strongly negative value of ΔG° corresponding to a low K_D and high affinity.

The molecular driving force of the interaction between **10** and PDE δ is the strongly favourable change in enthalpy ΔH° upon interaction (-11.5 kcal/mole), which is mainly due to the formation of two hydrogen bonds to the two benzimidazole units. The more rigid benzimidazole **12** displays a similarly exothermic thermodynamic binding profile (ΔH° -11.0 kcal/mole), however the entropic contribution $-T\Delta S^\circ$ to the free energy ΔG° is much less pronounced, which results in a lower affinity of 1400 nM. The strongly enthalpy driven binding of the benzimidazole fragments **10** and **12** makes them *bona fide* starting points for the design of highly efficient and selective binders of PDE δ .^{69,73}

In parallel the previously identified PDE δ inhibitor Atorvastatin was docked into the farnesyl binding site. According to the best scoring docking poses, the amide of Atorvastatin functions as a hydrogen bond acceptor and interacts with the deeply buried Arg61 (Figure 20).

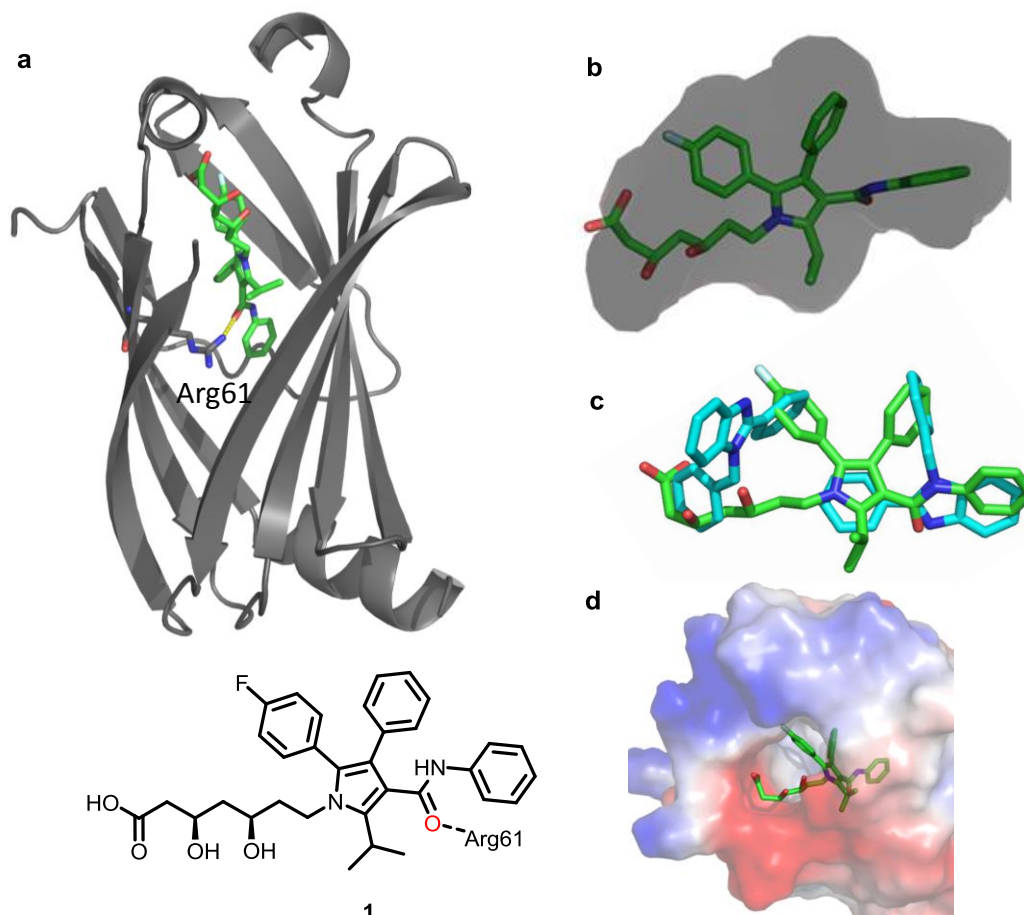
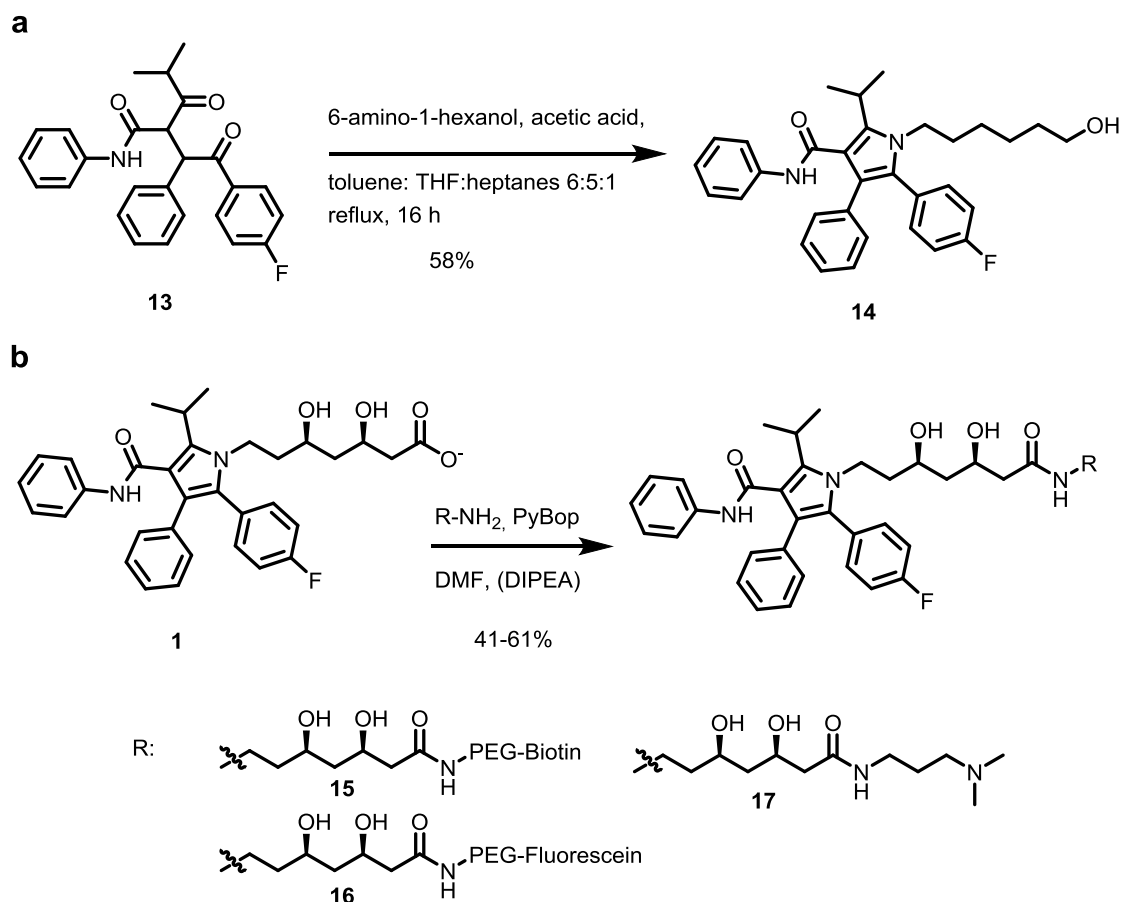


Figure 20 Best scoring docking pose for the Atorvastatin-PDE δ interaction. a) Overall structure of Atorvastatin (colored sticks)-PDE δ model, hydrogen bond of amide to Arg61 is highlighted; b) Surface representation of PDE δ cavity (PDB 4JV6) with docked Atorvastatin, highlighting the good fit of Atorvastatin into the binding pocket according to best scoring docking pose; c) Overlay with benzimidazole fragments; d) Surface charge representation of protein around Atorvastatin, showing a potentially unfavourable interaction of the carboxylate with the negatively charged protein surface.

Closer inspection of the docking pose revealed that the substituted pyrrole core efficiently fills the binding pocket (Figure 20, b). The flexible acid side chain of Atorvastatin on the other hand does not show any key interactions. Therefore Atorvastatin-derivatives were synthesized in which the acid side chain was replaced by a simple aliphatic alcohol of similar length (Scheme 2). Notably, Tyr149 is not targeted by Atorvastatin. Consequently the acid was converted into a strong hydrogen bond acceptor by formation of an amide bond. It was also reasoned that the negative charge of Atorvastatin might lead to unfavourable electrostatic interactions with the

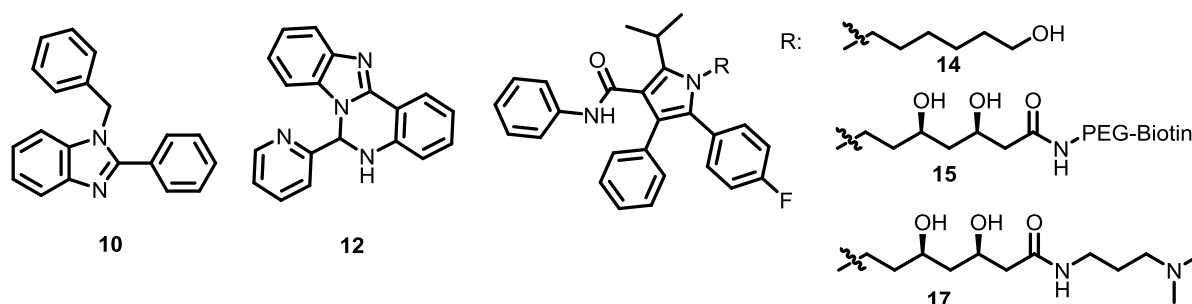
negatively charged protein surface ((Figure 20, d). Consequently, a tertiary amine was incorporated into novel Atorvastatin-derivatives.



Scheme 2 Synthesis of Atorvastatin derivatives. a) by Paal-Knorr-synthesis or b) by amide bond formation.

The highest yields were obtained when a large excess of the amine component was used which suppressed the competing intramolecular lactonization. With the synthesized Atorvastatin derivatives in hand, the potency of this compound class was evaluated using ITC experiments (Table 1).

Table 1 Thermodynamic profiles derived from isothermal titration calorimetry for different compounds. For compounds marked with an asterisk the error is based on the fit.



Entry	Cpd (rac)	K_D / nM	ΔH° / (kcal/mole)
1	10	217 ± 15	-11.5
2	12	1420 ± 480	-11.0
3	17	118 ± 22 *	-8.0
4	15	67 ± 16 *	-10.0
5	14	170 ± 56	-2.5

Similar to the benzimidazole fragments **10** and **12** (Table 1, entries 1 and 2), binding of Atorvastatin derivatives **15** and **17** is strongly enthalpy driven (Table 1, entries 3 and 4). The binding affinity of Atorvastatin derivative **14** is similar to benzimidazole **10**, however **14** features only one strong hydrogen bond acceptor (amide), as a result the binding is much less enthalpy driven (Table 1, entry 5). Surprisingly, the flexible lipid chain of Atorvastatin derivative **10** does not result in an observable entropic penalty upon interaction with the protein. These data may suggest a high residual mobility of **14** in the protein bound state, since PDE δ is a very flexible protein.

4.3. Development of a fluorescence polarization assay to evaluate small molecule-PDE δ interactions

ITC is a highly reliable, label-free technique for the determination of K_D values. However, protein consumption is high, throughput is low and compounds have to be soluble at least to double digit micromolar concentrations.⁷⁴ Therefore, alternative assays for the determination of compound affinities were needed. Fluorescence polarization had been previously used to determine the affinities of lipidated peptides for PDE δ .^{40,75-77} Due to the low affinity of the peptides large protein concentrations would be needed to perform displacement assays with small molecules, since only at high nanomolar protein concentrations a significant amount of peptide would be protein-bound. High protein concentrations additionally also lead to difficulties in the determination of the affinity of very potent binders.

In biophysical assays, low affinity, labeled Ras peptides can be readily replaced with high affinity small molecules like Fluorescein-Atorvastatin **16** since both target the prenyl binding cavity of PDE δ . Atorvastatin derivatives proved to be strong binders to PDE δ in ITC experiments. In particular the biotinylated Atorvastatin derivative **15** showed the highest binding affinity of all compounds tested in ITC. These data suggest that the structurally similar Fluorescein-Atorvastatin **16** would bind with a similarly low K_D which would allow the use of **16** in displacement titrations at low nanomolar protein concentrations. Therefore Fluorescein-Atorvastatin **16** was used as a starting point for the development of fluorescence polarization assays.

The rationale behind this fluorescence polarization assay is that Fluorescein-Atorvastatin can rotate freely in bulk solution, whereas rotation in the protein-bound state is restricted. If linear polarized light is used to excite Fluorescein-Atorvastatin, the polarization of the emitted light is dependent on the rotational movement of the fluorophore within the fluorescence lifetime. If the molecule rotates quickly within the fluorescence lifetime, the emitted light will be depolarized. As a result the unbound Fluorescein-Atorvastatin exhibits a low fluorescence polarization, whereas protein-bound Fluorescein-Atorvastatin shows a high polarization. If unlabeled small molecules are used to displace Fluorescein-Atorvastatin from the prenyl binding cavity of PDE δ , the unbound Fluorescein-Atorvastatin will then also exhibit a low fluorescence polarization (Figure 21,a).

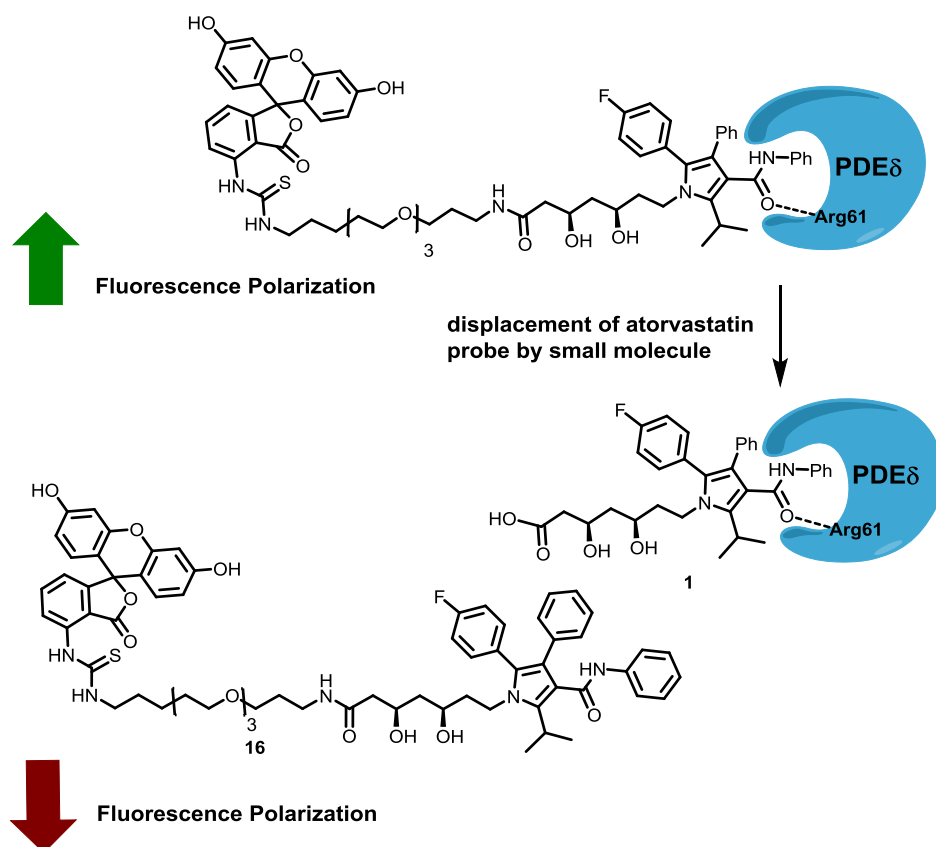


Figure 21 Displacement assay employing Fluorescein-Atorvastatin and unlabeled small molecules (e.g. Atorvastatin (**1**)). Displacement of Fluorescein-Atorvastatin is detected via the change in fluorescence polarization. Fluorescein-Atorvastatin can rotate freely in bulk solution, whereas rotation in the protein-bound state is restricted. If linear polarized light is used to excite Fluorescein-Atorvastatin, the polarization of the emitted light is dependent on the rotational movement of the fluorophore within the fluorescence lifetime. If the molecule rotates quickly within the fluorescence lifetime, the emitted light will be depolarized. Therefore, unbound Fluorescein-Atorvastatin exhibits a low fluorescence polarization, whereas protein-bound Fluorescein-Atorvastatin shows a high polarization. If unlabeled small molecules are used to displace Fluorescein-Atorvastatin from the prenyl binding cavity of PDE δ , the unbound Fluorescein-Atorvastatin will then also exhibit a low fluorescence polarization.

As expected Fluorescein-Atorvastatin **16** bound tightly in a direct titration with PDE δ (K_D 7.1 ± 4.0 nM, Figure 22, a). Therefore, low nanomolar concentrations of fluorophore and protein could be used for the competition assay which simplified the measurement of small molecules with very high affinity (Figure 21, b).

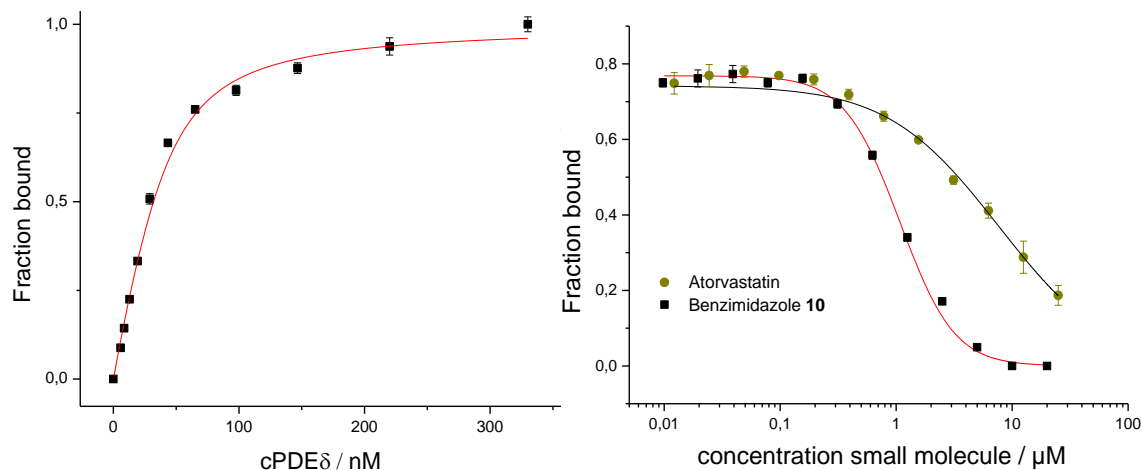
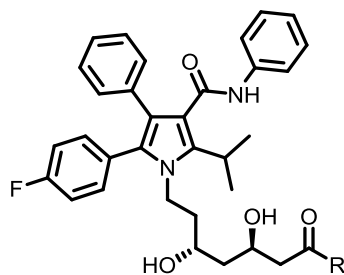


Figure 22 Fluorescence polarization assays employing Fluorescein-Atorvastatin and PDE δ ; a) Direct titration of Fluorescein-Atorvastatin **16** (50 nM) with PDE δ , on the y-axis the fraction of Fluorescein-Atorvastatin that is bound to PDE δ is shown; b) Displacement titrations using unlabeled small molecules and **16** as probe (conditions: Fluorescein Atorvastatin 24 nM, PDE δ 40 nM).

Displacement titrations with unlabeled small molecules were performed to obtain the K_D values of their interaction with PDE δ .⁷⁸ Atorvastatin (K_D , 1250 nM, Table 2, entry 1) proved to be a stronger binder than Sildenafil ($K_D > 5 \mu\text{M}$), therefore the Atorvastatin amide compound collection was further enlarged (in collaboration with LDC, Dortmund).

Table 2 Affinities of Atorvastatin derivatives measured by means of fluorescence polarization (using **16** as probe). Compounds marked with an asterisk were synthesized by LDC/Taros.



Entry	Compound	R	K _D / nM
1	1		1250 ± 234
2	18		35 ± 9
3	19		16 ± 5
4	20		36 ± 15
5	15		26 ± 10

Conversion of the carboxylic acid of Atorvastatin to an amide increased the affinity of the resulting pyrroles compared to Atorvastatin itself by more than one of order of magnitude. We reasoned that this striking increase in affinity could be explained by the formation of a second strong hydrogen bond to the amide. These Atorvastatin derivatives could potentially form two hydrogen bonds to Arg61 and Tyr149 instead of only one, which is to be expected for Atorvastatin itself.

In parallel, the highly ligand efficient benzimidazole fragments were investigated. Benzimidazole **10** displayed an affinity of 165 ± 23 nM in the Fluorescein-Atorvastatin displacement assay (Table 3), whereas the closely related 1-benzyl 2-phenylindole showed no measurable binding. A number of simple benzimidazoles like **10** are found in the MPI Dortmund compound library and it was therefore decided to test whether the existing

benzimidazole library contained more potent compounds than **10**. The library of simple *N*-substituted benzimidazoles was tested at a concentration of 1 μ M in the fluorescence polarization assay employing Fluorescein-Atorvastatin and the best compounds were retested in a dose-response binding assay. From these experiments a simple benzimidazole containing an azepane moiety emerged as the most potent compound (Table 3, entry 2). The high affinity can be explained by the very high hydrophobicity of this saturated heterocycle, which apparently fills the hydrophobic cavity of PDE δ with high efficiency. The introduction of a tertiary amine and thus presumably a positive charge is tolerated by the protein. Consistent with the fluorescence polarization data, the compound shows a high affinity ($K_{D,app}$ of 110 nM, see appendix) in the Alpha screen assay employing a *C*-terminal K-Ras peptide.

Table 3 Averaged affinities of simple benzimidazoles determined by means of fluorescence polarization employing Fluorescein- Atorvastatin.

The image shows the chemical structure of a benzimidazole derivative. It consists of a benzene ring fused to an imidazole ring. The nitrogen at position 1 of the imidazole ring is substituted with an R¹ group, and the nitrogen at position 2 is substituted with an R² group.

Entry	Cpd	R ¹	R ²	K _D / nM
1	10			165
2	21			52
3	22			83
4	23			149
5	24			250

4.4 Design, synthesis and biophysical evaluation of a *bis*-benzimidazole library

Comparison of the K_D values determined in different investigations suggested that the fragment-sized benzimidazole **10** binds to PDE δ with a higher binding affinity than the farnesylated K-Ras4B protein (165 vs 302 nM).^{40,79} Very high affinity compounds are often required to obtain high target occupancy and specificity in a biological environment. Therefore, it was decided to link the two benzimidazole fragments identified in the cocrystal structure of **10** in order to improve potency. Molecular modelling (Schrödinger, Maestro suite) enabled the *in silico* analysis of different linker moieties. The best scoring poses were analysed and compared to the cocrystal structure of **10** (Figure 23, a,b). Phenyl rings A and B (Figure 23, a) of the two different benzimidazole fragments **10** were well aligned for a T-stacking interaction in the cocrystal structure and thus these two rings were left unaltered. Phenyl ring C on the other hand was found to be in close proximity to the benzylic position (4.3 Å) of benzimidazole fragment **10**. Consequently a short linker was used for connecting the two fragments at the indicated positions (Figure 23, b, c).

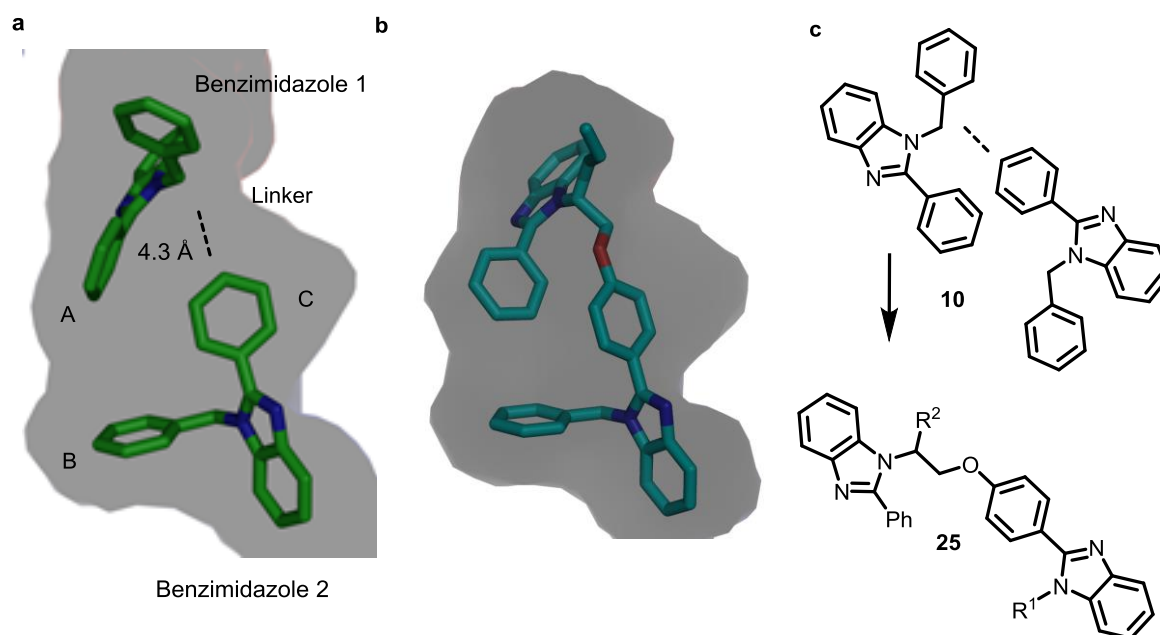
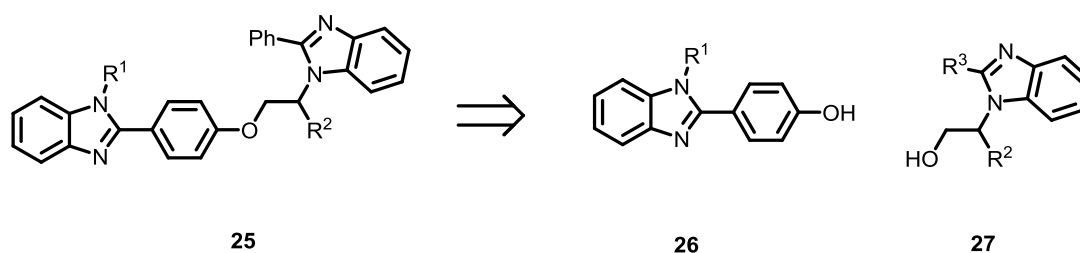


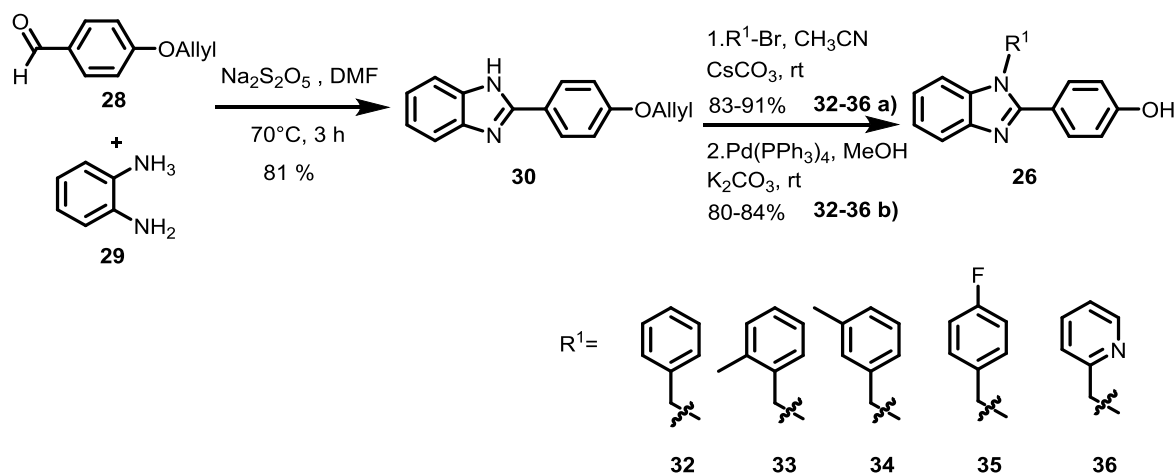
Figure 23 Design of linked benzimidazoles; a) Surface representation of PDE δ cavity (PDB 4JV6). The distance between linked atoms is highlighted; b) Best scoring docking pose obtained by docking an allyl substituted (R^2) *bis*-benzimidazole into crystal structure of benzimidazole fragment **10** (PDB 4JV6); c) Design of linked *bis*-benzimidazole ethers **25**.

Retrosynthetically, the *bis*-benzimidazoles were disconnected to phenols **26** and alcohols **27** (Scheme 3).



Scheme 3 Disconnection of *bis*-benzimidazoles into fragments **26** und **27**.

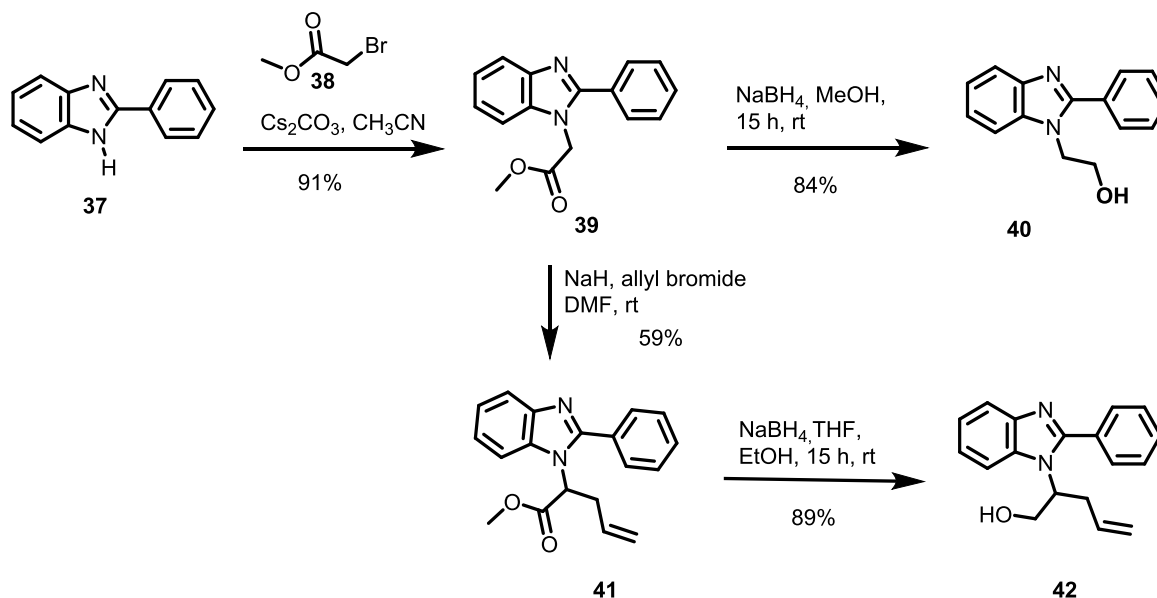
The synthesis of benzimidazole fragments **26** started with commercially available phenylenediamine, which was reacted with 4-allyloxy benzaldehyde in the presence of sodium metabisulfite to yield the desired benzimidazole **30**. *N*-benzylation of the benzimidazole followed by allyl deprotection of the phenol furnished the desired products **32-36** in good yields (80-84%).



Scheme 4 Synthesis of benzimidazole fragments **26**.

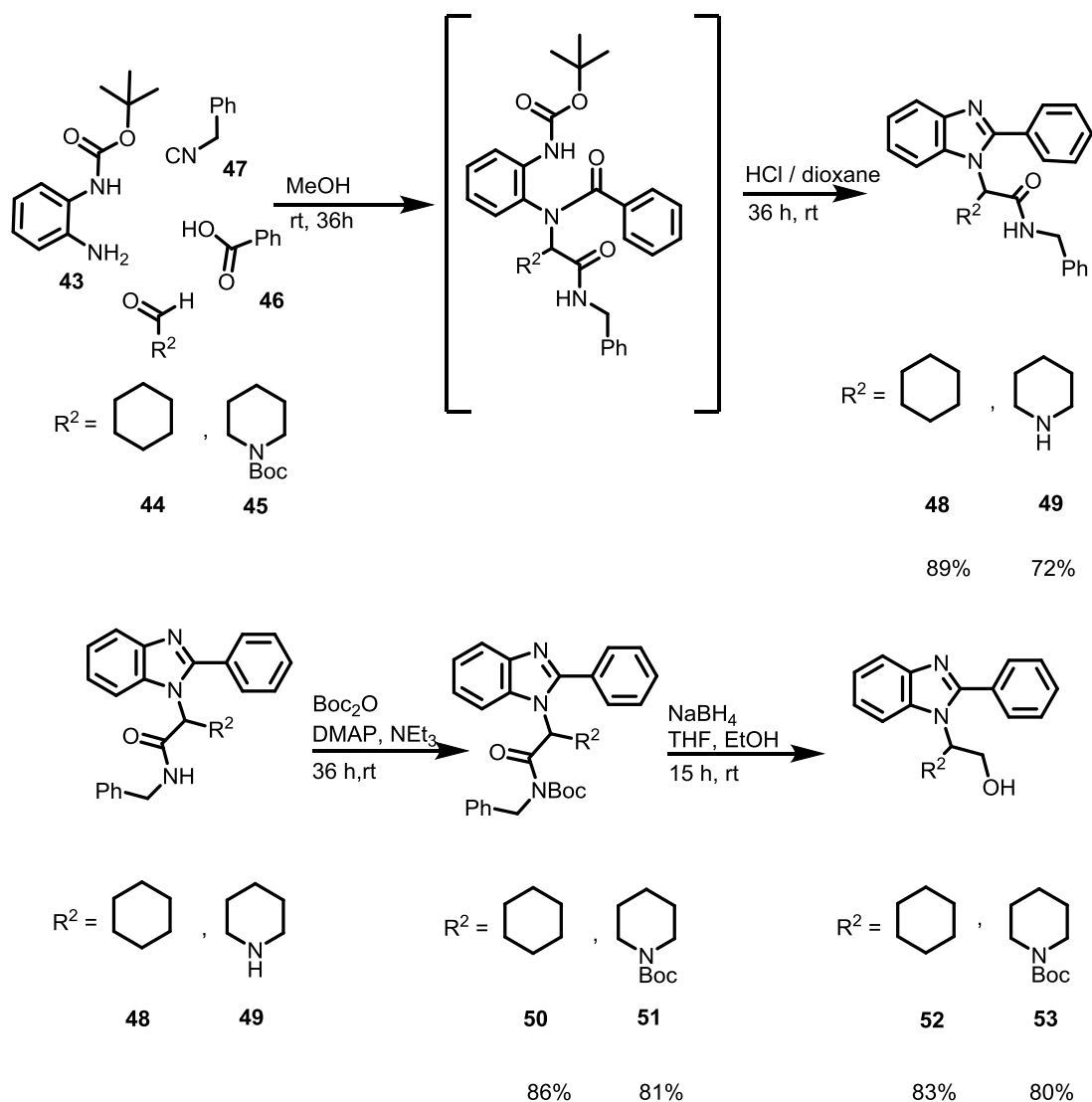
Benzimidazole fragments **27** were synthesized either by an alkylation/reduction route or by a strategy based on a Ugi multi component reaction. Initially, *bis*-benzimidazoles containing small, flexible substituents like an allyl group at position R² were synthesized to avoid clashes with the surface of the protein and to validate that fragment linking leads to higher affinity. Such benzimidazole fragments **27** were synthesized by alkylation of commercially available

2-phenyl benzimidazole with methyl bromoacetate (Scheme 5). The intermediate ester **39** was either directly reduced to the alcohol **40** or further alkylated with allyl bromide and then reduced with sodium borohydride.



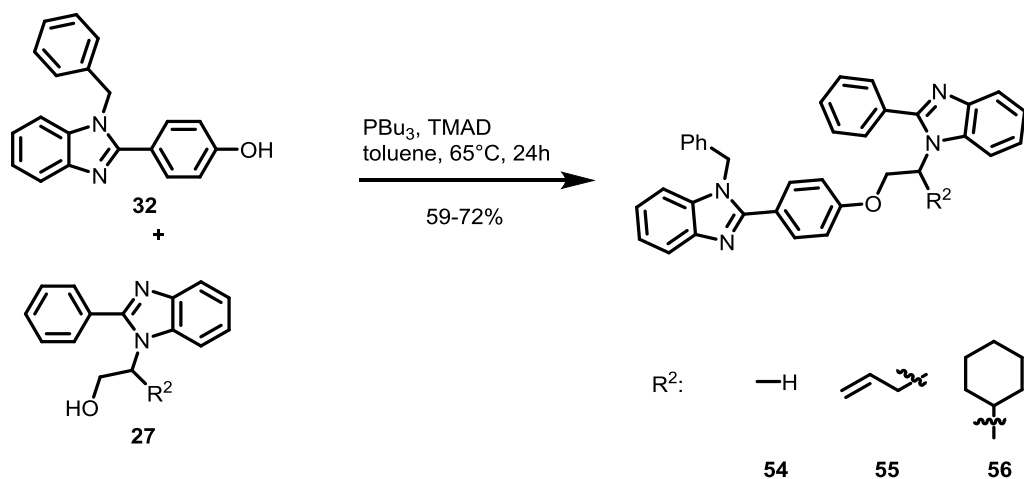
Scheme 5 Synthesis of benzimidazole fragments **40** and **42** by alkylation/reduction sequence.

Benzimidazole fragments **27** containing more bulky substituents were synthesized by a strategy that is based on a Ugi-four-component reaction.⁸⁰ Commercially available *o*-phenylenediamine, benzoic acid, benzyl isocyanate and the appropriate aldehyde were stirred for 36 h in MeOH to obtain the initial Ugi-product, which was then Boc-protected and cyclized using HCl /dioxane to yield the intermediate branched amides **48** and **49** respectively in one pot and good yields (72-89%, Scheme 6). Activation of the amide by reaction with di-*tert*-butyl dicarbonate, followed by reductive cleavage of the amide led to the desired free alcohols **52** and **53** in good overall yields.



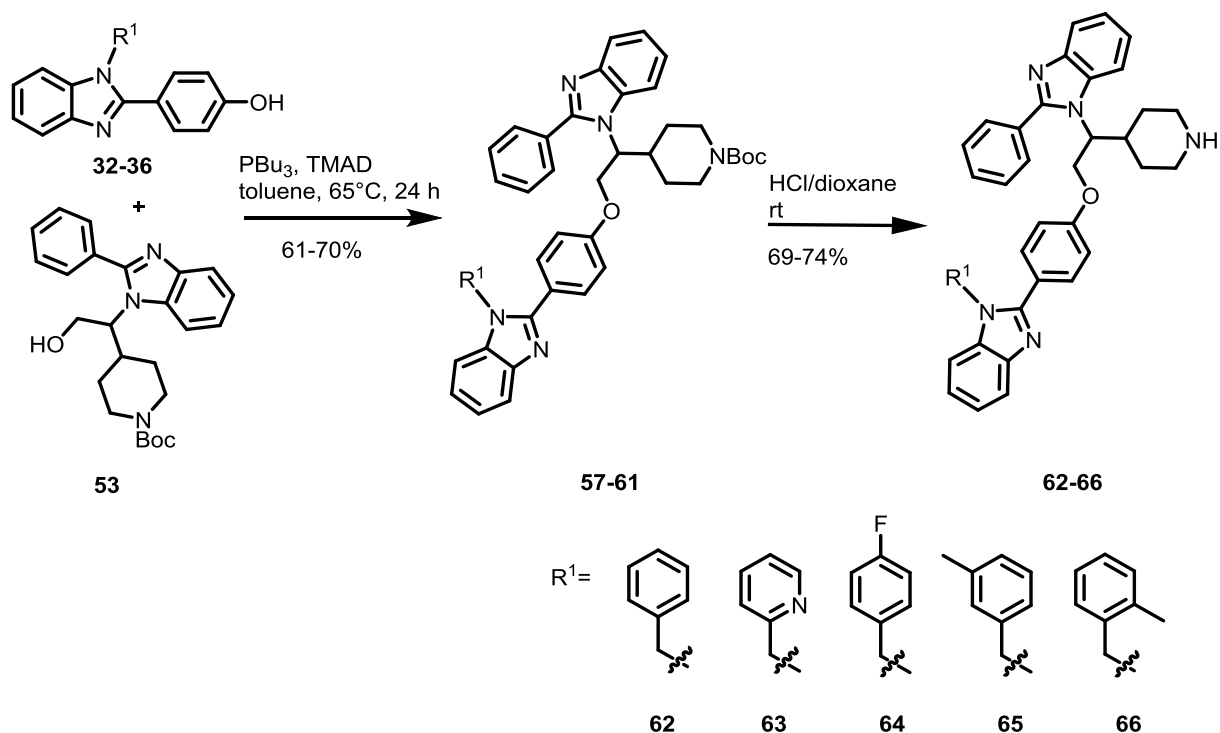
Scheme 6 Synthesis of benzimidazole fragments **27** by a Ugi-4-component strategy.

Benzimidazole fragments **26** and **27** were subsequently connected via a modified Mitsunobu reaction with *n*-tributylphosphine and tetramethyl azadicarboxamide (TMAD).⁸¹ When fresh PBU_3 and TMAD were used the reaction proceeded well with yields ranging from 59% to 72% (Scheme 7).



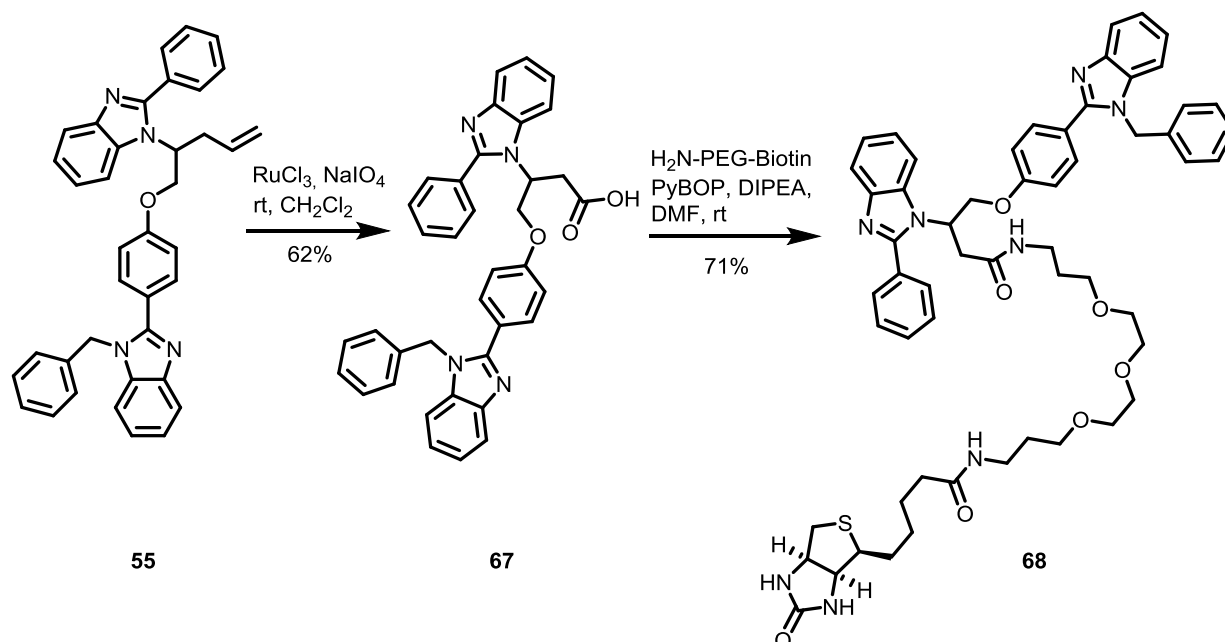
Scheme 7 Fragment linking of benzimidazoles via Mitsunobu reaction employing PBu_3 , TMAD.

Boc-protected piperidines were linked in an analogous fashion (Scheme 8). Mitsunobu reaction of alcohol **53** with benzimidazoles **32-36** yielded the intermediate Boc-protected piperidines (61-70%). Deprotection of the piperidines and purification by reverse phase chromatography afforded the final inhibitors (69-74%).



Scheme 8 Synthesis of piperidine containing bis-benzimidazoles via Mitsunobu reaction.

In order to obtain a suitable probe for pull down experiments in cell lysates the *bis*-benzimidazole **55** was equipped with a biotin moiety. For this purpose the allyl-substituted *bis*-benzimidazole **55** was oxidatively cleaved and coupled to a biotinylated linker to yield **68** (Scheme 9).



Scheme 9 Synthesis of acid **67** and subsequent biotinylation to yield **68**.

4.4.1 Evaluation of *bis*-benzimidazole affinities for PDE δ by means of fluorescence polarization assays and T_m shift measurements

Due to the large hydrophobic surface area and the high abundance of aromatic rings, linked *bis*-benzimidazoles were generally sparingly soluble. Compound **56** for example shows a solubility below 1 μM (Solrank, LDC Dortmund). This low solubility in aqueous buffers may result in experimental artifacts, which lead to an underestimation of the real affinity for this compound. Therefore, in addition to fluorescence polarization assays an orthogonal direct binding assay was needed which is not sensitive to compound solubility. T_m shift assays measure changes in the protein melting point T_m upon binding of a small molecule to the protein. The experiments should be performed by using a stoichiometry of protein to small molecule of approximately 1:1, which avoids precipitation of the small molecule, since the protein solubilizes the small molecule by soaking it into the hydrophobic cavity. Additionally, precipitation is avoided by the gradual increase in temperature during the experiment.

Different methodologies have been used for the detection of changes in the protein melting point upon binding of small molecules. Fluorophores which bind to unfolded patches of the protein may be used for the detection of protein melting points.^{82,83} CD-spectroscopy has a relatively low throughput but it has the advantage of being label free.^{84,85} To ensure orthogonality with the fluorescence polarization assays CD-spectroscopy was employed here to determine the melting point of PDE δ in the absence and presence of small molecule (Figure 24).

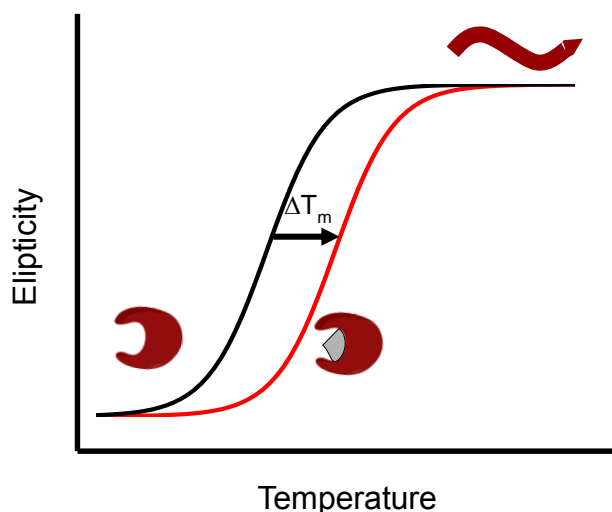


Figure 24 Schematic representation of the T_m shift assay. The ellipticity is proportional to the difference in absorption of left and right circular polarized light. Upon heating the chiral secondary structure elements of the protein (red) start to unfold, resulting in a decrease in the absolute value of ellipticity. In the presence of a small molecules (grey) the melting curve of the protein is shifted towards higher temperatures (red curve), leading to a higher T_m .

CD-spectroscopy measures the difference in absorption of left and right circular polarized light. The measured so-called ellipticity is proportional to the difference in absorption of left and right circular polarized light. Upon heating, the chiral secondary structure elements of the protein (Figure 24) start to unfold, resulting in a decrease in ellipticity. In the presence of small molecules (grey) the melting curve of the protein is shifted towards higher temperatures, leading to a higher T_m .

Under the assumption that the thermodynamic binding profile within a compound series is constant, it has been shown that the T_m shift correlates with the affinity of the compound.⁸³ PDE δ displays a typical CD-spectrum for a beta-barrel protein, consisting mainly of beta sheets. Measurements in DMSO containing buffer solutions (due to compound storage in DMSO) have

to be carried out at relatively long wavelengths, because of the strong absorption of DMSO at wavelengths below 230 nm. Consequently a wavelength of 232 nm was chosen. The absolute value of ellipticity at that wavelength decreased clearly when the protein unfolds at elevated temperatures (Figure 25). Strikingly, all benzimidazoles shift the melting curve to substantially higher temperatures.

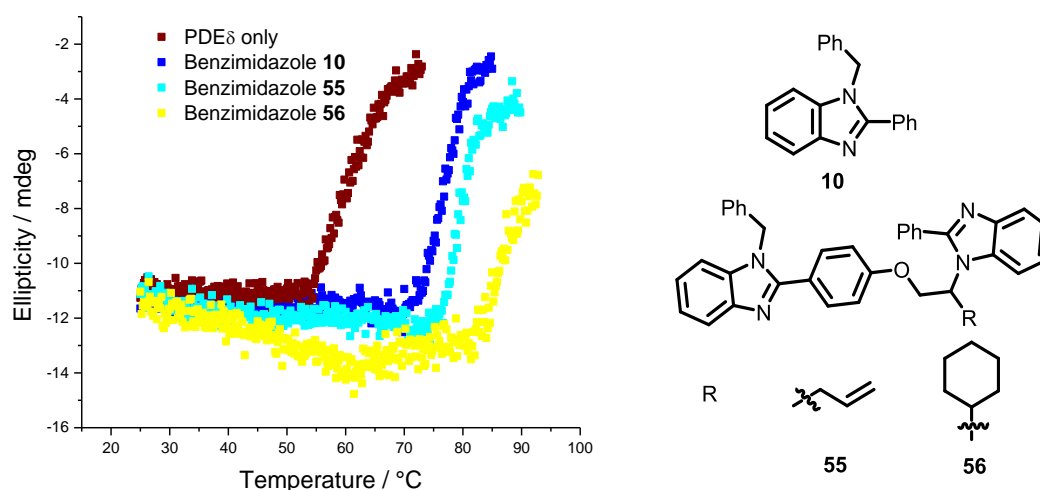


Figure 25 Determination of melting point (T_m) with CD-spectroscopy in the absence or presence of benzimidazole compounds.

Bis-benzimidazole **56** even shifts the melting point of the protein close to the detection limit of the instrument, since for technical reasons the ellipticity could not be reliably measured above 90°C. Thus, linkage of the benzimidazole fragments indeed leads to higher affinities.

The very large increase in the melting point ΔT_m for all compounds can be explained by a decrease of the protein flexibility upon ligand binding.^{86,87} Unliganded PDE δ does not crystallize suggesting a high intrinsic flexibility of the protein. Addition of a ligand causes the protein to rigidify. This interpretation is substantiated by recent ultrasound velocimetry data which show that the complex of a simple farnesyl derivative with PDE δ is much less dynamic than free PDE δ .⁸⁷

Subsequently cocrystallization of the validated *bis*-benzimidazole-based PDE δ inhibitors was attempted by Dr. Shehab Ismail. Gratifyingly, the **55**-PDE δ complex gave well-diffracting crystals with a resolution down to 1.75 Å. The x-ray structure revealed an almost complete

overlap of the *bis*-benzimidazole with the guiding benzimidazole fragment **10** and a very good overlay with the highest scoring docking pose (Figure 26). Inspection of the **55**-PDE δ structure revealed a hydrophobic cavity around the allyl group, which could also be filled by larger substituents.

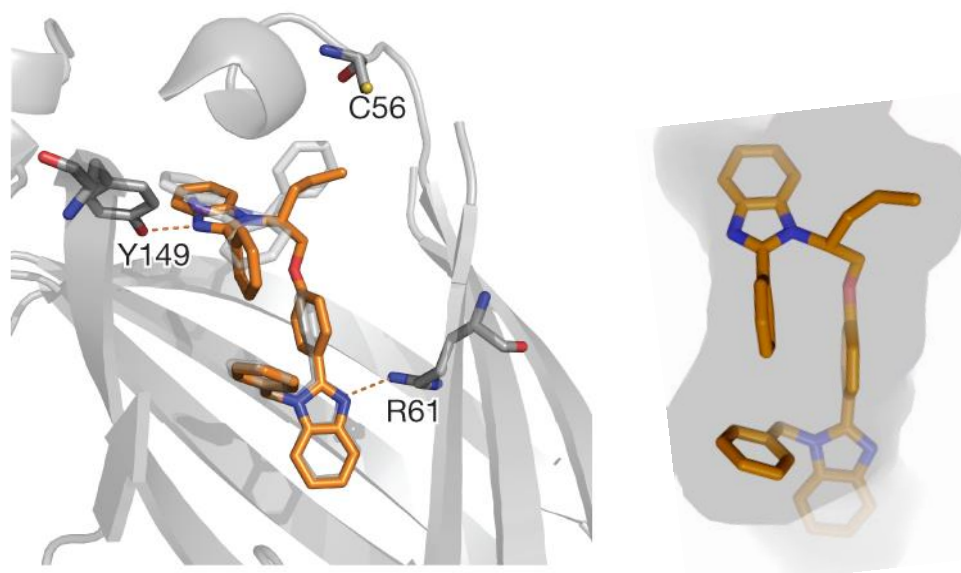
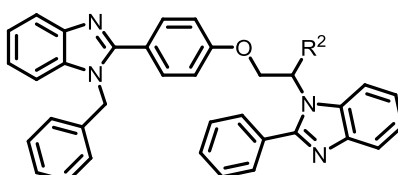


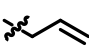
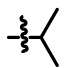
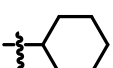
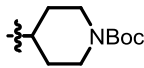
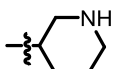
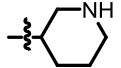
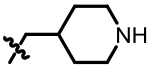
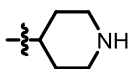
Figure 26 Cocrystal structure of *bis*-benzimidazole **55** with PDE δ ; left) Overlay of the *bis*-benzimidazole (coloured sticks) with the guiding benzimidazole fragments (faint grey sticks); right) view of cavity surrounding the *bis*-benzimidazole.

Binding of linked benzimidazole **55** was also analysed by means of fluorescence polarization. Consistent with the T_m shift, PDE δ bound to **55** with a 4-5 fold higher affinity compared to fragment **10**. A library with varying substituents at position R^2 (Table 4) was designed and evaluated with the T_m shift – and the fluorescence polarization assay. Increasing the size of the substituent R^1 with the use of a isopropyl and a cyclohexyl group increased both the affinity and the protein melting point (Table 4, entries 2+3), whereas introduction of a negative charge and omission of the substituent R^1 led to no improvement (Table 4, entry 4). Coupling of the *bis*-benzimidazole core to a PEG-linker and biotinylation resulted in decreased affinity (Table 4, entry 5). Due to a presumed steric clash with the surface of the binding pocket, a Boc-protected piperidine showed only weak interaction with PDE δ (Table 4, entry 6). Owing to the proximity of the allyl group to the backbone carbonyl of Cys56 in the cocrystal of **55** with PDE δ , an additional hydrogen bond was envisaged. Therefore, piperidines were used to replace the allyl group. Amongst the tested piperidines, piperidine **62** proved to be the most potent (entry 10). Unexpectedly the affinity of piperidine **62** was slightly lower compared to the allyl

and cyclohexyl substituted *bis*-benzimidazoles. However, introduction of the piperidine groups substantially increased the solubility of the small molecules in aqueous solutions, and the idea of installing a piperidine functionality as a hydrogen bonding donor was investigated further.

Table 4 Library of *bis*-benzimidazoles with varying substituents at the position R². Compounds marked with an asterisk were synthesized by LDC/Taros.



Entry	Cpd (rac)	R ²	K _D / nM	T _m shift / °C
1	55		39±11	19.7
2	69		20 ± 5	nd
3	56		16±2	25.8
4	67	CH ₂ COOH	870 ± 290	10.0
5	68	PEG-Biotin	328 ± 38	11.6
6	57		>2000	7.2
7	70	 *	>400	nd
		Diastereomer 1		
8	71	 *	207 ± 42	nd
		Diastereomer 2		
9	72	 *	162 ± 50	nd
10	62		87 ± 35	20.5

Further structural variations were conducted with the piperidine moiety in place, and focused on the variation of the benzyl moiety. The distance between the benzyl group of benzimidazole **55** and Trp32 is below 4 Angstrom such that it can undergo a T-stacking interaction with the electron rich indole moiety (Figure 27). T-stacking interactions are usually strongly dependent on the electronic nature of the interacting aromatic moieties.^{88,89} Therefore, electron-donating and electron withdrawing groups were introduced at position R¹ (Table 2).

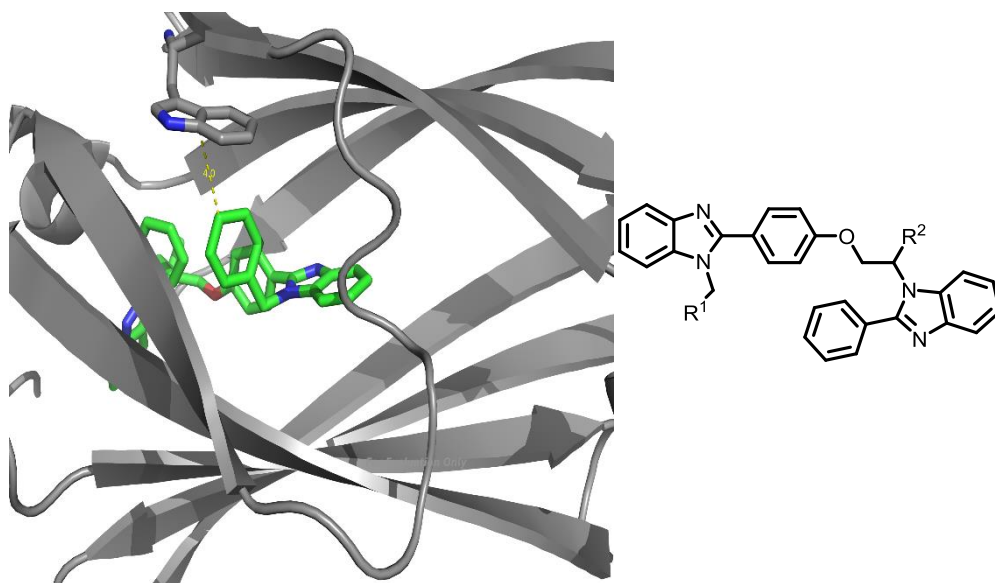
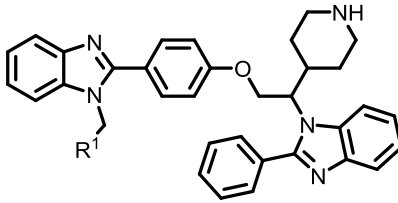
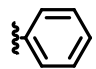
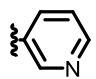
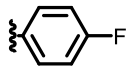
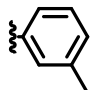
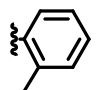


Figure 27 T-stacking interaction between benzimidazole **55** and PDE8

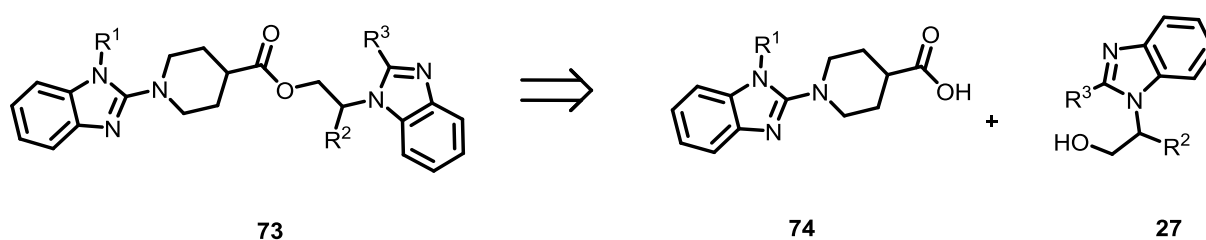
Unexpectedly neither the synthesis of electron-poor aromatic systems (4-fluorobenzene, pyridine; Table 5, entries 2-3) nor electron-rich toluene derivatives (Table 5, entries 4-5) resulted in more potent compounds. Owing to these disappointing results the benzyl moiety was retained in further studies.

Table 5 Variation of the substituent R¹ which undergoes a T-stacking with Trp32.


Entry	Cpd (rac)	R ¹	K _D / nM	T _m shift / °C
1	62		87 ± 35	20.5
2	63		231 ± 28	17.4
3	64		251 ± 36	nd
4	65		191 ± 45	nd
5	66		474 ± 121	nd

4.4.2 Synthesis and biophysical evaluation of ester linked *bis*-benzimidazoles

The results in Table 4 suggest that the rigid ether linker might make the backbone carbonyl of Cys56 unavailable for interaction with the piperidine group. Consequently the length of the linker moiety was increased and the ether replaced by a more flexible ester. In analogy to the disconnection of the ether compounds, ester linked *bis*-benzimidazoles were divided into two benzimidazole fragments: **74** and **27** (Scheme 10).

**Scheme 10** Disconnection of linked *bis*-benzimidazoles esters.

Benzimidazole fragments **74** were synthesized starting from 2-chloro benzimidazole (**75**). Nucleophilic aromatic substitution with ethyl piperidine-4-carboxylate (**76**) afforded compound **77** in 81 % yield. The free benzimidazole was subsequently either benzylated with caesium carbonate and benzyl bromides in acetonitrile (**78-79**) or underwent a Mitsunobu reaction with 3-hydroxymethyl thiophene (61%) using tributyl phosphine and TMAD (**80**). Cleavage of the ester under basic or strongly acidic, aqueous conditions furnished the free carboxylic acids **81-83**.

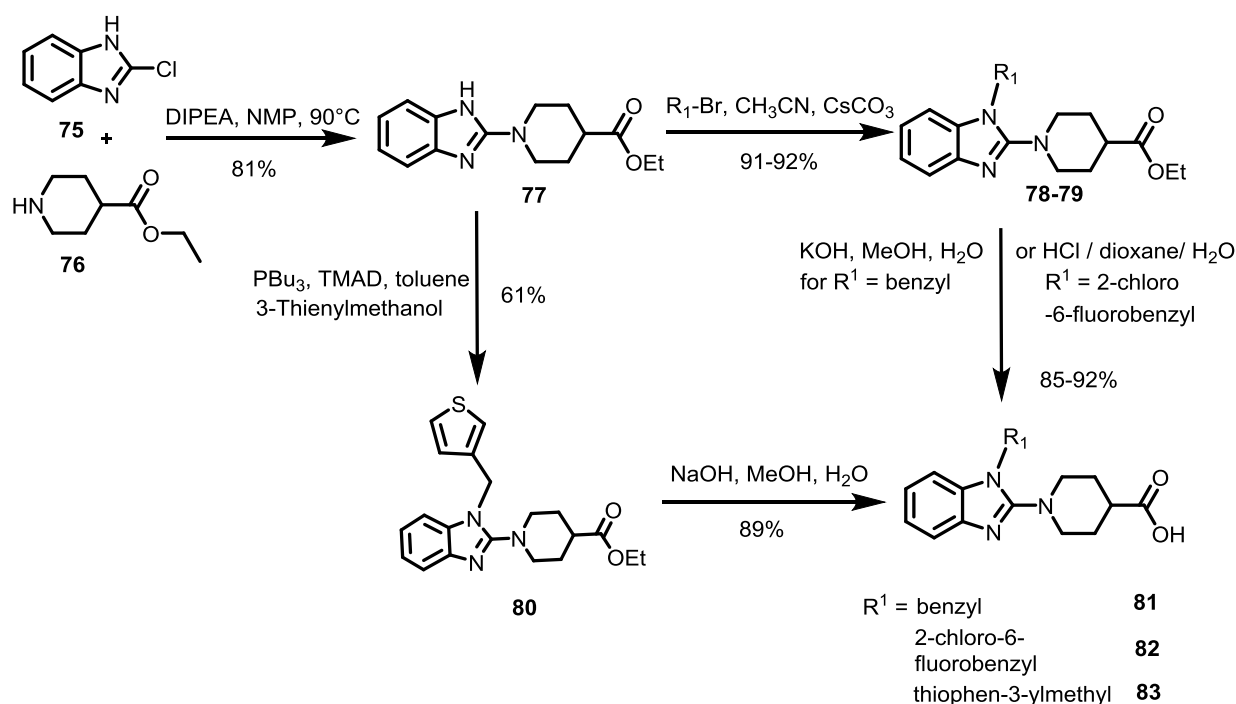


Figure 28 Synthesis of benzimidazole fragments **74**.

Benzimidazole fragments **74** were then reacted with fragments **27** under Mitsunobu reaction conditions ($PS-PPh_3$, DtBAD) and deprotected, if necessary, to yield the linked *bis*-benzimidazoles (Figure 29).

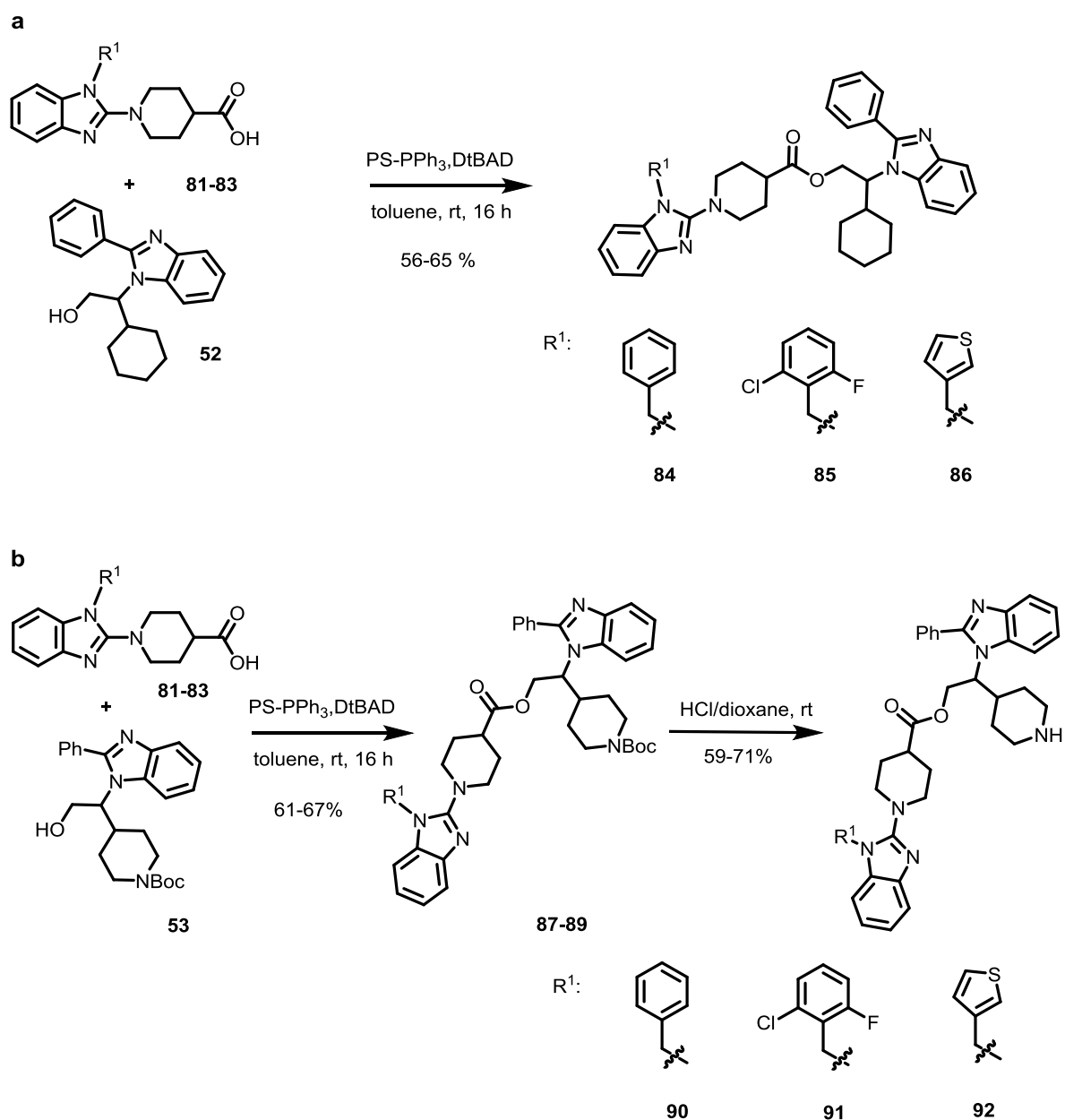


Figure 29 Synthesis of ester-linked *bis*-benzimidazoles from fragments **81-83** and **27** containing a) a cyclohexyl group or b) a piperidine moiety.

The ester compound collection was evaluated subsequently in fluorescence polarization assays and the data in Table 6 show that replacement of the phenyl ether with a piperidyl ester in this compound class leads generally to higher affinities. Gratifyingly, ester **90** bound to PDE δ with an affinity of 10 nM. The increased affinity of ester **90** compared to the related ether compound series might be explained by the formation of an additional H-bond to Cys56 as it was envisaged by docking experiments.

Indeed, a cocrystal structure of **90** with PDE δ confirmed the presence of a third hydrogen bond between the backbone carbonyl of Cys56 and the piperidine moiety (Figure 30).

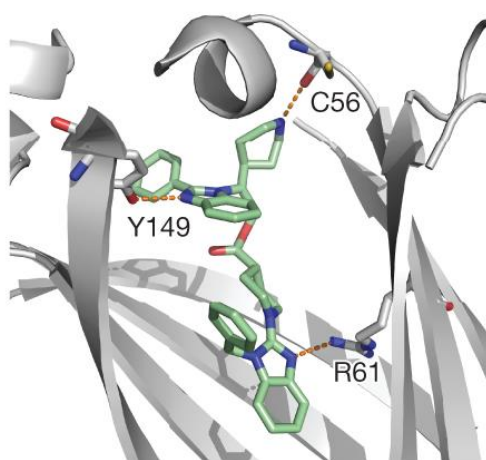
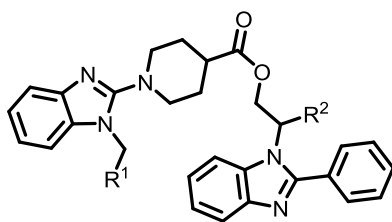


Figure 30 Cocrystal structure of **90** with PDE δ confirms third hydrogen bond of the *bis*-benzimidazole with the backbone carbonyl of Cys56 (PDB 4JVF).⁷⁹

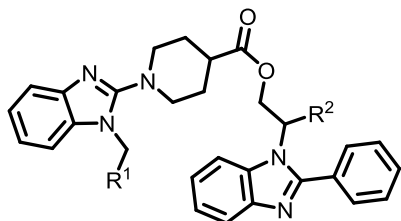
Compared to the guiding piperidine containing ester **90**, cyclohexyl and isopropyl substituted esters (R^1) displayed lower affinity (Table 6, entries 2 and 3). Consistent with the data shown in Table 1 additional electron withdrawing substituents on the benzyl ring reduce the binding affinity and thus yield higher K_D values (Table 6, entries 4 and 5). The replacement of the benzyl moiety at R^1 with a 3-methyl thiophene however resulted in similar affinities (Table 6, entries 6 and 7). In general, the cyclohexyl substituted benzimidazoles which cannot form a third H-bond to Cys56 bind with lower affinities to the protein than the piperidines (Table 6, entries 1,4,6 vs 2,5,7).

Table 6 Affinities of ester linked *bis*-benzimidazoles measured by means of competitive titrations employing Fluorescein-Atorvastatin.

Entry	Cpd (rac)	R ¹	R ²	K _D / nM
1	90			10 ± 3
2	84			25 ± 8
3	93			17 ± 3
4	91			77 ± 20
5	85			115 ± 35
6	92			9 ± 2
7	86			16 ± 4

Since the cocrystal structure of **90** with PDE δ revealed a third hydrogen to Cys56 it was envisaged to further explore how strongly the additional hydrogen bond affects affinity. Replacement of the 4-piperidyl moiety at R² by a 3-piperidyl substituent (Table 7, entries 2 and 3), a pyrrolidine (entries 4 and 5) and a 4-methylene piperidine (entry 6) resulted in compounds with slightly reduced or similar affinity compared to ester **90**. Notably, all ester-linked benzimidazoles bind with higher affinities than the related ethers.

Table 7 Affinities of ester linked *bis*-benzimidazoles measured by means of competitive titrations employing Fluorescein-Atorvastatin. Compounds other than **90** were synthesized by Taros/LDC.

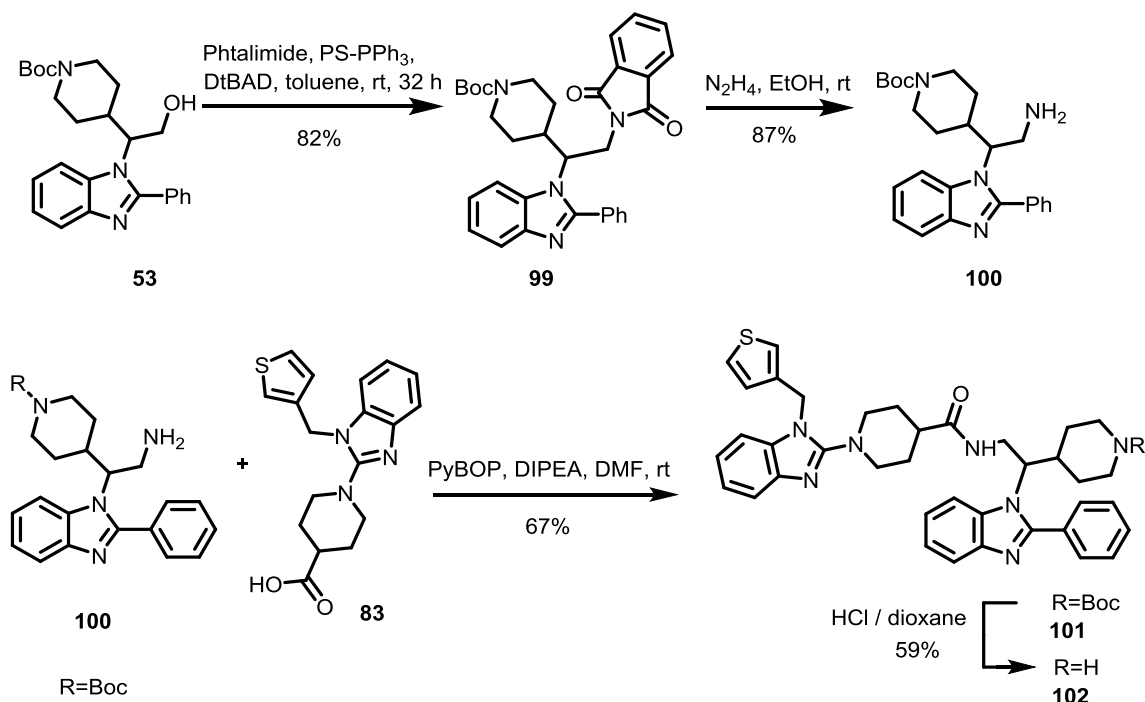


Entry	Cpd (rac)	R ¹	R ²	K _D / nM
1	90			10 ± 3
2	94		 Diastereomer 1	18 ± 5
3	95		 Diastereomer 2	11 ± 3
4	96		 Diastereomer 1	13 ± 3
5	97		 Diastereomer 2	14 ± 6
6	98			14 ± 5

4.4.3 Synthesis and biophysical evaluation of amide and carbamate linked *bis*-benzimidazoles

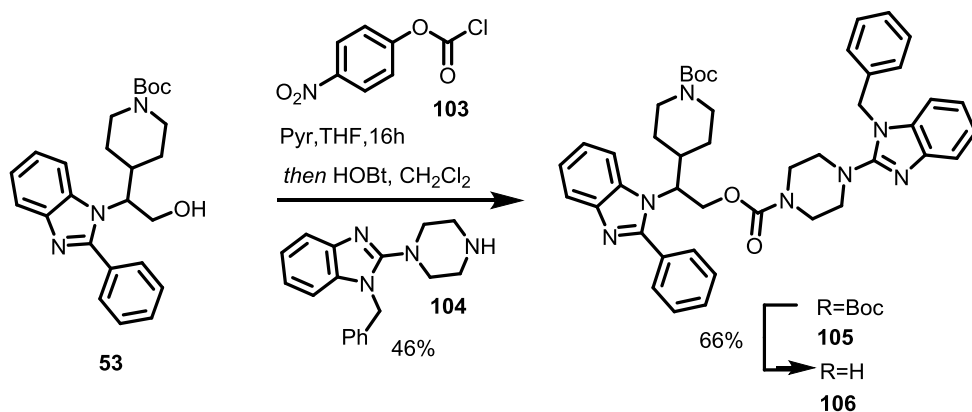
The higher potency of the ester linked *bis*-benzimidazoles was attributed to the increased flexibility and length of the linker moiety. Due to a possible susceptibility of the ester compounds towards cleavage by hydrolases in prospective cellular investigations, the ester moiety was replaced by more stable linkers. Therefore, similarly long linkers like amides and carbamates were investigated. Amide linked *bis*-benzimidazoles were synthesized from alcohol **53** (Scheme 11). The alcohol was transformed into the phthalimide by means of a Mitsunobu

reaction. Deprotection with hydrazine afforded the free amine **100**, which was coupled with the free acid **83** using PyBop/DIPEA. Boc-protected benzimidazole **101** was deprotected with HCl in dioxane to afford the free piperidine.



Scheme 11 Synthesis of amide linked *bis*-benzimidazoles starting from alcohol **53**.

Amide **102** was evaluated in fluorescence polarization assays and it was found that the rigid amide **102** binds to PDE δ with lower affinity than the related ester (Table 8). This can be attributed to the planarity/rigidity of the amide bond, the different hydrogen bonding properties and/or a different conformation. In another effort it was attempted to replace the ester by a similarly flexible carbamate. For the synthesis of the carbamate, alcohol **53** was reacted with 4-nitrophenyl chloroformate (**103**). The intermediate carbonate was *in situ* activated with HOBt and then reacted with piperazine **104** to afford the Boc-protected carbamate **105**. Boc-deprotection furnished the desired carbamate **106**.



Scheme 12 Synthesis of carbamate linked *bis*-benzimidazoles.

Carbamate **106** showed much stronger binding compared to the rigid amide **102**, yet it was not as good as the best ester compounds (Table 8).

Table 8 Affinities of ester, carbamate and amide linked *bis*-benzimidazoles.

Entry	Cpd (rac)	R ¹	X	Y	R ²	K _D / nM	T _m shift
1	90		O	C		10 ± 3	26.0
2	92		O	C		9 ± 2	nd
3	102		NH	C		720 ± 240	nd
4	106		O	N		35 ± 13	21.4

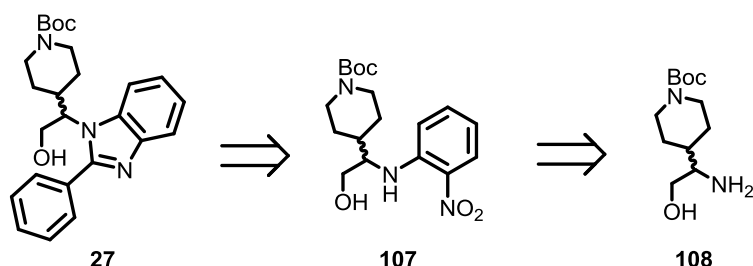
4.4.4 Separation of racemic *bis*-benzimidazoles and biophysical evaluation

With the aim of investigating if the different enantiomers of the *bis*-benzimidazole compounds bound with strongly different affinities, the enantiomers of the Boc-protected *bis*-

benzimidazoles **57** and **89** were separated by preparative chiral HPLC. Deprotection using HCl/dioxane and subsequent biophysical experiments revealed a 4-6 fold difference in potency for each pair of enantiomer with affinities of 38 ± 16 nM vs 190 ± 55 nM for compounds **62**, and K_D values of 7 ± 3 nM and 39 ± 18 nM for compound **92**. Although the absolute configuration of these compounds could in principle be obtained by cocrystallization with PDE δ , a very high resolution would be needed. Since such highly diffracting crystals were not available, it was decided to assign the absolute configuration by analogy to well established enantioselective syntheses.

4.4.5 Enantioselective synthesis of *bis*-benzimidazoles

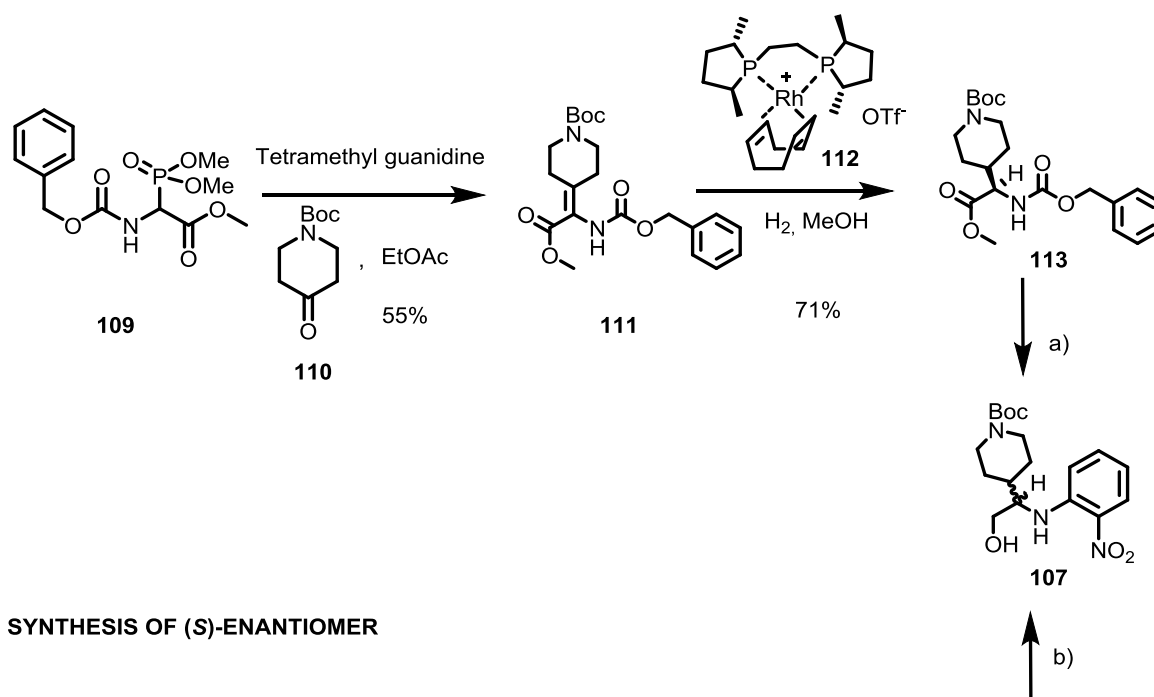
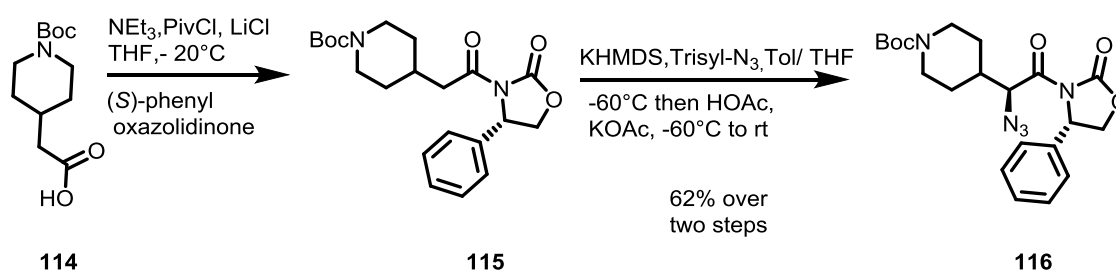
The racemic ester and ether linked benzimidazoles displayed low nanomolar K_D values, it was however at this stage unclear which enantiomer bound with higher affinity. It was realized that the chiral benzimidazole fragments **27** can be retrosynthetically traced back to amino alcohols (Scheme 13).



Scheme 13 Disconnection of chiral benzimidazole into amino alcohol.

Since the chiral synthesis of amino acids and alcohols is well established, it was planned to assign the absolute stereochemistry according to literature precedent. In addition, the enantioselective synthesis should provide gram quantities of chiral building blocks for the synthesis of **62** and **92**. Two well-established routes for the enantioselective synthesis of chiral amino alcohols were investigated in parallel; asymmetric hydrogenation and Evans azidation methodology. Both asymmetric hydrogenation and azidation have been successfully applied to the synthesis of chiral amino acid and alcohol building blocks including (*R*)-piperidinyl glycine.^{90,91} Both approaches were used to synthesize gram quantities of the two different enantiomers of key intermediate **107** (Scheme 14). The asymmetric hydrogenation approach started with *N*-boc 4-piperidone which was reacted with *N*-Cbz-phosphonoglycine trimethyl ester (**110**) in a Horner-Woodsworth-Emmons reaction.⁹¹ The resulting Cbz-protected enamine was then subjected to asymmetric hydrogenation using [(*R,R*)Me-BPE_Rh-COD]OTf (**112**) as

a catalyst (4% mol) at 3-5 bar hydrogen pressure. The ester was Cbz deprotected by hydrogenolysis employing H₂ on Pd/C and the ester functionality reduced with sodium borohydride. Nucleophilic aromatic substitution with 1-fluoro 2-nitrobenzene provided the key alcohol **107**, which was used to evaluate enantiomeric purity since it is a common intermediate in both enantioselective approaches.

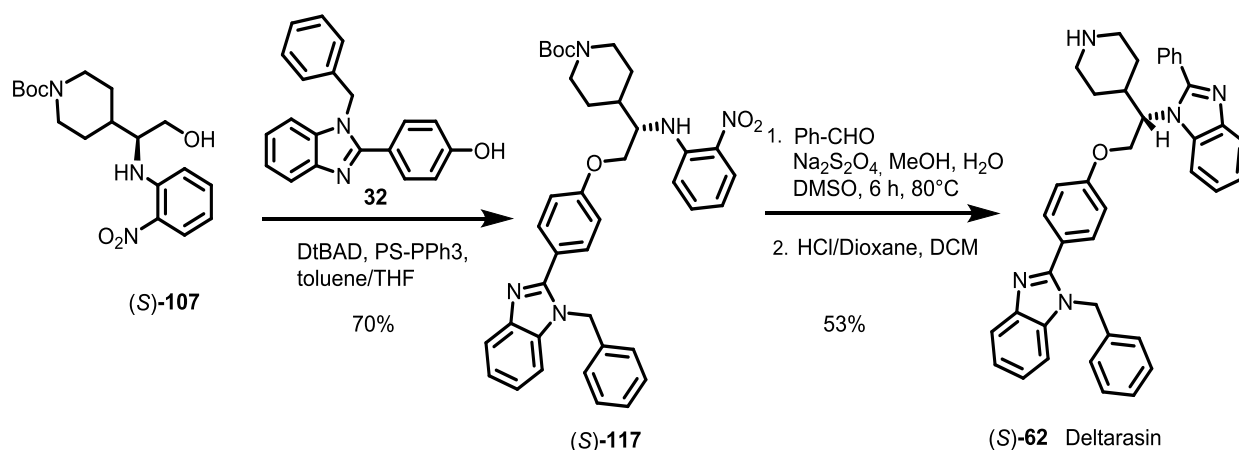
SYNTHESIS OF (*R*)-ENANTIOMERSYNTHESIS OF (*S*)-ENANTIOMER

Scheme 14 Enantioselective synthesis of chiral alcohol **107** by asymmetric hydrogenation with [(*R,R*)-Me-BPE-Rh-COD]OTf or by Evans azidation. Reaction conditions. a) 1. NaBH₄, MeOH 2. H₂, Pd/C, EtOH 3. 1-Fluoro-2-nitrobenzene, DIPEA, NMP, 100°C, 6h.; 21% over three steps b) 1. H₂, Pd/C, EtOH; 2. NaBH₄, MeOH 3. 1-Fluoro-2-nitrobenzene, DIPEA, NMP, 100°C, 6h, 45% over three steps.

The alternative synthesis based on Evans azidation started from the commercially available *N*-Boc-protected acid **114**, which was activated with PivCl and *in situ* coupled to deprotonated (*S*)-4-phenyl-2-oxazolidinone. On gram scale an alternate synthesis of oxazolidinone **115** was preferred: To avoid the use of butyl lithium, LiCl was employed to mediate the coupling of

N-Boc-protected acid **114** with (*S*)-4-phenyl-2-oxazolidinone.⁹² The resulting oxazolidinone **115** was obtained in high purity after recrystallization and was thus directly subjected to azidation with trisyl azide in a mixture of toluene/THF at -60°C. As preceded in literature, quenching the intermediate sulfonyl triazene intermediate with buffered acid, avoids diazo transfer and provides the azide **116** in good yields.⁹³ Reduction with sodium borohydride in methanol, followed by hydrogenation with palladium over carbon and nucleophilic aromatic substitution provided the intermediate alcohol **107**.

Analysis of the chiral HPLC traces of intermediate **107** revealed that asymmetric hydrogenation gave an ee of only 88%. Evans azidation on the other hand led to the completely enantiopure intermediate alcohol **107**. Therefore, the Evans methodology was used for all further syntheses of enantiopure compounds. Key chiral alcohol **107** was reacted with phenol **32** using Mitsunobu conditions to yield ether (*S*)-**117** (Scheme 15). The intermediate was cyclized under reductive conditions and Boc-deprotected to yield (*S*)-**62**. This compound was termed Deltarasin due its ability to break the Ras-PDE δ interaction *in cellulo* (see below).



Scheme 15 Enantioselective synthesis of the *bis*-benzimidazole Deltarasin.

Boc-protected Deltarasin was evaluated in terms of chiral purity by analytical, chiral HPLC. As references the racemic compound mixture and the separated enantiomers (prep. HPLC) were used.

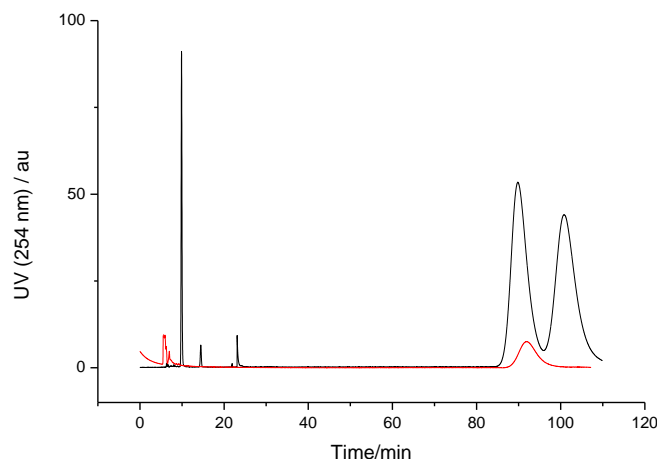
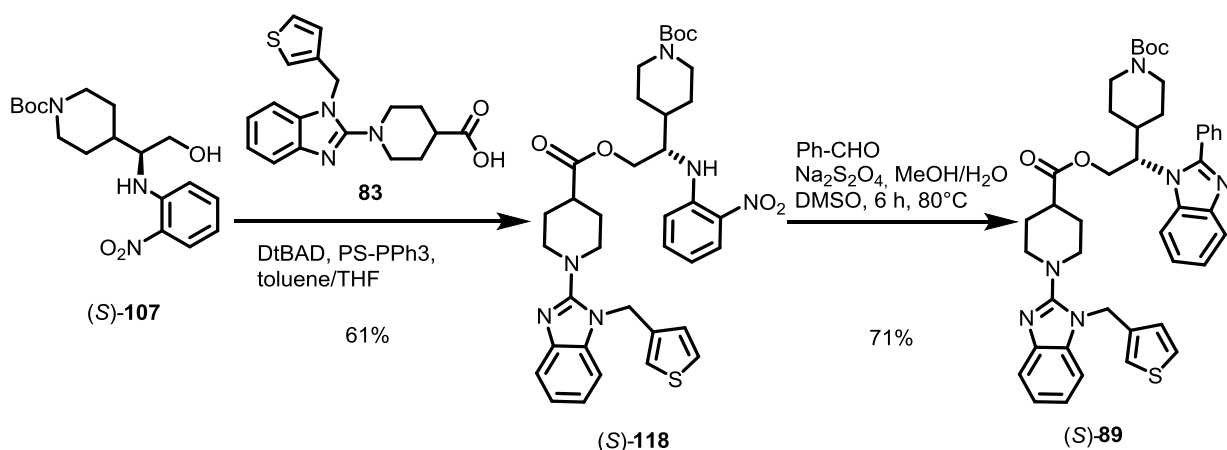


Figure 31 Chiral HPLC trace for racemic benzimidazoles **57** (Boc-Deltarasin) and for the (*S*)-enantiomers (red) obtained by both preparative chiral HPLC and enantioselective synthesis.

Analysis of the chiral HPLC traces allowed for the assignment of the two peaks to the respective enantiomers, with the faster eluting compound being the (*S*)-enantiomer. In an analogous approach for the assignment of the absolute configuration of ester compound **92**, Boc protected alcohol (*S*)-**107** was reacted with acid **83** using Mitsunobu conditions to yield nitro aniline (*S*)-**118**, which was cyclized with benzaldehyde (Scheme 16). Coinjection of the racemate, the separated enantiomers (prep. HPLC) and the (*S*)-enantiomer allowed for the assignment of the enantiomers (Figure 32). For both ether **62** and ester **92**, the (*S*)-enantiomers proved to be more potent than the (*R*) enantiomers.



Scheme 16 Enantioselective synthesis of ester (*S*)-**118** by Mitsunobu reaction, followed by cyclization of a nitro aniline intermediate.

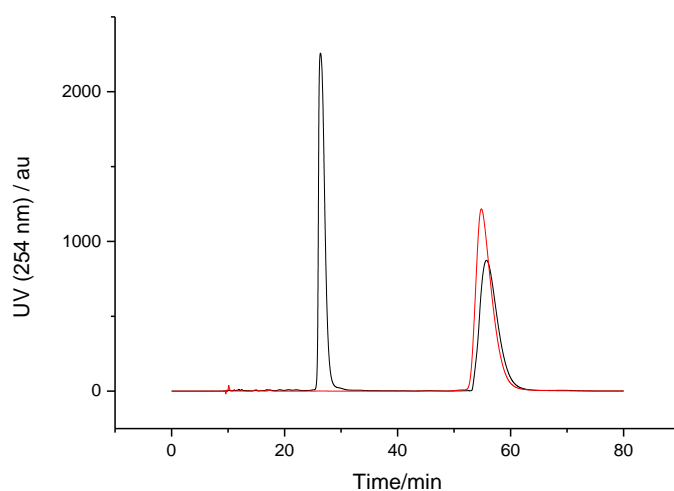


Figure 32 Chiral HPLC traces for racemic benzimidazole **89** (black) and for the (*S*)-enantiomers (red) obtained by both preparative chiral HPLC and enantioselective synthesis. Stereochemistry was assigned according to literature precedents.

Despite the good results obtained with the described enantioselective approaches, the whole synthetic sequence was rather long. Therefore, shorter enantioselective routes towards *bis*-benzimidazoles were investigated. It was planned to synthesize alcohol (*S*)-**53** via a sequence of enantio- and regioselective iridium catalysed alkylation followed by ozonolysis and reduction.

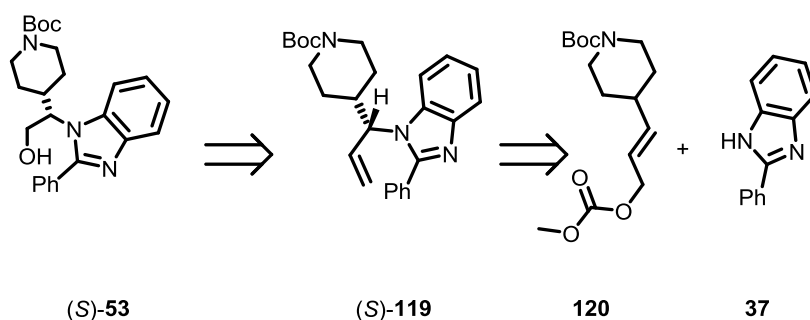
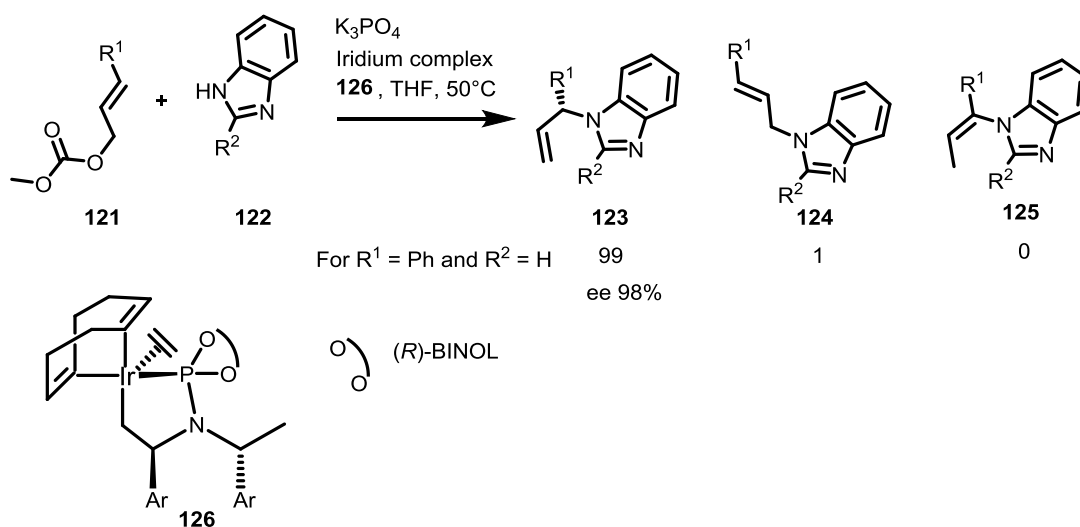


Figure 33 Alternative retrosynthetic analysis of alcohol (*S*)-**53**

Hartwig and coworkers describe an iridium catalyzed enantio- and regioselective alkylation of benzimidazoles in very high yields.⁹⁴ Substrates tested include a cyclohexyl group at position R^1 and a phenyl group at R^2 (but not both together, Scheme 17). However, the catalyst of the reactions was synthesized in a glove box, due to its instability. Only one example is presented

where the iridium catalyst is formed *in situ*, although the whole reaction is still carried out in the glove box.



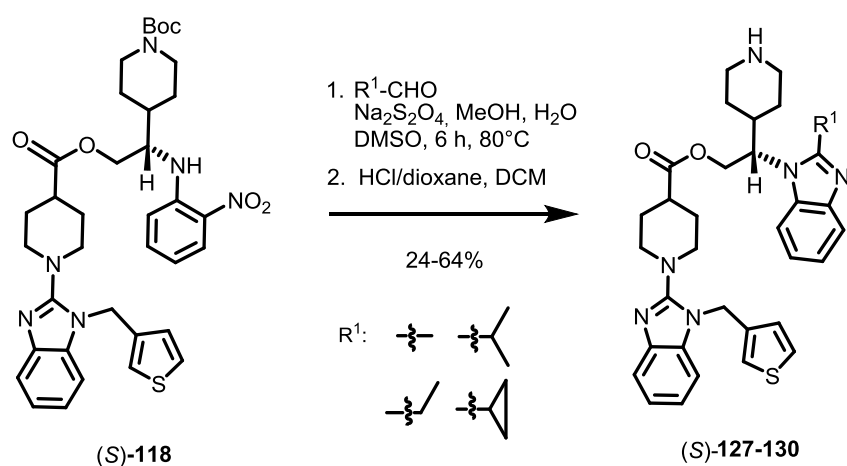
Scheme 17 Enantioselective asymmetric allylation of benzimidazoles using iridium catalyst.⁹⁴

Nevertheless the reaction was investigated as an alternative to synthesize the desired enantiomers. Initial attempts under normal Schlenk conditions and *in situ* formation of the catalyst did not lead to the desired product in acceptable yields. The attempted reaction ($R^1=Ph$, $R^2=Ph$, Scheme 17) resulted in a complex reaction mixture which includes two regioisomeric products with the expected mass along with the dialkylation product in a 1:1.5:2.2 ratio (Coronona detector, LC-MS). Due to these discouraging results no further optimization was attempted.

4.4.6. Biophysical evaluation of enantiomerically pure ester and ether linked compounds

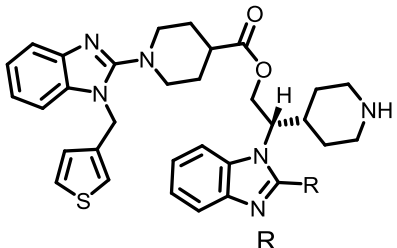
While highly potent molecules were identified among the *bis*-benzimidazoles, ligand efficiency, solubility and drug likeness of the compounds still left room for improvement.⁶⁷ It was therefore envisaged to reduce the number of aromatic rings and the size of the benzimidazoles while trying to maintain potency. With the enantioselective route towards the *bis*-benzimidazoles in

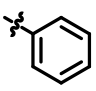


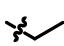

hand, initial attempts focused on replacing the 2-phenyl substituent in the ester compound series by alkyl residues (Scheme 18, Table 9).



Scheme 18 Enantioselective synthesis of esters (S)-127-130 by cyclization of a common nitro aniline intermediate.

Indeed, replacement of the phenyl group in the guiding benzimidazole (S)-92 with an isopropyl, an ethyl or a cyclopropyl group yielded similarly potent compounds (Table 9, entries 2-4). However, the introduction of a methyl group resulted in reduced affinity.

Table 9: Affinities of ester-linked benzimidazoles as measured by fluorescence polarization


Entry	Cpd	R	K_D / nM
1	(S)- 92		7 ± 3
2	(S)- 127		8 ± 2
3	(S)- 128		12 ± 4
4	(S)- 129		9 ± 3
5	(S)- 130		35 ± 16

4.4.7 Structural simplification of *bis*-benzimidazoles

In a further effort to decrease the size of the compounds the stereocenter was eliminated in both the ester and the ether series. Surprisingly high affinity compounds were identified which bind with improved ligand efficiency (Table 10, entries 1-5). These data suggest that a third hydrogen bond to Cys56 might not necessary for the development of highly potent compounds targeting the K-Ras-PDE δ interaction. Additionally the dataset suggests that large hydrophobic substituents like cyclohexyl and isopropyl are also not essential for high affinity. Analysis of the existing crystal structures and docking experiments do not provide any simple explanation for this finding.

A possible explanation might be revealed by an analysis of protein dynamics. Biophysical experiments showed that in the farnesyl bound state PDE δ is conformationally constrained compared to the free state, which results in an entropic penalty upon binding of ligands into the

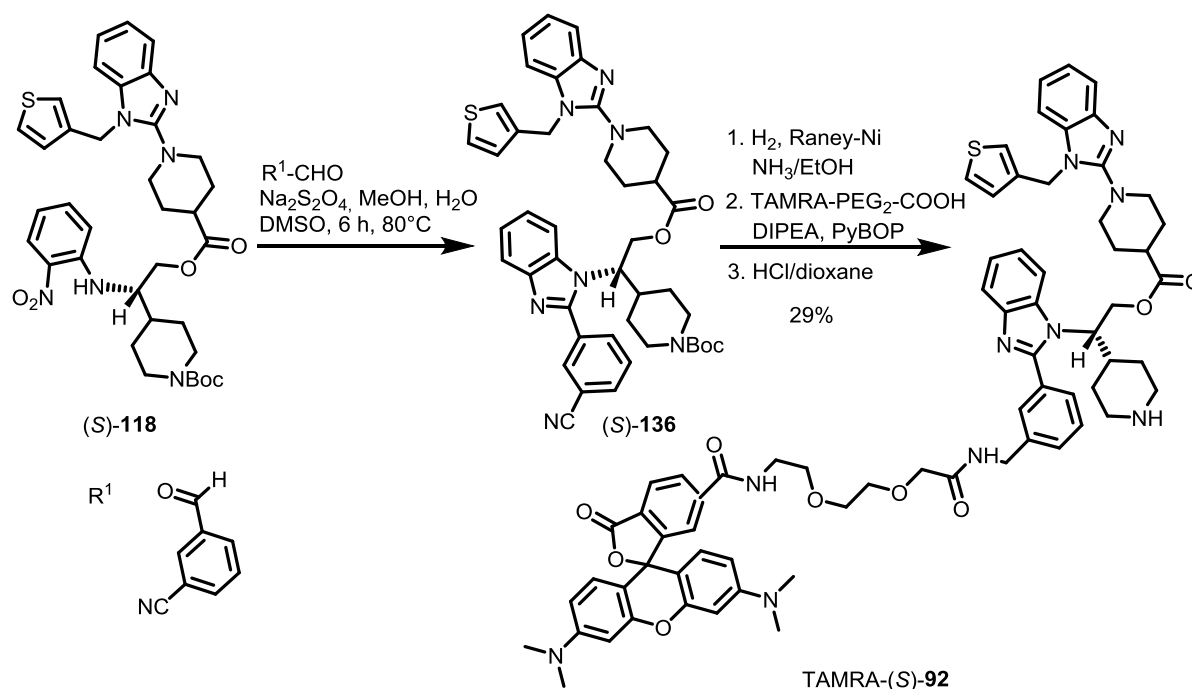
farnesyl cavity.⁸⁶ In addition, PDE δ does not crystallize in the absence of bound ligands, highlighting the high intrinsic flexibility of the protein. Therefore, the unexpectedly high affinity of the *bis*-benzimidazoles in Table 10 might be due to the less pronounced restriction of proteins dynamics, resulting in a lower entropic penalty upon binding of a small molecule.⁸⁶

Table 10: Affinities of smaller benzimidazoles measured by means of fluorescence polarization. Compounds were synthesized by LDC/Taros.

Entry	Cpd	R	K _D / nM
1	131		7 ± 2
2	132		6 ± 2
3	133		14 ± 2
4	134		7 ± 3
5	135		17 ± 2

4.4.8 Synthesis of TAMRA-labeled *bis*-benzimidazoles and evaluation of specificity

As shown above, *bis*-benzimidazoles bind strongly to PDE δ in biophysical displacement titrations employing Fluorescein-Atorvastatin. In order to validate the strong interaction, the *bis*-benzimidazoles (S)-62 Deltarasin and ester (S)-92 were labeled with the rhodamine-based dye TAMRA (Scheme 19) and their interaction with PDE δ was further investigated.



Scheme 19 Synthesis of TAMRA-labeled (S)-92. TAMRA-Deltarasin was synthesized by analogy.

Both labeled compounds display very high affinities for PDE δ with K_D values in the single digit nanomolar range (Figure 34). In direct titrations employing labeled compounds these values can be regarded as upper limits, since picomolar affinities cannot be measured under these experimental conditions. For fluorophores like TAMRA low signal to background ratios (fluorescence intensity) are commonly observed at low nanomolar fluorophore concentrations which introduce artifacts into binding isotherms. For the differentiation of high affinity, labeled compounds two solutions exist: a) competitive titrations using unlabeled compounds of known affinity or b) kinetic experiments which allow for the determination of the K_D from the ratio of association and dissociation rate constants (see below). For competitive titrations the two TAMRA-labeled compounds were subjected to titrations with PDE δ in the presence of an excess of unlabeled Atorvastatin.

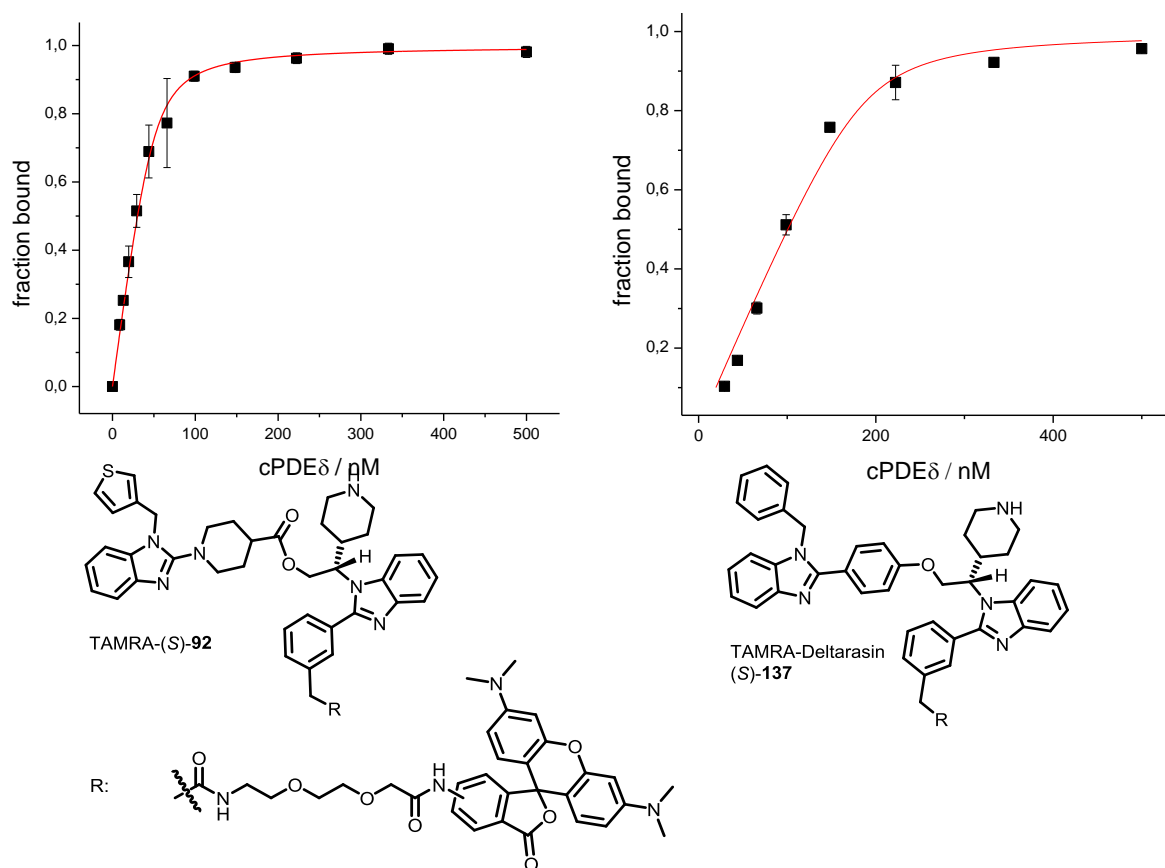


Figure 34 Direct Titration of TAMRA-(S)-92 (100 nM, left) and TAMRA-Deltarasin (175 nM, right) with PDE δ . Fit to a one-site binding model derived from the law of mass action yields the the corresponding K_D values (TAMRA-(S)-92 K_D 5.3 ± 1.5 nM and TAMRA-Deltarasin 7.6 ± 1.3 nM). The titrations for TAMRA-Deltarasin were also repeated at lower concentrations (35 nM) resulting in similar K_D values.

The data can be approximately fit by a single site model, however no standard binding model is available for this experimental setup (Figure 35).⁹⁵ Even in the presence of competitor the binding isotherms for TAMRA-(S)-92 still display a stepwise shape suggesting a higher affinity than the fit suggests. Under these conditions the TAMRA-labeled compounds, however, can be differentiated in terms of their relative affinities, and the data suggest that the ester TAMRA-(S)-92 binds more strongly than TAMRA-Deltarasin.

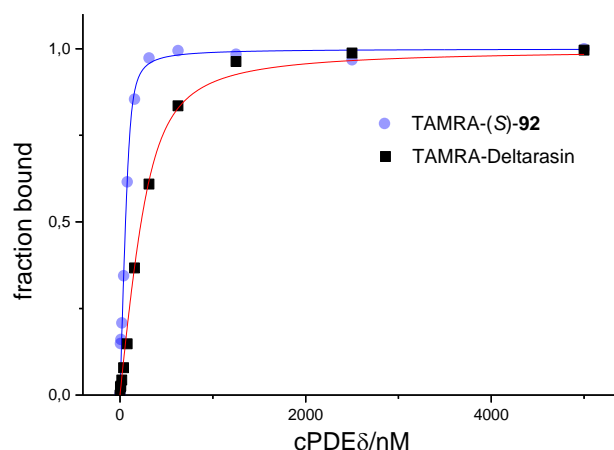


Figure 35 Titrations of TAMRA-(S)-92 (60 nM) and TAMRA-Deltarasin (100 nM) with PDE δ in the presence of 1000 nM unlabeled Atorvastatin.

Although both TAMRA-labeled compounds bind with high affinity to PDE δ it was unclear how specific the interaction between PDE δ and these *bis*-benzimidazoles is. Therefore, binding to the related solubilizing factors UNC119a/HRG4 and UNC119b was investigated, which feature a high degree of structural similarity to PDE δ .³² Both contain a beta barrel structure which can accommodate a lipid moiety. In contrast to PDE δ , UNC119a/b bind myristoylated peptides with low nanomolar affinity. Additionally specificity was tested against the presumed Ras specific lipid binding proteins Galectins1/3.^{25,96,97}

To test the specificity both TAMRA-labeled compounds were titrated with the mentioned lipid binding proteins (Figure 36). Only PDE δ led to an increase in fluorescence polarization upon addition of protein to the labeled probes TAMRA-(S)-92 and TAMRA-Deltarasin. The TAMRA-labeled *bis*-benzimidazoles did not bind to any other lipid binding proteins and are therefore selective probes for exploring the interaction of small molecules with PDE δ .

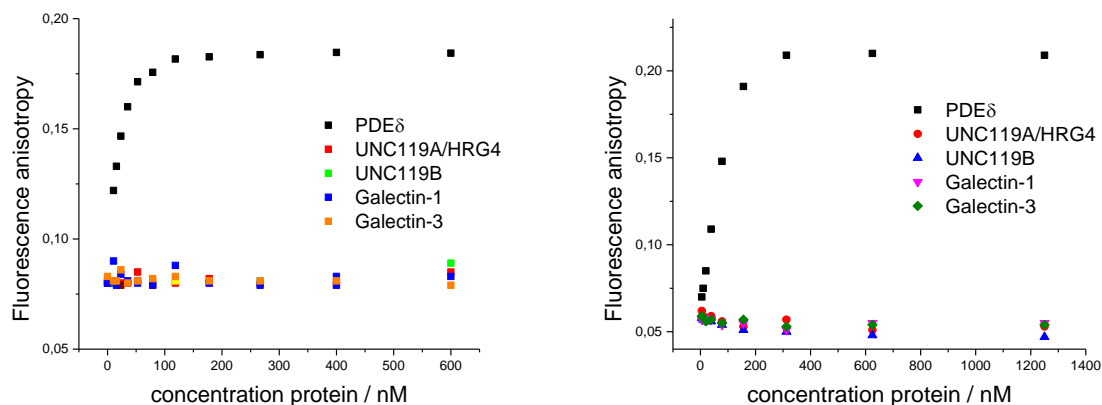


Figure 36 Titration of TAMRA-(S)-92 (100 nM, left) and TAMRA-Deltarasin (175 nM, right) with PDE δ , UNC119A/HRG4, UNC119B, Galectin-1 and Galectin-3 in PBS buffer (containing 0.05% Chaps). Solely addition of PDE δ led to a change in fluorescence anisotropy of the TAMRA-labeled probes.

4.5 Displacement titrations of TAMRA-Deltarasin with benzimidazoles

TAMRA-(S)-92 and TAMRA-Deltarasin were also investigated for their suitability in displacement titrations. Initial qualitative experiments suggested that TAMRA-Deltarasin unlike Fluorescein-Atorvastatin and TAMRA-(S)-92 displays a relatively fast dissociation rate from the protein (half lives on the minute scale, see also kinetic analysis below). The advantage of using probes with relatively fast dissociation rates is that precipitation effects can be avoided, because equilibration times with unlabeled small molecules are shorter. This is of particular interest for sparingly soluble small molecules like *bis*-benzimidazoles (see discussion T_m shift). Therefore, displacement titrations of TAMRA-Deltarasin with the benzimidazole fragment **10** and the *bis*-benzimidazole Deltarasin were also investigated (Figure 37). Both compounds showed a dose dependent decrease of fluorescence anisotropy and thus the fraction of protein-bound fluorophore (K_D values: Benzimidazoles fragment **10**: 21 nM, Deltarasin 4 nM). The affinities for the unlabeled compounds are markedly higher compared to the dataset obtained with Atorvastatin-Fluorescein.

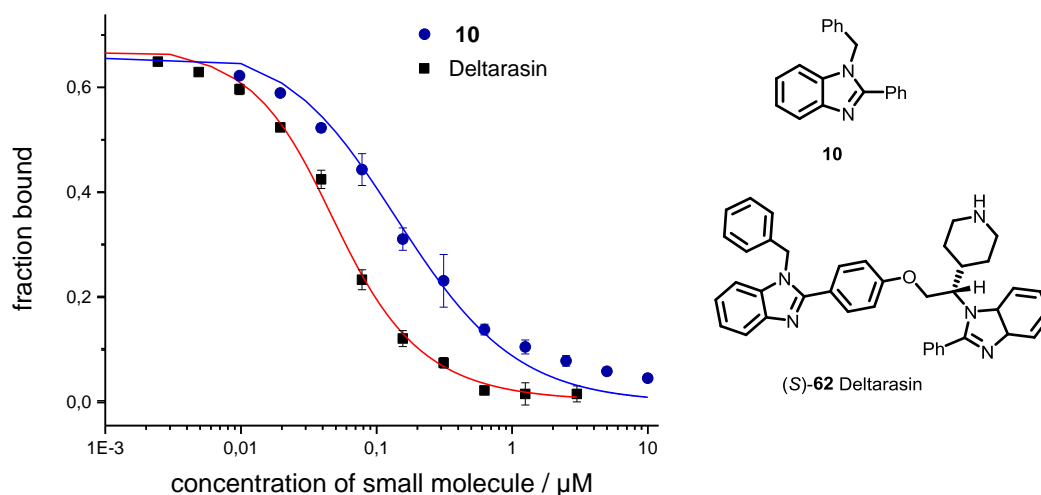


Figure 37 Representative displacement titrations of TAMRA-Deltarasin with benzimidazole fragment **10** (fit in blue) and Deltarasin (fit in red). Conditions: TAMRA-Deltarasin 33 nM, PDE δ 40 nM. Data were fit to an exact competition model based on the law of mass action.

4.6 Displacement Alpha screen with biotinylated Atorvastatin

Although fluorescence polarization and T_m shift assays were successfully used to evaluate compound libraries, other assay formats were investigated. Alpha technology was successfully used with a biotinylated K-Ras peptide as described above. However, due to the low affinity of K-Ras4B peptides for PDE δ high protein concentrations were needed and thus the affinity of highly potent inhibitors remained elusive. Biotin-Atorvastatin **15** on the other hand showed a very high affinity in the T_m shift assay (22.8°C), and ITC (67 nM). Therefore, in analogy to the direct titration of biotinylated K-Ras4B with PDE δ (Figure 13, Figure 15) Atorvastatin was titrated with PDE δ and an apparent $K_{D,app}$ of around 7 nM was obtained (Figure 38).

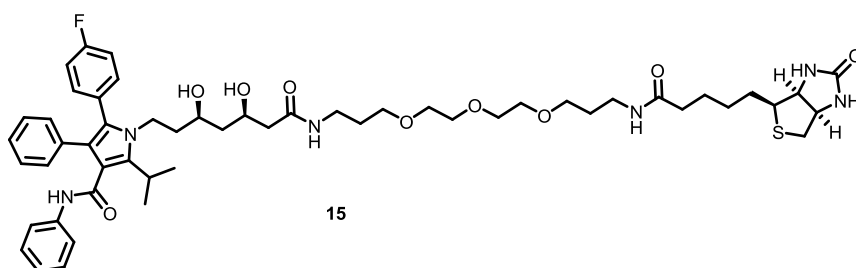
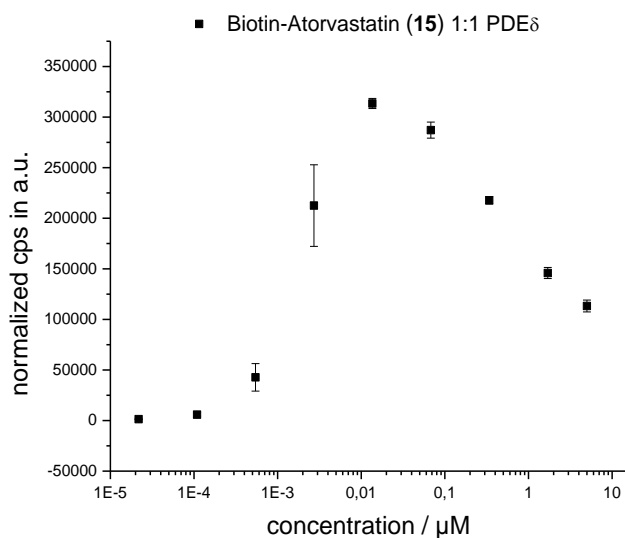


Figure 38 Dilution series of Biotin-Atorvastatin **15** with PDE δ using Alpha screen readout.

Notably, the binding curve for Biotin-Atorvastatin **15** displays a bell-like shape which can be explained by the so-called hooking effect.⁹⁸ The Biotin-Atorvastatin **15** / PDE δ / donor bead / acceptor bead system can be regarded as a four body binding equilibrium. Some ternary and higher-order equilibria exhibit a bell-shaped dose response curve in which increasing the total concentration of the central species can actually cause reduction in ternary or higher-order complex concentration, and thus lead to a decreased signal (for a three body illustration see Figure 39).

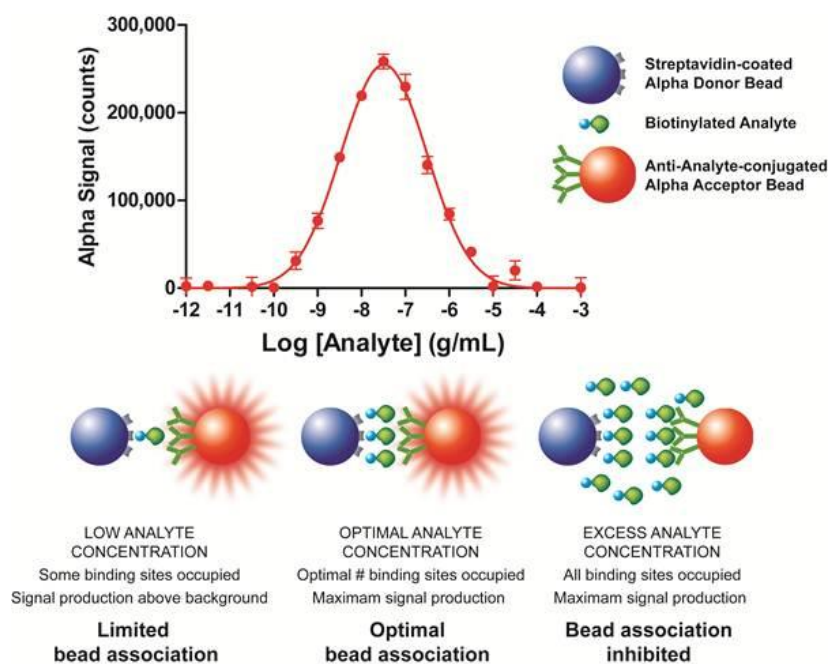


Figure 39 Illustration of the hooking effect, a general property of three body binding equilibria, applied to Alpha technology.⁹⁹

In the case of a three body system using Alpha technology with just one analyte (e.g. a biotinylated, His-tagged protein, Figure 39), it means that excess analyte concentrations lead to decreased ternary complex formation because all binding sites on the donor and the acceptor beads are already occupied. In this situation excess analyte will not bring the two beads together, rather a situation results where the bridging species, which causes the signal, will compete with excess analyte that binds only to one bead and not to the other.

In the case of a four body system as observed with Biotin-Atorvastatin **15** / PDE δ / donor bead / acceptor bead, the system can be reduced to a three body problem as in Figure 39 at high concentrations of compound and protein. If compound and protein are used at a 1:1 stoichiometry, at concentrations above the K_D virtually all of the compound will be bound to protein. Under these conditions neither free compound nor free protein exist, therefore the system can be reduced to a three body binding equilibrium containing the Biotin-Atorvastatin-Protein-complex, the donor bead and the acceptor bead. Therefore, the illustration in Figure 39 can also be applied to the discussed four body equilibrium.

Displacement titrations employing Atorvastatin derivative **17** and *bis*-benzimidazole **55** lead to apparent affinities of 45 ± 20 and 55 ± 10 nM (Figure 40). The affinity for *bis*-benzimidazole **55** is therefore in the same range as measured by fluorescence polarization (39 nM).

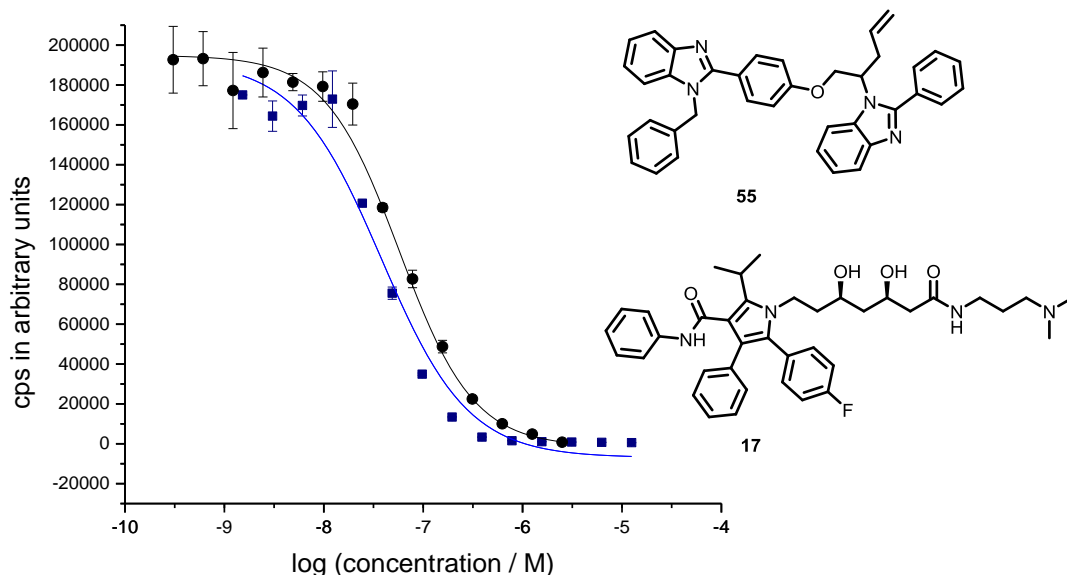


Figure 40 Representative displacement titrations of Biotin-Atorvastatin **15** with Atorvastatin derivative **17** (blue) and *bis*-benzimidazole **55** (black). Data were fit to an empirical dose response model. $K_{D,app}$ values of 45 ± 20 (**17**) and 55 ± 10 nM (**55**) can be derived from two independent sets of experiments employing different orders of compound addition. (Atorvastatin 6 nM, PDE δ 24 nM).

The displacement assay with Biotin-Atorvastatin is thus a viable alternative to the other assays (ITC, fluorescence polarization, T_m shift).

4.7 Kinetic analysis of small molecule-PDE δ interactions

For medicinal chemistry the rate constant k_{off} is of particular interest, because arguably k_{off} is more predictive of cellular activity than the equilibrium constant K_D .¹⁰⁰ Various methods have been described to measure the kinetic rate constants, k_{on} and k_{off} , for a protein/ligand interaction.¹⁰¹⁻¹⁰³ Very fast association and dissociation kinetics for example are readily obtainable by stopped flow measurements employing for example fluorescence anisotropy as readout.⁴⁴ Slow dissociation rates of labeled small molecules can be determined by means of time resolved fluorescence anisotropy measurements in standard 96 well plates. In a standard assay setup with PDE δ , the TAMRA labeled small molecules were preincubated with PDE δ and

then a large excess of unlabeled competitor was added to determine the displacement of labeled compound in real time.

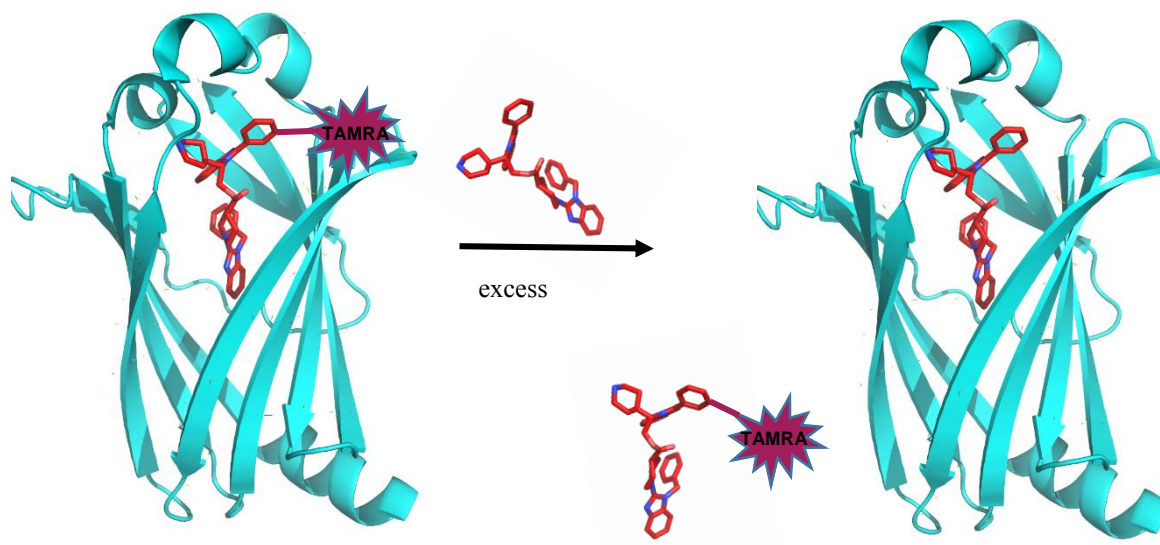


Figure 41 Displacement assay for measuring k_{off} of labeled compounds using an excess of the unlabeled molecule. The addition of an excess of small molecule ensures that no rebinding of the labeled compound to the proteins occurs.

When TAMRA-(*S*)-**92** and TAMRA-Deltarasin were used, the high initial fluorescence anisotropy decreased over time after addition of unlabeled Deltarasin (Figure 42). Strikingly, the rate constants for TAMRA-Deltarasin k_{off} ($(6 \pm 1) \times 10^{-4} \text{ s}^{-1}$) and for TAMRA-(*S*)-**92** ($(9 \pm 5) \times 10^{-5} \text{ s}^{-1}$) are several orders of magnitude lower than the previously determined k_{off} of 3 s^{-1} for a farnesylated peptide mimicking the Ras-family protein Rheb (Table 11, entries 1-3).⁴⁴

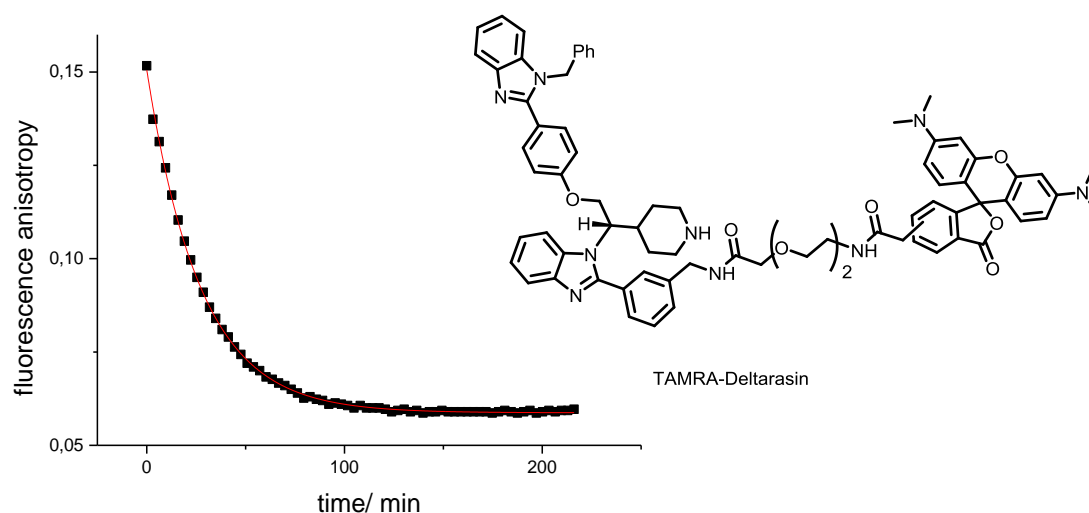


Figure 42 Representative competition experiment of TAMRA-Deltarasin with an excess of unlabeled Deltarasin, observed by a fluorescence anisotropy time course.

Table 11 Rate constant k_{off} for labeled small molecules and peptides. & K_{D} values derived from direct titration measured by fluorescence polarization. Adopted from references.^{40,44}

Entry	Compound	$k_{\text{off}} / \text{s}^{-1}$	K_{D} / nM
1	Dansyl-GKSSC(Far)-OMe from RheB	3 &	102 &
2	TAMRA-Deltarasin	6.1×10^{-4}	7.6
3	TAMRA-(S)-92	9.0×10^{-5}	5.3

While fluorescence polarization experiments allow for the determination of rate constants for labeled molecules like TAMRA-Deltarasin, these experiments necessitate a label, which may influence the interaction. Therefore, label-free experimental techniques were investigated. Surface plasmon resonance (SPR) allows for the determination of affinities and kinetic parameters in a single experiment.^{102,103} In SPR experiments with unlabeled small molecules, the protein is immobilized via its affinity tag. The small molecule is added to a flow cell and the adsorption of the small molecule onto the solid phase is monitored over time and in a concentration dependent manner. In collaboration with the company Biaffin, Kassel an assay

system employing immobilized GST-PDE δ was established. To this end, GST-PDE δ was reversibly immobilized on an anti GST capturing surface. In these binding experiments simple benzimidazole **10** showed a fast association and a fast dissociation from immobilized PDE δ (Figure 43, left).

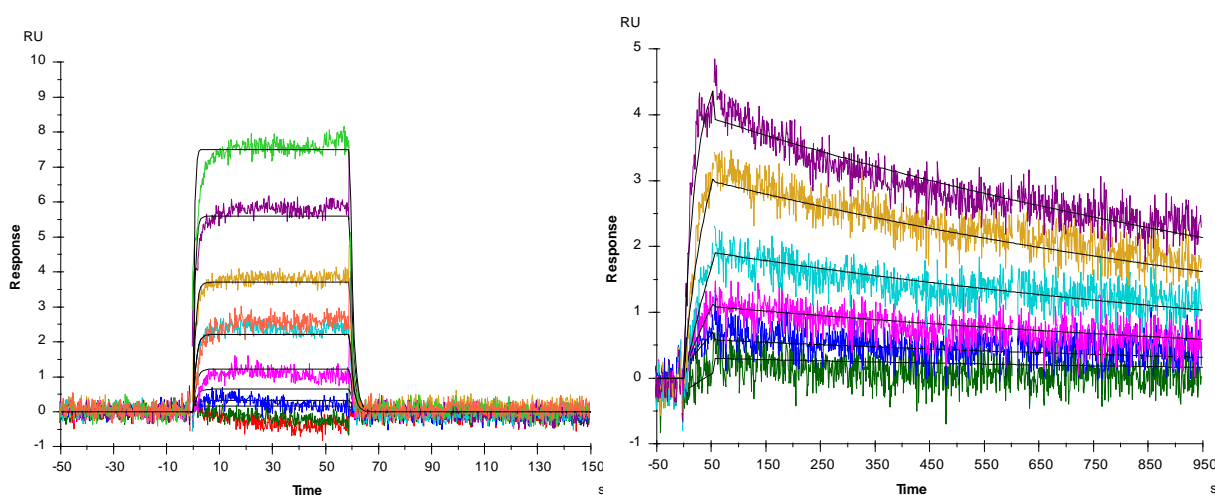
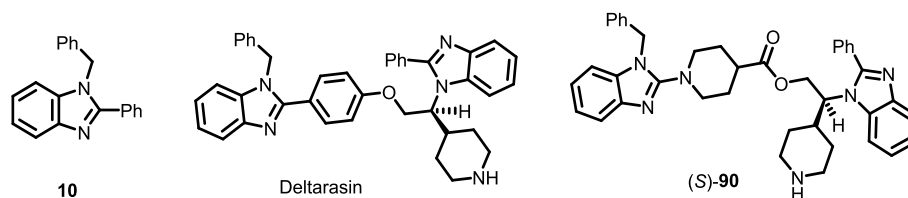


Figure 43. Representative SPR experiments carried out at 35°C on a Biacore T100. For benzimidazole **10** compound concentrations were varied from 63 to 8000 nM (left), for the *bis*-benzimidazole Deltarasin a concentration range of 2-64 nM was used (right). Experiments were carried out by Biaffin GmbH, Kassel.

The *bis*-benzimidazoles (*S*)-**90** and Deltarasin displayed a similarly fast association, whereas the dissociation rate was strongly reduced (Table 12, entries 2 and 3). The dissociation rates k_{off} derived from SPR experiments agree well with fluorescence polarization data (see above). The equilibrium constants K_D derived from kinetic experiments are higher for the benzimidazole fragment **10**, whereas they are much lower for the *bis*-benzimidazole Deltarasin and (*S*)-**90**. According to the SPR experiments ester (*S*)-**90** displays very tight binding with an affinity of 77 pM (Table 12, entry 3).

Table 12 Surface plasmon resonance data for the interaction of benzimidazoles with PDE δ . K_D values marked with an asterisk are derived from the ratio of rate constants. Value in parenthesis is derived from steady state analysis.



Entry	Compound	$k_{on} / M^{-1}s^{-1}$	k_{off} / s^{-1}	K_D / nM
1	10	3.9×10^5	0.9	2900* (2400)
2	(S)- 62 Deltarasin	6.3×10^5	6.9×10^{-4}	1.1*
3	(S)- 90	8.6×10^5	6.5×10^{-5}	0.077*

4.8 Effect of GppNHp-loaded Arl2/3 on the small molecule-PDE δ interaction

It was previously shown that the Arl2/3 GTPases actively released farnesylated cargo proteins from PDE δ and that farnesylated Rheb and K-Ras display K_D -values for binding to PDE δ in the higher nanomolar range (Rheb $K_D = 394$ nM, K-Ras $K_D = 302$ nM).⁴⁰ Therefore, it was explored whether Arl2/3 can also displace cargo with much lower K_D -values, as for instance TAMRA-labeled Deltarasin and ester (S)-**92**.

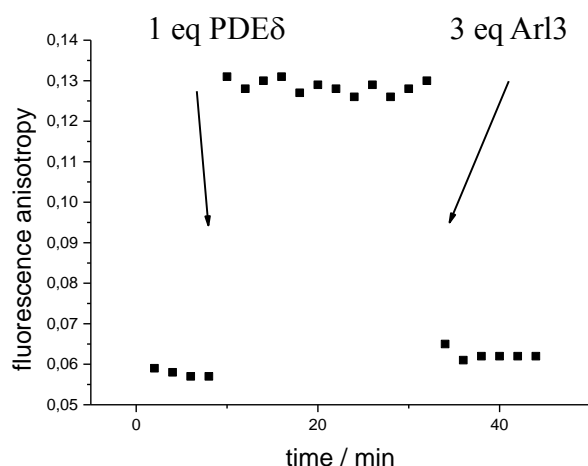


Figure 44 Active displacement of TAMRA-(*S*)-**92** (50 nM) with an excess of Arl3 observed by fluorescence anisotropy.

Interestingly, the TAMRA-labeled ester (*S*)-**92** was readily displaced by GppNHp-loaded Arl3 (Figure 44). Therefore, it was tested whether Arl2/3 release high-affinity ligands in a concentration dependent manner. Preformed PDE δ / TAMRA-Deltarasin or ester (*S*)-**92** complex were treated either with Arl2 or Arl3. The PDE δ -TAMRA-Deltarasin complex was disrupted by both Arl2 and Arl3 as seen by the rapid and concentration-dependent release of the inhibitor from the prenyl-binding protein (Figure 45, left). Arl3 released the labeled small molecule more efficiently from the farnesyl binding site than Arl2. Using a simplified competition model K_D values of 24 nM for Arl2 and 1 nM for Arl3 are obtained from this dataset. Surprisingly, Arl2 was not able to readily displace the labeled ester TAMRA-(*S*)-**92** from the farnesyl binding site (Figure 45, right).

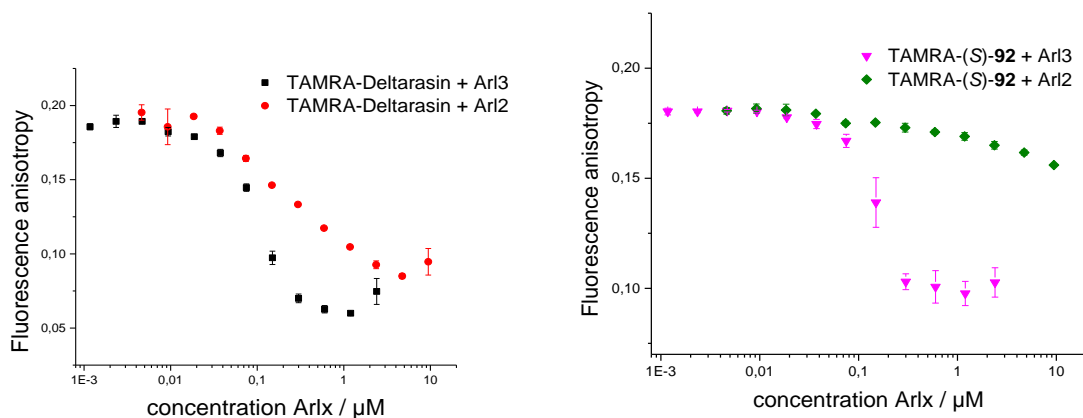


Figure 45 Representative displacement titrations showing the release of high-affinity ligands from PDE δ by Arl2/3. Displacement titrations of TAMRA-Deltarasin (left) or TAMRA-(S)-92 (right) bound to PDE δ (both 100 nM) with different concentrations of GppNHp-loaded Arl2/3 measured by fluorescence anisotropy.

These experiments suggest that very high-affinity compounds like TAMRA-(S)-92 can only be efficiently released by Arl3, whereas Arl2 does not efficiently displace these tight binding ligands from the farnesyl binding site.

Similar to the TAMRA-(S)-92-PDE δ complex, the Fluorescein-Atorvastatin-PDE δ complex displays dissociation half lives on the hour scale, suggesting very high affinity. Therefore, this different chemotype was also investigated in qualitative experiments employing labeled Atorvastatin and Arl2/3 (Figure 46). Like TAMRA-(S)-92, Fluorescein-Atorvastatin is stable towards displacement by Arl2, but readily released by Arl3.

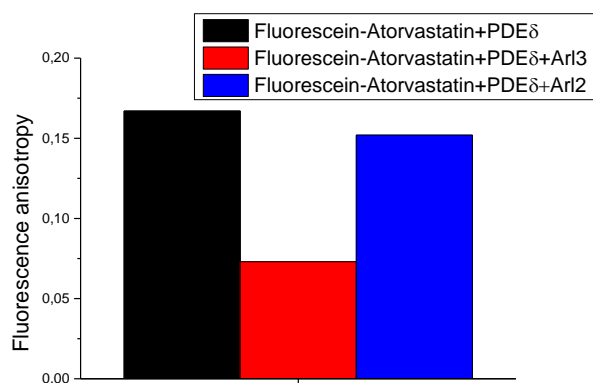


Figure 46 Qualitative release experiments of Fluorescein-Atorvastatin with GppNHp-loaded Arl2/3. A complex of Fluorescein-Atorvastatin and PDE δ was treated with equal amounts of Arl2 and Arl3. Only Arl3 can efficiently release Fluorescein-Atorvastatin.

High to medium affinity cargo like TAMRA-Deltarasin and farnesylated peptides on the other hand are susceptible to displacement by both Arl2 and Arl3. In a direct titration with PDE δ TAMRA-Deltarasin shows a similar K_D compared to Fluorescein-Atorvastatin and TAMRA-(*S*)-**92** (5-7 nM), but even at the lowest technically possible protein concentrations these compounds cannot be differentiated in terms of affinity in a direct titration. The dissociation rates of the three compounds however are clearly different (see above), suggesting that Fluorescein-Atorvastatin and TAMRA-(*S*)-**92** both indeed bind with higher affinity than TAMRA-Deltarasin.

Notably, Arl3 but not Arl2 displaces the farnesylated ciliary phosphatase INPP5E from PDE δ in cell lysates (Figure 47).⁵⁶ suggesting a higher affinity complex of INPP5E-PDE δ compared to Ras-PDE δ .

Consistent preliminary direct titrations performed with a C-terminal TAMRA-labeled INPP5E peptide show higher affinities compared to Ras peptides, with a labeled peptide INPP5E peptide displaying an affinity of 48 nM.



Figure 47 Differential release of farnesylated phosphatase INPP5E by Arl2 and Arl3, measured by Thomas *et al.*⁵⁶ LAP6-PDE δ and myc-INPP5E in RPE cells were incubated with increasing amount of either GDP (TN)- or GTP (QL)-mimicking mutant GST-ARL2 or GST-ARL3 as indicated. Immunoprecipitation of PDE δ with anti-GFP antibodies and detection of co-immunoprecipitated INPP5E by anti-Myc immunoblotting reveal specific ARL3 QL-dose dependent interaction between INPP5E and PDE δ .⁵⁶

These findings have important consequences for the cellular effect of small molecules targeting PDE δ . Since Arl2/3 and PDE δ are present in cells in comparable concentrations (low micromolar),¹⁰⁴ the cargo-releasing ability of Arl2/3 would necessitate higher compound concentrations to observe a cellular effect than to be expected based on the affinity constant K_D .

The displacement titration data suggest that Arl2 and Arl3 have different binding affinities for PDE δ , with Arl3 being the more potent interactor. Preliminary SPR experiments and fluorescence polarization data support this notion.¹⁰⁵ The binding data also hints at different roles for Arl2 and Arl3 in the cell. Arl2/3 are both expressed in the cytoplasm, where they may unload low-affinity, prenylated cargo like Ras from PDE δ . Therefore their roles may be interchangeable in that part of the cell. Arl3 on the other hand is also strongly expressed in cilia, where it may release high affinity cargo like INPP5E from PDE δ . Interestingly, for UNC119a/b high affinity myristoylated peptides can also be only released by Arl3 and not by Arl2.¹⁰⁶ Here, the Arl3 *N*-terminal helix has been described as a pocket opener. The interaction of Arl3 with PDE δ must be structurally different since the lipid binding site of UNC119 is on the other side of the protein compared to PDE δ .¹⁰⁶ Since Arl3 regulates targeting of both farnesylated and myristoylated cargo to the primary cilium,^{106,107} it can be reasoned that it is the central release factor for transport of lipidated cargo to the cilium.

The high affinity cargo identified for UNC119a/b and PDE δ are all of ciliary origin,^{106,107} suggesting two differential roles for the lipid binding proteins. Apparently this class of lipid binding proteins controls the localization of low affinity cargo like Src kinases for UNC119a and Ras GTPases for PDE δ in the cell body, whereas high affinity cargo is transported to the primary cilium and released by Arl3.

4.9 Effect of GppNHp-Arl2 on the displacement kinetics of cargo from PDE δ

In addition to equilibrium titrations, the influence of GppNHp-Arl2 on the kinetics of cargo release was investigated. Since Arl2 forms a low affinity ternary complex with farnesylated Rheb and PDE δ , which rapidly dissociates, the addition of Arl2 to PDE δ should increase the dissociation rate of bound cargo. Consequently the impact of Arl2 on the dissociation rate of TAMRA labeled small molecules was investigated.

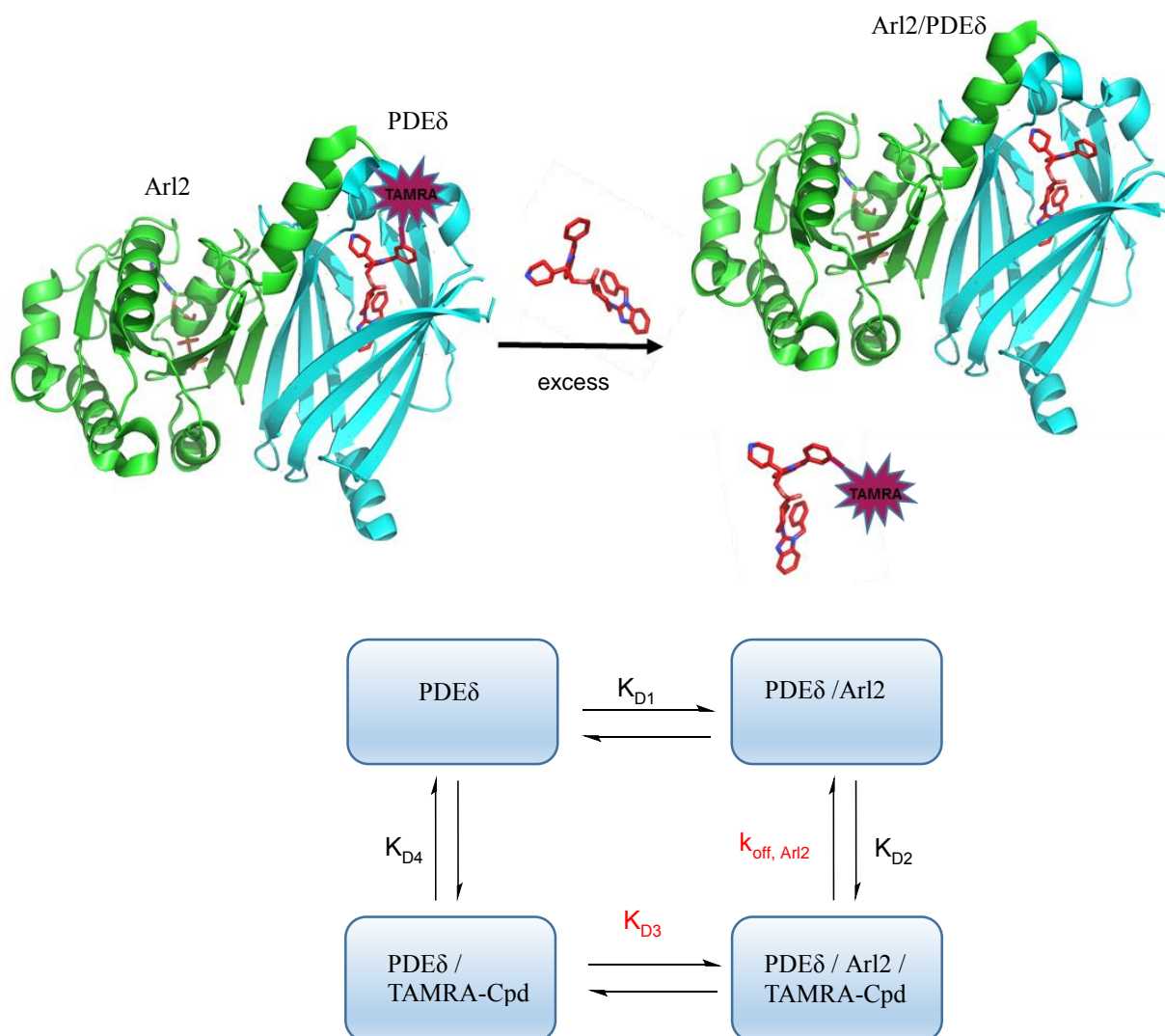


Figure 48 Principle of kinetic experiments involving TAMRA-labeled compounds (Cpd), Arl2 and PDEδ. When Arl2 is added to a complex of TAMRA-labeled small molecule and PDEδ, formation of a ternary complex is observed. The amount of ternary complex formed is dependent on the relative concentration of Arl2 compared to PDEδ and the equilibrium constant K_{D3} . The exchange reaction between TAMRA-labeled and unlabeled small molecule is then initiated by adding an excess of the free small molecule, which allows for the calculation of apparent dissociation rate constants $k_{\text{off,obs}}$. The maximum value of $k_{\text{off,obs}}$ corresponds to $k_{\text{off,Arl2}}$ of the TAMRA-labeled small molecule from the ternary Arl2-PDEδ-TAMRA-Cpd complex.

When a preformed PDEδ-TAMRA-Deltarasin complex (both 33 nM) was treated with a 20-fold excess of unlabeled compound a slow dissociation with a half life around 20 min was observed (Figure 49). If the competitor was added after preincubation with different concentrations of GppNHp-Arl2 the dissociation rate was readily increased, with two equivalents already showing a significant effect (4 fold increase). Further excess of GppNHp-Arl2 led to the release of the labeled small molecule from the binding site with a half-life in the second range (lower detection limit).

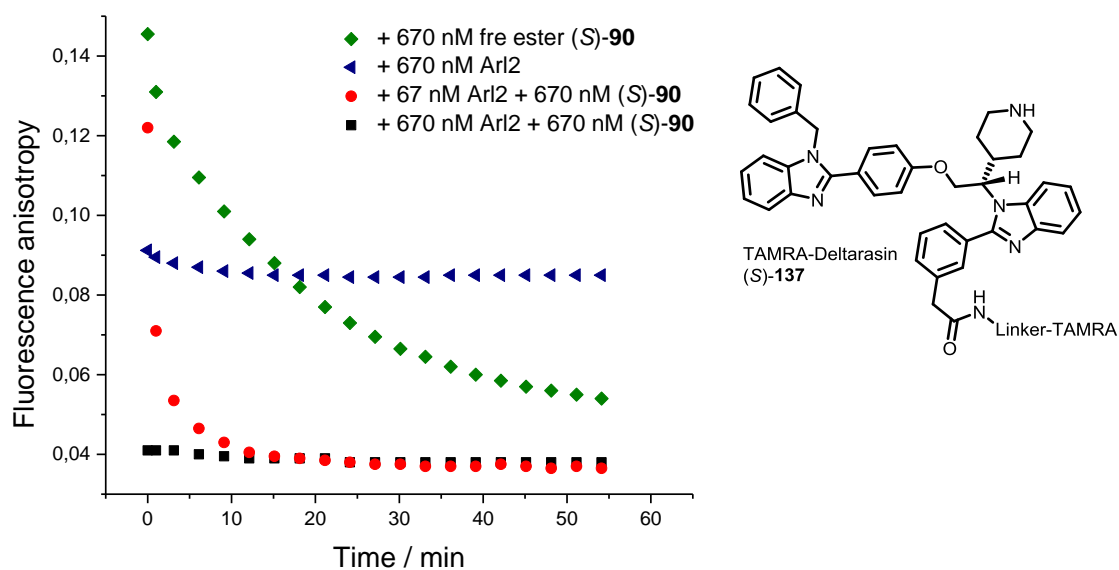


Figure 49 Time-resolved fluorescence anisotropy measurement of premixed TAMRA-Deltarasin (lower panel) and PDE δ (33 nM) after initializing the dissociation with a 20-fold excess of unlabeled ester (green dots). The experiments were also carried out in the presence of different concentrations of GppNHp loaded Arl2 protein (blue, red and black dots).

It was also tested if GppNHp-Arl2 could affect the kinetics of cargo release when the very high affinity TAMRA-(S)-92 was used as probe. TAMRA-(S)-92 cannot be efficiently displaced by Arl2, however it was reasoned that the binding kinetics of TAMRA-(S)-92 to PDE δ might be altered (Figure 50).

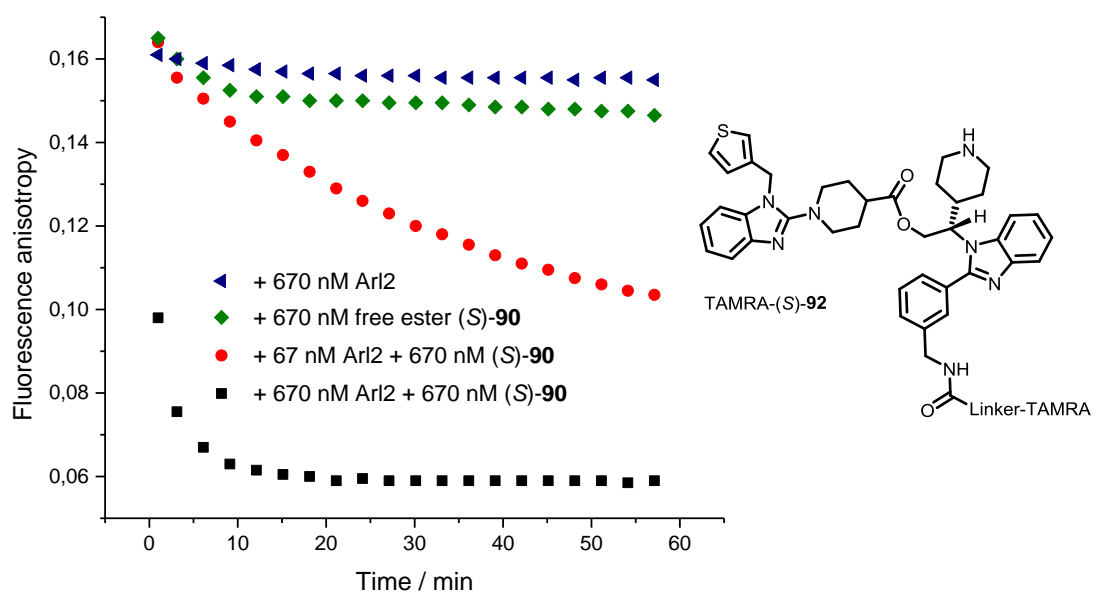


Figure 50 Time-resolved fluorescence anisotropy measurement of premixed TAMRA-(S)-92 (33nM) after initializing the dissociation with a 20-fold excess of unlabeled ester (green dots). The experiments were also carried out in the presence of different concentrations of GppNHp loaded Arl2 protein (blue, red and black dots).

When a preformed PDE δ -TAMRA-(S)-92 complex (both 33 nM) was treated with an excess of unlabeled compound in the presence of Arl2 a similar dissociation rate enhancement was observed compared to TAMRA-Deltarasin. Two equivalents of Arl2 increased the measured dissociation rate by a factor 5, a 20:1 ratio of Arl2:PDE δ resulted in a 63-fold dissociation rate enhancement (Figure 51). This suggests that the apparent dissociation rate constant $k_{\text{off,obs}}$ for TAMRA-(S)-92-PDE δ correlates linearly with the initial Arl2 concentration.

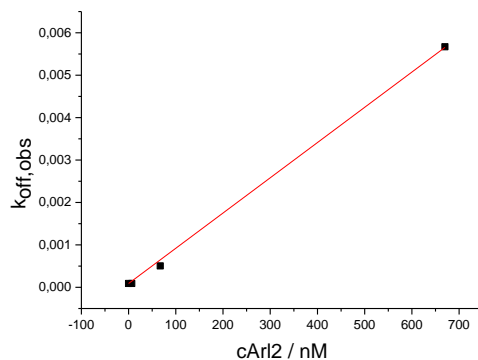


Figure 51 Dependence of apparent dissociation rate constant $k_{\text{off,obs}}$ on the initial Arl2 concentration for the dissociation of the TAMRA-(S)-92-PDE δ complex.

Since $k_{\text{off,obs}}$ has to correlate with the amount of the ternary TAMRA-Cpd-PDE δ -Arl2 complex it has to level off when the TAMRA-Cpd-PDE δ complex is fully saturated with Arl2. The observed rate $k_{\text{off,obs}}$ is actually indicative of the fraction bound of TAMRA-small molecule-PDE δ to Arl2 and the data can be fitted according to the law of mass action to obtain the equilibrium constant K_{D3} . A simulation of the experimental conditions using a K_{D3} in the low micromolar range reveals good agreement between theory and experiments (Figure 52). At the experimentally used nanomolar concentrations, a micromolar affinity constant K_{D3} would result in a low fraction bound of TAMRA-Cpd-PDE δ to Arl2. At low Arl2 concentrations relative to the K_{D3} a linear increase of $k_{\text{off,obs}}$ with the concentration of Arl2 is expected. Since the observed experimental data is in agreement with this analysis it can be concluded that K_{D3} must be in the micromolar range.

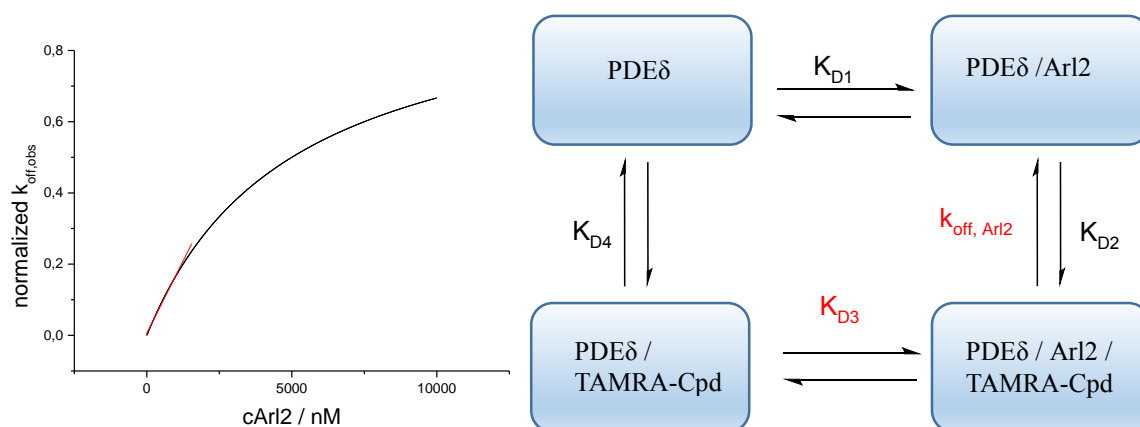


Figure 52 Simulated values for $k_{\text{off,obs}}$ (normalized) in dependence of Arl2 concentrations reveal a hyperbolic relationship. A region of linear increase of k_{obs} with increased Arl2 concentrations (red) is observed for a K_{D3} 5 μM . (cPDE δ -TAMRA-(S)-92 33 nM).

These data have also important implications for the release of small molecules from the PDE δ binding site in the living cell. Since ternary Arl2-Cpd-PDE δ complexes display relatively low affinity and rapidly dissociate, high Arl2 concentrations may locally lower the affinity of the Cpd-PDE δ complex so that even low affinity, locally enriched farnesylated proteins can displace the small molecule.

Small molecule screen for finding Arl2/3 like allosteric inhibitors of the Ras- PDE δ interaction

Arl2/3 and small molecule inhibitors can both antagonize the Ras-PDE δ interaction. In contrast to small molecules, which bind to the hydrophobic cavity of PDE δ , Arl2/3 increase the dissociation rate of bound cargo by forming ternary complexes. Kinetic experiments allow for the differentiation of small molecules which bind to the hydrophobic cavity of PDE δ and allosteric binders. In order to identify small molecules which bind allosterically, displacement experiments of TAMRA-(S)-**92** with small molecules were carried out. The tested small molecule library consisted of 300 selected high-affinity binders which were identified by the Ras-PDE δ Alpha screen. The library was tested at a concentration of 20 μ M and Arl3 was used as a control since it rapidly displaces cargo from the prenyl-binding cavity of PDE δ . Unfortunately no allosteric inhibitor could be identified by this screen. Due to the large, flat and flexible interaction surface area this finding is not surprising. Screening of a larger set of compounds however might reveal starting points for the design of potent allosteric binders of PDE δ .

4.10 Synthesis of benzimidazole-pyrrole hybrid inhibitors

The results obtained for the *bis*-benzimidazoles and the Atorvastatin derivatives demonstrate that the farnesyl-binding site of PDE δ is amenable to structure guided improvement of compound affinity. Since both compound classes display high affinities it was decided to combine structural elements from both compound classes into hybrid inhibitors, with the goal of achieving high ligand efficiency.

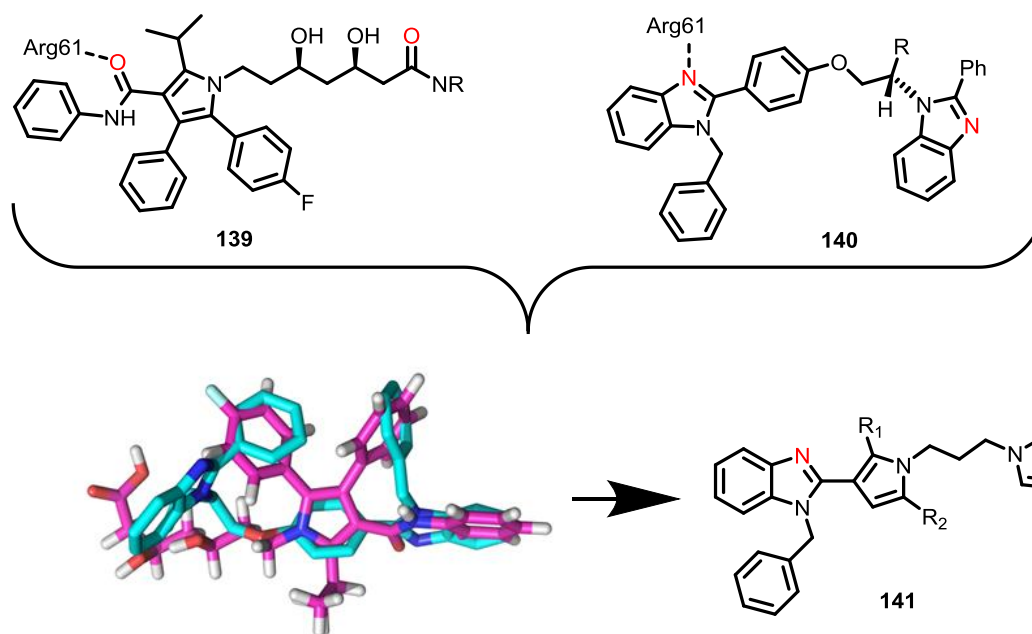


Figure 53 Design of hybrid Atorvastatin-benzimidazole inhibitors. Top panel: Key hydrogen bond acceptors are highlighted. Lower panel: Overlay of *bis*-benzimidazole (cyan) and Atorvastatin (pink) from best scoring docking pose. In a hybrid approach it was envisaged to keep the isopropyl substituted pyrrole moiety of Atorvastatin which according to docking extends into a hydrophobic pocket that was not targeted by the *bis*-benzimidazole compounds.

The reduced number of non-H atoms could lead to a decrease in logD, an increase in ligand efficiency and possibly improved solubility.

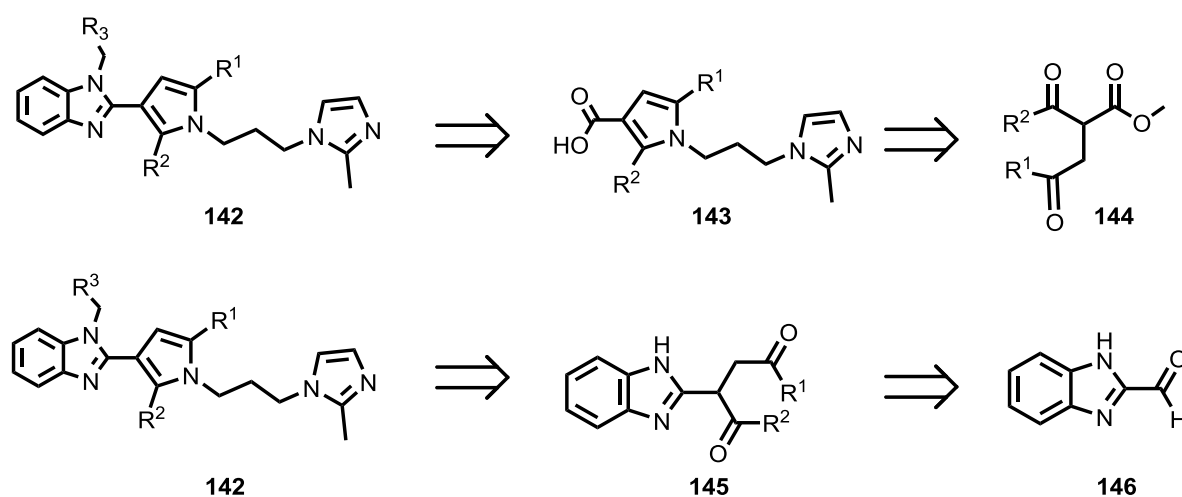


Figure 54 Retrosynthetic analysis of benzimidazole-pyrrole hybrid molecules.

Initially it was envisaged to install the pyrrole moiety by a Paal-Knorr synthesis (Figure 54, upper panel). Coupling of the acid **143** to phenylendiamine, followed by cyclization would then

furnish the benzimidazole. This route, however, allowed for little diversity and low step efficiency. Consequently, it was decided to start with commercially available benzimidazole 2-carboxaldehyde and install the pyrrole at a later stage of the synthesis (Figure 54, lower panel). The aldehyde was therefore subjected to aldol condensation with acetophenone resulting in an α,β -unsaturated ketone (Figure 55). Stetter reaction with aliphatic aldehydes, followed by Paar-Knorr synthesis furnished the benzimidazole pyrrole core structure and alkylation as previously described led to the *N*-substituted benzimidazoles.

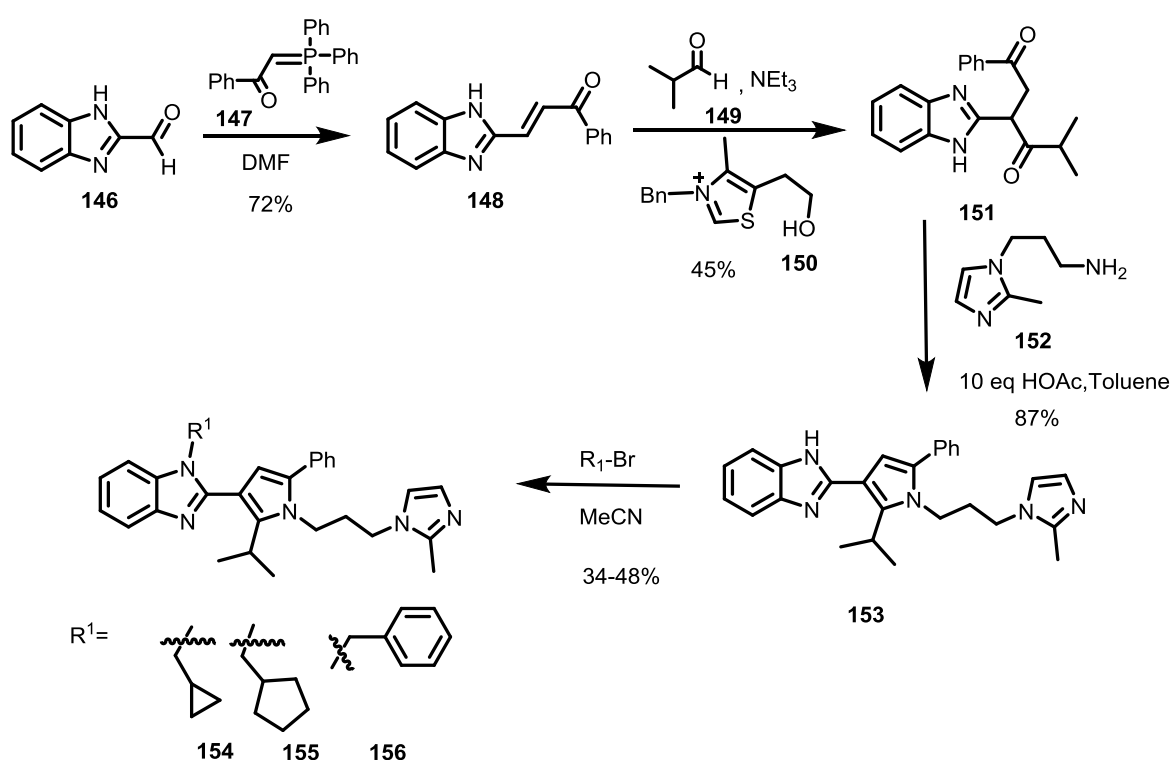


Figure 55 Synthesis of benzimidazole-pyrrole hybrid inhibitors.

Unfortunately, the resulting hybrid benzimidazole-pyrrole compound series did not show strong binding to PDE δ (Table 13). Consistent with other benzimidazole binding data, the free, non-alkylated benzimidazole did not display notable binding to PDE δ (Table 13, entry 4).

Table 13: Affinities of benzimidazole-pyrrole- hybrid compounds measured by fluorescence polarization and T_m shift assays.

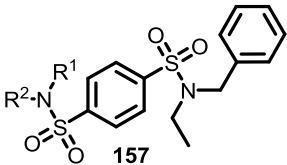
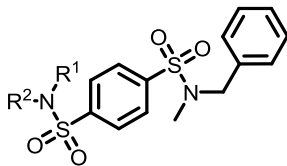
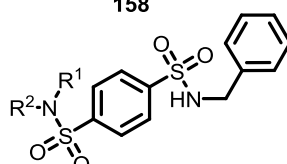
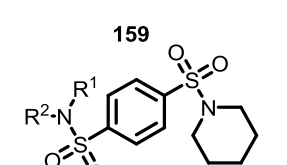
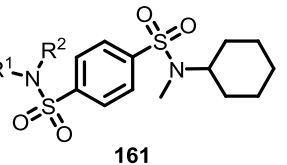
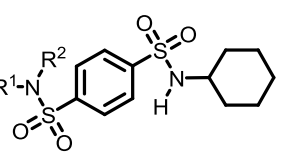
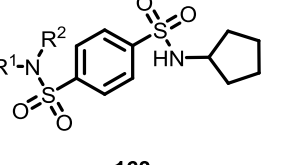
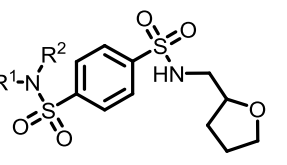
Entry	Cpd (rac)	R ¹	R ²	K _D / nM	T _m shift / °C
1	154			251 ± 33	18.3
2	155			347 ± 47	19.6
3	156			689 ± 223	nd
4	153	H		>1000	nd

4.11 Evaluation of *bis*-sulfonamides as PDE δ inhibitors

By means of the biophysical Alpha Screen assay employing a K-Ras4B peptide and PDE δ (described above, conducted by COMAS, Dortmund), alternative chemotypes were identified by high-throughput screening. Among these, commercially available *bis*-sulfonamides were identified as potent PDE δ binders. High inhibitory potency in the Alpha screen assay was independently confirmed by the competitive FP assay with labeled Atorvastatin (Table 14).

RESULTS AND DISCUSSION

Table 14 Hit cluster derived from screening of 56 commercially available *bis*-sulfonamides. R¹ and R² are carbocycles and heterocycles.

	Cluster average K _D / nM	Nr of compounds in cluster	Top hit K _D / nM
 <p>157</p>	10	4	<5
 <p>158</p>	681	6	<5
 <p>159</p>	477	6	<5
 <p>160</p>	838	8	47
 <p>161</p>	157	4	6
 <p>162</p>	321	4	8
 <p>163</p>	381	5	108
 <p>164</p>	456	5	8

From Table 14 it is apparent that all clusters contain highly potent molecules. For the understanding of structure activity relationships, representative *bis*-sulfonamides were docked into the cocrystal structure of ester (*S*)-**90** with PDE δ (Figure 56, a). As expected the *bis*-sulfonamides are able to interact with both Tyr149 and Arg61. Gratifyingly, Shehab Ismail was able to obtain a cocrystal structure of compound **165** with the protein which confirmed the representative docking pose (Figure 56, b). In addition to the expected hydrogen bonds with Tyr149 and Arg61 a clear H-bond with a glutamine (Gln78) is observed.

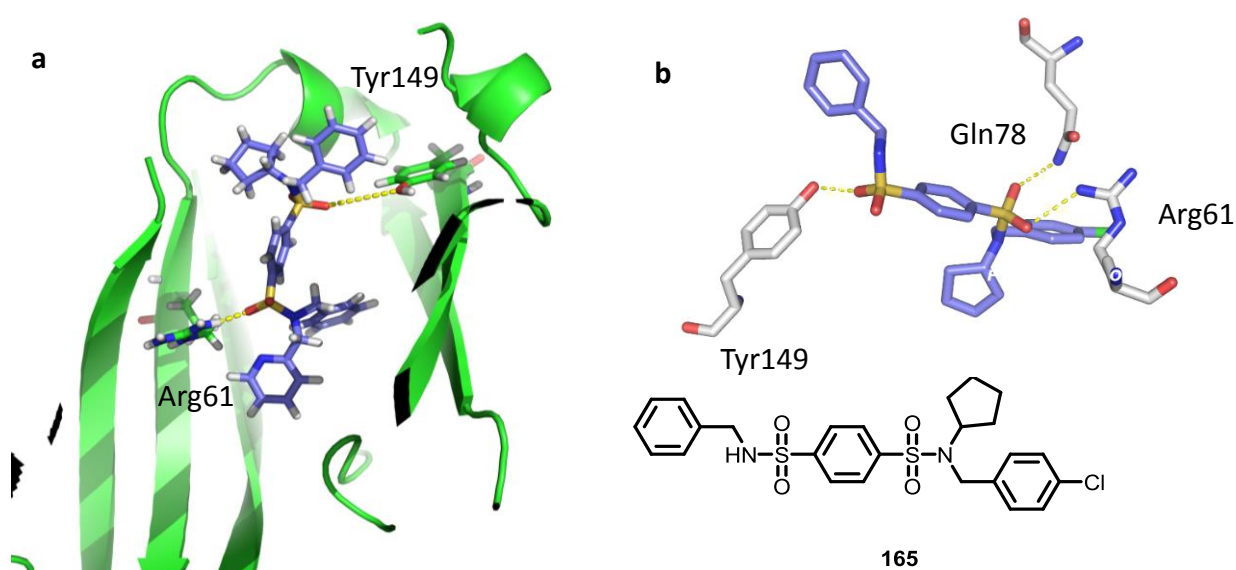
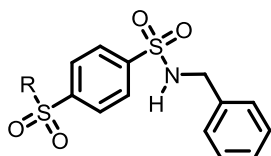


Figure 56 Structural models for binding of *bis*-sulfonamides to PDE δ a) Docking pose of a representative *bis*-sulfonamide, hydrogen bonds to Arg61 and Tyr149 are highlighted; b) Snapshot from cocrystal structure of **165** with PDE δ (solved by Dr. Shehab Ismail).

In contrast to the Atorvastatin derivatives and the *bis*-benzimidazoles, the *bis*-sulfonamides contain a short linker (phenyl ring), whereas the other compound classes use longer linking moieties to bridge the distance between Tyr149 and Arg61. In the *bis*-sulfonamides series the pharmacophore is therefore concentrated on a much smaller scaffold and features an additional hydrogen bond. With the structural data in hand, the hit clusters were analysed, and structure activity relationships were derived. Generally, the analysis of the 56 compound dataset proved to be very difficult, which can be attributed to the symmetry of the molecules. Here the analysis will be limited to the hit cluster containing the cocrystallized *bis*-sulfonamide. The combination of a saturated carbocycle and phenyl derivatives revealed highly potent compounds (Table 15, entries 1 and 2). Exchanging the cyclopentyl substituent with a methyl furfuryl group decreased

the affinity by one order of magnitude (Table 15, entries 1 vs 3). Replacement of the *para*-chlorobenzyl group (Table 15, entry 3) with an *ortho*-fluoro substituent increased the K_D strongly (Table 15, entry 4), while very bulky secondary sulfonamides (Table 15, entry 5) were also unfavorable suggesting clashes with the protein surface.

Table 15 Structure activity relationships for representative hit cluster members. Averaged affinities of triplicate measurements are shown.



Entry	Cpd	R	K_D / nM
1	164		<5
2	165		5
3	166		58
4	167		1941
5	168		280

Based on the cocrystal structure of **164** with PDE δ it is apparent that this *bis*-sulfonamide does not extend into the pocket close to Cys56, therefore improvement in analogy to the *bis*-benzimidazoles seems readily possible. Indeed, the results shown in Table 14 revealed that the most potent hit cluster features two secondary sulfonamides (also compare the docking Figure

56, a), which presumably extend into that pocket. Secondary sulfonamides incorporating a piperidine for targeting Cys56 are currently being synthesized by Pablo Martin-Gago.

4.12 Cellular Experiments with PDE δ inhibitors

4.12.1 “Pull down” experiments in cell lysates with biotinylated probes

With a library of very potent *bis*-benzimidazoles in hand, it was decided to test whether these compounds also bind to PDE δ in cell lysates. Therefore, *bis*-benzimidazole (*S*)-**169** was hydrogenated employing Raney-Ni, and the resulting amine coupled to a biotin unit to yield Biotin-Deltarasin (**170**). Biotin is commonly used for immobilization of compounds on Streptavidin-coated beads which allows for the enrichment of interacting proteins by affinity isolation.

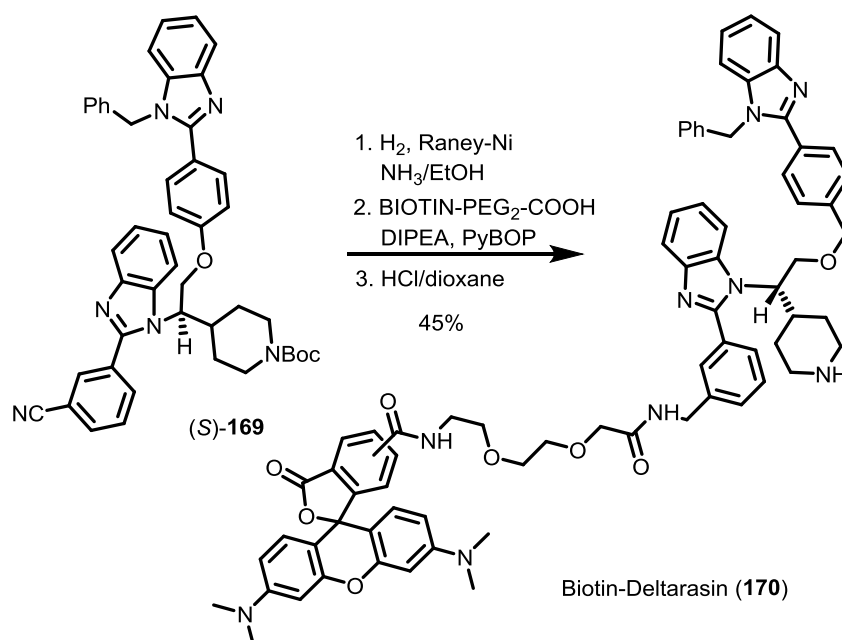


Figure 57: Synthesis of Biotin-Deltarasin (**170**).

An excess of Biotin-Deltarasin (**170**) and Biotin-Atorvastatin (**15**) were treated with Streptavidin-coated magnetic beads, washed and then subjected to “pull down” experiments with MDCK cell lysates (For principle see Figure 58)

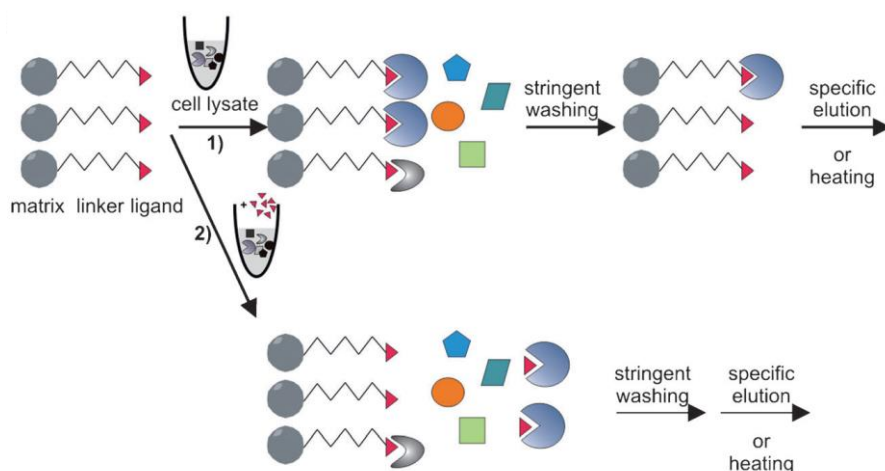


Figure 58 Principle of direct binding assay with immobilized compounds (upper panel, 1) or competition experiment (lower panel, 2) of immobilized compound with free compound. (modified from reference¹⁰⁸).

The fraction of PDE δ in the cell lysate that bound to the immobilized compounds was analysed by Western blotting using an anti-PDE δ antibody (Santa Cruz). In Figure 59 a) it is apparent that compared to control, both immobilized compounds can enrich PDE δ at the solid phase, and thus bind to PDE δ in cell lysates.

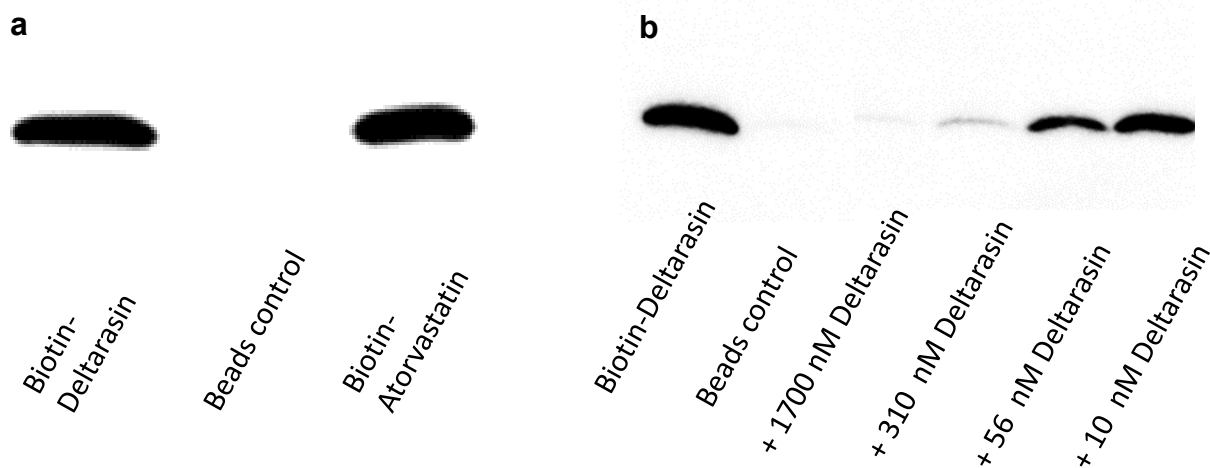


Figure 59 Representative pull-down experiments using immobilized Biotin-Deltarasin and Biotin-Atorvastatin in MDCK cell lysates. Western Blots were stained with anti-PDE δ antibody. a) qualitative “pull down” experiments employing biotinylated compounds; b) competition experiments employing Biotin-Deltarasin and free Deltarasin.

Additionally, independent competition experiments with varying concentrations of free compound (Figure 59, b) validated the interaction of both biotinylated and free Deltarasin with PDE δ in MDCK cell lysates. The binding data generated with the immobilized and the free

benzimidazole in cell lysates show that the structure guided approach towards the development of small molecule inhibitors of PDE δ was successful.

4.12.2 *In cell* measurements of the effect of Deltarasin on the interaction of Ras with PDE δ and resulting delocalization of K-Ras

To address whether the synthesized compounds also break the interaction of Ras family proteins with PDE δ in the cell, FRET-FLIM experiments were conducted by Björn Papke, Anchal Chandra und Nachiket Vartak from the group of Prof. Bastiaens. Since K-Ras4B localizes predominantly to the plasma membrane, it is difficult to monitor its interaction with cytosolic PDE δ in the living cell. The Rheb-PDE δ interaction was therefore used as a model system, because Rheb as well as PDE δ are enriched in the cytosol (Figure 60). The fraction of interacting Rheb with PDE δ is relatively high, and a change in fluorescence lifetime upon inhibition with a small molecule can be easily monitored.

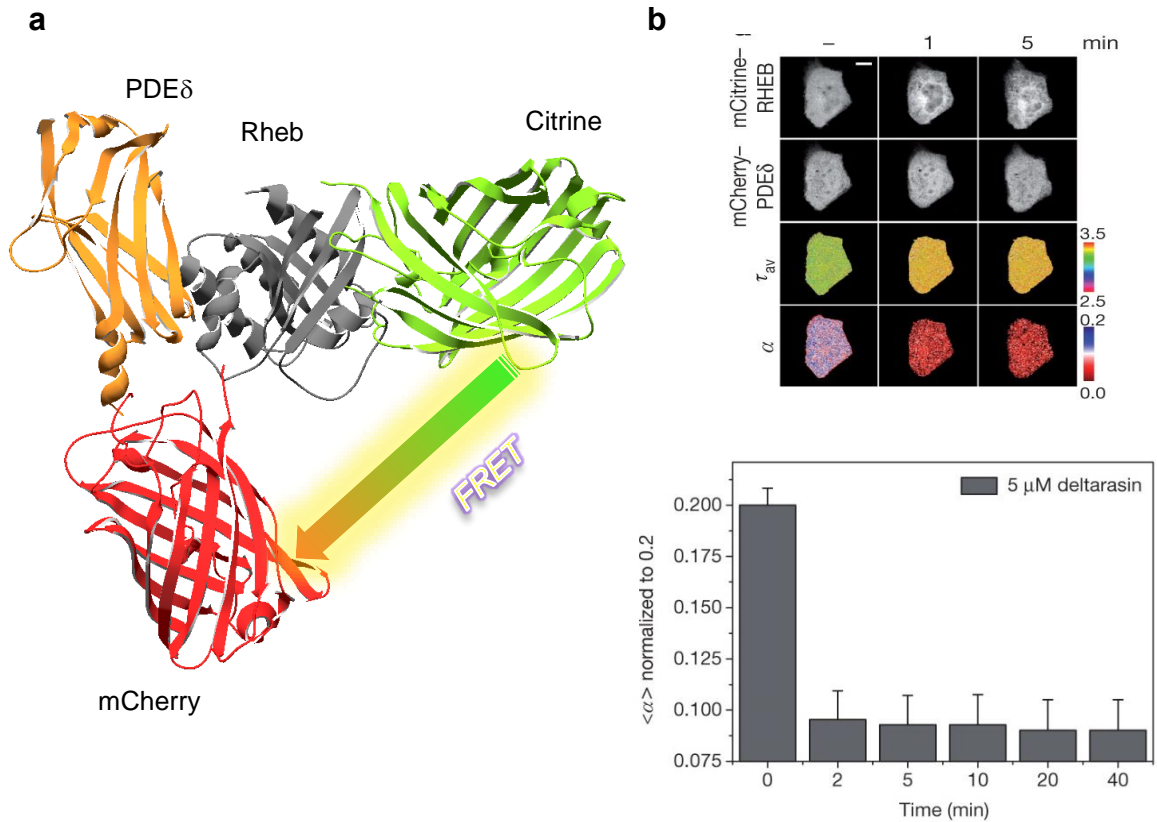


Figure 60 Live-cell imaging using mCherry-PDE δ and mCitrine-Rheb. a) Principle of assay: If mCherry-PDE δ and mCitrine-Rheb interact, the two fluorophores come close to each other and upon excitation of mCitrine-Rheb, energy may be transferred to mCherry-PDE δ . The resulting Förster-Resonance-Energy-Transfer (FRET) decreases the lifetime of the excited state of Citrine Rheb. Therefore, Fluorescence-Lifetime-Imaging (FLIM) can be used to quantify the fraction α of interacting Rheb and PDE δ ; b) FRET-FLIM time series on MDCK cells treated with Deltarasin. Treatment with Deltarasin resulted in an increase in fluorescence lifetime τ_{av} and decrease in fraction bound α of Rheb. The normalized quantification is shown in the lower panel.⁷⁹

Treatment of MDCK cells with Deltarasin led to a loss of interaction between mCherry-PDE δ and mCitrine-Rheb, resulting in an increase in fluorescence lifetime τ_{av} and decrease in fraction of interacting Rheb (α) (Figure 60, b, upper panel). The loss of interaction between Rheb and PDE δ was visible within 2 minutes. This observation is similar to *in vitro* data showing a rapid displacement of farnesylated Rheb from PDE δ . A dose-response study of the effect of Deltarasin on the Rheb-PDE δ interaction revealed that the compound breaks the interaction efficiently at concentrations as low as double digit nanomolar (Figure 61) in the living cell.

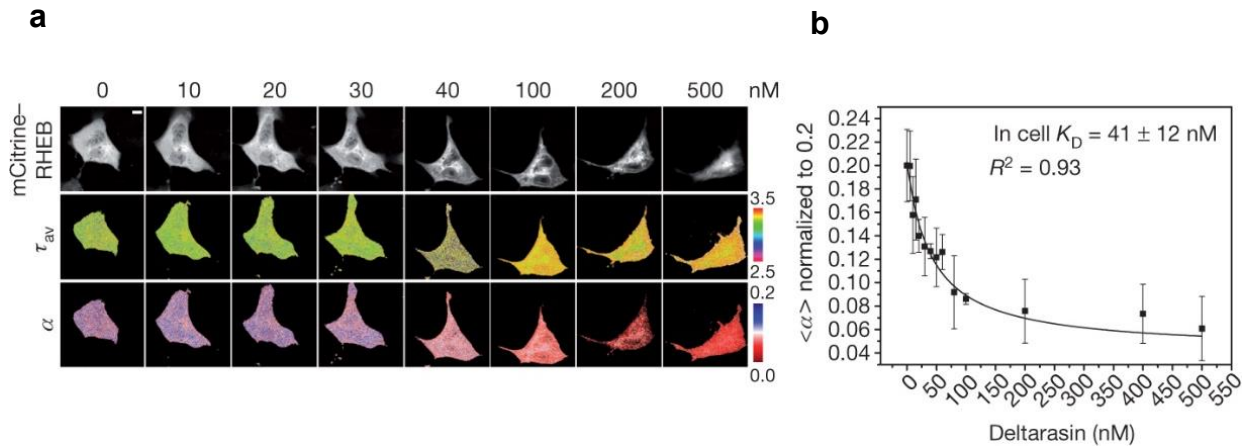


Figure 61 Effect of different concentrations of Deltarasin on the Rheb-PDE δ interaction. a) Concentration dependent FRET-FLIM measurements using the mCitrine-Rheb-mCherry-PDE δ interaction; b) Quantification of FRET-FLIM data using a simple dose response model and the Cheng-Prusoff equation.⁷⁹

It was also of interest to confirm that the small molecules directly interact with PDE δ in the living cell. Therefore, cells were treated with TAMRA-Deltarasin which resulted in a reduction of the donor lifetime of mTFP-PDE δ . This experiment confirmed the binding of the small molecule to PDE δ in the living cell (Figure 62).

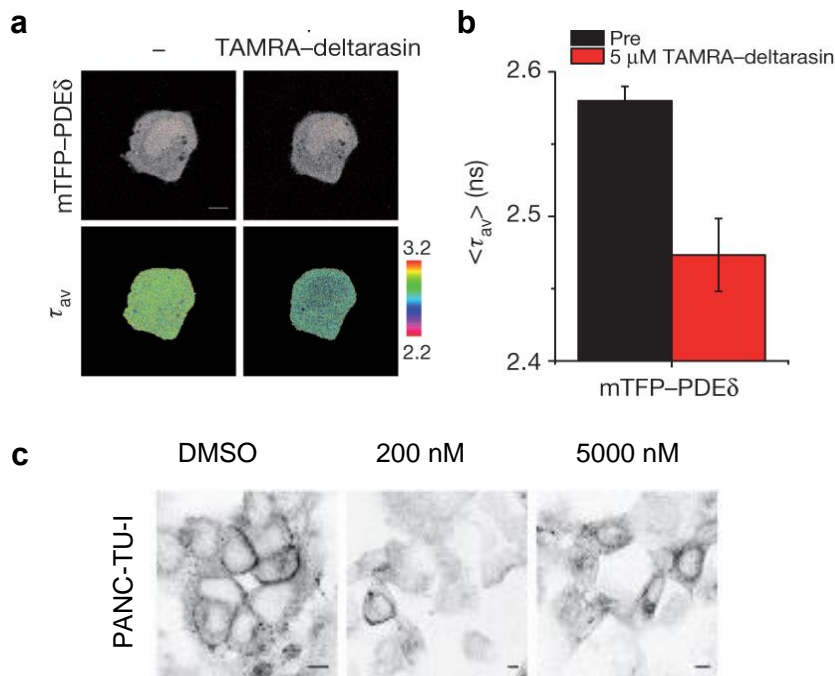


Figure 62 a) Effect of TAMRA-Deltarasin on the donor lifetime of mTFP-PDE δ in MDCK cells transfected with mTFP-PDE δ ; b) Quantification of the observed impact on donor lifetime; c) Relocalization of Ras in PANC-TU-I cells upon treatment of different concentrations of Deltarasin.

In addition, immunofluorescence staining of fixed and permeabilized human pancreatic ductal adenocarcinoma cells (hPDAC) with a pan-antibody against Ras showed a relocalisation of endogenous Ras in PANC-TU-I cells after 2 h (Figure 62, c). In summary, it has been shown that Deltarasin binds to endogenous PDE δ in cells, thereby breaks the interaction of Ras family proteins with PDE δ and alters the localization of Ras proteins in the cell.

4.12.3 Evaluation of PDE δ inhibitors in Ras signaling

The effect of Ras-PDE δ inhibitors on oncogenic K-Ras signaling was subsequently studied in hPDAC cells by the Bastiaens group.⁷⁹ Singh *et al.* had previously shown that shRNA can be used to deplete K-Ras in pancreatic cancer cell lines harboring *K-Ras* mutations in order to classify these cell lines whether they require K-Ras for survival.¹⁰⁹ Thus, the effect of Deltarasin on cell survival of K-Ras dependent (CAPAN-1 and PANC-TUI) and K-Ras independent pancreatic cancer cell lines (PANC-1 and BxPC3) was compared by real time cell analysis (RTCA).¹⁰⁹ In parallel it was tested whether survival of these four cell lines is dependent on PDE δ expression levels by transfecting the cells with a lentiviral construct for doxycycline inducible shRNA expression against PDE δ . Treatment of cells with 5 μ M Deltarasin or doxycycline induced knock-down of PDE δ resulted in reduced cell proliferation of the K-Ras dependent PANC-TUI and CAPAN1 hPDAC cell lines and had only a slight effect on the growth of K-Ras independent PANC-1 and BcPX3 hPDAC cells. This experiment clearly showed that survival signaling from oncogenic K-Ras is attenuated by the inhibition of the K-Ras-PDE δ interaction by Deltarasin that leads to relocalization of K-Ras to endomembranes. In addition, only K-Ras dependent pancreatic tumor cells showed a clear effect of PDE δ inhibition on their overall proliferation. In order to assess whether the Deltarasin induced proliferation inhibition of K-Ras dependent hPDAC cells was caused by programmed cell death, a fluorescence assisted cell sorting (FACS) cell death assay was performed. Both oncogenic K-Ras dependent mPDAC cell lines (PANC-TUI and CAPAN1) displayed a strong increase in programmed cell death after 24h incubation with Deltarasin, whereas the K-Ras independent hPDAC cells (Panc1 and BxPC3) showed little effect.

To address if inhibition of the PDE δ -K-Ras interaction by Deltarasin has an effect on oncogenic K-Ras signal transduction, the epidermal growth factor (EGF) mediated Erk1/2 response was studied by the Bastiaens group. Quantitative Western blot analysis of phosphorylated Erk1/2 revealed that the K-Ras dependent PANC-TUI had a high basal Erk activity that was reduced upon inhibition of PDE δ by Deltarasin. Importantly, the two oncogenic K-Ras dependent

hPDAC cell lines (PANC-TUI and CAPAN-1) showed a reduction in the EGF mediated transient Erk signal response as compared to the K-Ras independent hPDAC cells (PANC-1 and BcPX3). The loss of the spatial organization of oncogenic K-Ras after inhibition of the PDE δ -K-Ras interaction thus impaired survival and proliferative signaling that specifically causes cell death in K-Ras dependent hPDAC cells.

In further experiments the effect of Deltarasin on human cancer cells xenografted into mice was evaluated by Prof. Hahn and coworkers, Uni Bochum. Deltarasin was administered to nude mice bearing subcutaneous human PANC-TUI tumour cell xenografts. Deltarasin was delivered to the mice bearing human tumour cells by intra-peritoneal injection once (QD) or twice (BID) a day (Figure 63, a). Treatment of mice with Deltarasin resulted in a dose-dependent reduction in PANC-TUI tumour growth rate compared to controls. Mice that were treated with Deltarasin (10 mg kg⁻¹ twice a day), displayed virtually no tumour growth within the first nine days. Administration of the compound also resulted in a reduced variance of tumour size compared to control at the end of day nine (Figure 63, b).

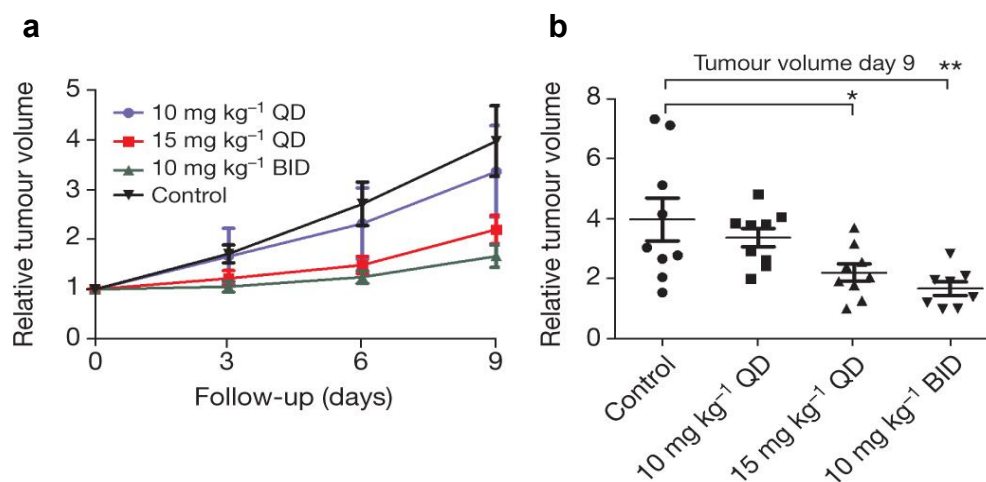


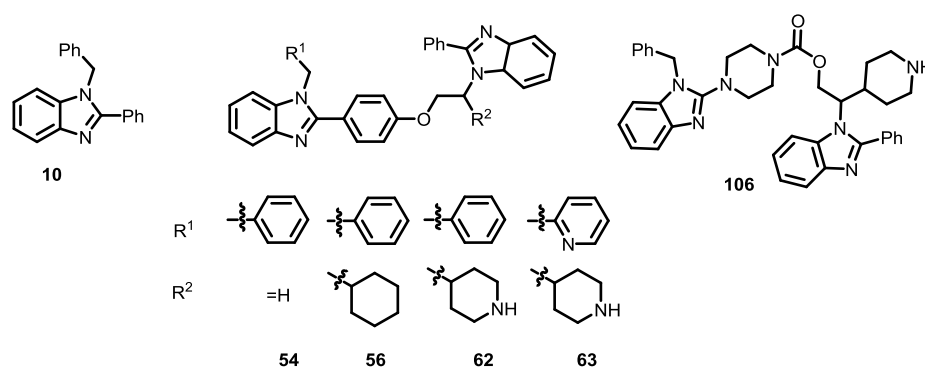
Figure 63 Deltarasin impairs dose-dependent *in vivo* growth of xenografted pancreatic carcinoma in nude mice.⁷⁹

a) Tumour volume measurements: Deltarasin was administered by the group of Prof. Hahn by intra-peritoneal injection once (QD) or twice (BID) per day at 10 mg kg⁻¹ QD, 15 mg kg⁻¹ QD and 10 mg kg⁻¹ BID. Changes in mean tumour volumes are given relative to the volumes at treatment initiation; b) Tumour volume at day 9 of Panc-Tu-I xenograft experiments. *P* values derived from *t*-test. ***P* ≤ 0.01, **P* ≤ 0.05 indicate statistical significance.⁷⁹

4.12.4 Evaluation of PDE δ inhibitors in Hedgehog signaling

Due to the involvement of PDE δ in ciliopathies and the crosstalk between oncogenic K-Ras and Hedgehog signaling, the benzimidazole library was evaluated for its impact on signal

transduction in mouse embryonic mesoderm fibroblasts by COMAS, Dortmund. Multipotent mesenchymal cells (C3H10T1/2) are able to differentiate into osteoblasts after treatment with the Smoothed (SMO) agonist Purmorphamine. The differentiation process is coupled to the expression of osteoblast specific genes such as alkaline phosphatase. Upon addition of a chemoluminescent substrate (e.g. CDP-star), alkaline phosphatase induces luminescence by a hydrolysis reaction. In the presence of a Hedgehog pathway inhibitor a reduced signal is expected, since less alkaline phosphatase is expressed. Pleasingly, the benzimidazole library contained various inhibitors of the Hedgehog pathway (Table 16). The best compounds showed activities in the low micromolar range. Piperidine-containing compounds, however, displayed undesired toxicity in the control viability experiments (Table 16, entries 4-7).

Table 16 Inhibition of Hedgehog signaling by benzimidazole compounds.

Entry	Cpd	IC ₅₀ / μ M	Viability / μ M
1	10	10.3	>30
2	54	2.8	>30
3	56	4.6	>30
4	(<i>R</i>)- 62	2.0	2.9
5	Deltarasin (<i>S</i>)- 62	1.9	2.8
6	63	6.0	7.0
7	106	1.8	4.1

C3H10T1/2 cells have been described as an ideal screening system for monitoring cilia function,¹¹⁰ which is linked strongly to Hedgehog signal transduction. Joubert syndrome is a developmental disease, which may be caused by a mislocalization of the farnesylated phosphatase INPP5E in the cell. INPP5E exclusively localizes to the primary cilium if functional PDE δ is present. A homozygous mutation of PDE δ completely abrogates binding of prenylated proteins to PDE δ and leads to impaired transport of farnesylated INPP5E to the cilium. PDE δ -mutated patients display eye defects due to mislocalization of the rhodopsin kinases GRK1 and 7, but additionally show limb, renal, and cerebral anomalies.⁵⁶ These anomalies are typical developmental disorders which might be accounted for by impaired

Hedgehog signaling from the primary cilium. Due to the developmental anomalies of PDE δ -mutated patients, it is not surprising that PDE δ inhibitors are active in Hedgehog signaling. Most likely the effect of the small molecules on Hedgehog signaling is caused by a mislocalization of INPP5E or another prenylated ciliary protein (e.g. RAB28), which functional PDE δ normally transports to the primary cilium. In addition, the crosstalk between Ras and Hedgehog signaling may account for the observed effect.⁵⁸ Oncogenic K-Ras activates Hedgehog signaling in pancreatic adenocarcinoma cells through activation of a downstream effector pathway involving RAF/MEK/ERK. Whether this crosstalk also exists in embryonic fibroblasts is currently unclear.

Since INPP5E plays an essential role in the primary cilium by controlling ciliary growth factor and PI3K signaling,¹¹¹ small molecule inhibitors of PDE δ should affect PI3K signaling in ciliated cells. Testing of these inhibitors in ciliated cells might provide novel insight into the function of cilia as signaling hubs in developmental cells.

4.13 Evaluation of the prenyl-specificity of PDE δ *in vitro*

To date conflicting data has been reported on the prenyl specificity of PDE δ .^{30,31,40,46,112} While some reports indicate a significantly higher affinity of farnesylated vs geranylgeranylated peptides for PDE δ , this selectivity could not be confirmed in more elaborate model systems. Pull down experiments identified similar amounts of farnesylated and geranylgeranylated proteins.^{54,56} Proteomics experiments by Philipp Kuchler, MPI Dortmund show also no clear preference of PDE δ for farnesylated proteins. Biophysical investigations thus far have not explored the same peptide sequence with either a geranylgeranyl or a farnesyl modification. Therefore, fluorescein labeled peptides derived from the C-terminus of G- α were tested in fluorescence polarization measurements for their binding to PDE δ (Figure 64).

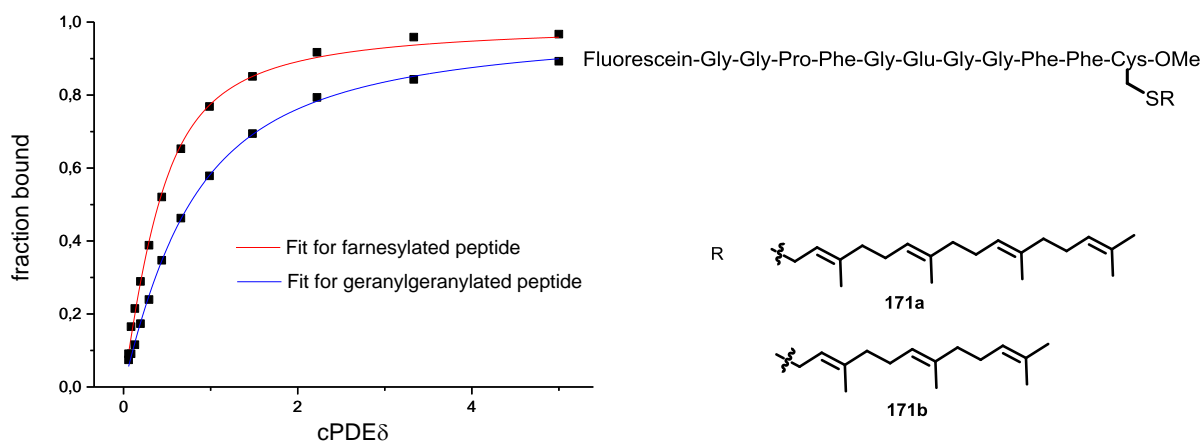


Figure 64 Representative titrations of G α derived peptides differing only in the lipid modification (geranylgeranyl vs farnesyl). Fitting of the data yields K_D values of 200 nM for the farnesylated and 499 nM for the geranylgeranylated peptide.

The titrations indicated a slight preference of PDE δ for farnesylated peptides over geranylgeranylated peptides (K_D values 200 vs 499 nM), but the difference in affinity was not as strong as previously measured using peptides with different amino acid sequences.⁴⁰ These data clearly suggest that due to the flexibility and size of the prenyl binding pocket both lipids can be accommodated by PDE δ with high affinity. *In vivo* distinct differences between the shuttling of geranylgeranylated vs farnesylated proteins exist. RhoGDI has been shown to bind the geranylgeranylated RhoA GTPase with an affinity in the low picomolar range, suggesting that at least for RhoGTPases proteins other than PDE δ regulate membrane trafficking.¹¹³ The extremely high affinity of RhoA for RhoGDI is due to lipid protein interactions and additional protein-protein backbone interactions. For PDE δ such protein-protein backbone contacts have not been identified thus far. It is generally expected that solubilizing factors for geranylgeranylated proteins display a higher affinity for their cargo since these proteins show a 40-60 fold higher affinity for membranes compared to farnesylated proteins.¹¹⁴ Future cellular experiments using a set of geranylgeranylated proteins should clarify whether PDE δ also maintains the spatial organization of these lipidated proteins.

4.14 Rational design of UNC119a/b inhibitors

Similar to PDE δ , UNC119a/HRG4 and UNC119b are lipid binding proteins.^{32,115} However unlike PDE δ they recognize *N*-myristoylated proteins. UNC119a/HRG4 has been shown to shuttle Src kinases and to participate in targeting transducin- α to the outer segment of

photoreceptors via interaction with its acylated *N*-terminus.^{34,116-118} UNC119b shuttles nephrocystin-3 (NPHP3) and targets it to the primary cilium.¹⁰⁷ Therefore, UNC119a/b are interesting targets for tool compound development and potentially also for drug development. The paralogs UNC119a/b share a very high sequence identity, and feature very similar lipid binding sites (Figure 65). So far, only crystal structures with UNC119a have been obtained. Interestingly, the hydrophobic lipid binding pocket in UNC119a/b is located on the other side of the protein compared to PDE δ and RhoGDI.

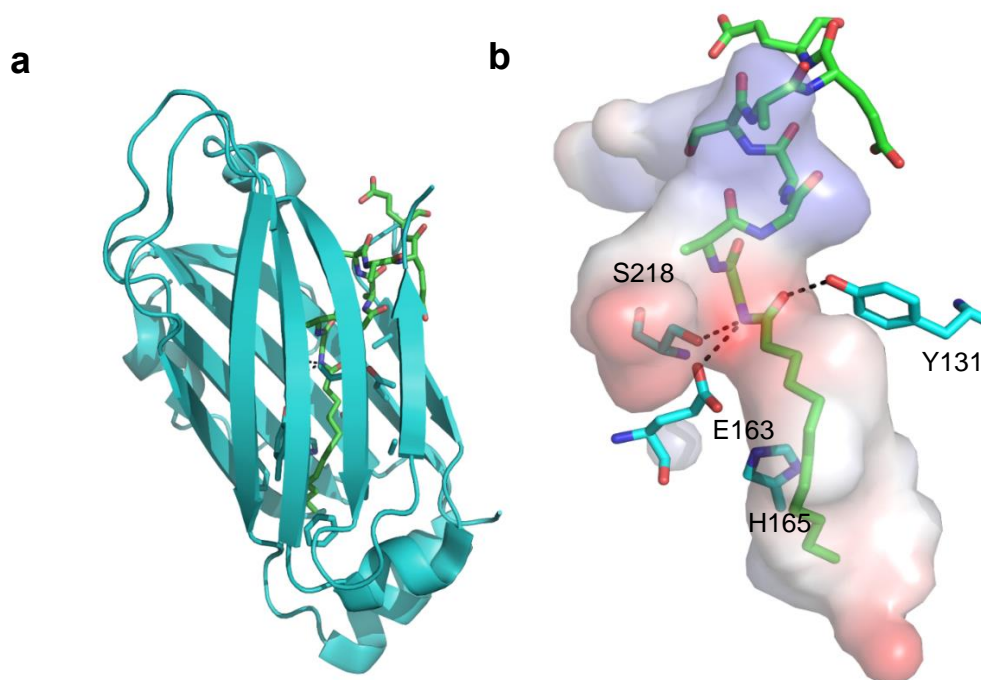
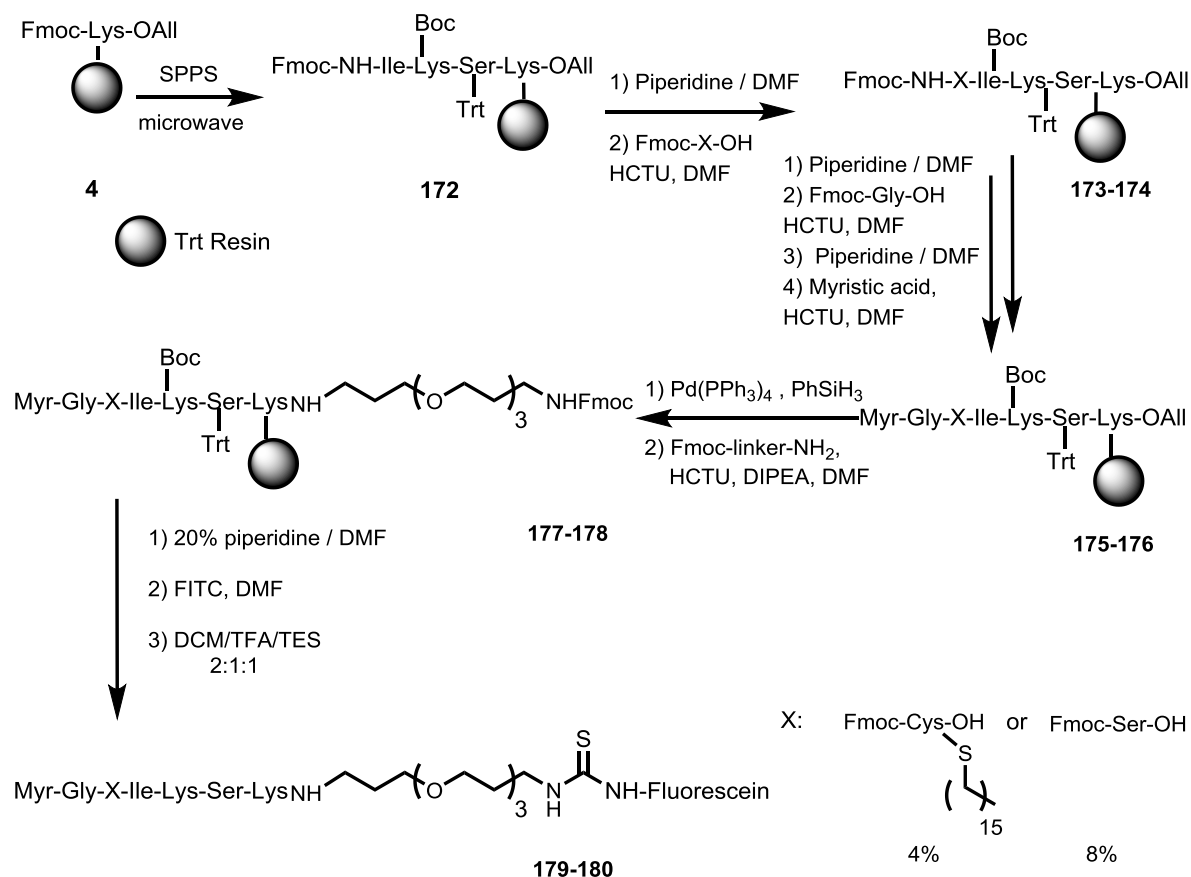


Figure 65 Structural analysis of UNC119a in complex with a lauroylated peptide a) Overall structure of UNC119a in complex with a lauroylated peptide (green sticks) derived from the *N*-terminus of the transducin- α subunit; b) Hydrophobic binding pocket of UNC119a (PDB 3RBQ), key H-bonds are highlighted in black dashes.

Binding of a lauroylated peptide mimicking the *N*-terminus of transducin- α to UNC119a is mediated by hydrophobic interactions as well as hydrogen bonding. The cocrystal structure reveals that although the fatty acid chain and six *N*-terminal amino acids are deeply buried, the hydrophobic cavity is still far from being completely filled (Figure 65, b). Notably, the relatively short lauroyl C-12 chain leaves unexplored hydrophobic space deep in the binding site. Consistent with this finding the longer myristoyl group shows stronger binding. Key H-bonds are observed mainly with the *N*-terminal amide bond, highlighting its significance for inhibitor development (Figure 65). Tyr149 donates an H-bond to the carbonyl of the amide, whereas Ser218 and Glu163 interact with the NH of the amide. Ser218 points directly towards the amide NH forming an H-bond suggesting that Ser218 may at least partially be deprotonated.

The long lipid group seemed central to activity and was used as a starting point for the rational design of small molecule inhibitors. The previously identified APT1/2 inhibitor Palmostatin B features a long lipid chain and incorporates a lactone, which may act as a hydrogen bond acceptor for Tyr131. In addition it can covalently modify nucleophilic serins.^{19,119,120}

For an investigation of the binding of Palmostatin B to UNC119a, a fluorescent probe was needed for competition experiments. Therefore, an *N*-terminal, myristoylated peptide of Src family kinase Lyn was synthesized by standard solid phase peptide synthesis (Scheme 20).



Scheme 20 Solid phase peptide synthesis of a mono and double lipidated Lyn peptide starting from an orthogonally protected lysine building block (see above).

Subsequently the binding of Palmostatin B to UNC119a was investigated by means of a competitive assay using fluorescence polarization as readout. The fluorescence polarization decreases in a dose dependent manner upon addition of Palmostatin B (Figure 66). Although the binding curve does not level off at low micromolar concentrations, concentrations as low as 100 nM already affected the binding of the fluorescently labeled Lyn peptide. To additionally validate the binding TAMRA-Palmostatin B was employed and yielded a K_D value of $2.5 \pm 1 \mu\text{M}$ for UNC119a and $3.5 \pm 1.1 \mu\text{M}$ for UNC119b. It is of note that TAMRA-Palmostatin bound

to UNC-119a/b although the compound is labeled on the lipid tail. Although the affinity of Palmostatin B for UNC119a/b is only in the low micromolar range these results suggest that lipidated beta-lactones might be valuable starting points for the synthesis of high affinity UNC119a/b inhibitors. Screening of a larger set of strained lactones might reveal much better inhibitors, which could potentially also form a covalent bond to a serine residue (like the buried Ser218) of the protein.

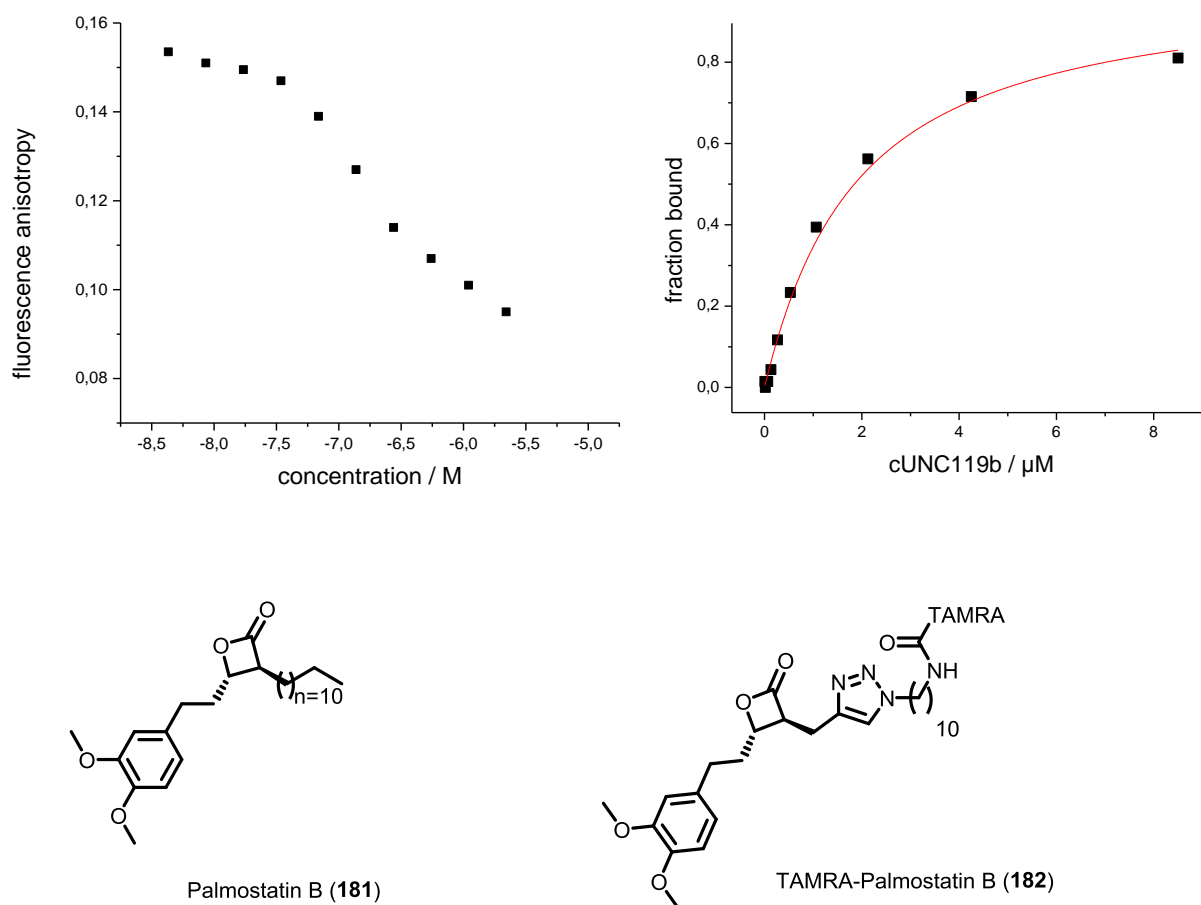


Figure 66 Binding of Palmostatin B to UNC119b measured by means of a competitive fluorescence polarization assay employing labeled *N*-terminal Lyn kinase peptide (left); direct binding of TAMRA-labeled Palmostatin B to UNC119b (right).

In an additional approach towards the rational design of UNC119a inhibitors the helical conformation of the *N*-terminal transducin- α peptide in the complex with UNC119a was exploited. Generally conformational preorganization of peptides in their protein bound conformation can lead to increased affinities. Hydrocarbon-peptide stapling has emerged as a powerful tool for conformational preorganization.¹²¹ Stapling requires the introduction of two

methylated and alkenylated amino acids into the peptide sequence of interest and macrocycle formation by ring closing metathesis to generate a bridging moiety connecting two turns of an α -helix. Commonly two modified amino acids are incorporated at positions i and $i+4$ to form an eight-carbon bridge because these residues usually display an $\text{NH}_i\text{-CO}_{i+4}$ -hydrogen bond within a helix. On the other hand i and $i+3$ staples are also frequently used to generate peptide macrocycles. Bridging positions i and $i+3$ of the peptide does not strongly stabilize helical peptide conformation, but it rigidifies the peptide backbone and potentially reduces the entropic penalty of binding by conformational preorganization.

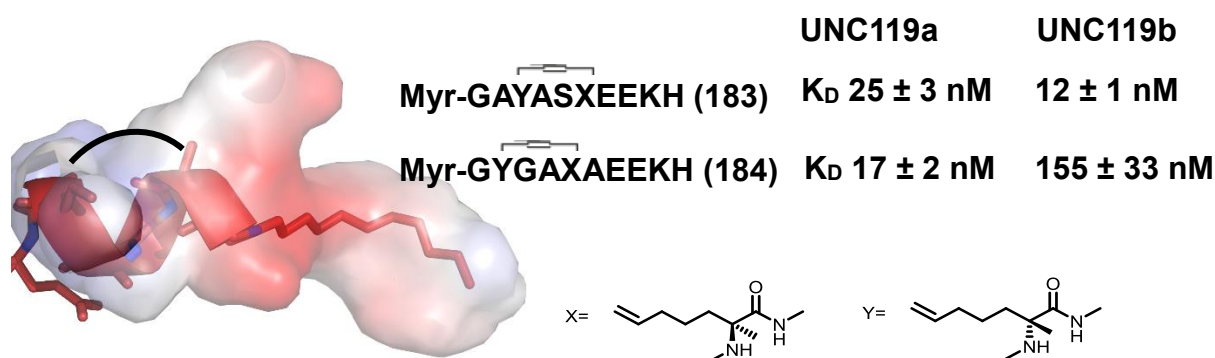


Figure 67 Hydrocarbon stapling of transducin- α peptides for lead generation of UNC119a/b binders. Left) helical conformation of transducin- α peptide bound to UNC, right) sequences of two stapled peptides incorporating an hydrocarbon bridge. Numbers are K_D values in nM.

An initial screen of four stapled, unlabeled peptides in a competitive fluorescence polarization assay revealed two promising binders featuring an i and $i+3$ hydrocarbon bridge. In order to validate the binding the corresponding fluorescein-labeled peptides were resynthesized by Philipp Cromm and evaluated in direct fluorescence polarization assays. Gratifyingly, the stapled peptides showed affinities down to double digit nanomolar (Figure 67), and at least one peptide showed a 9-fold selectivity between UNC119a and b (Figure 67). Due to the lipid modification and their overall hydrophobicity these peptides are expected to be membrane permeable and at least partially protease resistant due to the potential binding to lipid transport proteins. Further structure guided design and library synthesis by Philipp Cromm might enable finding peptides with higher affinities than wild type transducin- α (7 nM to UNC119a).¹⁰⁶ In this context it seems particularly promising to replace the myristoyl group with hydrophobic small molecules and create hybrid small molecule-stapled peptide inhibitors.

5 SUMMARY

Ras proteins are molecular switches, which regulate cellular growth and differentiation. Mutations in the Ras encoding genes lock Ras proteins in a permanent “on” state which may result in sustained cellular growth and ultimately carcinogenesis. Due to the high abundance of Ras mutations in tumors, these proteins have been at the focus of anti-cancer treatment for decades. Of particular interest has been the medicinally most relevant isoform K-Ras. The localization of K-Ras in the cell is strongly linked to its function as a biological switch, since K-Ras enrichment at the plasma membrane is required for proper Ras signaling. The shuttling protein PDE δ regulates the cellular localization of K-Ras and thus oncogenic K-Ras signaling. PDE δ features a large hydrophobic binding pocket, which accommodates the prenyl group of proteins like K-Ras in the cell. In contrast to K-Ras, PDE δ turned out to be readily druggable and inhibitors of the K-Ras-PDE δ interaction should impair oncogenic K-Ras signaling.

Identification and optimization of benzimidazole based K-Ras-PDE δ inhibitors

For the identification of small molecules targeting the K-Ras-PDE δ interaction, a high throughput assay based on the Alpha technology was employed and the highly ligand-efficient benzimidazole fragment **10** was identified. ITC experiments as well as cocrystallization of the benzimidazoles with PDE δ revealed that two benzimidazoles moieties may bind to the farnesyl-binding cavity (Figure 68, a and b). Binding of the fragment **10** was clearly enthalpy driven, consistent with the formation of two hydrogen bonds to the protein (Arg61, Tyr149). In order to increase affinity and specificity, the two benzimidazole moieties of fragment **10** were linked. The best ether-linked *bis*-benzimidazoles showed significantly improved affinities down to 16 nM and an increase of the protein melting temperature of more than 25°C. The cocrystal structure of *bis*-benzimidazole **55** with PDE δ revealed that the allyl group points to the backbone carbonyl of Cys56 (Figure 68, c). Further structure based optimization focused on targeting this carbonyl group by an additional H-bond. Therefore, the allyl group was replaced by a piperidine moiety and the bridging phenyl ether was substituted by a more flexible piperidyl ester. Gratifyingly the resulting ester-linked *bis*-benzimidazoles showed higher affinities. A cocrystal structure of (*S*)-**92** with PDE δ confirmed the additional hydrogen bond to Cys56 (Figure 68, d).

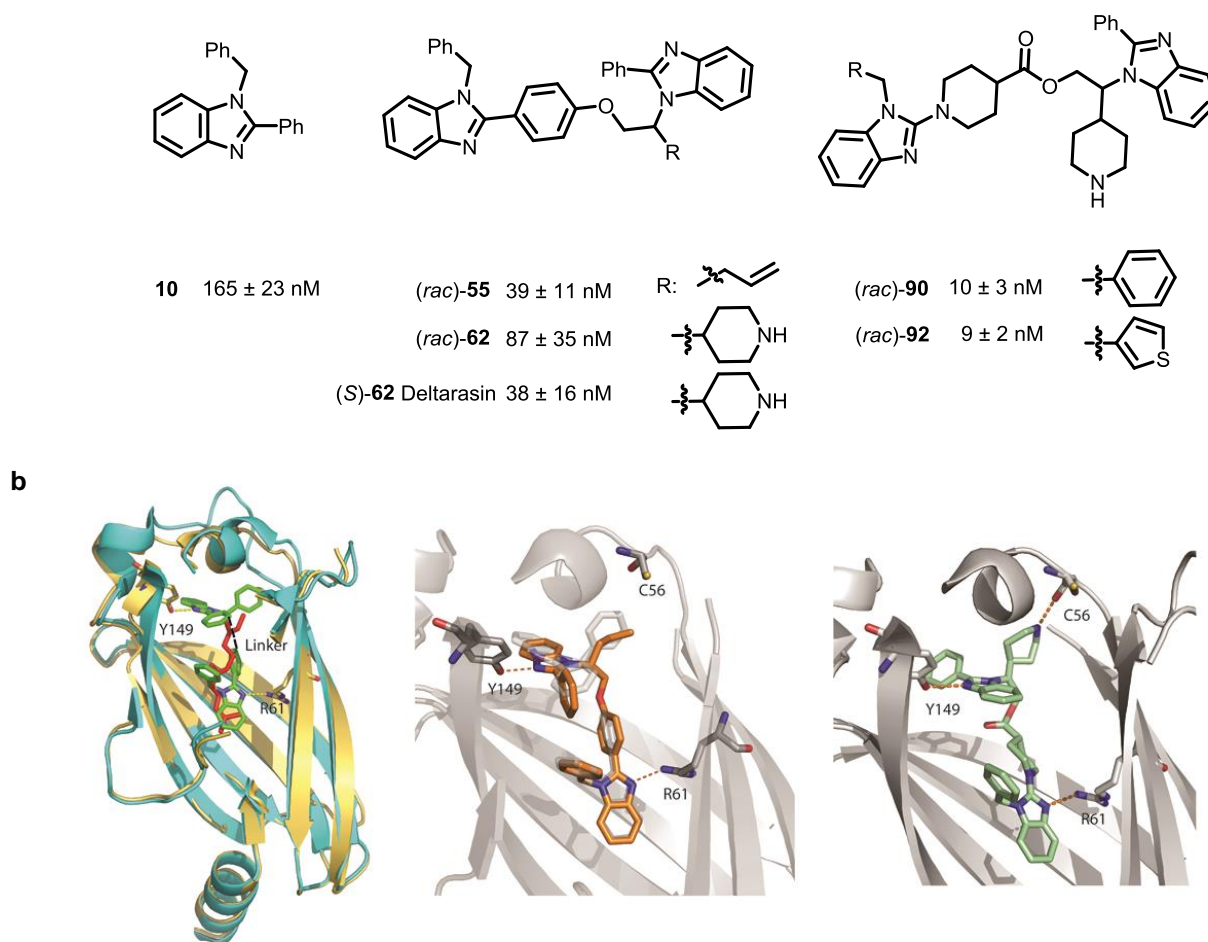


Figure 68 a) Structure and binding affinities of benzimidazole compounds as determined by displacement titrations employing Fluorescein-Atorvastatin and fluorescence polarization as readout; b) Ribbon diagram of PDE δ structure in complex with **10** (yellow), and overlay with the previously obtained crystal structure of farnesylated Rheb peptide with PDE δ (cyan). Benzimidazole fragment **10** (green) and farnesyl group (red) are shown as ball and sticks. Hydrogen bonding interactions between two molecules of **10** and Tyr149 and Arg61 in the cocrystal structure are highlighted; c) Structure of *(rac)*-**55** (orange sticks) in complex with PDE δ . Overlaid is the structure of two molecules of **10** (faint grey sticks) in complex with PDE δ ; d) Cocrystal structure of *(S)*-**90** with PDE δ confirms the presence of a hydrogen bond between the piperidine and the backbone carbonyl of Cys56. Cocrystal structures were obtained by Dr. Shehab Ismail.

Direct titrations of TAMRA-labeled compounds *(S)*-**62** Deltarasin and *(S)*-**92** revealed affinities for PDE δ in the single digit nanomolar range, close to the detection limit assays employing fluorescence polarization. These compounds were therefore employed in direct titrations with other lipid binding proteins, showing no interaction with UNC119a/b and Galectin 1/3. Consistent with the high affinity time resolved fluorescence anisotropy measurements revealed very slow dissociation rates with half lives in the range of hours for TAMRA-labeled *(S)*-**92**.

SPR experiments confirmed the very high affinity of ester-linked *bis*-benzimidazoles also for unlabeled benzimidazoles with affinities down to 77 pM for ester (*S*)-**90**.

Small molecule inhibition of the K-Ras-PDE δ interaction impairs oncogenic K-Ras signaling

Due to the potential instability of ester containing *bis*-benzimidazoles in the cell, the biological evaluation of this compound class was carried out with the well-soluble, ether-linked (*S*)-**62** Deltarasin. Pull down experiments with biotinylated Deltarasin revealed very strong binding to PDE δ in cell lysates. Competition experiments with biotinylated and free compound highlighted the high affinity of the benzimidazole compounds for PDE δ in cell lysates. In collaboration with the group of Prof. Bastiaens FRET-FLIM experiments were carried out in the living cell which showed that Deltarasin can break the Ras-PDE δ interaction and induce relocalization of Ras family proteins, particularly of the clinically relevant K-Ras protein. The inhibition of the K-Ras-PDE δ interaction by Deltarasin also impaired oncogenic K-Ras signaling, as judged by the decrease in ERK phosphorylation and selective growth inhibition of K-Ras dependent cells. The group of Prof. Hahn showed that Deltarasin also inhibits the growth of xenografted pancreatic carcinoma cells in nude mice.

Further structure-based optimization of small molecules targeting the prenyl binding cavity of PDE δ

Further structure-based optimization and synthesis of *bis*-benzimidazoles led to a decrease in molecular weight of the inhibitors, a decrease in hydrophobicity and an increase in ligand efficiency. In a further attempt to find other compound classes, which target PDE δ , the known inhibitor Atorvastatin was modified and binding affinity was increased by almost two orders of magnitude. Additionally high-throughput screening enabled the identification of *bis*-sulfonamides as very potent binders to PDE δ . Altogether 56 sulfonamides were tested and revealed very high affinities down to the low nanomolar range.

Allosteric release of PDE δ inhibitors by Arl2/3

Although the most potent *bis*-benzimidazoles display K_D values for PDE δ in the low nanomolar range, no inhibitor with nanomolar potency in cells could be identified. Previously it was shown that Arl2/3 actively release low affinity, farnesylated cargo proteins from PDE δ by an allosteric

displacement mechanism. Therefore, it was tested whether the Arl2/3 GTPases could also impair the binding of small molecules to PDE δ and whether these allosteric release factors may reverse the biological effect of small molecules targeting PDE δ in the cell. To investigate the effect of Arl2/3 on the high-affinity complexes between TAMRA-labeled small molecules and PDE δ , the preformed complexes were titrated with increasing concentrations of Arl2/3, making use of time-resolved fluorescence polarization measurements. In the case of TAMRA-Deltarasin both Arl2 and Arl3 were able to release the small molecule from the farnesyl binding cavity, whereas the very high-affinity TAMRA-(*S*)-**92**-PDE δ complex could only be disrupted by Arl3 in analogous experiments. These displacement titrations showed that Arl3 has a much higher binding affinity for PDE δ than Arl2 and suggested two differential roles for Arl2 and Arl3. While Arl2 regulates the localization of low-affinity Ras GTPases in the cytoplasm, Arl3 is essential for the release of high-affinity prenylated cargo like the inositol phosphatase INPP5E, which is transported to the primary cilium.

Prenyl specificity of the interaction between lipidated proteins and PDE δ

PDE δ functions as a shuttling protein for farnesylated proteins like K-Ras in the cell. The interaction with geranylgeranylated proteins however remains controversial. Within this thesis binding of prenylated peptides to PDE δ was explored and fluorescence polarization experiments revealed a slight preference (factor 2.5) of PDE δ for farnesylated over geranylgeranylated peptides. These data suggest that the selectivity is much less pronounced than previously thought.

Effect of PDE δ inhibitors on Hedgehog signaling

In a further study together with COMAS, Dortmund it was shown that PDE δ inhibition affects the differentiation of mouse embryonic mesoderm fibroblasts, and therefore down regulates Hedgehog signaling. It was reasoned that this effect may be due to the impaired transport of prenylated proteins like INPP5E to the primary cilium, since the primary cilium is a signaling hub required for correct Hedgehog signal transduction.

Rational design of high potency binders of UNC119a and UNC119b

Similar to PDE δ , the related lipid binding proteins UNC119a and UNC119b feature a large hydrophobic cavity which can be addressed by small molecules. The previously identified

APT1 inhibitor Palmostatin B was shown to bind to UNC119a/b with affinities in the low micromolar range, whereas rationally designed stapled peptides displayed affinities in the low nanomolar range. Cellular studies with these high-affinity peptides should clarify the role of UNC119a/b in the transport of lipidated protein cargo in the cytoplasm and to the primary cilium.

In summary, a novel approach for targeting oncogenic K-Ras signaling has been presented within this thesis. Rational, structure guided design resulted in the generation of highly potent inhibitors which target the prenyl binding cavity of PDE δ . The optimized inhibitors break the K-Ras-PDE δ -interaction *in vitro* and *in cellulo* and impair oncogenic K-Ras signaling. The results presented within this thesis show that Ras could potentially be druggable and that drug discovery programs aimed at oncogenic K-Ras may be successful in the long run.

6 EXPERIMENTAL SECTION

Biochemical Experiments and experiments with cell lysates

General Buffers:

5x SDS-PAGE loading buffer (0.225 M Tris-HCl pH = 6.8, 50% glycerol, 5% SDS-b. 0.05% Bromophenol Blue, 0.25 M DTT), 1x Running buffer (1 M Tris-HCl, 0.9 M HEPES, 35 mM SDS-b), 10x PBS (phosphate buffered saline, 1.37 M NaCl, 27 mM KCl, 0.1 M NaH₂PO₄, 20 mM KH₂PO₄, pH= 7.4), 10x TBS (0.2 M Tris-HCl, 1.5 M NaCl, pH = 7.4), TBST (TBS + 0.1% Tween 20), Transfer or blotting buffer (25 mM Tris-HCl, 0.2 M Glycine, MeOH / H₂O = 1/4)

Protein Expression of His₆-PDE δ

His₆-PDE δ was expressed in *E. Coli* Rossetta cells (pet28a). A 10 L expression liquid culture was cultivated from 15 LB agar plates and the expression was carried out at a temperature of 28°C until the cells reached an OD of 0.5. Kanamycin and chloramphenicol were used as selection markers. The expression temperature was lowered then to 16°C and overexpression of His₆-PDE δ was induced with IPTG. After 16 hours the cells were centrifuged and the pellet was resuspended in 20 mM Tris (pH 7.5), 150 mM NaCl, 1 mM mercaptoethanol. Cells were lysed by sonication, centrifuged and to the supernatant was added PMSF to a final concentration of 1 mM. The lysate was applied to a Ni-NTA column and washed with 5 column volumes of buffer containing 20 mM imidazole. The protein was eluted with a gradient of imidazole. Precipitation of some eluted fractions containing imidazole was observed, therefore protein solutions were diluted with imidazole-free buffer and incubated at 4°C over night. Eluted protein was concentrated and applied in 4 runs to a gelfiltration column. Eluted fractions were pooled and concentrated yielding 210 mg of protein.

Alpha-Screen with biotinylated K-Ras4B

Screening for inhibitors of the His₆-PDE δ -K-Ras4B interaction was conducted in white, non-binding 384-well plates (Corning) in a final volume of 20 μ L. For the screen a mixture of His₆-PDE δ , and biotinylated K-Ras-peptide (final concentrations 600 nM and 900 nM in HEPES 20 mM, 100 mM NaCl, 0,005% Chaps pH 7.5) were added to the 1536-well plates. Compound solutions were directly added from 10 mM DMSO stock solutions to a final concentration of 10 μ M and the resulting mixture was incubated for 30 min (For Dose response curves,

compounds were tested at concentrations between 10 μ M and 5 nM). Premixed Nickel Chelate Acceptor Beads and Streptavidin Donor Beads were added to a final concentration of 10 μ g/mL. The resulting mixture was incubated at 4°C overnight. Plates were read on a Paradigm reader (Molecular devices, Alphascreen 1536 HTS detection cartridge, temperature 29°C-33°C). Screening (COMAS) based on Alpha-technology was conducted in white, non-binding 1536-well plates (Corning) in a final volume of 6 μ L. For the screen a mixture of His₆-PDE δ , and biotinylated K-Ras-peptide (final concentrations 100 nM and 250 nM in HEPES 20 mM, 100 mM NaCl, 0,005% Chaps pH 7.5) were added to the 1536-well plates. Compound solutions were directly added from 10 mM DMSO stock solutions to a final concentration of 10 μ M and the resulting mixture was incubated for 30 min (For Dose response curves, compounds were tested at concentrations between 10 μ M and 5 nM). Premixed Nickel Chelate Acceptor Beads and Streptavidin Donor Beads were added to a final concentration of 10 μ g/mL. The resulting mixture was incubated at 4°C overnight. Plates were read on a Paradigm reader (Molecular devices, Alphascreen 1536 HTS detection cartridge, temperature 29°C-33°C).

Dose response curves using Alpha technology with biotinylated Atorvastatin:

Assays were conducted in white, non-binding 384-well plates (Corning) in a final volume of 20 μ L. Biotin-Atorvastatin and His₆-PDE δ (final concentrations 6 nM and 24 nM in HEPES 20 mM, 100 mM NaCl, 0.005% Chaps, 0.1 % BSA pH 7.5) were added to 384-well plates. Compound solutions were added and the mixture incubated for 5 h at room temperature. The same assay was also conducted by adding unlabeled small molecule first to His₆-PDE δ , followed by addition of Biotin-Atorvastatin. Premixed Nickel Chelate Acceptor Beads and Streptavidin Donor Beads were added to a final concentration of 10 μ g/mL. The resulting mixture was incubated at 4°C overnight. Plates were read then on a Paradigm reader (Molecular devices, Alphascreen 384 HTS detection cartridge,

Fluorescence polarization measurements for the determination of the binding constant K_D of fluorophore-labeled compounds

PDE δ was serially diluted in a solution containing 100 nM of TAMRA-labeled small molecules in 200 μ L PBS-buffer (containing 0.05% Chaps, 0.5% DMSO). The 96-well plates were incubated at room temperature for 3 h. The fluorescence polarization values (Ex: 530 nM, Em: 580) were read on a Safire II plate reader (Tecan, temperature ~30°C).

Data was corrected for changes in fluorescence intensity and the fraction bound was fit to a one site binding model derived from the law of mass action using K_D as the only fitting parameter.⁷⁵

Non-linear regression was performed in OriginPro 8.6.
$$FSB = \frac{A - A_{free}}{A - A_{free} + Q(A_{bound} - A)}$$

FSB=fraction bound; A_{free} : anisotropy of free fluorophore A_{bound} : anisotropy of bound fluorophore; Q : change in fluorescence intensity between free and bound state; A: observed Anisotropy

$$FSB = \frac{K_D + L_{Tot} + P - \sqrt{(K_D + L_{Tot} + P)^2 - 4L_{Tot}P}}{2L_{Tot}}$$

L_{Tot} : total concentration of fluorophore, P: protein concentration

Data for Fluorescein-Atorvastatin were fit analogously.

All fluorescence polarization experiments were run in at least two different sets of experiments using triplicate determinations unless indicated otherwise.

Displacement titrations of labeled Atorvastatin-probe for the determination of K_D values:

To fluorescein-labeled Atorvastatin **15** (24 nM) and His₆-tagged PDE δ (40 nM) in 200 μ L PBS-buffer (containing 0.05% Chaps, 1% DMSO) in a black, non-binding 96-well plate (Greiner) the small molecule was added from a DMSO stock solution. The resulting solution was serially diluted, holding the concentrations of **15**, PDE δ and DMSO constant. The sealed plates were shaken overnight at room temperature and centrifuged at the beginning of the next day. The fluorescence polarization values (Ex: 470 nm, Em: 525 nm) were read on a Safire II plate reader (Tecan, temperature 28-32°C).

For the fitting of the data to a competition model the exact mathematical solution derived from the law of mass action was used as described by Roehrl *et al.*¹²² Fraction bound data was fit using KD2 as the only fitting parameter and total ligand concentration as independent variable (OriginPro8.6, function codec from origin).

$$FSB = \frac{2 * (\sqrt{(KD1 + KD2 + LST + LT - RT)^2 - 3 * ((LT - RT) * KD1 + (LST - RT) * KD2 + KD1 * KD2)}) * \cos(\arccos((-2 * (KD1 + KD2 + LST + LT - RT)^3 + 9 * (KD1 + KD2 + LST + LT - RT) * ((LT - RT) * KD1 + (LST - RT) * KD2 + KD1 * KD2) - 27 * (-KD1 * KD2 * RT)) / (2 * \sqrt{((KD1 + KD2 + LST + LT - RT)^2 - 3 * ((LT - RT) * KD1 + (LST - RT) * KD2 + KD1 * KD2))^3})) / 3) - (KD1 + KD2 + LST + LT - RT)) / (3 * KD1 + 2 * \sqrt{(KD1 + KD2 + LST + LT - RT)^2 - 3 * ((LT - RT) * KD1 + (LST - RT) * KD2 + KD1 * KD2)})}$$

$$RT) * KD2 + KD1 * KD2)) * \cos(\arccos((-2 * (KD1 + KD2 + LST + LT - RT)^3 + 9 * (KD1 + KD2 + LST + LT - RT) * ((LT - RT) * KD1 + (LST - RT) * KD2 + KD1 * KD2) - 27 * (-KD1 * KD2 * RT)) / (2 * \sqrt{((KD1 + KD2 + LST + LT - RT)^2 - 3 * ((LT - RT) * KD1 + (LST - RT) * KD2 + KD1 * KD2))^3})) / 3) - (KD1 + KD2 + LST + LT - RT)).$$

FSB: Fraction bound of fluorescent probe

KD1: Binding constant of fluorescent probe determined from direct titration

KD2: Fitting parameter (Binding constant of unlabeled competitor)

LST: Total concentration of unlabeled small molecule competitor

RT: Total protein concentration

For the fitting of data to a competition model with cooperative binding of two benzimidazole fragments the program Scientist 3.0 was used. An experimental system was defined as a series of partial equations including the equilibrium relationships between the various species. Anisotropy data was converted to fraction bound and fitting was carried out in analogy to a previously described set of equilibrium relationships by Goody and coworkers.¹²³

$$K_{D1} = \frac{[A][PDED_f]}{[APDED]}$$

$$K_{D2} = \frac{[L^2][PDED_f]}{[LPDED]}$$

A: equilibrium concentration of free fluorophore

L: equilibrium concentration of free ligand

APDED: equilibrium concentration of bound fluorescent probe

LPDED: equilibrium concentration of bound small molecule

PDEDf: equilibrium concentration of free protein

This model was used (together with equations describing the mass balance) to numerically simulate the FSB of fluorophore and compared with the experimental data.

Scientist input file:

```
//          Micromath          Scientist          Model          File
IndVars:                                     LST
DepVars:                                     A,L,APDED,LPDED,PDEDf,FSB
```

Params:

ATOT,PDED,KD1,KD2

LPDED=

$L^2 * PDEDf / KD2$

$APDED = A * PDEDf / KD1$

$ATOT = A + APDED$

$LST = L + LPDED$

$PDED = PDEDf + APDED + LPDED$

$0 < A < ATOT$

$0 < L < LST$

$0 < PDEDf < PDED$

$FSB = 1 - A / ATOT$

$LST = 0$

Kinetic experiments using TAMRA-labeled benzimidazoles

To labeled small molecule (33 nM) and His₆-tagged PDE δ (33 nM) in 300 μ L PBS-buffer in a black, non-binding 96-well plate (Greiner) was added a 20 fold excess of unlabeled small molecule from a DMSO stock solution (final DMSO concentration 0.3%). DMSO was used as control. The fluorescence polarization values (Ex: 530 nm, Em: 580 nm) were read on a Safire II plate reader (Tecan, temperature 28-32°C). Plates were shaken in between measurements and polarization values were read at appropriate time intervals.

Displacement titrations of TAMRA-labeled-probes with GppNHp-loaded Arl2/3

To labeled small molecule (33 nM) and His₆-tagged PDE δ (33 nM) in 250 μ L Tris-Buffer (20 mM Tris (pH 7.5), 150 mM NaCl, 5 mM MgCl₂) in a black, non-binding 96-well plate (Greiner) was added GppNHp-loaded Arl2/3 from a concentrated stock solution (200 μ M). The mixture was serially diluted with respect to Arl2/3 holding the concentration of labeled small molecule and PDE δ constant. The proteins Arl2/3 were provided by Dr Shehab Ismail.

Kinetic experiments using TAMRA-labeled benzimidazoles in the presence of Arl2

To labeled small molecule (33 nM), His₆-tagged PDE δ (33 nM) and Arl2 in 300 μ L Tris-Buffer (20 mM Tris (pH 7.5), 150 mM NaCl, 5 mM MgCl₂) in a black, non-binding 96-well plate (Greiner) was added a 20 fold excess of unlabeled small molecule from a DMSO stock solution (final DMSO concentration 0.3%). The fluorescence polarization values (Ex: 530 nm, Em: 580 nm) were read on a Safire II plate reader (Tecan, temperature 28-32°C). Plates were shaken in between measurements and polarization values were read at appropriate time intervals.

Isothermal titration calorimetry

Titration were carried out on an iTC₂₀₀ calorimeter (MicroCal Inc). PDE δ protein (280 μ M) was titrated to small molecule (30 μ M) in 50 mM Tris, pH 7.5, 150 mM NaCl containing a final amount of 5% DMSO. Titrations were carried out at 25°C and data were fit by using a single site binding model as implemented in the software of the instrument supplier.

SPR experiments:

SPR experiments were carried out by Biaffin GmbH, Kassel. GST-PDE δ was used for site-directed affinity capture of the GST fusion construct. A second anti-GST capture surface was

used as reference. For reversible immobilization of GST-PDE δ running buffer (see below) containing 500 mM NaCl and 0.05% Tween 20 was used to minimize/prevent aggregation on the chip surface. Experiments were carried out at 35°C using 20 mM Tris (pH 7.4), 150 mM NaCl, 20 μ M EDTA, 0.005% Tween 20, 5% DMSO as running buffer on a Biacore T100 instrument.

T_m-Shift assays

Protein melting points in the presence of small molecules were detected by CD-spectroscopy (Jasco J-815, 0.1 cm path length cell). Melting curves were run in PBS-buffer (1% DMSO) containing 30 μ M of small molecule and 25 μ M PDE δ . Due to absorption of DMSO unfolding of PDE δ was detected at 232 nm (heating rate 1°C per minute, starting from 30°C).

Pull-down experiments with cell lysates

MDCK cells were provided by Philipp Kuchler. The cells were washed 3x with cold PBS puffer and then treated with lysis buffer (25 mM sodium hydrogenphosphate, 150 mM NaCl, 5 mM MgCl, 300 mM sucrose, 1 mM EDTA, protease inhibitor cocktail) for 15 min, transfered into eppendorf cups, sonicated for 10 min and repeatedly pressed through a syringe needle. The heterogeneous mixture was centrifuged for 30 min at 13000 rpm and the supernatant collected. The protein concentration was measured to be between 0.5-1.5 mg/mL. Lysates were frozen at -80°C and used within a month.

For pull down experiments 500 μ L Streptavidin beads (Pierce) were washed with PBS buffer, incubated with 500 μ L 10 μ M Biotin-Deltarasin in PBS buffer for 2 h at room temperature and then washed 4 x with PBS buffer containing 0.05% Chaps. The beads were incubated with 500 μ L cell lysate for 2h. For competition experiments the cell lysate was preincubated with an appropriate concentration of the soluble inhibitor (up to 10 μ M) for 10 min and treated with the beads containing the immobilized compound. The beads were washed 5x with PBS buffer containing 0.05% Chaps.

The immobilized proteins were eluted using boiling SDS sample buffer and separated by SDS-PAGE. Proteins were transfered to PVDF membranes by electroblotting. Membranes were blocked with 5% milk in Tris buffered saline/ Tween (TBST) buffer for 15 min, washed with TBST buffer and treated with PDE δ antibody for 1.5 h at room temperature (Santa Cruz, N15,

1:500 in 5% milk). After washing with TBST the membrane was incubated with HRP coupled secondary anti-goat antibody for 1 h at room temperature. Chemiluminescence was observed with a licor odyssey machine employing Super Signal West Pico solution.

Molecular modelling:

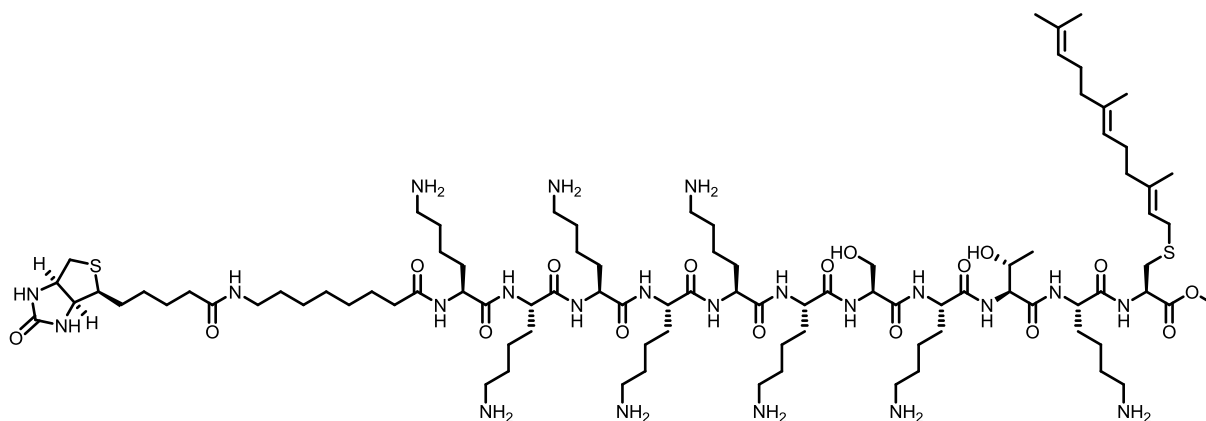
Molecular modelling experiments were carried out with the Maestro 9.1 suite (Schrödinger). Both ligand and receptor flexibility were taken into account by using receptor docking (Glide) in combination with the protein structure prediction embedded in the program Prime. For protein preparation, the program Protein Preparation Wizard embedded in the Schrödinger Maestro suite was used to prepare the PDE δ cocrystal structure before carrying any out docking experiments. Water molecules were removed from the protein crystal structure, hydrogen atoms were added and resulting structure was refined by OPLS2005 force-field. The minimization was ended when the RMSD reached 0.18 Å. Then, the Receptor Grid Preparation option present in Glide was used to generate the protein grid that was subsequent utilized in docking experiments. The Van der Waals radius scaling factor was set to 0.5 with a partial charge cutoff of 0.25. In the Constraints options, tyrosine (Y149) and arginine (R61) were selected as sites for hydrogen bonding. Ligand preparation for docking was carried out with LigPrep in Maestro 9.1 and the OPLS_2005 force-field. Epika was used to generate possible states at target pH 7.0 ± 4.0 . Desalt, Generate tautomers and Retain specified chiralities were selected. In case of rings, 20 low energy ring conformations were generated per ligand. Ligand docking options in Glide were used for the first round of docking experiments. Under Setting, XP (extra precision), Dock flexibly, Sample nitrogen inversions, Sample ring conformation and Epik state penalties to docking score were selected, amide bonds were penalized for nonplanar conformation. Under the Ligands section, the Van der Wals radius scaling factor was set to 0.5 and the docking was set to match at least 1 out of two constraints. Several poses were generated and cocrystallized compounds were redocked and analysed in terms of overlay with the X-ray structure. Then, all poses with a GScore of more than two orders of magnitude lower than that of the cocrystallized compound were discarded. Furthermore, the remaining poses were visually inspected and those with significant clashes were not considered any further. If the clash was found in a region where the protein was expected to be flexible the pose was however taken account.

Chemical Synthesis

General considerations. NMR spectroscopic data were recorded on a 400 MHz or 600 MHz instrument at room temperature. NMR spectra were calibrated to the solvent signals of deuterated DMSO- d_6 or $CDCl_3$. The following abbreviations are used to indicate the signal multiplicity: s (singlet), d (doublet), t (triplet), q (quartet), br (broad), m (multiplet). Analytical HPLC-MS data were recorded on a HPLC system with a C18 reverse column coupled to an ESI spectrometer, flow rate: 1.0 mL/min; time: 15 min; solvent A: 0.1% HCOOH in water, Solvent B: 0.1% HCOOH in Acetonitrile; 1 min 10% B, in 10 min to 100% B. High resolution mass spectra (HR-MS) were measured using electrospray ionization (ESI). Chiral HPLC analysis was performed on a Chiralpak IC Column 250 mm x 4.6 mm, flow rate: 0.5 mL/min; ethanol in *iso*-hexane. Preparative HPLC separations were carried out using a reversed-phase C18 column (RP C18, flow 20.0 mL/min, solvent A: 0.1% TFA in water, solvent B: 0.1% TFA in Acetonitrile, from 10 % B to 100 % B. In addition to analytical HPLC, U-HPLC was employed using the following methods indicated for each compound: Column: Acquity UPLC® BEH 18, 1.7 μ m, 2.1 x 50mm, 5min_A:flow 0.5mL/min,0.0min: 95% (water+0.05%TFA) + 5% (ACN + 0.05% TFA),0.5min: 95% (water+0.05%TFA) + 5% (ACN + 0.05% TFA),2.5min: 0% (water+0.05%TFA) + 100% (ACN + 0.05% TFA), 5.0min: 0% (water+0.05%TFA) + 100% (ACN + 0.05% TFA);5min_B:flow 0.5mL/min,0.0min: 100% (water+0.05%TFA) + 0% (ACN + 0.05% TFA),0.1min: 100% (water+0.05%TFA) + 0% (ACN + 0.05% TFA), 5.0min: 0% (water+0.05%TFA) + 100% (ACN + 0.05% TFA);10min_C:flow 0.5mL/min,0.0min: 95% (water+0.05%TFA) + 5% (ACN + 0.05% TFA), 0.5min: 95% (water+0.05%TFA) + 5% (ACN + 0.05% TFA), 8.0min: 0% (water+0.05%TFA) + 100% (ACN + 0.05% TFA), 10.0min: 0% (water+0.05%TFA) + 100% (ACN + 0.05% TFA);10min_D:flow 0.5mL/min,0.0min: 100% (water+0.05%TFA) + 0% (ACN + 0.05% TFA) 0.1min: 100% (water+0.05%TFA) + 0% (ACN + 0.05% TFA)10.0min: 0% (water+0.05%TFA) + 100% (ACN + 0.05% TFA. Atorvastatin was purchased from Sequoia Reseach Products. Biotin-PEG-COOH and Biotin-PEG-NH₂ were purchased from PolyPeptide Group. The library of simple benzimidazoles and the *bis*-sulfonamides shown in the supporting information were purchased from Enamine and Chemdiv. All other commercially available chemicals were purchased from Alfa Aesar, Aldrich, Acros, ABCR, TCI, Chess, MerckMillipore, Strem. Peptides **171a/b** were synthesized by Sasikala Thavam. TAMRA-Palmostatin and Palmostatin were synthesized by Dr. Marion Rusch, Stapled peptides **184** and **185** were synthesized by Philipp Cromm. Compounds synthesized by LDC and Taros are marked with asterisks in the corresponding tables. All biochemically tested

compounds, whether synthesized or purchased, possess a purity of at least 95%, as measured by LC-MS.

Synthesis of biotinylated, C-terminal K-Ras4B peptide

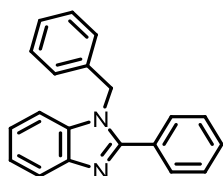


Biotinylated K-Ras4B peptide 9 The C-terminal K-Ras4B peptide was synthesized by means of solid-phase peptide synthesis (scale: 0.1 mmol, loading 0.5 mmol/g trityl resin) similar to a previously described procedure employing immobilized Fmoc-Lys-Cys-Far-OMe.⁴⁰ Fmoc cleavage was achieved using 5 mL of 20% piperidine, 2% DBU in DMF twice for 10 minutes. Subsequently the resin was washed 5 times with DMF. All amino acids were coupled twice employing 4 eq of amino acid, 4 eq of HCTU and 8 eq of DIPEA in 5 ml DMF. Double couplings were carried out at 60°C for 30 minutes each cycle. The resulting N-terminal amino acid was coupled with 5eq Biotin-NHS ester at room temperature in DMF. Cleavage from the solid support was performed by treating the resin with 10 mL of 1 % TFA in dry DCM containing 2 % TES for for 1 hour, then with 1.5 % TFA for 1 h and with 2% TFA in DCM for an additional hour. After each treatment the resin was washed DCM/MeOH 1:1 and MeOH. Finally toluene was added to the mixture and the solvent was evaporated under reduced pressure. The resulting crude product was dissolved in a minimal amount of MeOH, filtered through a syringe filter and slowly added to an ice-cold solution of Et₂O. The precipitate was dissolved in DMSO and after purification by preparative HPLC using a C18 column the peptide was obtained (40 mg, 20%). ¹H NMR (600 MHz, DMSO-*d*₆) δ 8.51 – 7.68 (m, 31H), 6.42 (s, 1H), 6.38 (s, 1H), 5.19 – 5.01 (m, 3H), 4.52 – 4.10 (m, 11H), 4.01 – 3.94 (m, 1H), 3.66 – 3.53 (m, 5H), 3.22 – 2.94 (m, 4H), 2.90 – 2.59 (m, 18H), 2.19 – 1.85 (m, 8H), 1.77 – 1.14 (m, 64H), 1.02 (d, *J* = 6.2 Hz, 3H). ¹³C NMR (151 MHz, DMSO-*d*₆) δ 173.45, 172.74, 172.59, 172.23, 172.20, 172.15, 171.64, 170.70, 170.20, 163.44, 159.59, 159.39, 159.18, 158.97, 139.40,

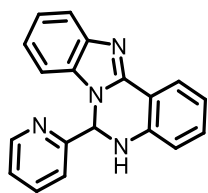
135.27, 131.33, 124.76, 124.31, 120.73, 120.68, 118.75, 116.77, 67.33, 62.50, 61.75, 59.91, 58.49, 56.10, 55.59, 53.29, 53.22, 52.97, 52.68, 35.89, 35.81, 32.18, 32.05, 31.95, 31.81, 31.65, 29.84, 29.46, 29.33, 29.16, 28.88, 28.72, 27.29, 27.25, 27.01, 26.85, 26.54, 26.14, 26.04, 25.87, 23.11, 22.90, 22.70, 19.99, 19.91, 18.20, 16.46, 16.41. LC-MS (ESI): calcd for $C_{92}H_{170}N_{22}O_{17}S_2$: 960.63506 $[M+2H]^{2+}$, found 960.97 $[M+2H]^{2+}$, $R_t = 4.80$ min; HR-MS found 960.63545 $[M+2H]^{2+}$. $[\alpha]_D^{20}$: -66.5° ($c=0.72$, H_2O).

General Procedure A for the *N*-Alkylation of benzimidazoles

To a suspension of the benzimidazole in acetonitrile (1 mL/ 0.1 mM benzimidazole) was added caesium carbonate (1.5 eq) and the corresponding alkyl bromide (1.05 eq). The reaction mixture was stirred at room temperature for 1-3 hours and after this time it was concentrated in vacuo. The residue was suspended in a mixture of DCM and sat. $NaHCO_3$ (vol % 50:50, 10 mL/0.1 mmol benzimidazole). The aqueous layer was extracted with DCM (2 x, 10 mL/0.1 mmol benzimidazole). The combined organic layers were dried over Na_2SO_4 , filtered and the solvent was removed under reduced pressure. The crude product was purified by flash chromatography as described below.

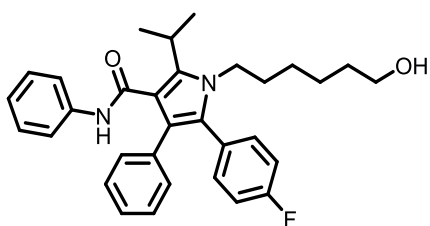


1-Benzyl-2-phenyl-1H-benzo[d]imidazole (10) The *N*-benzylation of 2-phenyl benzimidazole (185 mg, 0.92 mmol) was performed following the general procedure described above. The crude product was purified by flash column chromatography (gradient of cyclohexane:ethylacetate 10:1 to 1:1) to yield the desired compound (212 mg, 0.74 mmol, 86%). 1H NMR (400 MHz, $DMSO-d_6$) δ 7.76 – 7.67 (m, 3H), 7.57 – 7.47 (m, 3H), 7.47 – 7.42 (m, 1H), 7.31 – 7.16 (m, 5H), 6.98 (d, $J = 7.3$ Hz, 2H), 5.57 (s, 2H). ^{13}C NMR (101 MHz, $DMSO-d_6$) δ 153.94, 143.37, 137.60, 136.57, 130.84, 130.50, 129.72, 129.45, 128.15, 126.77, 123.37, 122.89, 119.95, 111.78, 48.15. LC-MS (ESI): calcd for $C_{20}H_{16}N_2$: 285.13863 $[M+H]^+$, found 285.01 $[M+H]^+$, $R_t = 5.90$ min; HR-MS found 285.13883 $[M+H]^+$.

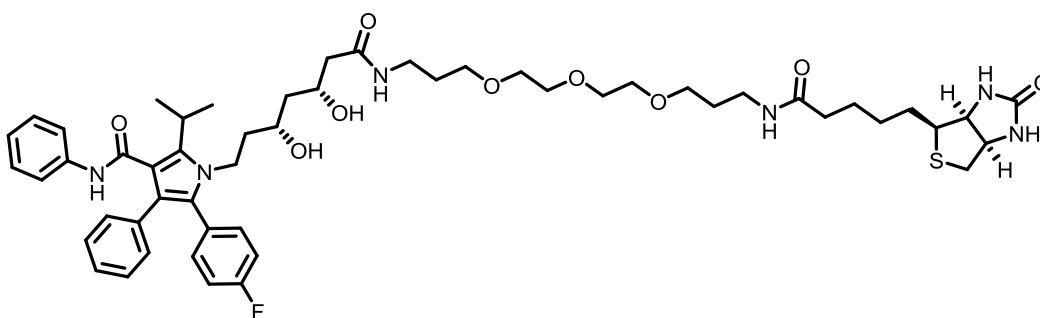


6-Pyridyl-5,6-dihydrobenzo[4-5]imidazo[1,2-c]quinazoline (12) A mixture of 2-pyridinecarboxaldehyde (99 mg, 0.93 mmol) and 2-(2-aminophenyl)-1*H*-benzimidazole (200 mg, 0.93 mmol) was dissolved in acetic acid (2 mL). The reaction mixture was stirred at 65°C for 16 h. After cooling to room temperature the reaction mixture was diluted with DCM (15 mL) and a sat. NaHCO₃ – solution was slowly added until a basic pH was reached. The aqueous layer was extracted with DCM (2 x 15 mL). The combined organic phases were dried over Na₂SO₄, filtered and the solvent was removed under reduced pressure. The crude product was purified by flash column chromatography (gradient of DCM: MeOH 50:1 to 5:1) to yield the desired compound (196 mg, 0.66 mmol, 71%). ¹H NMR (400 MHz, DMSO-*d*₆) δ 8.51 – 8.35 (m, 1H), 7.92 (d, *J* = 7.7 Hz, 1H), 7.73 (td, *J* = 6.1, 3.0 Hz, 1H), 7.69 (d, *J* = 2.0 Hz, 1H), 7.65 – 7.59 (m, 1H), 7.35 – 7.30 (m, 1H), 7.30 – 7.24 (m, 1H), 7.24 – 7.06 (m, 5H), 6.84 (d, *J* = 8.2 Hz, 1H), 6.81 – 6.70 (m, 1H). ¹³C NMR (101 MHz, DMSO-*d*₆) δ 159.05, 150.14, 147.51, 144.46, 143.64, 138.10, 133.69, 132.20, 125.25, 124.61, 122.85, 122.70, 120.87, 119.25, 118.70, 115.36, 112.70, 111.07, 69.04. LC-MS (ESI): calcd for C₁₉H₁₄N₄: 299.12912 [M+H]⁺, found 299.01 [M+H]⁺, R_t = 2.70 min; HR-MS found 299.12929 [M+H]⁺.

Synthesis of Atorvastatin derivatives

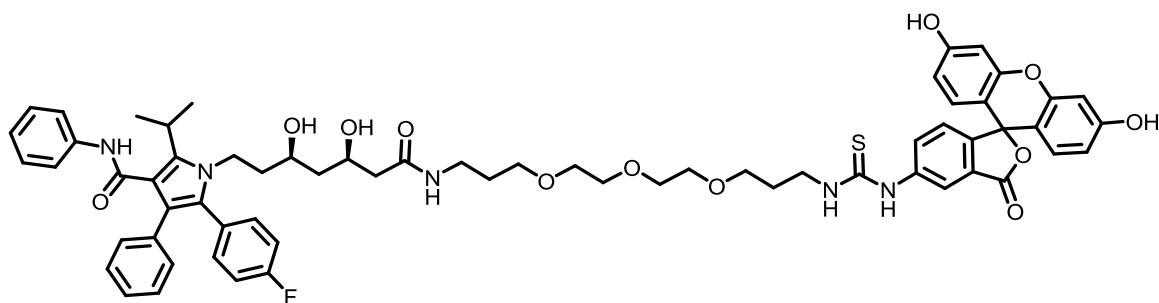
**5-(4-fluorophenyl)-1-(6-hydroxyhexyl)-2-isopropyl-N,4-diphenyl-1H-pyrrole-3-**

carboxamide 14 To a suspension of commercially available 2-[2-(4-Fluorophenyl)-2-oxo-1-phenylethyl]-4-methyl-3-oxopentanoic acid phenylamide (Atorvastatin derivative M, **13**, 100 mg, 0.24 mmol) in a mixture of toluene: heptane: THF 6:5:1 (5 mL) was added 6-aminohexan-1-ol (168 mg, 1.4 mmol) and acetic acid (0.2 mL). The resulting reaction mixture was heated under reflux conditions for 16 h. The reaction mixture was allowed to cool to room temperature. The reaction mixture was concentrated under reduced pressure, diluted with saturated sodium hydrogen carbonate solution and extracted with DCM (3x 20 mL). The combined organic phases were dried (Na₂SO₄), filtered and concentrated to dryness. Purification by automated flash chromatography (gradient cyclohexane : ethyl acetate 10:1 to 1:1) afforded the desired product (60 mg, 58%). ¹H NMR (400 MHz, CDCl₃) δ 7.16 – 7.02 (m, 9H), 7.02 – 6.88 (m, 5H), 6.79 (s, 1H), 3.77 – 3.70 (m, 2H), 3.52 – 3.39 (m, 3H), 1.50 – 0.75 (m, 15H). ¹³C NMR (101 MHz, CDCl₃) δ 164.91, 163.62, 161.17, 141.51, 138.57, 134.83, 133.37, 133.29, 130.67, 128.96, 128.80, 128.60, 128.57, 128.47, 126.69, 123.61, 121.84, 119.70, 115.57, 115.36, 62.80, 44.74, 32.56, 31.68, 26.66, 26.41, 25.29, 21.87. LC-MS (ESD): calcd for C₃₂H₃₅N₂O₂F 499.27553, found 499.27540 [M+H]⁺.



1-((23R,25R)-23,25-Dihydroxy-5,21-dioxo-1-((3aS,4S,6aR)-2-oxohexahydro-1H-thieno[3,4-d]imidazol-4-yl)-10,13,16-trioxa-6,20-diazaheptacosan-27-yl)-5-(4-fluorophenyl)-2-isopropyl-N,4-diphenyl-1H-pyrrole-3-carboxamide (15) To Atorvastatin Calcium (25 mg, 0.043 mmol) in DMF (1 mL) was added PyBob (39 mg, 0.08 mmol), DIPEA (72 μL, 0.4 mmol)

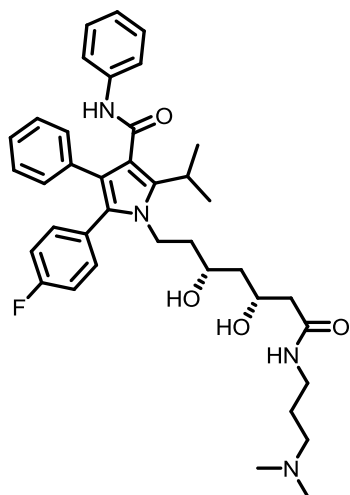
and Biotin-PEG₃-NH₂*TFA (126 mg, 0.23 mmol). The reaction mixture was stirred at room temperature for 18 h and then directly applied to reverse phase chromatography to yield the desired product as a TFA salt (20 mg, 41%). ¹H NMR (600 MHz, DMSO-*d*₆) δ 9.75 (s, 1H), 7.79 – 7.66 (m, 2H), 7.48 (d, *J* = 7.9 Hz, 2H), 7.25 – 7.13 (m, 6H), 7.08 – 7.03 (m, 4H), 7.00 – 6.94 (m, 2H), 4.28 (dd, *J* = 7.6, 4.7 Hz, 1H), 4.10 (dd, *J* = 7.7, 4.4 Hz, 1H), 3.53 – 3.47 (m, 5H), 3.46 – 3.41 (m, 4H), 3.39 – 3.33 (m, 4H), 3.24 – 3.18 (m, 1H), 3.10 – 3.01 (m, 5H), 2.82 – 2.77 (m, 1H), 2.13 – 2.08 (m, 2H), 2.02 (t, *J* = 7.4 Hz, 2H), 1.65 – 1.54 (m, 6H), 1.53 – 1.37 (m, 5H), 1.37 – 1.33 (m, 6H), 1.31 – 1.23 (m, 3H). ¹³C NMR (151 MHz, dms) δ 172.59, 171.25, 166.82, 163.37, 161.56, 159.12, 158.95, 140.11, 136.61, 135.58, 134.05, 129.82, 129.10, 128.29, 127.96, 126.11, 123.33, 121.26, 120.06, 116.10, 70.43, 70.20, 68.78, 68.75, 66.67, 66.47, 61.73, 59.88, 56.09, 44.46, 44.26, 36.40, 35.89, 30.08, 30.02, 28.89, 28.71, 26.33, 25.97, 22.98. LC-MS (ESI): calcd for C₅₃H₇₁N₆O₉FS: 987.50600 [M+H]⁺, HR-MS found: 987.50543.



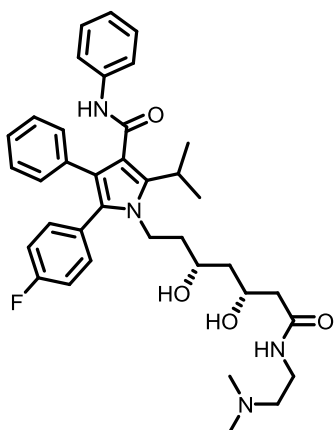
1-

((19R,21R)-1-(3',6'-Dihydroxy-3-oxo-3H-spiro[isobenzofuran-1,9'-xanthene]-5-ylamino)-19,21-dihydroxy-17-oxo-1-thioxo-6,9,12-trioxa-2,16-diazatricosan-23-yl)-5-(4-fluorophenyl)-2-isopropyl-N,4-diphenyl-1H-pyrrole-3-carboxamide (16) To Atorvastatin (20 mg, 35 μmol) in DMF (200 μL) was added DIPEA (24 μL, 140 μmol), FITC-PEG₃-NH₂¹²⁴ (90 mg, 148 μmol) and PyBOP (27 mg, 50 μmol). The reaction mixture was stirred for 36 hours and then directly applied to a reverse phase C-18 column (gradient water: acetonitrile 9:1 to 1:5 containing 0.1% TFA) to yield fluorescein-labeled atorvastatin (17 mg, 15 μmol, 41%). ¹H NMR (600 MHz, DMSO-*d*₆) δ 9.89 (s, 1H), 9.77 (s, 1H), 8.19 (s, 1H), 8.05 (s, 1H), 7.75 (t, *J* = 5.6 Hz, 1H), 7.69 (s, 1H), 7.47 (d, *J* = 8.0 Hz, 2H), 7.24 – 7.13 (m, 8H), 7.07 – 7.01 (m, 4H), 6.99 – 6.92 (m, 2H), 6.66 – 6.63 (m, 2H), 6.59 – 6.52 (m, 4H), 3.94 – 3.87 (m, 1H), 3.79 (dd, *J* = 11.9, 7.1 Hz, 1H), 3.75 – 3.68 (m, 2H), 3.24 – 3.15 (m, 2H), 3.10 – 2.98 (m, 3H), 2.09 (d, *J* = 6.3 Hz, 2H), 1.78 (p, *J* = 6.5 Hz, 2H), 1.64 – 1.53 (m, 4H), 1.53 – 1.43 (m, 1H), 1.41 – 1.30 (m, 8H), 1.28 – 1.17 (m, 2H). ¹³C NMR (151 MHz, DMSO-*d*₆) δ 171.26, 169.20, 166.81, 161.35, 160.14, 152.53, 136.57, 135.55, 129.79, 129.68, 129.32, 129.11, 128.30, 127.93,

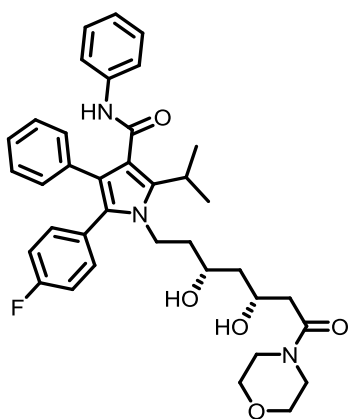
126.03, 123.65, 121.22, 120.04, 118.06, 116.11, 115.96, 113.25, 110.37, 102.88, 70.42, 70.39, 70.23, 70.19, 68.73, 66.63, 66.46, 44.45, 44.26, 41.48, 39.38, 36.36, 29.94, 29.19, 22.98; LC-MS (ESI): calcd for $C_{64}H_{68}FN_5O_{12}S$: 1150.46420 $[M+H]^+$, found: 1150.21 $[M+H]^+$, $R_t = 8.81$ min; HR-MS found 1151.46229 $[M+H]^+$.



1-((3R,5R)-7-(3-(Dimethylamino)propylamino)-3,5-dihydroxy-7-oxoheptyl)-5-(4-fluorophenyl)-2-isopropyl-N,4-diphenyl-1H-pyrrole-3-carboxamide (17) To Atorvastatin Calcium (10 mg, 0.017 mmol) in DMF (0.3 mL) was added N1,N1-dimethylpropane-1,3-diamine (67 μ L, 0.54 mmol) and PyBob (10 mg, 0.019 mmol). The reaction mixture was stirred at room temperature for 18 h and then directly applied to reverse phase chromatography to yield the product (7 mg, 61%) as a TFA salt. 1H NMR (600 MHz, DMSO- d_6) δ 9.76 (s, 1H), 9.35 (s, 1H), 7.93 (t, $J = 5.8$ Hz, 1H), 7.48 (d, $J = 7.8$ Hz, 2H), 7.24 – 7.14 (m, 5H), 7.08 – 7.02 (m, 4H), 7.00 – 6.94 (m, 2H), 4.70 (s, 1H), 4.62 (s, 1H), 3.96 – 3.88 (m, 1H), 3.86 – 3.80 (m, 1H), 3.77 – 3.69 (m, 1H), 3.54 – 3.48 (m, 1H), 3.24 – 3.16 (m, 1H), 3.14 – 3.01 (m, 2H), 2.98 (t, $J = 7.3$ Hz, 2H), 2.73 (s, 6H), 2.16 – 2.05 (m, 2H), 1.76 – 1.65 (m, 2H), 1.64 – 1.56 (m, 1H), 1.53 – 1.45 (m, 1H), 1.43 – 1.37 (m, 1H), 1.35 (d, $J = 7.0$ Hz, 6H), 1.29 – 1.23 (m, 1H). ^{13}C NMR (151 MHz, DMSO- d_6) δ 171.92, 166.81, 161.43, 140.09, 136.58, 135.54, 134.06, 134.00, 129.79, 129.39, 129.11, 128.32, 127.94, 126.05, 123.66, 121.24, 120.05, 118.19, 116.12, 115.98, 66.59, 66.38, 55.59, 55.27, 44.56, 44.31, 42.92, 41.50, 40.72, 39.51, 35.99, 26.32, 25.11, 23.01, 22.99. LC-MS (ESI): calcd for $C_{38}H_{47}N_4O_4F$: 643.36596 $[M+H]^+$, found: 643.31 $[M+H]^+$, $R_t = 6.4$ min, HR-MS : 643.36593.

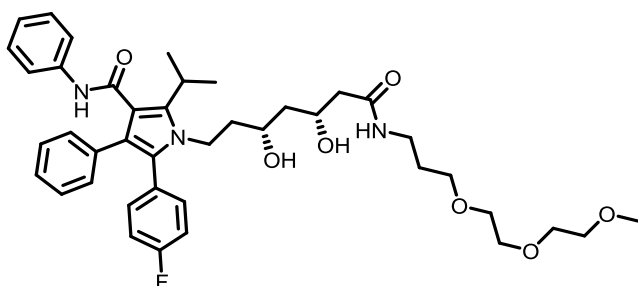


1-((3R,5R)-7-((2-(Dimethylamino)ethyl)amino)-3,5-dihydroxy-7-oxoheptyl)-5-(4-fluorophenyl)-2-isopropyl-N,4-diphenyl-1H-pyrrole-3-carboxamide (18) The compound was synthesized by Carsten Schultz-Fademrecht, LDC Dortmund. ^1H NMR (400 MHz, $\text{DMSO-}d_6$) δ 9.71 (s, 1H), 7.69 (t, $J = 5.6$ Hz, 1H), 7.45 (d, $J = 8.5$ Hz, 2H), 7.24 - 7.12 (m, 6H), 7.04 (m, 4H), 6.95 (m, 2H), 4.66 (br.s, 1H), 3.88 (m, 1H), 3.82 - 3.61 (m, 5H), 3.20 (quin, $J = 6.9$ Hz, 1H), 3.10 (q, $J = 6.3$ Hz, 2H), 2.25 (t, $J = 6.7$ Hz, 2H), 2.11 (m, 1H), 2.10 (s, 6H), 1.59 (m, 1H), 1.50 (m, 1H), 1.38 (m, 1H), 1.34 (d, $J = 7.0$ Hz, 6H), 1.27 (m, 1H). LC-MS:5min_A: $R_t = 1.92$ min, 10min_C: $R_t = 4.23$ min. LC-MS (ESI): calcd for $\text{C}_{37}\text{H}_{45}\text{N}_4\text{O}_4\text{F}$: 629.35031 $[\text{M}+\text{H}]$, HR-MS found: 629.35127.



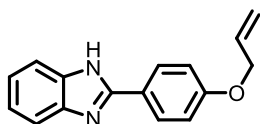
1-((3R,5R)-3,5-Dihydroxy-7-morpholino-7-oxoheptyl)-5-(4-fluorophenyl)-2-isopropyl-N,4-diphenyl-1H-pyrrole-3-carboxamide (19) The compound was synthesized by Carsten Schultz-Fademrecht, LDC Dortmund. ^1H NMR (400 MHz, CDCl_3) δ 7.21 - 7.13 (m, 9H), 7.06 (d, $J = 8.0$ Hz, 2H), 6.99 (m, 3H), 6.86 (s, 1H), 4.59 (br.s, 1H), 4.23 - 4.07 (m, 2H), 3.94 (m, 1H), 3.77 (m, 1H), 3.66 (m, 4H), 3.64 - 3.54 (m, 4H), 3.40 (t, $J = 4.9$ Hz, 2H), 2.31 (m, 2H), 1.65 (m, 2H), 1.54 (d, $J = 7.1$ Hz, 6H), 1.47 (m, 1H), 1.18 (dt, $J = 14.2$ Hz, $J = 2.1$ Hz, 1H). LC-

MS: 5min_A: $R_t=2.22\text{min}$, 10min_C: $R_t=5.02\text{min}$. LC-MS (ESI): calcd for $\text{C}_{37}\text{H}_{42}\text{N}_3\text{O}_5\text{F}$: 628.31867 [M+H], HR-MS found: 628.31974.

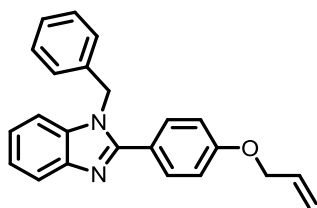


1-((15R,17R)-15,17-Dihydroxy-13-oxo-2,5,8-trioxa-12-azanonadecan-19-yl)-5-(4-fluorophenyl)-2-isopropyl-N,4-diphenyl-1H-pyrrole-3-carboxamide (20) The compound was synthesized by Carsten Schultz-Fademrecht, LDC Dortmund. ^1H NMR (400 MHz, CDCl_3) δ 7.20 - 7.10 (m, 9H), 7.06 (d, $J = 7.9$ Hz, 2H), 7.02 - 6.95 (m, 3H), 6.90 (s, 1H), 6.77 (t, $J = 5.3$ Hz, 1H), 4.83 (br.s, 1H), 4.11 (m, 2H), 3.92 (m, 1H), 3.73 (m, 1H), 3.65 - 3.51 (m, 12H), 3.36 (q, $J = 5.9$ Hz, 2H), 3.54 (s, 3H), 2.24 (m, 2H), 1.75 (quin, $J = 6.0$ Hz, 2H), 1.70 - 1.57 (m, 2H), 1.53 (d, $J = 7.1$ Hz, 6H), 1.45 (m, 1H), 1.25 (d, $J = 14.2$ Hz, 1H). LC-MS: 5min_A: $t_R=2.21\text{min}$, 10min_C: $t_R=5.02\text{min}$. LC-MS (ESI) $\text{C}_{41}\text{H}_{52}\text{FN}_3\text{O}_7$ calcd: 717, found: 718 [M+H] $^+$. LC-MS (ESI): calcd for $\text{C}_{41}\text{H}_{52}\text{N}_3\text{O}_7\text{F}$: 718.38621 [M+H] $^+$, HR-MS found: 718.38856.

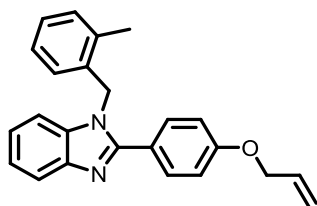
Procedures for synthesis of benzimidazole fragments



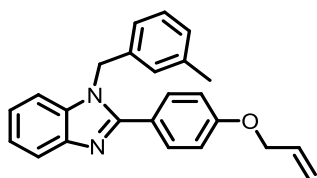
2-(4-(Allyloxy)phenyl)-1H-benzo[d]imidazole (30) To a mixture of 4-allyloxybenzaldehyde (4.00 g, 23.9 mmol) and phenyldiamine (2.72 g, 25.1 mmol) in DMF (50 mL) at room temperature was added $\text{Na}_2\text{S}_2\text{O}_5$ (4.50 g, 23.9 mmol). The reaction mixture was heated at 70°C for 3 h. To the reaction mixture was added ice water (150 mL) and the resulting suspension was stirred for 2 h at 0°C . The slightly brown precipitate was filtered, washed with cold water (100 mL), ethyl acetate (3x 20 mL) and dried *in vacuo* to afford the product. (4.85 g, 19.8 mmol, 81 %). ^1H NMR (400 MHz, $\text{DMSO}-d_6$) δ 8.11 (d, $J = 8.7$ Hz, 2H), 7.56 (dd, $J = 5.9, 3.1$ Hz, 2H), 7.23 - 7.06 (m, 4H), 6.11-5.99 (m, 1H), 5.41 (d, $J = 16.8$ Hz, 1H), 5.27 (d, $J = 10.6$ Hz, 1H), 4.64 (d, $J = 4.7$ Hz, 2H); ^{13}C NMR (101 MHz, $\text{DMSO}-d_6$) δ 160.3, 151.9, 139.7, 134.1, 128.8, 123.1, 122.6, 118.3, 115.8, 115.4, 69.02; LC-MS (ESI): calcd for $\text{C}_{16}\text{H}_{14}\text{N}_2\text{O}$: 251.11789 [M+H] $^+$, found 251.13 [M+H] $^+$, $R_t = 5.84$ min; HR-MS found 251.11800 [M+H] $^+$.



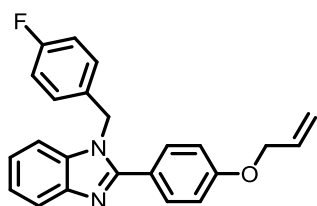
2-(4-(Allyloxy)phenyl)-1-benzyl-1H-benzo[d]imidazole (32a) Compound **32a** was synthesized according to Procedure (A) for the synthesis of N-alkylated benzimidazoles starting from **30** (262 mg, 1.04 mmol). The crude product was purified by automated flash chromatography using a gradient of cyclohexane : ethyl acetate 10:1 to 1:2 to yield the benzimidazole (325 mg, 0.95 mmol, 91%). ¹H NMR (400 MHz, DMSO-*d*₆) δ 7.70 – 7.60 (m, 3H), 7.43 – 7.37 (m, 1H), 7.30 – 7.14 (m, 5H), 7.07 (d, *J* = 8.8 Hz, 2H), 6.99 (d, *J* = 7.4 Hz, 2H), 6.11 – 5.93 (m, 1H), 5.55 (s, 2H), 5.40 (dd, *J* = 17.3, 1.7 Hz, 1H), 5.26 (dd, *J* = 10.5, 1.7 Hz, 1H), 4.62 (d, *J* = 5.2 Hz, 2H). ¹³C NMR (101 MHz, DMSO-*d*₆) δ 160.00, 153.89, 143.40, 137.68, 136.61, 134.08, 131.13, 129.47, 128.12, 126.72, 123.14, 123.07, 122.75, 119.72, 118.40, 115.60, 111.59, 68.99, 48.14. LC-MS (ESI): calcd for C₂₃H₂₀N₂O: 341.16484 [M+H]⁺, found: 341.25 [M+H]⁺, *R*_t = 7.43 min; HR-MS found 341.16508 [M+H]⁺.



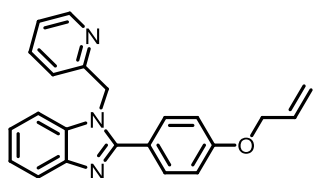
2-(4-(Allyloxy)phenyl)-1-(2-methylbenzyl)-1H-benzo[d]imidazole (33a) The product was synthesized according to Procedure A for the N-alkylation of benzimidazoles starting from **30** (291 mg, 1.27 mmol). The crude product was purified by automated flash chromatography (gradient cyclohexane : ethyl acetate 10:1 to 1:2) to yield the product (387 mg, 1.09 mmol, 86%). ¹H NMR (400 MHz, DMSO-*d*₆) δ 7.71 (dd, *J* = 7.9, 0.6 Hz, 1H), 7.61 – 7.54 (m, 2H), 7.30 (dd, *J* = 7.9, 0.7 Hz, 1H), 7.27 – 7.08 (m, 4H), 7.07 – 6.97 (m, 3H), 6.37 (d, *J* = 7.7 Hz, 1H), 6.03 (ddt, *J* = 17.3, 10.5, 5.3 Hz, 1H), 5.49 (s, 2H), 5.46 – 5.31 (m, 1H), 5.25 (dd, *J* = 10.5, 1.7 Hz, 1H), 4.63 – 4.54 (m, 2H), 2.29 (s, 3H). ¹³C NMR (101 MHz, DMSO-*d*₆) δ 160.01, 153.97, 143.37, 136.75, 135.62, 135.55, 134.06, 131.05, 130.84, 127.88, 126.93, 125.11, 123.07, 123.04, 122.79, 119.73, 118.41, 115.59, 111.53, 68.97, 46.56, 19.34; LC-MS (ESI): calcd for C₂₄H₂₂N₂O: 355.18049 [M+H]⁺, found: 355.19 [M+H]⁺, *R*_t = 7.75 min; HR-MS found 355.18092 [M+H]⁺.



2-(4-(Allyloxy)phenyl)-1-(3-methylbenzyl)-1H-benzo[d]imidazole (34a) Compound **34a** was synthesized according to Procedure A for the *N*-alkylation of benzimidazoles starting from **30** (316 mg, 1.26 mmol). The crude product was purified by automated flash chromatography (gradient cyclohexane : ethyl acetate 10:1 to 1:2) to yield the product (394 mg, 1.11 mmol, 88%). ¹H NMR (400 MHz, DMSO-*d*₆) δ 7.72 – 7.58 (m, 3H), 7.38 (dt, *J* = 6.7, 3.7 Hz, 1H), 7.25 – 7.11 (m, 3H), 7.09-7.03 (m, 3H), 6.85 (s, 1H), 6.74 (d, *J* = 7.6 Hz, 1H), 6.12 – 5.94 (m, 1H), 5.50 (s, 2H), 5.40 (dd, *J* = 17.3, 1.7 Hz, 1H), 5.26 (dd, *J* = 10.5, 1.7 Hz, 1H), 4.63-4.60 (m, 2H), 2.19 (s, 3H). ¹³C NMR (101 MHz, DMSO-*d*₆) δ 160.00, 153.89, 143.38, 138.65, 137.63, 136.62, 134.09, 131.13, 129.40, 128.82, 127.31, 123.75, 123.15, 123.06, 122.74, 119.70, 118.40, 115.61, 111.58, 68.99, 48.13, 21.68. LC-MS (ESI): calcd for C₂₄H₂₂N₂O: 355.18049 [M+H]⁺, found: 355.23 [M+H]⁺, *R*_t = 7.67 min; HR-MS found 355.18107 [M+H]⁺.

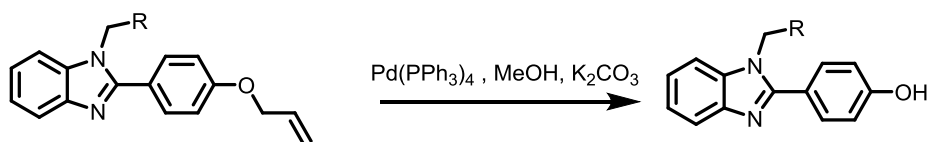


2-(4-(Allyloxy)phenyl)-1-(4-fluorobenzyl)-1H-benzo[d]imidazole (35a) Compound **35a** was synthesized according to Procedure A for the *N*-alkylation of benzimidazoles starting from **30** (243 mg, 0.97 mmol). The crude product was purified by automated flash chromatography (gradient cyclohexane : ethylacetate 10:1 to 1:2) to yield the product (301 mg, 0.84 mmol, 86%). ¹H NMR (400 MHz, DMSO-*d*₆) δ 7.72 – 7.58 (m, 3H), 7.46 – 7.37 (m, 1H), 7.24 – 7.16 (m, 2H), 7.14 – 6.93 (m, 6H), 6.05 (ddt, *J* = 17.3, 10.5, 5.2 Hz, 1H), 5.54 (s, 2H), 5.44 – 5.36 (m, 1H), 5.29 – 5.23 (m, 1H), 4.67 – 4.57 (m, 2H). ¹³C NMR (101 MHz, DMSO-*d*₆) δ 163.26, 160.84, 160.01, 153.82, 143.40, 136.49, 134.08, 133.86, 131.15, 128.89, 128.81, 123.13, 123.08, 122.80, 119.75, 118.41, 116.40, 116.19, 115.62, 111.56, 68.99, 47.48. LC-MS (ESI): calcd for C₂₃H₁₉FN₂O : 359.15542 [M+H]⁺, found: 359.19 [M+H]⁺, *R*_t = 7.41 min; HR-MS found 359.15576 [M+H]⁺.

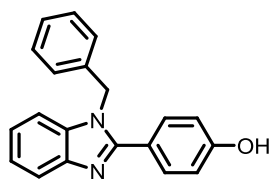


2-(4-(Allyloxy)phenyl)-1-(pyridin-2-ylmethyl)-1H-benzo[d]imidazole (36a) The product was synthesized according to Procedure A for the N-alkylation of benzimidazoles starting from **30**. The crude product was purified by automated flash chromatography (gradient DCM:MeOH 50:1 to 20:1) to yield the product (83%, 1.27 mmol, 432 mg). ¹H NMR (400 MHz, DMSO-*d*₆) δ 8.45 – 8.39 (m, 1H), 8.29 – 8.24 (m, 1H), 7.71 – 7.62 (m, 3H), 7.53 – 7.46 (m, 1H), 7.31 – 7.16 (m, 4H), 7.08 (t, *J* = 5.8 Hz, 2H), 6.10 – 5.98 (m, 1H), 5.61 (s, 2H), 5.41 (dd, *J* = 17.3, 1.7 Hz, 1H), 5.27 (dd, *J* = 10.5, 1.7 Hz, 1H), 4.63 (d, *J* = 5.2 Hz, 2H). ¹³C NMR (101 MHz, DMSO-*d*₆) δ 160.04, 153.86, 149.45, 148.47, 143.40, 136.40, 134.66, 134.08, 133.30, 131.21, 124.47, 123.22, 123.02, 122.90, 119.81, 118.43, 115.66, 111.54, 69.00, 45.91. LC-MS (ESI): calcd for C₂₀H₁₉N₃O : 342.16009 [M+H]⁺, found: 342.18 [M+H]⁺, R_t = 5.95 min.

General Procedure B for the deprotection of allyl-protected phenols

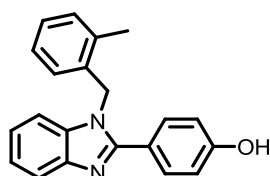


The allyl-protected phenol (1eq) was dissolved in degassed methanol (5 mL/mmol protected phenol). To this mixture was added K₂CO₃ (3 eq) and Pd(PPh₃)₄ (0.2 eq). The reaction mixture was stirred at room temperature for 1-3 hours and after this time it was concentrated *in vacuo*. The residue was resuspended in DCM (10 mL/mmol) and a sat. NH₄Cl-solution was subsequently added. The pH of the aqueous layer was adjusted to 8 and the aqueous layer was extracted with DCM (3 x 20 mL/mmol phenol). The combined organic layers were dried over Na₂SO₄, filtered and concentrated *in vacuo*. The crude product was purified as described below.

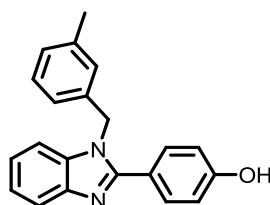


4-(1-Benzyl-1H-benzo[d]imidazol-2-yl)phenol (32b) Compound **32b** was synthesized according to Procedure B for the allyl-deprotection of benzimidazoles. The compound was purified by automated flash chromatography using a gradient of cyclohexane: ethyl acetate 20:1 to 1:1 to afford the desired compound (143 mg, 0.47 mmol, 83%). ¹H NMR (400 MHz, DMSO-*d*₆) δ 9.93 (s, 1H), 7.72 – 7.59 (m, 1H), 7.54 (d, *J* = 8.6 Hz, 2H), 7.41 – 7.33 (m, 1H), 7.32 – 7.12 (m, 5H), 6.99 (d, *J* = 7.4 Hz, 2H), 6.87 (d, *J* = 8.7 Hz, 2H), 5.53 (s, 2H); ¹³C NMR (101 MHz, DMSO-*d*₆) δ = 160.3, 151.9, 139.7, 134.1, 128.8, 123.1, 122.6, 118.3, 115.7, 115.4, 69.0

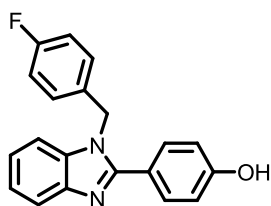
LC-MS (ESI): calcd for $C_{20}H_{16}N_2O$: 301.13354 $[M+H]^+$, found: 301.18 $[M+H]^+$, $R_t = 5.89$ min; HR-MS found 301.13367 $[M+H]^+$.



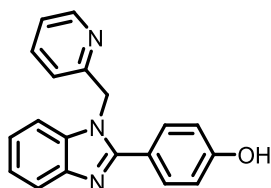
4-(1-(2-Methylbenzyl)-1H-benzimidazol-2-yl)phenol (33b) Compound **33b** was synthesized according to Procedure B for the allyl-deprotection of benzimidazoles. The crude product was purified by automated flash chromatography using a gradient of cyclohexane: ethyl acetate 20:1 to 1:1 to yield compound **33** (160 mg, 0.51 mmol, 81%). 1H NMR (400 MHz, $DMSO-d_6$) δ 9.92 (s, 1H), 7.68 (dd, $J = 7.9, 0.5$ Hz, 1H), 7.65 – 7.57 (m, 1H), 7.57 – 7.50 (m, 1H), 7.47 (t, $J = 5.6$ Hz, 2H), 7.32 – 7.10 (m, 5H), 7.01 (t, $J = 7.5$ Hz, 1H), 6.86 – 6.78 (m, 2H), 6.37 (d, $J = 7.6$ Hz, 1H), 5.46 (s, 2H), 2.28 (s, 3H). ^{13}C NMR (101 MHz, $DMSO-d_6$) δ 159.56, 154.42, 143.39, 136.72, 135.67, 135.54, 132.68, 132.20, 132.11, 131.02, 130.94, 129.48, 129.36, 127.84, 126.89, 125.15, 122.88, 122.68, 121.30, 119.61, 116.21, 111.45, 46.53, 19.33. LC-MS (ESI): calcd for $C_{21}H_{18}N_2O$: 315.14919 $[M+H]^+$, found: 315.09 $[M+H]^+$, $R_t = 6.29$ min; HR-MS found 315.14919 $[M+H]^+$.



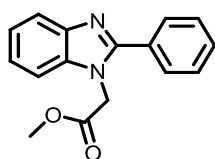
4-(1-(3-Methylbenzyl)-1H-benzimidazol-2-yl)phenol (34b) Compound **34b** was synthesized according to Procedure B for the allyl-deprotection of benzimidazoles. The crude product was purified by automated flash chromatography using a gradient of cyclohexane: ethyl acetate 20:1 to 1:1 to yield compound **34** (167 mg, 0.53 mmol, 83%). 1H NMR (400 MHz, $DMSO-d_6$) δ 9.98 (s, 1H), 7.70 – 7.64 (m, 1H), 7.57 – 7.48 (m, 2H), 7.39 – 7.33 (m, 1H), 7.23 – 7.10 (m, 3H), 7.03 (d, $J = 7.6$ Hz, 1H), 6.92 – 6.83 (m, 3H), 6.75 (d, $J = 7.5$ Hz, 1H), 5.48 (s, 2H), 2.18 (s, 3H). ^{13}C NMR (101 MHz, $DMSO-d_6$) δ 159.59, 154.36, 143.41, 138.63, 137.68, 136.60, 131.22, 129.36, 128.79, 127.35, 123.78, 122.89, 122.64, 121.40, 119.58, 116.26, 111.51, 48.13, 21.67. LC-MS (ESI): calcd for $C_{21}H_{18}N_2O$: 315.14919 $[M+H]^+$, found: 315.12 $[M+H]^+$, $R_t = 6.33$ min; HR-MS found: 315.14939 $[M+H]^+$.



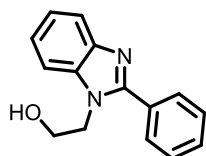
4-(1-(4-Fluorobenzyl)-1H-benzo[d]imidazol-2-yl)phenol (35b) Compound **35b** was synthesized according to Procedure B for the allyl-deprotection of benzimidazoles. The crude product was purified by automated flash chromatography using a gradient of cyclohexane: ethyl acetate 20:1 to 1:1 to yield compound 10 (156 mg, 0.49 mmol, 84%). ^1H NMR (400 MHz, $\text{DMSO-}d_6$) δ 9.94 (s, 1H), 7.69 – 7.63 (m, 1H), 7.56 – 7.48 (m, 2H), 7.44 – 7.37 (m, 1H), 7.24 – 7.14 (m, 2H), 7.10 (t, $J = 8.8$ Hz, 2H), 7.06 – 6.98 (m, 2H), 6.87 (d, $J = 8.4$ Hz, 2H), 5.52 (s, 2H). ^{13}C NMR (101 MHz, $\text{DMSO-}d_6$) δ 163.24, 160.82, 159.56, 154.27, 143.42, 136.46, 133.93, 133.90, 131.22, 128.91, 128.83, 122.95, 122.69, 121.31, 119.62, 116.37, 116.25, 116.16, 111.48, 47.45. LC-MS (ESI): calcd for $\text{C}_{20}\text{H}_{15}\text{FN}_2\text{O}$: 319.12412 $[\text{M}+\text{H}]^+$, found: 319.11 $[\text{M}+\text{H}]^+$, $R_t = 6.21$ min; HR-MS found 319.12438 $[\text{M}+\text{H}]^+$.



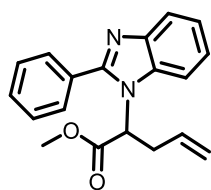
4-(1-(Pyridin-2-ylmethyl)-1H-benzo[d]imidazol-2-yl)phenol (36b) Compound **36b** was synthesized according to Procedure B for the allyl-deprotection of benzimidazoles. The crude product was purified by automated flash chromatography using a gradient of DCM: MeOH 100:1 to 10:1 to yield compound the product (123 mg, 0.41 mmol, 80%). ^1H NMR (400 MHz, $\text{DMSO-}d_6$) δ 9.95 (s, 1H), 8.42 (dd, $J = 4.3, 1.8$ Hz, 1H), 8.27 (s, 1H), 7.71 – 7.60 (m, 1H), 7.56 – 7.49 (m, 2H), 7.50 – 7.44 (m, 1H), 7.31 – 7.24 (m, 2H), 7.24 – 7.15 (m, 2H), 6.95 – 6.83 (m, 2H), 5.60 (s, 2H). ^{13}C NMR (101 MHz, $\text{DMSO-}d_6$) δ 159.59, 154.30, 149.41, 148.49, 143.42, 136.37, 134.68, 133.36, 131.27, 124.45, 123.04, 122.80, 121.25, 119.69, 116.30, 111.46, 45.89. LC-MS (ESI): calcd for $\text{C}_{19}\text{H}_{15}\text{N}_3\text{O}$: 302.12933. $[\text{M}+\text{H}]^+$. 302.13 $[\text{M}+\text{H}]^+$, $R_t = 4.13$ min.



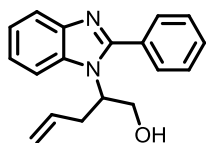
Methyl 2-(2-phenyl-1H-benzo[d]imidazol-1-yl)acetate (39) To a suspension of 2-phenyl benzimidazole (**37**) (0.32 g, 1.6 mmol) in acetonitrile (5 mL) was added caesium carbonate (0.80 g, 2.5 mmol) and methyl bromoacetate (0.16 mL, 1.7 mmol). The reaction mixture was stirred at room temperature for 3 hours and concentrated *in vacuo*. The residue was suspended in a mixture of DCM and sat. NaHCO₃ (vol % 50:50, 15 mL). The aqueous layer was reextracted with DCM (2 x 20 mL). The combined organic layers were dried over Na₂SO₄, filtered and concentrated in *in vacuo* to afford the product (0.40 g, 1.5 mmol, 91%). ¹H NMR (400 MHz, DMSO-*d*₆) δ 7.77 – 7.63 (m, 3H), 7.63 – 7.44 (m, 4H), 7.33 – 7.09 (m, 2H), 5.21 (s, 2H), 3.64 (s, 3H). ¹³C NMR (101 MHz, DMSO-*d*₆) δ 169.40, 153.91, 143.08, 136.91, 130.57, 130.51, 129.62, 129.53, 123.45, 123.00, 119.87, 111.36, 53.17, 46.57. LC-MS (ESI): calcd for C₁₆H₁₄N₂O₂: 267.11280 [M+H]⁺, found: 267.18 [M+H]⁺; HR-MS found 267.11311 [M+H]⁺.



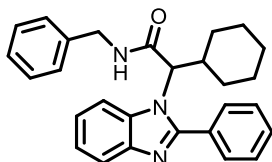
2-(2-Phenyl-1H-benzo[d]imidazol-1-yl)ethanol (40) To a solution of benzimidazole **39** (400 mg, 1.43 mmol) in MeOH (5 mL) was added NaBH₄ (376 mg, 10.0 mmol) at room temperature. The reaction mixture was stirred at room temperature for 12 h. To the reaction mixture was added sat. NH₄Cl-solution (15 mL), followed by DCM (30 mL). The pH of the aqueous layer was adjusted to 8 by addition of sat. NaHCO₃-solution. The aqueous layer was reextracted with DCM (2x 20 mL). The combined organic layers were dried (Na₂SO₄), filtered and concentrated *in vacuo* and the residue was purified by flash chromatography (gradient cyclohexane : ethyl acetate 100:1 to 1:1) to afford the product (302 mg, 1.26 mmol, 84%). ¹H NMR (400 MHz, DMSO-*d*₆) δ 7.97 – 7.84 (m, 2H), 7.76 – 7.60 (m, 2H), 7.60 – 7.45 (m, 3H), 7.34 – 6.99 (m, 2H), 5.08 (s, 1H), 4.33 (t, *J* = 5.5 Hz, 2H), 3.89 – 3.56 (m, 2H). ¹³C NMR (101 MHz, DMSO-*d*₆) δ 154.25, 143.32, 136.56, 131.27, 130.32, 130.20, 129.21, 122.93, 122.56, 119.71, 111.89, 59.92, 47.49. LC-MS (ESI): calcd for C₁₅H₁₄N₂O: 239.11789 [M+H]⁺, found: 239.19 [M+H]⁺, Rt = 4.32 min; HR-MS found 239.11806 [M+H]⁺.



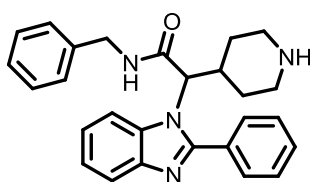
Methyl 2-(2-phenyl-1H-benzo[d]imidazol-1-yl)pent-4-enoate (41) To a solution of **39** (500 mg, 1.88 mmol) in DMF (5 mL) was added at 0°C NaH (83 mg, 60% mineral oil suspension). The reaction mixture was stirred for 60 minutes, then a solution of allyl bromide (244 μ L, 2.90 mmol) in DMF (2 mL) was added. The reaction mixture was allowed to warm to room temperature and stirred for 3 h. A saturated solution of NH₄Cl (10 mL) was added at 0°C to the reaction mixture. The aqueous suspension was extracted with DCM (3 x 20 mL). The combined organic phases were dried over Na₂SO₄, filtered and concentrated to dryness. The crude product was purified by automated flash chromatography using a of gradient cyclohexane : ethyl acetate 10:1 to 1:3 to yield the product (340 mg, 1.11 mmol, 59%). ¹H NMR (400 MHz, DMSO-*d*₆) δ 7.71 – 7.66 (m, 1H), 7.65 – 7.59 (m, 2H), 7.60 – 7.53 (m, 3H), 7.51 – 7.43 (m, 1H), 7.30 – 7.19 (m, 2H), 5.36 (dd, *J* = 9.5, 6.3 Hz, 1H), 5.32 – 5.16 (m, 1H), 4.76 (d, *J* = 10.2 Hz, 1H), 4.65 (d, *J* = 17.1 Hz, 1H), 3.68 (s, 3H), 2.99 – 2.77 (m, 2H). ¹³C NMR (101 MHz, DMSO-*d*₆) δ 170.08, 154.65, 143.50, 134.57, 133.12, 130.73, 130.61, 130.17, 129.53, 123.50, 122.94, 120.30, 119.37, 112.40, 58.12, 53.61, 33.85. LC-MS (ESI): calcd for C₁₉H₁₈N₂O₂ : 307.14410 [M+H]⁺, found: 307.16 [M+H]⁺; HR-MS found 307.14440 [M+H]⁺.



2-(2-Phenyl-1H-benzo[d]imidazol-1-yl)pent-4-en-1-ol (42) A solution of benzimidazole **41** (320 mg, 0.94 mmol) in EtOH:THF (1:5, 5 mL) was added to a suspension of NaBH₄ (188 mg, 5 mmol) in THF (4 mL) at room temperature over 1 h. The reaction mixture was stirred at room temperature for 12 h. NaBH₄ (94 mg, 2.5 mmol) was added to the reaction mixture and stirring was continued for 3 h. To the reaction mixture was added sat. NH₄Cl-solution (15 mL), followed by DCM (30 mL). The pH of the aqueous layer was adjusted to 9 by addition of sat. NaHCO₃-solution. The aqueous layer was again extracted with DCM (2x 20 mL). The combined organic layers were dried (Na₂SO₄), filtered, concentrated to dryness and the residue was purified by flash chromatography (gradient cyclohexane : ethyl acetate 100:1 to 1:1) to afford the product (217 mg, 0.77 mmol, 83%). ¹H NMR (400 MHz, CDCl₃) δ 7.69 – 7.62 (m, 1H), 7.63 – 7.56 (m, 2H), 7.47 (d, *J* = 7.9 Hz, 1H), 7.44 – 7.30 (m, 3H), 7.27 – 7.11 (m, 2H), 5.41 – 5.19 (m, 1H), 4.88 – 4.65 (m, 2H), 4.65 – 4.45 (m, 1H), 4.35 – 4.10 (m, 1H), 3.94 – 3.76 (m, 1H), 2.85 – 2.62 (m, 1H), 2.57 – 2.43 (m, 1H). ¹³C NMR (101 MHz, CDCl₃) δ 155.69, 143.40, 133.48, 133.05, 130.70, 130.37, 129.78, 128.62, 122.64, 122.53, 120.20, 118.56, 112.31, 62.97, 59.55, 34.09. LC-MS (ESI): calcd for C₁₈H₁₈N₂O: 279.14919 [M+H]⁺, found: 279.10 [M+H]⁺; HR-MS found 279.14941 [M+H]⁺.

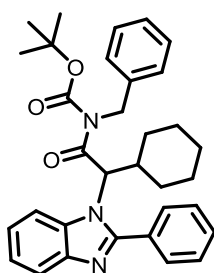


N-Benzyl-2-cyclohexyl-2-(2-phenyl-1H-benzo[d]imidazol-1-yl)acetamide (48) A mixture of the aniline **43** (1.80 g, 9.0 mmol) and cyclohexyl carbaldehyde **44** (1.10 g, 9.9 mmol) was stirred at room temperature in MeOH (4 mL) for 10 minutes. To the reaction mixture was added benzylisocyanide (1.10 mL, 9 mmol) and a solution of benzoic acid (1.10 g 9.0 mmol) in MeOH (4 mL). The reaction mixture was stirred at room temperature for 36 h. After this time HCl in dioxane (4 M, 2 mL) was added to the reaction mixture. The reaction mixture was stirred for 36 h at room temperature and then the solvent was removed under reduced pressure. The residue was redissolved in DCM (20 mL) and washed with a sat. NaHCO₃ solution (30 mL). The aqueous layer was extracted with DCM (3x 20 mL). The combined organic layers were dried (Na₂SO₄), filtered and concentrated to dryness under reduced pressure. The residue was purified by flash chromatography using a gradient of cyclohexane :ethyl acetate 50:1 to 1:2 to afford the product (3.42 g, 8.06 mmol, 89 %). ¹H NMR (400 MHz, CDCl₃) δ 7.97 – 7.86 (m, 1H), 7.81 – 7.69 (m, 1H), 7.56 – 7.35 (m, 5H), 7.36 – 7.19 (m, 5H), 7.10 (dd, *J* = 6.8, 2.4 Hz, 2H), 6.13 (s, 1H), 4.50 – 4.29 (m, 3H), 2.76 – 2.56 (m, 1H), 1.96 (d, *J* = 12.3 Hz, 1H), 1.71 – 1.41 (m, 3H), 1.36 – 1.18 (m, 1H), 1.12 – 0.86 (m, 3H), 0.86 – 0.69 (m, 1H), 0.66 – 0.46 (m, 1H). ¹³C NMR (101 MHz, CDCl₃) δ 168.50, 154.93, 143.37, 137.77, 134.33, 130.74, 130.24, 129.92, 129.14, 128.96, 127.91, 123.51, 123.12, 120.18, 113.97, 66.39, 43.97, 37.84, 31.36, 29.18, 26.13, 25.81. LC-MS (ESI): calcd for C₂₈H₂₉N₃O: 424.23834 [M+H]⁺, found 424.21 [M+H]⁺; HR-MS found 424.23733 [M+H]⁺.



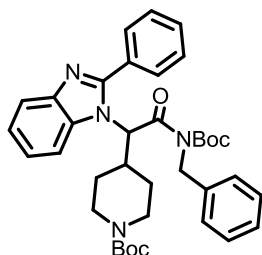
N-Benzyl-2-(2-phenyl-1H-benzo[d]imidazol-1-yl)-2-(piperidin-4-yl)acetamide (49) A mixture of the aniline **43** (1.20 g, 5.7 mmol) and the *tert*-butyl 4-formylpiperidine-1-carboxylate (**45**) (1.34 g, 6.3 mmol) was stirred at room temperature in MeOH (3 mL) for 10 minutes. To the reaction mixture was added benzylisocyanide (0.70 mL, 9.0 mmol) and a solution of benzoic acid (0.70 g 9.0 mmol) in MeOH (4 mL). The reaction mixture was stirred at room temperature for 36 h. To the reaction mixture was added HCl/dioxane (4 M, 2 mL). The reaction mixture

was stirred for 36 h at room temperature and then concentrated *in vacuo*. The residue was redissolved in DCM (20 mL) and washed with sat. NaHCO₃ solution (30 mL). The aqueous layer was reextracted with DCM (3x 20 mL). The combined organic layers were dried (Na₂SO₄), filtered and concentrated to dryness under reduced pressure. The residue was purified by automated flash chromatography (gradient cyclohexane : ethylacetate 100:1 to 1:2, containing 0.1% triethylamine) to afford the product (4.11 mmol, 1.75 g, 72%). ¹H NMR (400 MHz, DMSO-*d*₆) δ 8.89 (t, *J* = 5.6 Hz, 1H), 8.10 – 7.89 (m, 1H), 7.68 – 7.47 (m, 6H), 7.34 – 7.17 (m, 7H), 2.84 (d, *J* = 11.5 Hz, 1H), 2.67 – 2.51 (m, 2H), 2.37 (t, *J* = 12.4 Hz, 1H), 2.08 (t, *J* = 11.2 Hz, 1H), 1.60 (d, *J* = 13.0 Hz, 1H), 1.12 – 0.97 (m, 1H), 0.62 – 0.48 (m, 1H), 0.47 – 0.36 (m, 1H). ¹³C NMR (101 MHz, DMSO-*d*₆) δ 173.11, 155.19, 154.32, 152.61, 143.70, 138.15, 131.13, 130.49, 130.22, 129.37, 129.03, 127.91, 127.51, 123.29, 122.95, 120.05, 115.57, 84.79, 79.34, 63.36, 48.55, 37.71, 28.72, 27.85. LC-MS (ESI): calcd for C₂₇H₂₈N₄O: 425.23376 [M+H]⁺, found 425.17 [M+H]⁺, R_t = 5.15 min; HR-MS found 425.23359 [M+H]⁺.

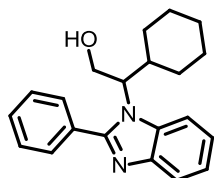


tert-Butyl benzyl(2-cyclohexyl-2-(2-phenyl-1H-benzo[d]imidazol-1-yl)acetyl)carbamate (50) To a solution of amide **48** (620 mg, 1.46 mmol) in DCM (5 mL) was added Boc-anhydride (639 mg, 2.92 mmol), triethylamine (405 μL, 2.92 mmol) and DMAP (179 mg, 1.46 mmol). The reaction mixture was stirred at room temperature for 5 h. After this time Boc-anhydride (639 mg, 2.92 mmol), triethylamine (405 μL, 2.92 mmol) and DMAP (179 mg, 1.46 mmol) were added to the reaction mixture and stirring was continued for an additional 12 h. The reaction mixture was concentrated to dryness under reduced pressure. Purification by automated flash chromatography using a gradient of cyclohexane : ethyl acetate 20:1 to 1:1 afforded the product (0.66 g, 1.26 mmol, 86%). ¹H NMR (400 MHz, CDCl₃) δ 8.07 (d, *J* = 7.4 Hz, 1H), 7.82 – 7.73 (m, 1H), 7.56 – 7.48 (m, 2H), 7.47 – 7.39 (m, 3H), 7.34 – 7.24 (m, 2H), 7.24 – 7.15 (m, 3H), 7.05 (d, *J* = 7.2 Hz, 2H), 6.38 (d, *J* = 10.6 Hz, 1H), 4.83 (d, *J* = 15.0 Hz, 1H), 4.68 (d, *J* = 14.9 Hz, 1H), 2.87 (d, *J* = 10.8 Hz, 1H), 1.84 – 1.68 (m, 2H), 1.72 – 1.50 (m, 2H), 1.38 – 0.74 (m, 15H). ¹³C NMR (101 MHz, CDCl₃) δ 173.81, 155.26, 152.49, 143.59, 137.78, 134.92, 131.22, 130.10, 129.81, 128.75, 128.56, 127.55, 127.42, 123.03, 122.68, 120.04, 115.08, 84.19, 64.13, 48.53, 39.52, 29.87, 29.66, 27.95, 26.38, 26.25, 26.16. LC-MS (ESI): calcd for

$C_{33}H_{37}N_3O_3$: 524.29077 $[M+H]^+$, found 524.18 $[M+H]^+$, $R_t = 11.55$ min; HR-MS found 524.29035 $[M+H]^+$.

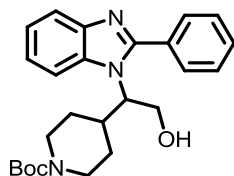


tert-Butyl 4-(2-(benzyl(tert-butoxycarbonyl)amino)-2-oxo-1-(2-phenyl-1H-benzo[d]imidazol-1-yl)ethyl)piperidine-1-carboxylate (51) To a solution of amide **49** (300 mg, 0.71 mmol) in DCM (5 mL) was added Boc-anhydride (463 mg, 2.13 mmol), triethylamine (293 μ L, 2.13 mmol) and DMAP (86 mg, 0.71 mmol). The reaction mixture was stirred at room temperature for 5 h. Boc-anhydride (463 mg, 2.13 mmol), triethylamine (293 μ L, 2.13 mmol) and DMAP (86 mg, 0.71 mmol) were added to the reaction mixture and stirring was continued for an additional 12 h. The reaction mixture was concentrated to dryness under reduced pressure. Purification by flash chromatography using a gradient of cyclohexane: ethyl acetate 20:1 to 1:1 afforded the product (0.36 g, 0.58 mmol, 81%). 1H NMR (400 MHz, $DMSO-d_6$) δ 8.04 (d, $J = 7.5$ Hz, 1H), 7.65 (d, $J = 8.0$ Hz, 1H), 7.55 – 7.37 (m, 5H), 7.31 – 7.10 (m, 5H), 7.04 (d, $J = 7.2$ Hz, 2H), 6.23 (d, $J = 10.4$ Hz, 1H), 4.77 (d, $J = 15.5$ Hz, 1H), 4.64 (d, $J = 15.1$ Hz, 1H), 3.95 (d, $J = 11.9$ Hz, 1H), 3.82 (d, $J = 11.2$ Hz, 1H), 2.97 (d, $J = 10.2$ Hz, 1H), 2.86 – 2.59 (m, 1H), 2.56 – 2.40 (m, 2H), 1.59 (d, $J = 11.7$ Hz, 1H), 1.47 – 1.24 (m, 10H), 1.25 – 1.05 (m, 9H), 1.05 – 0.88 (m, 2H). ^{13}C NMR (101 MHz, $DMSO-d_6$) δ 173.11, 155.19, 154.32, 152.61, 143.70, 138.15, 131.13, 130.49, 130.22, 129.37, 129.03, 127.91, 127.51, 123.29, 122.95, 120.05, 115.57, 84.79, 79.34, 63.36, 48.55, 37.71, 28.72, 27.85. LC-MS (ESI): calcd for $C_{37}H_{44}N_4O_5$: 625.33845 $[M+H]^+$, found 625.19 $[M+H]^+$, $R_t = 10.76$ min; HR-MS found 625.33840.



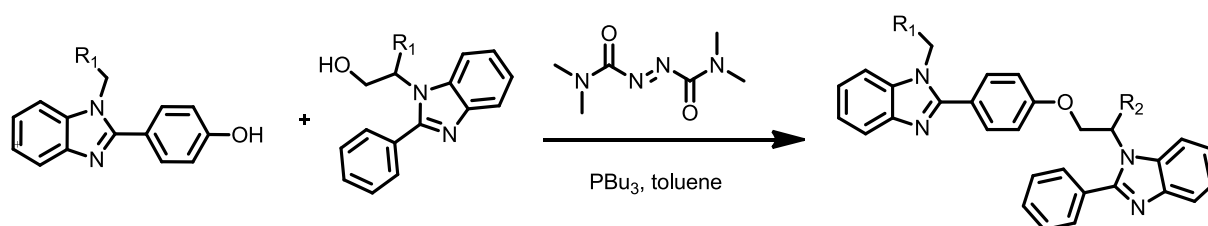
2-Cyclohexyl-2-(2-phenyl-1H-benzo[d]imidazol-1-yl)ethanol (52) A solution of Boc-protected amide **50** (650 mg, 1.24 mmol) in EtOH:THF (1:5, 5 mL) was added to a suspension of $NaBH_4$ (188 mg, 5 mmol) in THF (4 mL) at room temperature over 1 h. The reaction mixture was stirred at room temperature for 12 h. After this time $NaBH_4$ (94 mg, 2.5 mmol) was added to the reaction mixture and stirring was continued for 3 h. To the reaction mixture was added a

NH₄Cl-solution (15 mL), followed by DCM (20 mL). The pH of the aqueous layer was adjusted to 9 by addition of sat. NaHCO₃-solution. The aqueous layers were extracted with DCM (2x 20 mL). The combined organic layers were dried (Na₂SO₄), filtered and concentrated under reduced pressure and the residue was purified by flash chromatography (gradient cyclohexane: ethyl acetate 10:1 to 1:1) to afford the product (330 mg, 1.03 mmol, 83%). ¹H NMR (400 MHz, CDCl₃) δ 7.73 – 7.61 (m, 3H), 7.52 (d, *J* = 8.1 Hz, 1H), 7.48 – 7.35 (m, 3H), 7.25 – 7.10 (m, 2H), 4.36 – 4.21 (m, 2H), 4.06 – 4.02 (m, 1H), 3.13 (s, 1H), 2.18 – 2.05 (m, 1H), 1.80 (d, *J* = 11.9 Hz, 1H), 1.67 (d, *J* = 13.6 Hz, 1H), 1.53 (d, *J* = 10.0 Hz, 1H), 1.41 (d, *J* = 12.5 Hz, 1H), 1.31 – 1.10 (m, 1H), 1.04 – 0.77 (m, 4H), 0.57 – 0.37 (m, 1H). ¹³C NMR (101 MHz, CDCl₃) δ 156.21, 143.34, 133.52, 130.86, 130.56, 129.69, 128.63, 122.62, 122.51, 120.24, 112.34, 65.04, 61.68, 37.67, 30.88, 29.62, 26.06, 25.87, 25.74. LC-MS (ESI): calcd for C₃₇H₄₄N₄O₅: 321.19614 [M+H]⁺, found 321.18 [M+H]⁺, R_t = 6.24 min; HR-MS found 321.19642.

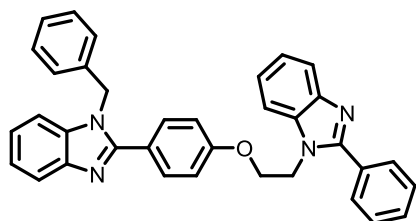


tert-Butyl 4-(2-hydroxy-1-(2-phenyl-1H-benzo[d]imidazol-1-yl)ethyl)piperidine-1-carboxylate (53) A solution of Boc-protected amide **51** (1.0 g, 1.6 mmol) in EtOH:THF (1:5, 15 mL) was added to a suspension of NaBH₄ (242 mg, 6.4 mmol) in THF (15 mL) at room temperature over 1 h. The reaction mixture was stirred at room temperature for 12 h. NaBH₄ (120 mg, 3.2 mmol) was added to the reaction mixture and stirring was continued for 3 h. To the reaction mixture was added NH₄Cl-solution (40 mL), followed by DCM (30 mL). The pH of the aqueous layer was adjusted to 8 by addition of sat. NaHCO₃-solution. The aqueous layers were reextracted with DCM (3x 30 mL). The combined organic layers were concentrated *in vacuo* and the residue was purified by flash chromatography (gradient cyclohexane: ethyl acetate 10:1 to 1:2) to afford the product (538 mg, 1.27 mmol, 80%). ¹H NMR (400 MHz, DMSO-*d*₆) δ 7.87 – 7.78 (m, 1H), 7.74 (d, *J* = 3.6 Hz, 2H), 7.70 – 7.62 (m, 1H), 7.58 – 7.46 (m, 3H), 7.26 – 7.11 (m, 2H), 5.29 – 5.07 (m, 1H), 4.30 – 4.07 (m, 2H), 4.04 – 3.73 (m, 2H), 3.71 – 3.44 (m, 1H), 2.79 – 2.56 (m, 1H), 2.45 – 2.23 (m, 2H), 1.81 (d, *J* = 12.2 Hz, 1H), 1.46 – 1.20 (m, 10H), 0.93 (d, *J* = 10.4 Hz, 1H), 0.68 – 0.38 (m, 2H). ¹³C NMR (101 MHz, DMSO-*d*₆) δ 155.95, 154.28, 143.86, 134.19, 131.67, 130.82, 130.09, 129.08, 122.74, 122.40, 120.11, 113.62, 79.18, 64.71, 60.33, 35.71, 30.18, 29.06, 28.67. LC-MS (ESI): calcd for C₂₅H₃₁N₃O₃: 422.24382 [M+H]⁺, found 422.20 [M+H]⁺, R_t = 6.31 min; HR-MS found 422.24271.

General Procedure C for the synthesis of phenol ethers via Mitsunobu reaction

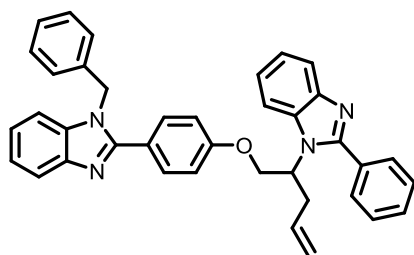


To a mixture of phenol, alcohol (1.0 eq) and tri-*n*-butyl phosphine (2 eq) in toluene (3 mL/mmol phenol) was added at 0°C TMAD (2 eq) in one portion. The resulting suspension was heated for 16 h at 60°C. If the reaction was not complete tri-*n*-butyl phosphine (1 eq) and TMAD (1 eq) were added at room temperature and the mixture was heated for 16 h at 60°C. The reaction mixture was diluted with DCM (20 mL/mmol phenol) and washed with sat. $NaHCO_3$ (10 mL/mmol phenol). The aqueous phase was reextracted with DCM (3 x 20 mL/mmol phenol). The combined organic phases were dried (Na_2SO_4), filtered and concentrated *in vacuo*. The crude product was purified by column chromatography as described below.

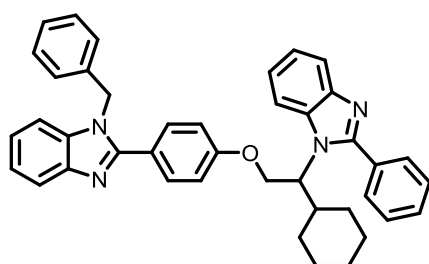


1-Benzyl-2-(4-(2-(2-phenyl-1H-benzo[d]imidazol-1-yl)ethoxy)phenyl)-1H-

benzo[d]imidazole (54) The product was synthesized from phenol **32** (50 mg, 0.17 mmol) and alcohol **40** according to Procedure C for the synthesis of phenol ethers via Mitsunobu reaction. The crude product was purified by automated flash chromatography using a gradient of cyclohexane: ethyl acetate 6:1 to 1:9 to yield the product (52 mg, 0.10 mmol, 59%). 1H NMR (400 MHz, $DMSO-d_6$) δ 7.86 – 7.79 (m, 2H), 7.77 (d, $J = 7.9$ Hz, 1H), 7.70 – 7.62 (m, 2H), 7.60 – 7.45 (m, 5H), 7.38 (d, $J = 6.8$ Hz, 1H), 7.33 – 7.13 (m, 7H), 6.96 (d, $J = 7.2$ Hz, 2H), 6.86 (d, $J = 8.7$ Hz, 2H), 5.49 (s, 2H), 4.70 (t, $J = 5.0$ Hz, 2H), 4.36 (t, $J = 5.1$ Hz, 2H). ^{13}C NMR (101 MHz, $DMSO-d_6$) δ 159.51, 154.48, 153.74, 143.35, 137.64, 136.56, 136.25, 131.22, 131.09, 130.27, 129.45, 129.29, 128.10, 126.68, 123.36, 123.14, 123.10, 122.77, 119.84, 119.71, 115.17, 111.94, 111.59, 66.71, 48.09, 44.41. LC-MS (ESI): calcd for $C_{35}H_{28}N_4O$: 521.23359 $[M+H]^+$, found: 521.34 $[M+H]^+$, $R_t = 6.37$ min; HR-MS found 521.23314 $[M+H]^+$.

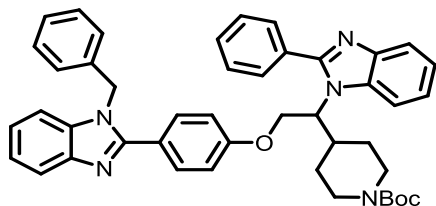


1-Benzyl-2-(4-(2-(2-phenyl-1H-benzo[d]imidazol-1-yl)pent-4-enyloxy)phenyl)-1H-benzo[d]imidazole (55) The product was synthesized from phenol **32** (76 mg, 0.25 mmol) and alcohol **42** according to Procedure C for the synthesis of phenol ethers via Mitsunobu reaction. The crude product was purified by automated flash chromatography using a gradient of cyclohexane: ethyl acetate 10:1 to 1:7 to yield the product (100 mg, 0.18 mmol, 72 %). ^1H NMR (400 MHz, $\text{DMSO-}d_6$) δ 7.99 – 7.89 (m, 1H), 7.75 – 7.63 (m, 4H), 7.57 (t, J = 11.0 Hz, 2H), 7.54 – 7.43 (m, 3H), 7.38 (dt, J = 8.8, 4.5 Hz, 1H), 7.34 – 7.06 (m, 8H), 6.98 (dd, J = 7.7, 5.4 Hz, 4H), 5.51 (s, 2H), 5.50 – 5.33 (m, 1H), 4.91 – 4.71 (m, 4H), 4.44 (dd, J = 10.1, 3.6 Hz, 1H), 3.08 – 2.91 (m, 1H), 2.81 – 2.68 (m, 1H). ^{13}C NMR (101 MHz, $\text{DMSO-}d_6$) δ 159.51, 155.59, 153.74, 143.91, 143.37, 137.66, 136.60, 133.94, 133.85, 131.47, 131.14, 130.59, 130.20, 129.47, 129.18, 128.11, 126.66, 123.48, 123.12, 123.01, 122.78, 122.61, 120.29, 119.73, 119.09, 115.33, 113.31, 111.59, 68.29, 56.84, 48.12, 33.72. LC-MS (ESI): calcd for $\text{C}_{38}\text{H}_{32}\text{N}_4\text{O}$: 561.26489 $[\text{M}+\text{H}]^+$, found: 561.36 $[\text{M}+\text{H}]^+$, R_t = 7.19 min; HR-MS found 561.26523 $[\text{M}+\text{H}]^+$.

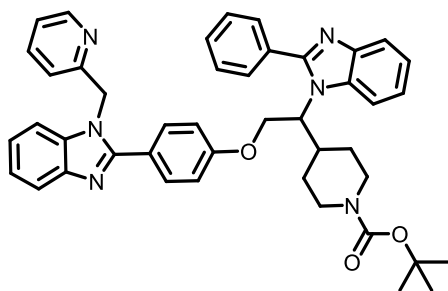


1-Benzyl-2-(4-(2-cyclohexyl-2-(2-phenyl-1H-benzo[d]imidazol-1-yl)ethoxy)phenyl)-1H-benzo[d]imidazole (56) The product was synthesized from phenol **32** (50 mg, 0.17 mmol) and alcohol **52** according to Procedure C for the synthesis of phenol ethers via Mitsunobu reaction. The crude product was purified by automated flash chromatography using a gradient of cyclohexane: ethyl acetate 10:1 to 1:7 to yield the product (63 mg, 0.11 mmol, 63%). ^1H NMR (600 MHz, $\text{DMSO-}d_6$) δ 7.91 (d, J = 7.3 Hz, 1H), 7.73 (d, J = 6.9 Hz, 2H), 7.66 (td, J = 7.1, 4.6 Hz, 2H), 7.58 (t, J = 10.6 Hz, 2H), 7.57 – 7.49 (m, 3H), 7.39 (d, J = 7.6 Hz, 1H), 7.28 – 7.15 (m, 7H), 7.04 (d, J = 8.6 Hz, 2H), 6.96 (d, J = 7.4 Hz, 2H), 5.51 (s, 2H), 4.85 (t, J = 9.9

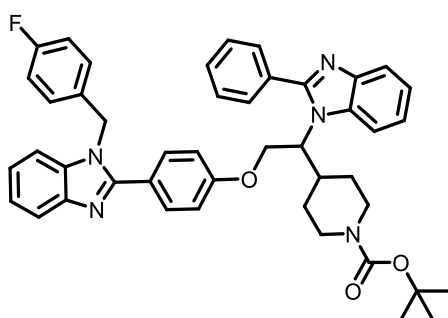
Hz, 1H), 4.61 – 4.54 (m, 1H), 4.45 (t, $J = 8.4$ Hz, 1H), 2.37 (d, $J = 10.8$ Hz, 1H), 1.99 – 1.92 (m, 1H), 1.64 (d, $J = 13.2$ Hz, 1H), 1.53 – 1.35 (m, 3H), 1.28 – 1.17 (m, 1H), 1.05 – 0.75 (m, 4H), 0.59 – 0.49 (m, 1H). ^{13}C NMR (151 MHz, DMSO- d_6) δ 159.71, 155.88, 153.73, 143.76, 143.29, 137.68, 136.58, 133.93, 131.13, 130.66, 130.27, 129.47, 129.28, 128.10, 126.64, 123.39, 123.13, 123.06, 122.80, 122.63, 120.24, 119.68, 115.39, 113.35, 111.61, 109.99, 67.38, 62.19, 48.08, 37.36, 30.74, 29.64, 26.11, 25.84, 25.79. LC-MS (ESI): calcd for $\text{C}_{41}\text{H}_{38}\text{N}_4\text{O}$: 603.31184 $[\text{M}+\text{H}]^+$, found: 603.39 $[\text{M}+\text{H}]^+$, $R_t = 8.14$ min; HR-MS found 603.31156 $[\text{M}+\text{H}]^+$.



tert-Butyl-4-(2-(4-(1-benzyl-1H-benzo[d]imidazol-2-yl)phenoxy)-1-(2-phenyl-1H-benzo[d]imidazol-1-yl)ethyl)piperidine-1-carboxylate (57) The product was synthesized from phenol **32** (60 mg, 0.14 mmol) and alcohol **53** according to Procedure C for the synthesis of phenol ethers via Mitsunobu reaction. The crude product was purified by automated flash chromatography using a gradient of cyclohexane: ethyl acetate 10:1 to 1:7 to yield the product (66 mg, 0.09 mmol, 66%). ^1H NMR (400 MHz, DMSO- d_6) δ 7.94 (d, $J = 6.3$ Hz, 1H), 7.78 – 7.64 (m, 4H), 7.64 – 7.49 (m, 5H), 7.40 (d, $J = 7.9$ Hz, 1H), 7.31 – 7.15 (m, 7H), 7.04 (d, $J = 8.2$ Hz, 2H), 6.97 (d, $J = 7.2$ Hz, 2H), 5.51 (s, 2H), 4.85 (d, $J = 9.5$ Hz, 1H), 4.58 (d, $J = 9.6$ Hz, 1H), 4.48 (s, 1H), 3.91 (d, $J = 12.6$ Hz, 1H), 3.70 (s, 1H), 2.80 – 2.52 (m, 2H), 2.45 – 2.31 (m, 1H), 1.92 (d, $J = 11.6$ Hz, 1H), 1.31 (s, 9H), 1.19–1.00 (d, $J = 9.6$ Hz, 2H), 0.92 – 0.63 (m, 2H). ^{13}C NMR (101 MHz, DMSO- d_6) δ 159.68, 155.83, 154.29, 153.69, 143.76, 143.18, 137.64, 136.56, 131.16, 130.69, 130.31, 129.46, 129.29, 128.11, 126.66, 123.39, 123.17, 122.84, 122.75, 120.29, 119.65, 115.42, 113.29, 111.62, 79.30, 67.12, 61.64, 48.13, 35.89, 29.79, 29.08, 28.71. LC-MS (ESI): calcd for $\text{C}_{45}\text{H}_{45}\text{N}_5\text{O}_3$: 704.35952 $[\text{M}+\text{H}]^+$, found: 704.31 $[\text{M}+\text{H}]^+$, $R_t = 7.68$ min; HR-MS found 704.36024 $[\text{M}+\text{H}]^+$. Chiral, analytical HPLC conditions: flow rate: 0.5 mL/min; solvent: 40 % ethanol in *iso*-hexane. (*S*)-**8** $R_t = 90.1$ min, (*R*)-**8** 100.9 min.

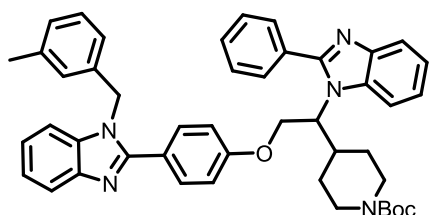


tert-Butyl 4-(1-(2-phenyl-1H-benzo[d]imidazol-1-yl)-2-(4-(1-(pyridin-2-ylmethyl)-1H-benzo[d]imidazol-2-yl)phenoxy)ethyl)piperidine-1-carboxylate (58) The product was synthesized from phenol **36** (61 mg, 0.14 mmol) according to Procedure C for the synthesis of phenol ethers via Mitsunobu reaction. The crude product was purified by automated flash chromatography using a gradient of DCM:MeOH 100:1 to 5:1 to yield the product (60 mg, 0.08 mmol, 61%). ^1H NMR (400 MHz, DMSO-*d*₆) δ 8.45 – 8.34 (m, 1H), 8.30 – 8.22 (m, 1H), 7.94 (d, J = 7.7 Hz, 1H), 7.78 – 7.39 (m, 10H), 7.30 – 7.14 (m, 6H), 7.06 (d, J = 8.6 Hz, 2H), 5.57 (s, 2H), 4.86 (t, J = 9.8 Hz, 1H), 4.63 – 4.53 (m, 1H), 4.53 – 4.43 (m, 1H), 3.91 (d, J = 12.2 Hz, 1H), 3.79 – 3.59 (m, 1H), 2.79 – 2.51 (m, 2H), 2.45 – 2.36 (m, 1H), 1.92 (d, J = 12.0 Hz, 1H), 1.30 (s, 9H), 1.18 – 0.93 (m, 1H), 0.88 – 0.55 (m, 2H). ^{13}C NMR (101 MHz, DMSO-*d*₆) δ 159.69, 155.85, 154.30, 153.72, 149.42, 148.39, 143.83, 143.36, 136.37, 134.58, 133.82, 133.28, 131.38, 131.23, 130.69, 130.30, 129.56, 129.29, 128.87, 125.98, 124.45, 123.38, 123.26, 123.15, 122.92, 122.72, 120.32, 119.81, 115.47, 113.30, 111.54, 79.30, 67.13, 61.64, 45.89, 35.87, 29.08, 28.71. LC-MS (ESI): calcd for C₄₄H₄₄N₆O₃: 705.35477 [M+H]⁺, found: 705.30 [M+H]⁺, R_t = 6.94 min; HR-MS found: 705.35474 [M+H]⁺.

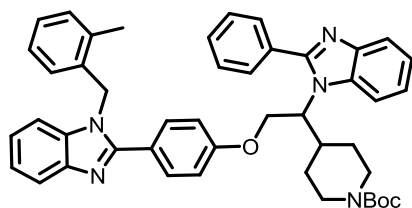


tert-Butyl 4-(2-(4-(1-(4-fluorobenzyl)-1H-benzo[d]imidazol-2-yl)phenoxy)-1-(2-phenyl-1H-benzo[d]imidazol-1-yl)ethyl)piperidine-1-carboxylate (59) The product was synthesized from phenol **35** (50 mg, 0.12 mmol) according to Procedure C for the synthesis of phenol ethers via Mitsunobu reaction. The crude product was purified by automated flash chromatography using a gradient of cyclohexane: ethyl acetate 10:1 to 1:7 to yield the product (58 mg, 0.08 mmol, 66%). ^1H NMR (400 MHz, CDCl₃) δ 7.88 – 7.79 (m, 2H), 7.71 (dd, J =

19.7, 5.3 Hz, 3H), 7.61 – 7.44 (m, 5H), 7.34 – 7.15 (m, 5H), 7.01 (p, $J = 8.8$ Hz, 4H), 6.92 (d, $J = 8.4$ Hz, 2H), 5.35 (s, 2H), 4.80 – 4.64 (m, 1H), 4.64 – 4.53 (m, 1H), 4.48 (d, $J = 9.7$ Hz, 1H), 4.21 – 4.02 (m, 1H), 4.01 – 3.87 (m, 1H), 2.71 (t, $J = 12.4$ Hz, 1H), 2.64 – 2.37 (m, 2H), 1.89 (d, $J = 12.9$ Hz, 1H), 1.34 – 1.19 (m, 10H), 1.02 – 0.79 (m, 2H). ^{13}C NMR (101 MHz, CDCl_3) δ 163.67, 161.22, 159.53, 155.80, 154.75, 153.84, 143.82, 143.28, 136.12, 133.57, 132.32, 132.29, 130.96, 130.82, 130.32, 130.08, 128.97, 127.85, 127.77, 123.43, 123.26, 123.01, 122.81, 120.83, 120.09, 116.38, 116.16, 114.95, 112.06, 110.44, 79.94, 67.47, 61.70, 47.92, 36.46, 30.16, 28.80, 28.60. LC-MS (ESI): calcd for $\text{C}_{45}\text{H}_{44}\text{FN}_5\text{O}_3$: 722.35009 $[\text{M}+\text{H}]^+$, found: 722.31 $[\text{M}+\text{H}]^+$, $R_t = 8.16$ min; HR-MS found: 722.35052 $[\text{M}+\text{H}]^+$.

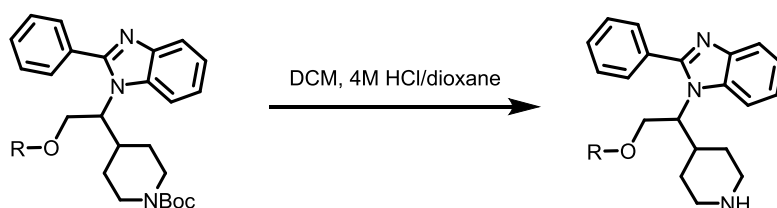


tert-Butyl 4-(2-(4-(1-(3-methylbenzyl)-1H-benzo[d]imidazol-2-yl)phenoxy)-1-(2-phenyl-1H-benzo[d]imidazol-1-yl)ethyl)piperidine-1-carboxylate (60) The product was synthesized from phenol **34** (70 mg, 0.17 mmol) according to Procedure C for the synthesis of phenol ethers via Mitsunobu reaction. The crude product was purified by automated flash chromatography using a gradient of cyclohexane: ethyl acetate 10:1 to 1:7 to yield the desired compound (86 mg, 0.12 mmol, 70%). ^1H NMR (400 MHz, cdcl_3) δ 7.82 – 7.74 (m, 2H), 7.69 – 7.57 (m, 4H), 7.55 – 7.48 (m, 2H), 7.47 – 7.39 (m, 3H), 7.24 – 7.08 (m, 7H), 7.05 – 6.99 (m, 1H), 6.87 – 6.72 (m, 5H), 5.28 (s, 2H), 4.69 – 4.55 (m, 1H), 4.55 – 4.43 (m, 1H), 4.43 – 4.34 (m, 1H), 4.12 – 3.95 (m, 1H), 3.91 – 3.73 (m, 1H), 2.63 (t, $J = 12.8$ Hz, 1H), 2.58 – 2.33 (m, 2H), 1.80 (d, $J = 12.6$ Hz, 1H), 1.32 (s, 9H), 1.20 – 1.13 (m, 1H), 0.81 (dd, $J = 24.7, 11.8$ Hz, 2H). ^{13}C NMR (101 MHz, CDCl_3) δ 159.63, 155.75, 154.75, 153.69, 143.70, 139.15, 136.34, 136.13, 133.55, 131.10, 130.72, 130.53, 130.32, 130.11, 129.23, 128.98, 128.84, 126.63, 123.37, 123.11, 123.07, 122.85, 120.77, 119.68, 114.97, 112.09, 110.75, 79.93, 67.47, 61.69, 48.62, 36.45, 30.15, 28.80, 28.60, 21.67. LC-MS (ESI): calcd for $\text{C}_{46}\text{H}_{47}\text{N}_5\text{O}_3$: 718.37517 $[\text{M}+\text{H}]^+$, found: 718.33 $[\text{M}+\text{H}]^+$, $R_t = 8.17$ min; HR-MS found: 718.37523 $[\text{M}+\text{H}]^+$.

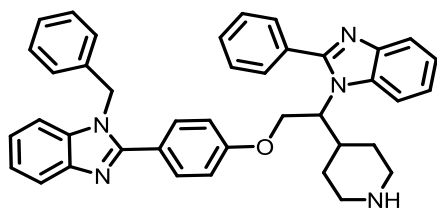


tert-Butyl 4-(2-(4-(1-(2-methylbenzyl)-1H-benzo[d]imidazol-2-yl)phenoxy)-1-(2-phenyl-1H-benzo[d]imidazol-1-yl)ethyl)piperidine-1-carboxylate (61) The product was synthesized from phenol **33** (39 mg, 0.12 mmol) according to Procedure C for the synthesis of phenol ethers via Mitsunobu reaction. The crude product was purified by automated flash chromatography using a gradient of cyclohexane: ethyl acetate 10:1 to 1:7 to yield the desired product (55 mg, 64%). ^1H NMR (400 MHz, CDCl_3) δ 7.90 – 7.78 (m, 2H), 7.78 – 7.64 (m, 3H), 7.64 – 7.45 (m, 5H), 7.35 – 7.17 (m, 6H), 7.16 – 7.06 (m, 2H), 6.93 – 6.83 (m, 2H), 6.74 (d, $J = 7.6$ Hz, 1H), 5.31 (s, 2H), 4.70 (t, $J = 8.2$ Hz, 1H), 4.63 – 4.51 (m, 1H), 4.51 – 4.36 (m, 1H), 4.18 – 4.04 (m, 1H), 4.02 – 3.74 (m, 1H), 2.70 (t, $J = 12.0$ Hz, 1H), 2.63 – 2.35 (m, 2H), 2.30 (s, 3H), 1.88 (d, $J = 12.4$ Hz, 1H), 1.44 – 1.30 (m, 9H), 1.29 – 1.18 (m, 1H), 1.00 – 0.73 (m, 2H). ^{13}C NMR (101 MHz, CDCl_3) δ 159.50, 155.80, 154.75, 153.98, 143.82, 143.22, 136.42, 134.69, 134.43, 130.83, 130.79, 130.48, 130.31, 130.07, 128.96, 127.84, 126.95, 125.39, 123.44, 123.18, 123.02, 122.94, 122.80, 120.82, 119.98, 114.92, 112.06, 110.55, 79.92, 67.46, 61.68, 46.89, 36.46, 30.15, 28.79, 28.60, 19.32. LC-MS (ESI): calcd for $\text{C}_{46}\text{H}_{47}\text{N}_5\text{O}_3$: 718.37517 $[\text{M}+\text{H}]^+$, found: 718.32 $[\text{M}+\text{H}]^+$, $R_t = 8.16$ min; HR-MS found: 718.37640 $[\text{M}+\text{H}]^+$.

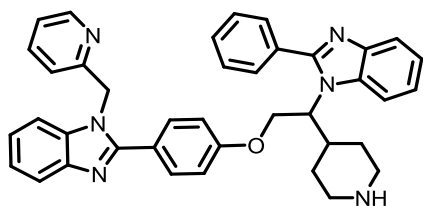
General Procedure D for the Boc-deprotection of piperidine-containing benzimidazoles



To a solution of Boc-protected piperidine in DCM (1 mL / 20 μM protected piperidine) was added a 4 M HCl/dioxane solution to a final concentration of 2 M HCl. The reaction mixture was stirred at room temperature for 3 h. The solvent was removed *in vacuo* to afford the product in quantitative yield as an HCl-salt. Further purification, if required, is described below.

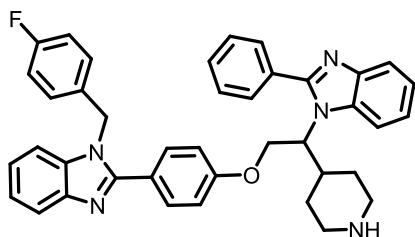


1-Benzyl-2-(4-(2-(2-phenyl-1H-benzo[d]imidazol-1-yl)-2-(piperidin-4-yl)ethoxy)phenyl)-1H-benzo[d]imidazole (62) The product was synthesized according to General Procedure (D) starting from **8** (32 mg, 0.046 mmol) to afford the HCl-salt in quantitative yield. The residue was dissolved in methanol (500 μ L) and applied to a preparative C18-RP column eluting with a gradient (CH₃CN: H₂O 1:5 to 9:1 containing 0.1% TFA), to afford the desired piperidine (20 mg, 0.033 mmol, 71%) as a TFA-salt. ¹H NMR (400 MHz, DMSO-*d*₆) δ 7.92 (d, *J* = 6.8 Hz, 1H), 7.77 – 7.71 (m, 2H), 7.69 – 7.63 (m, 2H), 7.63 – 7.49 (m, 5H), 7.41 – 7.36 (m, 1H), 7.30 – 7.14 (m, 7H), 7.05 (d, *J* = 8.6 Hz, 2H), 6.97 (d, *J* = 7.3 Hz, 2H), 5.51 (s, 2H), 4.86 (t, *J* = 9.9 Hz, 1H), 4.62 – 4.52 (m, 1H), 4.47 (t, *J* = 8.5 Hz, 1H), 2.89 (d, *J* = 12.0 Hz, 1H), 2.68 (d, *J* = 12.0 Hz, 1H), 2.46 – 2.34 (m, 1H), 2.28 – 2.11 (m, 1H), 1.89 – 1.80 (m, 1H), 1.13 – 0.98 (m, 1H), 0.77 – 0.51 (m, 2H). ¹³C NMR (101 MHz, DMSO-*d*₆) δ 159.70, 155.88, 153.74, 143.78, 143.36, 137.68, 136.61, 133.94, 131.49, 131.14, 130.68, 130.27, 129.46, 129.28, 128.10, 126.65, 123.48, 123.10, 122.78, 122.66, 120.27, 119.71, 115.40, 113.27, 111.58, 67.15, 62.29, 48.11, 46.11, 46.01, 36.24, 31.25, 29.88. LC-MS (ESI): calcd for C₄₀H₃₇N₅O: 604.30709 [M+H]⁺, found: 604.26 [M+H]⁺, *R*_t = 5.34 min; HR-MS found: 604.30716 [M+H]⁺. [α]_D²⁰: -140.0° for the (*S*)-enantiomer (*c*=0.6, DMSO, HCl salt).

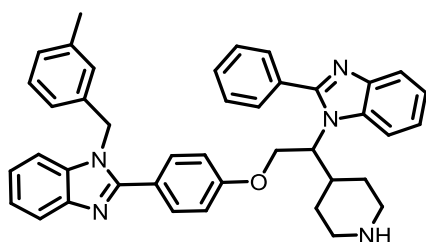


2-Phenyl-1-(1-(piperidin-4-yl)-2-(4-(1-(pyridin-2-ylmethyl)-1H-benzo[d]imidazol-2-yl)phenoxy)ethyl)-1H-benzo[d]imidazole (63) The product was synthesized according to General Procedure (D) to afford the HCl-salt in quantitative yield. The residue was dissolved in methanol (500 μ L) and applied to a preparative C18-RP column eluting with a gradient (CH₃CN: H₂O 1:5 to 9:1 containing 0.1% TFA), to afford the desired piperidine (27 mg, 0.044 mmol, 74%) as a TFA-salt. ¹H-NMR (600 MHz, DMSO-*d*₆) δ 9.35 – 9.24 (m, 1H), 9.00 – 8.86 (m, 1H), 8.72 – 8.65 (m, 2H), 8.34 – 8.26 (m, 1H), 8.03 – 7.96 (m, 1H), 7.93 – 7.85 (m, 4H), 7.80 – 7.67 (m, 6H), 7.59 – 7.48 (m, 4H), 7.20 (d, *J* = 8.5 Hz, 2H), 5.84 (s, 2H), 4.92 –

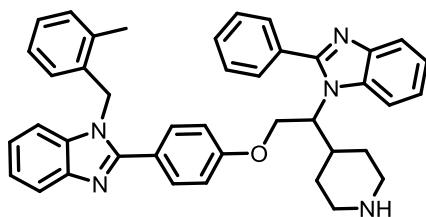
4.86 (m, 1H), 4.75 (d, $J = 8.3$ Hz, 1H), 4.69 – 4.53 (m, 1H), 3.26 (d, $J = 11.6$ Hz, 1H), 3.04 (d, $J = 12.1$ Hz, 1H), 2.97 – 2.84 (m, 2H), 2.70 (d, $J = 9.6$ Hz, 1H), 2.09 (d, $J = 12.5$ Hz, 1H), 1.64 – 1.53 (m, 1H), 1.28 – 1.18 (m, 2H). ^{13}C NMR (151 MHz, $\text{DMSO-}d_6$) δ 161.32, 153.01, 151.57, 133.82, 133.34, 132.85, 132.59, 131.32, 131.19, 130.03, 126.82, 126.49, 126.40, 126.12, 116.84, 116.09, 115.73, 115.28, 113.69, 66.71, 62.57, 46.64, 42.93, 40.70, 33.41, 26.16, 25.90. LC-MS (ESI): calcd for $\text{C}_{39}\text{H}_{36}\text{N}_6\text{O}$: 605.30234 $[\text{M}+\text{H}]^+$, found: 605.28 $[\text{H}]^+$, $R_t = 4.89$ min; HR-MS found 605.30247 $[\text{M}+\text{H}]^+$.



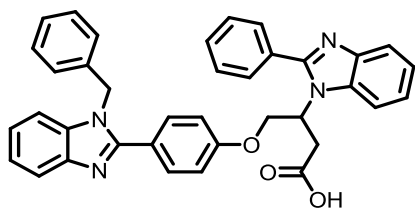
1-(4-Fluorobenzyl)-2-(4-(2-(2-phenyl-1H-benzo[d]imidazol-1-yl)-2-(piperidin-4-yl)ethoxy)phenyl)-1H-benzo[d]imidazole (64) The product was synthesized according to General Procedure (D) to afford the HCl salt. The residue was dissolved in methanol (500 μL) and applied to a preparative C18-RP column eluting with a gradient ($\text{CH}_3\text{CN}:\text{H}_2\text{O}$ 1:5 to 9:1 containing 0.1% acetic acid), to afford the desired piperidine (16 mg, 65%). ^1H NMR (600 MHz, $\text{DMSO-}d_6$) δ 7.92 (d, $J = 7.4$ Hz, 1H), 7.73 (d, $J = 6.9$ Hz, 2H), 7.66 (d, $J = 8.0$ Hz, 2H), 7.61 – 7.49 (m, 5H), 7.44 – 7.37 (m, 1H), 7.25 – 7.16 (m, 4H), 7.12 – 7.02 (m, 4H), 7.02 – 6.96 (m, 2H), 5.49 (s, 2H), 4.85 (t, $J = 9.9$ Hz, 1H), 4.58 (d, $J = 8.1$ Hz, 1H), 4.46 (t, $J = 8.6$ Hz, 1H), 2.92 (d, $J = 12.1$ Hz, 1H), 2.70 (d, $J = 11.9$ Hz, 1H), 2.26 – 2.15 (m, 1H), 1.88 (d, $J = 11.9$ Hz, 1H), 1.12 – 0.99 (m, 1H), 0.78 – 0.59 (m, 2H). ^{13}C NMR (151 MHz, $\text{DMSO-}d_6$) δ 173.50, 162.82, 161.20, 159.69, 155.87, 153.67, 143.76, 143.32, 136.45, 133.85, 133.83, 131.43, 131.16, 130.68, 130.30, 129.30, 128.80, 128.74, 123.39, 123.18, 123.12, 122.84, 122.70, 120.28, 119.73, 116.36, 116.22, 115.41, 113.28, 111.57, 67.07, 62.18, 47.41, 45.64, 45.55, 35.89, 30.68, 29.35, 22.85. LC-MS (ESI): calcd for $\text{C}_{40}\text{H}_{36}\text{FN}_5\text{O}$: 622.29767 $[\text{M}+\text{H}]^+$, found: 622.28 $[\text{M}+\text{H}]^+$, $R_t = 5.70$ min; HR-MS found 622.29806 $[\text{M}+\text{H}]^+$.



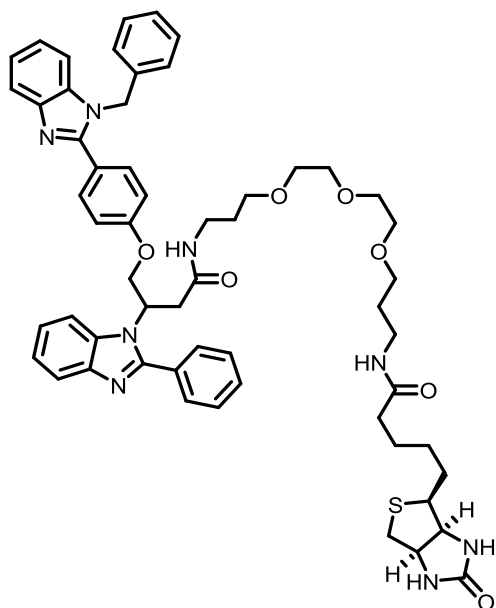
1-(3-Methylbenzyl)-2-(4-(2-(2-phenyl-1H-benzo[d]imidazol-1-yl)-2-(piperidin-4-yl)ethoxy)phenyl)-1H-benzo[d]imidazole (65) The product was synthesized according to General Procedure (D) to afford the HCl salt. The residue is dissolved in methanol (500 μ L) and applied to a preparative C18-RP column eluting with a gradient (ACN: H₂O 1:5 to 9:1 containing 0.1% acetic acid), to afford the desired piperidine (69%, 15 mg). ¹H NMR (600 MHz, DMSO-*d*₆) δ 7.91 (d, *J* = 7.3 Hz, 1H), 7.77 – 7.67 (m, 2H), 7.70 – 7.62 (m, 2H), 7.58 (t, *J* = 8.3 Hz, 2H), 7.57 – 7.49 (m, 3H), 7.37 (d, *J* = 7.9 Hz, 1H), 7.25 – 7.10 (m, 5H), 7.09 – 7.00 (m, 3H), 6.82 (s, 1H), 6.70 (d, *J* = 7.7 Hz, 1H), 5.45 (s, 2H), 4.85 (t, *J* = 10.0 Hz, 1H), 4.58 (d, *J* = 8.1 Hz, 1H), 4.46 (t, *J* = 8.5 Hz, 1H), 2.91 (d, *J* = 12.1 Hz, 1H), 2.70 (d, *J* = 12.1 Hz, 1H), 2.25 – 2.16 (m, 1H), 1.94 – 1.83 (m, 1H), 1.16 – 1.00 (m, 1H), 0.83 – 0.56 (m, 2H). ¹³C NMR (151 MHz, DMSO-*d*₆) δ 159.67, 155.86, 153.72, 151.53, 148.65, 143.75, 143.29, 138.64, 137.61, 136.59, 133.86, 131.42, 131.12, 130.68, 130.30, 129.39, 129.30, 128.78, 127.20, 123.66, 123.45, 123.12, 122.77, 122.69, 120.27, 119.68, 115.39, 113.27, 111.58, 67.07, 62.18, 48.06, 45.63, 35.92, 30.73, 29.41, 22.5, 21.66. LC-MS (ESI): calcd for C₄₁H₃₉N₅O: 618.32274 [M+H]⁺, found: 618.30[M+H]⁺, R_t = 5.79 min; HR-MS found 618.32299 [M+H]⁺.



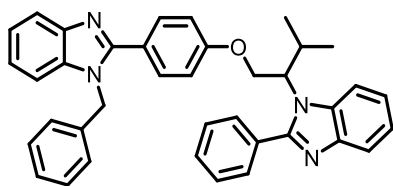
1-(2-Methylbenzyl)-2-(4-(2-(2-phenyl-1H-benzo[d]imidazol-1-yl)-2-(piperidin-4-yl)ethoxy)phenyl)-1H-benzo[d]imidazole (66) The product was synthesized according to General Procedure (D) (38 mg, 0.061 mmol) to afford the product as an HCl-salt in quantitative yield. ¹H NMR (400 MHz, DMSO-*d*₆) δ 8.64 (d, *J* = 10.7 Hz, 1H), 8.22 – 8.07 (m, 1H), 7.99 (d, *J* = 5.1 Hz, 1H), 7.87 – 7.68 (m, 4H), 7.67 – 7.55 (m, 5H), 7.48 (d, *J* = 8.2 Hz, 1H), 7.42 (t, *J* = 7.6 Hz, 1H), 7.38 – 7.29 (m, 3H), 7.24 (d, *J* = 7.1 Hz, 1H), 7.20 – 7.07 (m, 3H), 7.02 (t, *J* = 7.5 Hz, 1H), 6.49 (d, *J* = 7.7 Hz, 1H), 5.54 (s, 2H), 4.86 (t, *J* = 9.8 Hz, 1H), 4.64 (d, *J* = 10.3 Hz, 1H), 4.58 – 4.42 (m, 1H), 3.27 (d, *J* = 11.7 Hz, 1H), 3.06 (d, *J* = 11.5 Hz, 1H), 2.94 – 2.60 (m, 3H), 2.27 (s, 3H), 2.08 (d, *J* = 12.8 Hz, 1H), 1.41 (d, *J* = 12.5 Hz, 1H), 1.19 – 0.90 (m, 2H). ¹³C NMR (101 MHz, DMSO-*d*₆) δ 160.65, 158.66, 152.61, 135.68, 135.15, 134.48, 133.14, 131.49, 131.15, 131.00, 130.80, 129.84, 129.52, 128.21, 127.00, 125.23, 124.98, 123.94, 123.71, 119.60, 117.61, 115.81, 113.67, 112.75, 66.96, 61.61, 47.16, 43.20, 33.49, 26.65, 25.93, 19.34. LC-MS (ESI): calcd for C₄₁H₃₉N₅O: 618.32274 [M+H]⁺, found: 618.26 [M+H]⁺, R_t = 5.85 min; HR-MS found 618.32318 [M+H]⁺.

Procedures for the labeling of benzimidazole 55 with biotin

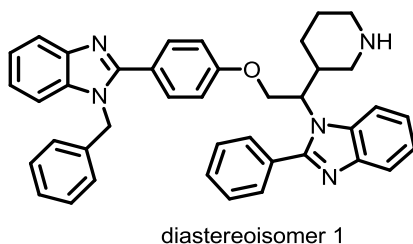
4-(4-(1-Benzyl-1H-benzo[d]imidazol-2-yl)phenoxy)-3-(2-phenyl-1H-benzo[d]imidazol-1-yl)butanoic acid (67) To a suspension of **55** (20 mg, 36 μmol) in a mixture of CCl_4 , acetonitrile and water 1:1:1.5 (2 mL) was added sodium periodate (31 mg, 140 μM) and RuCl_3 (0.3 mg). After 24h of stirring, sodium periodate (31 mg, 140 μM) and RuCl_3 (0.3 mg) were added. The reaction mixture was stirred for an additional 2 d. The reaction mixture was concentrated *in vacuo*. The aqueous residue was extracted with DCM (3x10 mL). The combined organic phases were dried (Na_2SO_4), filtered and concentrated *in vacuo*. The crude reaction mixture was subjected to automated flash chromatography (gradient DCM: MeOH 100:1 to 15:1) to afford compound **67** (13 mg, 22 μmol , 62%). ^1H NMR (400 MHz, $\text{DMSO}-d_6$) δ 7.91 (d, $J = 7.1$ Hz, 1H), 7.76 (dd, $J = 7.2, 2.0$ Hz, 2H), 7.65 (dd, $J = 10.7, 4.8$ Hz, 2H), 7.56 (d, $J = 8.7$ Hz, 2H), 7.48 (dd, $J = 8.2, 2.8$ Hz, 3H), 7.39 (d, $J = 6.4$ Hz, 1H), 7.32 – 7.14 (m, 7H), 6.96 (t, $J = 8.0$ Hz, 4H), 5.50 (s, 2H), 5.23 (s, 1H), 4.71 (t, $J = 9.9$ Hz, 1H), 4.39 (dd, $J = 10.7, 4.0$ Hz, 1H), 3.25 – 3.14 (m, 2H). ^{13}C NMR (101 MHz, $\text{DMSO}-d_6$) δ 159.42, 155.70, 153.73, 143.95, 143.35, 137.67, 136.57, 133.90, 131.60, 131.12, 130.59, 130.07, 129.47, 128.95, 128.11, 126.68, 123.49, 123.11, 122.77, 122.60, 120.24, 119.72, 115.25, 113.18, 111.60, 68.23, 53.52, 48.10, 34.96, 29.68. LC-MS (ESI): calcd for $\text{C}_{37}\text{H}_{30}\text{N}_4\text{O}_3$: 579.23907 $[\text{M}+\text{H}]^+$, found: 579.36 $[\text{M}+\text{H}]^+$, $R_t = 6.26$ min; HR-MS found 579.23912 $[\text{M}+\text{H}]^+$.



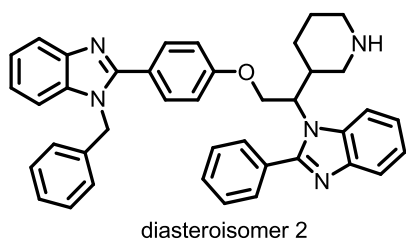
N-(18-(4-(1-Benzyl-1H-benzo[d]imidazol-2-yl)phenoxy)-15-oxo-17-(2-phenyl-1H-benzo[d]imidazol-1-yl)-4,7,10-trioxa-14-azaoctadecyl)-5-((3a*S*,4*S*,6a*R*)-2-oxohexahydro-1H-thieno[3,4-*d*]imidazol-4-yl)pentanamide (68) To a mixture of acid **67** (13 mg, 22 μ mol), Biotin-PEG-NH₂TFA (38 mg, 67 μ mol) in DMF (1 mL) at room temperature was added DIPEA (32 μ L, 180 μ mol) and PyBOP (54 mg, 100 μ mol). The reaction mixture was stirred at room temperature for 2 d and then concentrated *in vacuo*. The residue was dissolved in methanol (500 μ L) and applied to a preparative C18-RP column eluting with a gradient (CH₃CN:H₂O 1:4 to 9:1 containing 0.1% TFA), to afford the product as a mixture of diastereoisomers (16 mg, 16 μ mol, 71%). ¹H NMR (400 MHz, DMSO-*d*₆) δ 8.12 (d, *J* = 7.3 Hz, 1H), 8.06 (t, *J* = 5.6 Hz, 1H), 7.91 – 7.84 (m, 2H), 7.84 – 7.74 (m, 2H), 7.75 – 7.62 (m, 4H), 7.62 – 7.54 (m, 3H), 7.53 – 7.39 (m, 4H), 7.35 – 7.22 (m, 3H), 7.14 – 7.01 (m, 4H), 6.40 (s, 2H), 5.64 (s, 2H), 5.35 (s, 1H), 4.83 – 4.74 (m, 1H), 4.47 (dd, *J* = 11.0, 3.7 Hz, 1H), 4.28 (dd, *J* = 7.8, 5.0 Hz, 1H), 4.10 (dd, *J* = 7.7, 4.5 Hz, 1H), 3.51 – 3.38 (m, 6H), 3.38 – 3.30 (m, 4H), 3.30 – 3.20 (m, 1H), 3.18 – 3.10 (m, 3H), 3.10 – 2.97 (m, 4H), 2.96 – 2.86 (m, 1H), 2.83 – 2.73 (m, 1H), 2.55 (d, *J* = 12.4 Hz, 1H), 2.51 – 2.44 (m, 2H), 2.10 – 1.96 (m, 2H), 1.68 – 1.54 (m, 3H), 1.54 – 1.36 (m, 5H), 1.36 – 1.15 (m, 2H). ¹³C NMR (101 MHz, DMSO-*d*₆) δ 172.62, 168.60, 163.40, 160.84, 159.10, 158.76, 153.98, 151.92, 135.88, 134.17, 132.06, 131.90, 130.91, 129.60, 129.45, 128.65, 127.04, 125.90, 125.68, 125.22, 118.05, 117.71, 116.58, 115.82, 115.36, 114.63, 113.38, 70.41, 70.37, 70.20, 70.14, 68.78, 68.27, 61.74, 59.90, 56.10, 54.84, 48.86, 36.41, 36.36, 35.89, 35.21, 30.09, 29.71, 28.89, 28.72, 25.98. LC-MS (ESI): calcd for C₅₇H₆₆N₈O₇S: 1007.48479 [M+H]⁺, found: 1007,60 [M+H]⁺, Rt = 5.89 min; HR-MS found 1007.48529 [M+H]⁺.



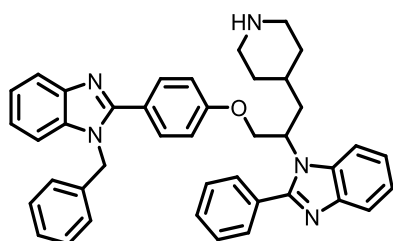
1-Benzyl-2-(4-(3-methyl-2-(2-phenyl-1H-benzo[d]imidazol-1-yl)butoxy)phenyl)-1H-benzo[d]imidazole (69) The product was synthesized by Carsten Schultz-Fademrecht, LDC Dortmund. ^1H NMR (400 MHz, CD_3OD) δ 7.95 - 7.86 (m, 1H), 7.79 (d, $J = 5.0$ Hz, 2H), 7.73 (d, $J = 8.0$ Hz, 2H), 7.63 - 7.53 (m, 6H), 7.44 - 7.23 (m, 8H), 7.08 - 7.01 (m, 3H), 5.52 (s, 2H), 4.69 - 4.45 (m, 3H), 2.82 (s, 1H), 1.16 (d, $J = 6.5$ Hz, 3H), 0.64 (d, $J = 6.6$ Hz, 3H). LC-MS: 5min_A: $t_{\text{R}}=1.98\text{min}$, 10min_C: $t_{\text{R}}=4.39\text{min}$. MS (ES) $\text{C}_{38}\text{H}_{34}\text{N}_4\text{O}$ calcd: 562, found: 563 $[\text{M}+\text{H}]^+$. LC-MS (ESI): calcd for $\text{C}_{38}\text{H}_{34}\text{N}_4\text{O}$: 563.28054 $[\text{M}+\text{H}]^+$, found 563.28190 $[\text{M}+\text{H}]^+$.



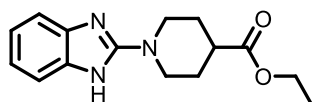
1-Benzyl-2-(4-(2-(2-phenyl-1H-benzo[d]imidazol-1-yl)-2-(piperidin-3-yl)ethoxy)phenyl)-1H-benzo[d]imidazole (diastereoisomer 1) (70) The product was synthesized by Carsten Schultz-Fademrecht, LDC Dortmund. ^1H NMR (400 MHz, CD_3OD) δ 7.95 (d, $J = 7.6$ Hz, 1H), 7.83 - 7.71 (m, 4H), 7.69 - 7.58 (m, 5H), 7.53 - 7.33 (m, 5H), 7.28 (m, 3H), 7.14 (d, $J = 8.5$ Hz, 2H), 7.06 (d, $J = 6.6$ Hz, 2H), 5.59 (s, 2H), 4.81 (m, 1H), 4.68 (d, $J = 9.8$ Hz, 1H), 3.67 (d, $J = 13.0$ Hz, 1H), 3.30 (m, 2H), 3.09 (m, 1H), 2.91 (t, $J = 12.1$ Hz, 1H), 2.83 (dt, $J = 2.7$ Hz, $J = 12.7$ Hz, 1H), 1.74 (d, $J = 14.3$ Hz, 1H), 1.54 (q, $J = 14.0$ Hz, 1H), 1.18 (d, $J = 12.1$ Hz, 1H), 1.09 (q, $J = 11.2$ Hz, 1H). LC-MS: 5min_A: $t_{\text{R}}=1.65\text{min}$, 10min_C: $t_{\text{R}}=3.37\text{min}$. LC-MS (ESI) $\text{C}_{40}\text{H}_{37}\text{N}_5\text{O}$ calcd: 603, found: 604 $[\text{M}+\text{H}]^+$. LC-MS (ESI, HR-MS): calcd for $\text{C}_{40}\text{H}_{37}\text{N}_5\text{O}$: 604.30709. $[\text{M}+\text{H}]^+$ found 604.30876 $[\text{M}+\text{H}]^+$.



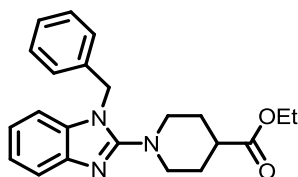
1-Benzyl-2-(4-(2-(2-phenyl-1H-benzo[d]imidazol-1-yl)-2-(piperidin-3-yl)ethoxy)phenyl)-1H-benzo[d]imidazole (diastereoisomer 2) (71) The product was synthesized by Carsten Schultz-Fademrecht, LDC Dortmund. ^1H NMR (400 MHz, CD_3OD) δ 8.05 (d, $J = 7.6$ Hz, 1H), 7.79 (m, 3H), 7.74 (d, $J = 7.3$ Hz, 1H), 7.68 - 7.63 (m, 5H), 7.60 - 7.33 (m, 5H), 7.30 (m, 3H), 7.12 (d, $J = 8.5$ Hz, 2H), 7.07 (dd, $J = 2.4$ Hz, $J = 7.7$ Hz, 2H), 5.62 (s, 2H), 4.77 (m, 1H), 4.71 (d, $J = 10.1$ Hz, 1H), 3.32 (m, 1H), 3.14 (m, 1H), 2.85 (dt, $J = 2.9$ Hz, $J = 13.2$ Hz, 1H), 2.69 (d, $J = 12.8$ Hz, 1H), 2.55 (m, 1H), 2.22 (d, $J = 10.5$ Hz, 1H), 1.89 (d, $J = 15.0$ Hz, 1H), 1.84 (m, 1H), 1.40 (m, 2H). LC-MS: 5min_A: $t_{\text{R}} = 1.61$ min, 10min_C: $t_{\text{R}} = 3.26$ min. MS (ESI) $\text{C}_{40}\text{H}_{37}\text{N}_5\text{O}$ calcd: 603, found: 604 $[\text{M}+\text{H}]^+$. LC-MS (ESI, HR-MS): calcd for $\text{C}_{40}\text{H}_{37}\text{N}_5\text{O}$: 604.30709. $[\text{M}+\text{H}]^+$ found 604.30839 $[\text{M}+\text{H}]^+$.



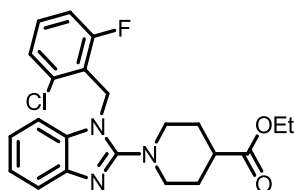
1-Benzyl-2-(4-(2-(2-phenyl-1H-benzo[d]imidazol-1-yl)-3-(piperidin-4-yl)propoxy)phenyl)-1H-benzo[d]imidazole (72) The product was synthesized by Carsten Schultz-Fademrecht, LDC Dortmund. ^1H NMR (400 MHz, CD_3OD , 300K) δ 7.89 (d, $J = 8.2$ Hz, 1H), 7.83 (m, 2H), 7.72 (m, 2H), 7.59 (m, 5H), 7.44 - 7.23 (m, 8H), 7.06 (d, $J = 8.6$ Hz, 2H), 7.02 (d, $J = 6.9$ Hz, 2H), 5.52 (s, 2H), 5.09 (m, 1H), 4.93 (t, $J = 10.1$ Hz, 1H), 4.53 (dd, $J = 4.2$ Hz, 10.1 Hz, 1H), 3.17 (m, 3H), 2.72 (m, 2H), 2.41 (t, $J = 11.5$ Hz, 1H), 1.86 (m, 1H), 1.52 (d, $J = 15.4$ Hz, 1H), 1.31 (m, 2H), 1.16 (m, 1H). LC-MS: 5min_A: $t_{\text{R}} = 1.60$ min, 10min_C: $t_{\text{R}} = 3.23$ min. MS (ESI) $\text{C}_{41}\text{H}_{39}\text{N}_5\text{O}$ calcd: 617, found: 618 $[\text{M}+\text{H}]^+$. LC-MS (ESI, HR-MS): calcd for $\text{C}_{41}\text{H}_{39}\text{N}_5\text{O}$: 618.32479 $[\text{M}+\text{H}]^+$, found 618.30839 $[\text{M}+\text{H}]^+$.

Procedures for the synthesis of benzimidazole fragments

Ethyl 1-(1H-benzo[d]imidazol-2-yl)piperidine-4-carboxylate (77) To a solution of 2-chloro benzimidazole (6.0 g, 39.3 mmol) in NMP (40 mL) was added 4-carboxyethyl piperidine (16.5 g, 105 mmol) and diisopropylethylamine (13.4 mL, 78.2 mmol). The reaction mixture was heated to 90°C and stirred for 16 h. Water (100 mL) was added and stirring was continued for an additional 20 min. The precipitate was collected by filtration and washed with water (3x 100 mL) and EtOAc (3x 30 mL) to yield the desired compound (8.67 g, 81% mmol). ¹H NMR (400 MHz, CDCl₃) δ 7.33 – 7.08 (m, 2H), 7.03 – 6.81 (m, 2H), 4.18 – 3.98 (m, 4H), 3.20 – 3.00 (m, 2H), 2.52 – 2.38 (m, 1H), 1.94 (d, *J* = 12.5 Hz, 2H), 1.83 – 1.66 (m, 2H), 1.29 – 1.07 (m, 3H). ¹³C NMR (101 MHz, CDCl₃) δ 174.59, 156.47, 120.45, 60.73, 46.33, 41.05, 27.65, 14.39. LC-MS (ESI): calcd for C₁₅H₁₉N₃O₂: 274.15500 [M+H]⁺, found: 274.16 [H]⁺, R_t = 5.75 min; HR-MS found 274.15523 [M+H]⁺.

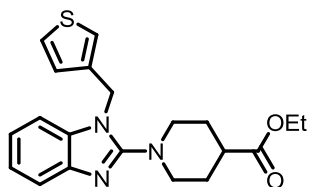


Ethyl 1-(1-benzyl-1H-benzo[d]imidazol-2-yl)piperidine-4-carboxylate (78) The product was synthesized by procedure A starting from compound **77** (140 mg, 0.38 mmol, 85%). ¹H NMR (400 MHz, DMSO-*d*₆) δ 7.46 – 6.96 (m, 9H), 5.25 (s, 2H), 4.15 – 3.99 (m, 2H), 3.41 (d, *J* = 12.3 Hz, 2H), 2.95 (t, *J* = 11.2 Hz, 2H), 2.60 – 2.50 (m, 1H), 1.93 – 1.62 (m, 4H), 1.16 (t, *J* = 6.9 Hz, 3H). ¹³C NMR (101 MHz, DMSO-*d*₆) δ 174.73, 158.51, 141.99, 137.66, 135.78, 129.37, 128.02, 127.09, 121.93, 121.50, 118.02, 110.43, 60.61, 50.42, 47.53, 40.57, 28.09, 14.77. LC-MS (ESI): calcd for C₂₂H₂₅N₃O: 364.19 [M+H]⁺, found: 364.22 [H]⁺, R_t = 8.01 min.

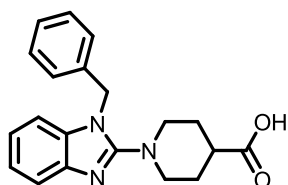


Ethyl 1-(1-(2-chloro-6-fluorobenzyl)-1H-benzo[d]imidazol-2-yl)piperidine-4-carboxylate (79) The product was synthesized from ethyl 1-(1H-benzo[d]imidazol-2-yl)piperidine-4-

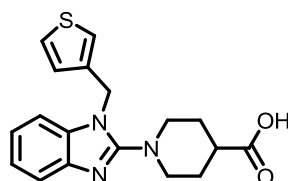
carboxylate (**77**) (100 mg, 0.37 mmol) according to General Procedure A for the alkylation of benzimidazoles. The crude product was purified by automated flash chromatography using a gradient of cyclohexane and ethyl acetate 20:1 to 1:2 to yield compound **79** (141 mg, 0.34 mmol, 92%). ^1H NMR (400 MHz, DMSO- d_6) δ 7.42 – 7.33 (m, 2H), 7.31 – 7.26 (m, 1H), 7.25 – 7.17 (m, 1H), 7.00 (d, J = 8.4 Hz, 1H), 6.95 – 6.90 (m, 2H), 5.39 (s, 2H), 4.08 (q, J = 7.1 Hz, 2H), 3.43 – 3.37 (m, 2H), 3.01 – 2.89 (m, 2H), 2.58 – 2.49 (m, 1H), 1.95 – 1.83 (m, 2H), 1.80 – 1.67 (m, 2H), 1.18 (t, J = 7.1 Hz, 3H). ^{13}C NMR (101 MHz, DMSO- d_6) δ 174.81, 161.97 ($^{\text{C-F}}J$ = 249.2 Hz), 159.01, 142.06, 135.14 ($^{\text{C-F}}J$ = 5.4 Hz), 134.52, 131.53 ($^{\text{C-F}}J$ = 9.9 Hz), 126.60 ($^{\text{C-F}}J$ = 3.2 Hz), 122.17 ($^{\text{C-F}}J$ = 16.5 Hz), 121.72, 121.42, 118.33, 115.41 ($^{\text{C-F}}J$ = 22.2 Hz), 109.94, 60.61, 50.59, 28.22, 14.79. LC-MS (ESI): calcd for $\text{C}_{22}\text{H}_{23}\text{ClFN}_3\text{O}_2$: 416.15356 $[\text{M}+\text{H}]^+$, found: 416.13 $[\text{H}]^+$, R_t = 7.03 min; HR-MS found 416.15341 $[\text{M}+\text{H}]^+$.



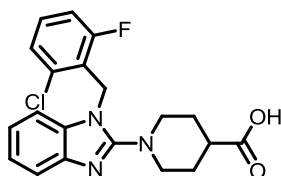
Ethyl 1-(1-(thiophen-3-ylmethyl)-1H-benzo[d]imidazol-2-yl)piperidine-4-carboxylate (80**)** To a mixture of benzimidazole (2.0 g, 7.3 mmol), 3-hydroxymethyl thiophene (2.5 g, 22.0 mmol) and tri-*n*-butyl phosphine (5.4 mL, 22.0 mmol) in THF (20 mL) was added at 0°C TMAD (3.8 g, 22.0 mmol) in one portion. The resulting suspension was allowed to warm to room temperature and stirred at this temperature for 3 h. The reaction mixture was concentrated *in vacuo* and the residue was purified by column chromatography (petroleum ether : ethyl acetate 5:1 to 1:1) to afford the desired compound (61%, 1.6 g). ^1H NMR (400 MHz, CDCl_3) δ 7.62 (dt, J = 7.9, 1.0 Hz, 1H), 7.32 (dd, J = 5.0, 3.0 Hz, 1H), 7.21 – 7.16 (m, 1H), 7.12 – 7.09 (m, 2H), 7.02 (dd, J = 3.0, 1.3 Hz, 1H), 6.96 (dd, J = 5.0, 1.3 Hz, 1H), 5.18 (s, 2H), 4.16 (q, J = 7.1 Hz, 2H), 3.49 (dt, J = 6.7, 3.1 Hz, 2H), 3.02 (td, J = 12.5, 2.7 Hz, 2H), 2.48 (tt, J = 11.1, 4.1 Hz, 1H), 2.05 – 1.95 (m, 2H), 1.95 – 1.79 (m, 2H), 1.27 (t, J = 7.1 Hz, 3H). ^{13}C NMR (101 MHz, CDCl_3) δ 174.81, 158.38, 141.80, 137.71, 135.44, 127.28, 126.23, 122.15, 121.71, 121.70, 118.40, 109.49, 60.77, 50.73, 44.18, 41.10, 28.32, 14.45. LC-MS (ESI): calcd for $\text{C}_{20}\text{H}_{23}\text{N}_3\text{O}_2\text{S}$: 370.15837 $[\text{M}+\text{H}]^+$, found: 370.13 $[\text{M}+\text{H}]^+$, R_t = 6.60 min; HR-MS found 370.15890 $[\text{M}+\text{H}]^+$.



1-(1-Benzyl-1H-benzo[d]imidazol-2-yl)piperidine-4-carboxylic acid (81) To ester **78** (1.10 g, 3.0 mmol) in MeOH/H₂O (30 mL, 10/1 vol/vol) was added KOH (0.84 g, 15 mmol) at room temperature. The resulting reaction mixture was stirred at room temperature for 5 h. The pH was adjusted with 20% acetic acid in H₂O to 6 and the aqueous phase was extracted with DCM (4x 30 mL). The combined organic phases were dried over Na₂SO₄, filtered and concentrated *in vacuo* to afford **81** (0.93 g, 92 %). ¹H NMR (400 MHz, DMSO-*d*₆) δ 12.17 (s, 1H), 7.43 (d, *J* = 7.8 Hz, 1H), 7.31 (t, *J* = 7.6 Hz, 2H), 7.24 (t, *J* = 7.3 Hz, 1H), 7.16 (d, *J* = 7.5 Hz, 3H), 7.09 (t, *J* = 7.4 Hz, 1H), 7.03 (t, *J* = 7.5 Hz, 1H), 5.27 (s, 2H), 3.49 – 3.40 (m, 2H), 3.04 – 2.90 (m, 2H), 2.47 – 2.39 (m, 1H), 1.88 – 1.80 (m, 2H), 1.78 – 1.63 (m, 2H). ¹³C NMR (101 MHz, CDCl₃) δ 176.35, 172.61, 137.46, 135.50, 129.38, 128.06, 127.08, 122.17, 121.72, 117.56, 110.55, 50.42, 47.68, 28.12, 21.71. LC-MS (ESI): calcd for C₂₀H₂₁N₃O₂: 336.17065 [M+H]⁺, found: 336.17 [M+H]⁺, R_t = 5.82 min; HR-MS found 336.17101 [M+H]⁺.



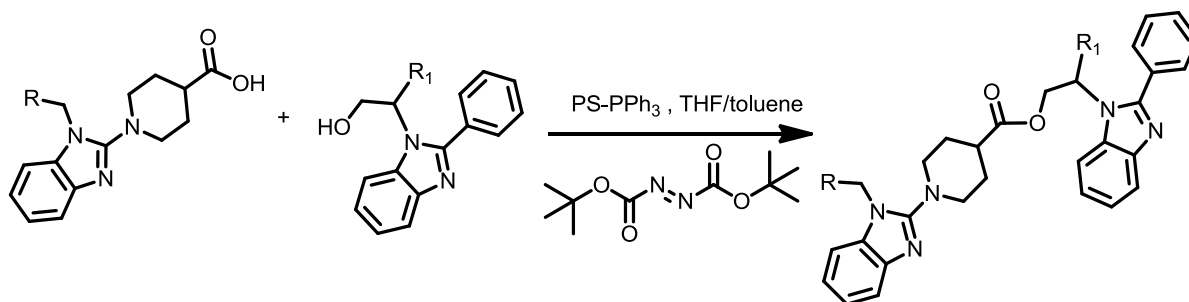
1-(1-(Thiophen-3-ylmethyl)-1H-benzo[d]imidazol-2-yl)piperidine-4-carboxylic acid (82) To ester **80** (1.6 g, 4.5 mmol) in MeOH/H₂O (40 mL, 10/1 vol/vol) was added KOH (1.3 g, 23 mmol) at room temperature. The resulting reaction mixture was stirred at room temperature for 5 h. The pH was adjusted with 20% acetic acid in H₂O to 6 and the aqueous phase was extracted with DCM (4 x 40 mL). The combined organic phases were dried over Na₂SO₄ and concentrated *in vacuo* to afford the desired compound (1.4 g, 89 %). ¹H NMR (400 MHz, DMSO-*d*₆) δ 12.23 (s, 1H), 7.49 (dd, *J* = 5.0, 3.0 Hz, 1H), 7.40 (d, *J* = 7.1 Hz, 1H), 7.29 (s, 1H), 7.23 (d, *J* = 7.5 Hz, 1H), 7.08 – 7.00 (m, 2H), 6.94 (d, *J* = 4.9 Hz, 1H), 5.21 (s, 2H), 3.47 – 3.41 (m, 2H), 3.00 – 2.89 (m, 2H), 2.47 – 2.39 (m, 1H), 1.93 – 1.83 (m, 2H), 1.82 – 1.69 (m, 2H). ¹³C NMR (151 MHz, DMSO) δ 176.50, 158.34, 138.47, 135.64, 127.85, 127.34, 125.99, 123.01, 121.88, 121.46, 117.96, 110.40, 50.59, 43.63, 28.22, 21.73. LC-MS (ESI): calcd for C₁₈H₁₉N₃O₂S: 342.12707 [M+H]⁺, found: 342.10 [M+H]⁺, R_t = 5.74 min; HR-MS found 342.12747 [M+H]⁺.



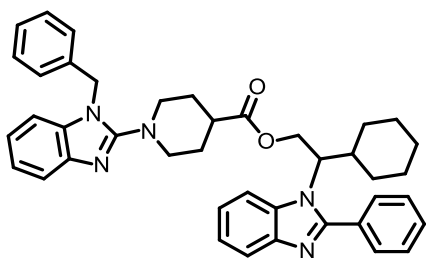
1-(1-(2-Chloro-6-fluorobenzyl)-1H-benzo[d]imidazol-2-yl)piperidine-4-carboxylic acid

(83) To a solution of the ester **79** (0.82 g, 2.0 mmol) in HCl/dioxane (4 M, 10 mL) was added water until the formation of a precipitate was observed. The reaction mixture was stirred at room temperature for 2 d, concentrated *in vacuo*, the pH of the aqueous residue was adjusted to 6 with sat. NaHCO₃ and the aqueous layer was extracted with DCM (5 x 40 mL). The combined organic phases were dried (Na₂SO₄), filtered and concentrated *in vacuo* to afford the desired product (0.65 g, 85%). ¹H NMR (400 MHz, DMSO-*d*₆) δ 7.41 – 7.34 (m, 2H), 7.29 (d, *J* = 7.8 Hz, 1H), 7.21 (t, *J* = 9.1 Hz, 1H), 7.04 – 6.97 (m, 1H), 6.97 – 6.90 (m, 2H), 5.40 (s, 2H), 3.46 – 3.37 (m, 2H), 3.02 – 2.87 (m, 2H), 2.47 – 2.39 (m, 1H), 1.90 (dd, *J* = 13.2, 3.2 Hz, 2H), 1.80 – 1.64 (m, 2H). ¹³C NMR (101 MHz, DMSO-*d*₆) δ 176.51, 163.22, 160.74, 159.08, 142.07, 135.18, 135.12, 134.53, 131.56, 131.46, 126.60, 126.57, 122.26, 122.10, 121.72, 121.40, 118.32, 115.51, 115.29, 109.94, 67.04, 50.74, 28.31. LC-MS (ESI): calcd for C₂₀H₁₉ClFN₃O₂: 388.12226 [M+H]⁺, found: 388.10 [M+H]⁺, R_t = 6.27 min; HR-MS found 388.12330 [M+H]⁺.

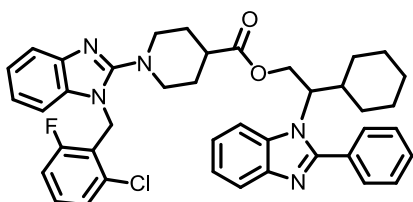
General Procedure E for esterification of two benzimidazole units



To a mixture of carboxylic acid, alcohol (1.0 eq) and polymer bound triphenylphosphine (3 meq) in THF/toluene (1:1, 3 mL/ mmol benzimidazole) was added at 0°C di-*tert*-butyl azodicarboxylate (3eq). The reaction mixture is stirred at room temperature for 16 h, diluted with DCM (15 mL/mmol benzimidazole) and filtered. The filtrate was concentrated *in vacuo* and purified by automated flash chromatography as described below.

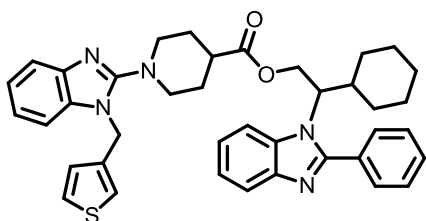


2-Cyclohexyl-2-(2-phenyl-1H-benzo[d]imidazol-1-yl) ethyl 1-(1-benzyl-1H-benzo[d]imidazol-2-yl)piperidine-4-carboxylate (84) The product was synthesized from alcohol **52** (40 mg, 0.12 mmol) and carboxylic acid **81** according to Procedure E for the esterification via Mitsunobu reaction. The crude product was purified by automated flash chromatography using a gradient of cyclohexane and ethyl acetate 50:1 to 1:2 to yield the product (57 mg, 0.09 mmol, 61%). ^1H NMR (600 MHz, DMSO-*d*6) δ 8.03 (s, 1H), 7.77 – 7.69 (m, 3H), 7.66 – 7.56 (m, 3H), 7.54 (t, $J = 7.8$ Hz, 1H), 7.42 – 7.21 (m, 10H), 5.38 (s, 2H), 4.84 (t, $J = 10.7$ Hz, 1H), 4.62 – 4.52 (m, 1H), 4.43 (t, $J = 8.0$ Hz, 1H), 3.66 – 3.55 (m, 1H), 3.56 – 3.43 (m, 1H), 3.28 – 3.10 (m, 2H), 2.62 – 2.52 (m, 1H), 2.40 (d, $J = 10.4$ Hz, 1H), 1.87 (d, $J = 10.8$ Hz, 1H), 1.72 – 1.57 (m, 3H), 1.57 – 1.32 (m, 4H), 1.32 – 1.14 (m, 1H), 1.09 – 0.83 (m, 4H), 0.73 – 0.57 (m, 1H). ^{13}C NMR (151 MHz, DMSO-*d*6) δ 173.73, 159.32, 159.09, 158.86, 158.63, 154.12, 153.28, 135.48, 132.98, 131.61, 130.74, 129.67, 129.63, 128.58, 126.89, 125.00, 124.71, 124.46, 118.46, 117.82, 115.87, 114.20, 113.41, 112.03, 109.99, 63.47, 62.19, 49.29, 48.97, 39.23, 37.42, 30.54, 29.64, 27.43, 27.36, 26.01, 25.75. LC-MS (ESI): calcd for $\text{C}_{41}\text{H}_{43}\text{N}_5\text{O}_2$: 638.34895 $[\text{M}+\text{H}]^+$, found: 638.34 $[\text{M}+\text{H}]^+$, $R_t = 7.79$ min; HR-MS found 638.34934 $[\text{M}+\text{H}]^+$.

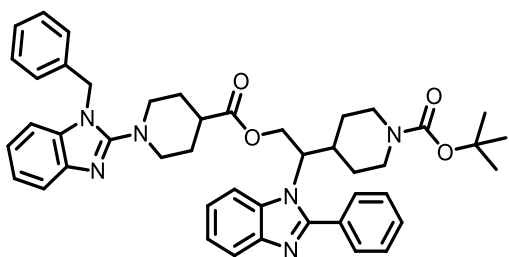


2-Cyclohexyl-2-(2-phenyl-1H-benzo[d]imidazol-1-yl)ethyl 1-(1-(2-chloro-6-fluorobenzyl)-1H-benzo[d]imidazol-2-yl)piperidine-4-carboxylate (85) The product was synthesized from alcohol **52** (40 mg, 0.12 mmol) and carboxylic acid **83** according to Procedure E for the esterification via Mitsunobu reaction. The crude product was purified by automated flash chromatography using a gradient of cyclohexane and ethyl acetate 20:1 to 1:2 to yield the product (56 mg, 0.08 mmol, 56%). ^1H NMR (400 MHz, CDCl_3) δ 7.86 – 7.77 (m, 1H), 7.70 (d, $J = 5.5$ Hz, 2H), 7.61 – 7.44 (m, 5H), 7.33 – 7.24 (m, 3H), 7.24 – 7.07 (m, 3H), 7.06 – 6.83 (m, 3H), 5.31 (s, 2H), 4.87 – 4.70 (m, 1H), 4.56 (dd, $J = 11.7, 3.7$ Hz, 1H), 4.49 (td, $J = 10.3, 3.9$ Hz, 1H), 3.47 – 3.11 (m, 2H), 3.09 – 2.84 (m, 2H), 2.48 – 2.15 (m, 2H), 1.98 – 1.83 (m, 1H),

1.86 – 1.51 (m, 7H), 1.29 – 0.93 (m, 5H), 0.80 – 0.53 (m, 1H). ^{13}C NMR (101 MHz, CDCl_3) δ 174.36, 163.26, 160.77, 158.67, 141.76, 135.72, 135.67, 133.90, 130.46, 130.37, 130.18, 129.93, 128.83, 126.08, 126.05, 122.94, 122.66, 121.89, 121.71, 121.61, 121.45, 120.64, 118.66, 114.77, 114.54, 112.11, 109.78, 63.70, 61.52, 50.93, 50.70, 40.95, 40.00, 39.96, 38.37, 31.14, 30.40, 29.78, 28.08, 28.00, 26.05, 25.94, 25.84. LC-MS (ESI): calcd for $\text{C}_{41}\text{H}_{41}\text{ClFN}_5\text{O}_2$: 690.30056 $[\text{M}+\text{H}]^+$, found: 690.30 $[\text{M}+\text{H}]^+$, $R_t = 7.81$ min; HR-MS found 690.30137 $[\text{M}+\text{H}]^+$.

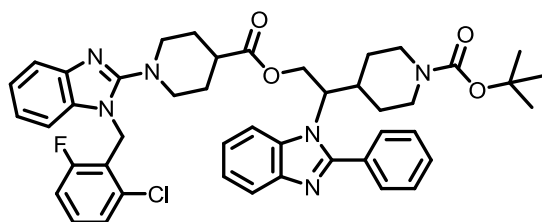


2-Cyclohexyl-2-(2-phenyl-1H-benzo[d]imidazol-1-yl)ethyl 1-(1-(thiophen-3-ylmethyl)-1H-benzo[d]imidazol-2-yl)piperidine-4-carboxylate (86) The product was synthesized from alcohol **52** (40 mg, 0.12 mmol) and carboxylic acid **82** according to Procedure E for the esterification via Mitsunobu reaction. The crude product was purified by automated flash chromatography using a gradient of cyclohexane and ethyl acetate 20:1 to 1:2 to yield the product (52 mg, 0.08 mmol, 65%). ^1H NMR (400 MHz, CDCl_3) δ 7.81 (d, $J = 8.4$ Hz, 1H), 7.72 – 7.63 (m, 2H), 7.63 – 7.42 (m, 4H), 7.34 – 7.21 (m, 4H), 7.21 – 7.15 (m, 1H), 7.14 – 7.05 (m, 2H), 7.01 – 6.97 (m, 1H), 6.92 (d, $J = 5.0$ Hz, 1H), 5.11 (s, 2H), 4.84 – 4.72 (m, 1H), 4.61 – 4.39 (m, 2H), 3.46 – 3.24 (m, 2H), 3.04 – 2.71 (m, 2H), 2.39 – 2.11 (m, 2H), 1.97 – 1.81 (m, 1H), 1.84 – 1.47 (m, 7H), 1.34 – 0.92 (m, 5H), 0.81 – 0.62 (m, 1H). ^{13}C NMR (101 MHz, CDCl_3) δ 174.29, 158.15, 141.72, 137.61, 135.39, 130.18, 129.95, 128.83, 127.29, 126.22, 122.94, 122.66, 122.16, 121.75, 121.73, 120.65, 118.40, 109.49, 63.65, 61.45, 50.56, 50.38, 44.10, 40.90, 38.39, 31.12, 29.80, 27.97, 27.94, 26.05, 25.94, 25.84. LC-MS (ESI): calcd for $\text{C}_{39}\text{H}_{41}\text{N}_5\text{O}_2\text{S}$: 644.30537 $[\text{M}+\text{H}]^+$, found: 644.31 $[\text{M}+\text{H}]^+$, $R_t = 7.53$ min; HR-MS found 644.30594 $[\text{M}+\text{H}]^+$.



tert-butyl 4-(2-(1-(1-benzyl-1H-benzo[d]imidazol-2-yl)piperidine-4-carboxyloxy)-1-(2-phenyl-1H-benzo[d]imidazol-1-yl)ethyl)piperidine-1-carboxylate (87) The product was

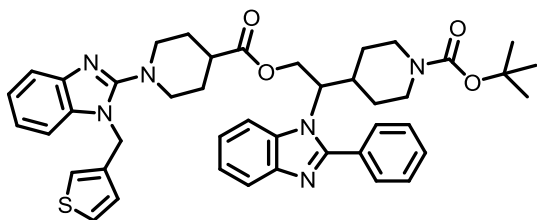
synthesized from alcohol **53** (63 mg, 0.15 mmol) and carboxylic acid **81** according to Procedure E for the esterification via Mitsunobu reaction. The crude product was purified by automated flash chromatography using a gradient of cyclohexane and ethyl acetate 20:1 to 1:2 to yield the desired product (70 mg, 0.10 mmol, 64%). ¹H NMR (400 MHz, CDCl₃) δ 7.74 (d, *J* = 7.6 Hz, 1H), 7.63 – 7.50 (m, 3H), 7.50 – 7.38 (m, 4H), 7.31 – 7.16 (m, 5H), 7.15 – 6.98 (m, 4H), 6.95 (d, *J* = 7.8 Hz, 1H), 5.08 (s, 2H), 4.75 (t, *J* = 10.2 Hz, 1H), 4.51 – 4.30 (m, 2H), 4.14 – 3.96 (m, 1H), 3.95 – 3.69 (m, 1H), 3.41 – 3.14 (m, 2H), 2.97 – 2.72 (m, 2H), 2.63 (t, *J* = 12.0 Hz, 1H), 2.51 – 2.14 (m, 3H), 1.84 – 1.41 (m, 4H), 1.39 – 1.04 (m, 10H), 1.04 – 0.63 (m, 3H). ¹³C NMR (101 MHz, CDCl₃) δ 174.16, 158.09, 155.58, 154.75, 143.80, 136.34, 135.40, 133.42, 130.67, 130.15, 130.10, 129.23, 128.99, 127.93, 126.24, 123.18, 122.92, 122.34, 121.91, 120.87, 118.24, 111.79, 109.67, 79.97, 63.33, 60.90, 50.50, 50.35, 47.86, 40.80, 36.99, 30.13, 28.82, 28.60, 27.92, 27.88. LC-MS (ESI): calcd for C₄₅H₅₀N₆O₄: 739.39663 [M+H]⁺, found: 739.39 [M+H]⁺, R_t = 7.38 min; HR-MS found 739.39738 [M+H]⁺. Chiral HPLC conditions: flow rate: 0.35 mL/min; solvent: 75 % ethanol in *iso*-hexane. R_T: (*R*)-26.5 min, (*S*)-56.8 min.



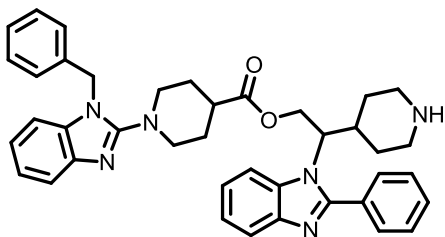
tert-Butyl 4-(2-(1-(1-(2-chloro-6-fluorobenzyl)-1H-benzo[d]imidazol-2-yl)piperidine-4-carboxyloxy)-1-(2-phenyl-1H-benzo[d]imidazol-1-yl)ethyl)piperidine-1-carboxylate (88)

The product was synthesized from alcohol **53** (75 mg, 0.18 mmol) and carboxylic acid **83** according to Procedure E for the esterification via Mitsunobu reaction. The crude product was purified by automated flash chromatography using a gradient of cyclohexane and ethyl acetate 20:1 to 1:2 to yield the desired compound (86 mg, 0.11 mmol, 61%). ¹H NMR (400 MHz, CDCl₃) δ 7.91 – 7.77 (m, 1H), 7.76 – 7.63 (m, 2H), 7.63 – 7.41 (m, 5H), 7.35 – 7.24 (m, 2H), 7.24 – 7.06 (m, 3H), 7.05 – 6.87 (m, 3H), 5.31 (s, 2H), 4.84 (t, *J* = 10.1 Hz, 1H), 4.61 – 4.44 (m, 2H), 4.23 – 4.06 (m, 1H), 4.00 – 3.85 (m, 1H), 3.42 – 3.24 (m, 2H), 3.06 – 2.88 (m, 2H), 2.71 (t, *J* = 12.2 Hz, 1H), 2.53 – 2.31 (m, 3H), 1.92 – 1.58 (m, 4H), 1.42 (s, 9H), 1.31 – 1.14 (m, 2H), 1.09 – 0.79 (m, 2H). ¹³C NMR (101 MHz, CDCl₃) δ 174.29, 163.25, 160.76, 158.60, 155.61, 154.76, 143.79, 141.68, 135.70, 135.65, 133.87, 133.43, 130.66, 130.50, 130.40, 130.16, 130.13, 129.00, 126.09, 126.05, 123.20, 122.94, 121.94, 121.76, 121.58, 121.42, 120.87, 118.64, 114.78, 114.55, 111.84, 109.82, 79.98, 63.35, 60.95, 50.88, 50.68, 40.93, 40.00, 39.96, 36.99, 30.14, 28.82, 28.60, 28.08, 28.00, 27.13. LC-MS (ESI): calcd for

$C_{45}H_{48}ClFN_6O_4$: 791.34824 $[M+H]^+$, found: 791.30 $[M+H]^+$, $R_t = 8.00$ min; HR-MS found 791.34737 $[M+H]^+$.

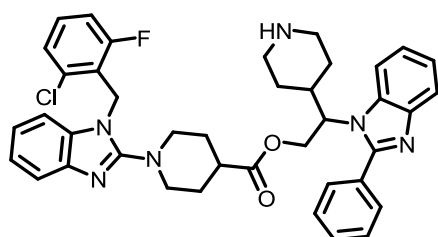


tert-Butyl 4-(1-(2-phenyl-1H-benzo[d]imidazol-1-yl)-2-(1-(1-(thiophen-3-ylmethyl)-1H-benzo[d]imidazol-2-yl)piperidine-4-carboxyloxy)ethyl)piperidine-1-carboxylate (89) The product was synthesized from alcohol **53** (80 mg, 0.19 mmol) and carboxylic acid **82** according to Procedure E for the esterification via Mitsunobu reaction. The crude product was purified by automated flash chromatography using a gradient of cyclohexane and ethyl acetate 20:1 to 1:2 to afford the desired compound (95 mg, 0.13 mmol, 67%). 1H NMR (400 MHz, $CDCl_3$) δ 7.82 (d, $J = 7.7$ Hz, 1H), 7.66 (s, 2H), 7.59 (t, $J = 8.4$ Hz, 1H), 7.57 – 7.45 (m, 4H), 7.36 – 7.22 (m, 3H), 7.23 – 7.14 (m, 1H), 7.14 – 7.05 (m, 2H), 6.97 (d, $J = 1.6$ Hz, 1H), 6.91 (d, $J = 5.0$ Hz, 1H), 5.11 (s, 2H), 4.83 (t, $J = 10.0$ Hz, 1H), 4.59 – 4.42 (m, 2H), 4.15 (d, $J = 11.3$ Hz, 1H), 4.03 – 3.86 (m, 1H), 3.50 – 3.23 (m, 2H), 3.02 – 2.79 (m, 2H), 2.78 – 2.62 (m, 1H), 2.54 – 2.25 (m, 3H), 1.85 (d, $J = 11.8$ Hz, 1H), 1.79 – 1.53 (m, 4H), 1.40 (s, 9H), 1.23 (d, $J = 11.9$ Hz, 1H), 1.00 (d, $J = 26.4$ Hz, 1H), 0.92 (d, $J = 9.8$ Hz, 1H). ^{13}C NMR (101 MHz, $CDCl_3$) δ 174.21, 158.07, 155.60, 154.75, 143.82, 141.66, 137.58, 135.36, 133.42, 130.69, 130.16, 130.12, 129.00, 127.32, 126.20, 123.18, 122.93, 122.20, 121.79, 121.72, 120.88, 118.39, 111.79, 109.50, 79.98, 63.31, 60.90, 50.53, 50.36, 44.10, 40.88, 37.01, 30.13, 28.83, 28.60, 27.97, 27.93. LC-MS (ESI): calcd for $C_{43}H_{48}N_6O_4S$: 745.35305 $[M+H]^+$, found: 745.33 $[M+H]^+$, $R_t = 7.35$ min; HR-MS found 745.35302 $[M+H]^+$. Chiral HPLC conditions: flow rate: 0.35 mL/min; solvent: 75 % ethanol in *iso*-hexane. R_T : (*R*)-26.8 min, (*S*)-54.6 min.

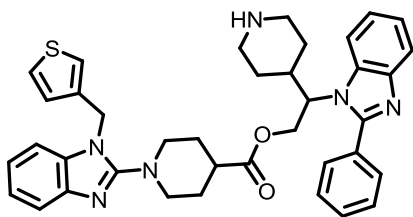


2-(2-Phenyl-1H-benzo[d]imidazol-1-yl)-2-(piperidin-4-yl)ethyl 1-(1-benzyl-1H-benzo[d]imidazol-2-yl)piperidine-4-carboxylate (90) The product was synthesized according to General Procedure (D) starting from the protected piperidine **87** (15 mg, 0.02 mmol) to afford the HCl-salt in quantitative yield. The residue was dissolved in methanol (500 μ L) and applied to a preparative C18-RP column eluting with a gradient (CH_3CN : H_2O 1:5 to 9:1 containing

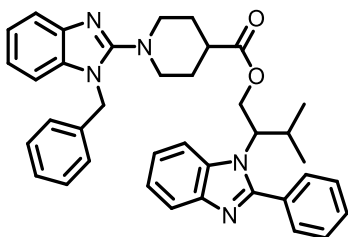
0.1% TFA), to afford piperidine **90** (9 mg, 0.01 mmol, 71%) as a TFA-salt. ^1H NMR (600 MHz, $\text{DMSO-}d_6$) δ 9.08 (s, 1H), 8.78 (s, 1H), 8.07 (s, 1H), 7.81 – 7.72 (m, 3H), 7.72 – 7.59 (m, 3H), 7.56 (d, $J = 7.8$ Hz, 1H), 7.43 (s, 2H), 7.39 – 7.30 (m, 5H), 7.28 (t, $J = 7.7$ Hz, 1H), 7.24 (d, $J = 7.5$ Hz, 2H), 5.39 (s, 2H), 4.83 (t, $J = 10.4$ Hz, 1H), 4.57 (d, $J = 11.3$ Hz, 1H), 4.54 – 4.43 (m, 1H), 3.65 (d, $J = 12.1$ Hz, 1H), 3.57 (d, $J = 11.9$ Hz, 1H), 3.33 – 3.17 (m, 3H), 3.04 (d, $J = 11.3$ Hz, 1H), 2.85 – 2.72 (m, 2H), 2.72 – 2.54 (m, 2H), 1.97 (d, $J = 12.3$ Hz, 1H), 1.69 – 1.58 (m, 2H), 1.58 – 1.44 (m, 2H), 1.40 (d, $J = 10.8$ Hz, 1H), 1.28 – 1.07 (m, 2H). LC-MS (ESI): calcd for $\text{C}_{40}\text{H}_{42}\text{N}_6\text{O}_2$: 639.34420 $[\text{M}+\text{H}]^+$, found: 639.36 $[\text{M}+\text{H}]^+$, $R_t = 5.41$ min; HR-MS found 639.34491 $[\text{M}+\text{H}]^+$.



2-(2-Phenyl-1H-benzo[d]imidazol-1-yl)-2-(piperidin-4-yl)ethyl 1-(1-(2-chloro-6-fluorobenzyl)-1H-benzo[d]imidazol-2-yl)piperidine-4-carboxylate (91) The product was synthesized according to General Procedure (D) starting from the protected piperidine **88** (15 mg, 0.02 mmol) to afford the HCl-salt in quantitative yield. The residue was dissolved in methanol (500 μL) and applied to a preparative C18-RP column eluting with a gradient ($\text{CH}_3\text{CN}:\text{H}_2\text{O}$ 1:5 to 9:1 containing 0.1% TFA), to afford the product (9 mg, 0.01 mmol, 65%) as the TFA-Salt. ^1H NMR (400 MHz, $\text{DMSO-}d_6$) δ 9.58 – 9.37 (m, 1H), 9.34 – 9.07 (m, 1H), 8.38 – 8.20 (m, 1H), 7.98 – 7.81 (m, 3H), 7.80 – 7.71 (m, 3H), 7.64 – 7.55 (m, 3H), 7.49 – 7.37 (m, 1H), 7.37 – 7.15 (m, 5H), 7.16 – 7.01 (m, 1H), 5.54 (s, 2H), 4.94 – 4.78 (m, 1H), 4.77 – 4.46 (m, 2H), 3.88 – 3.73 (m, 2H), 3.40 – 3.32 (m, 2H), 3.32 – 3.15 (m, 1H), 3.07 – 2.96 (m, 1H), 2.96 – 2.77 (m, 2H), 2.77 – 2.57 (m, 2H), 2.09 – 1.88 (m, 1H), 1.80 – 1.40 (m, 4H), 1.40 – 1.12 (m, 3H). ^{13}C NMR (101 MHz, $\text{DMSO-}d_6$) δ 173.66, 162.99, 160.51, 153.22, 152.23, 134.92, 134.87, 133.23, 132.54, 132.44, 131.22, 131.03, 130.15, 129.97, 126.92, 126.61, 125.28, 124.71, 120.13, 119.98, 116.37, 115.90, 115.68, 115.39, 113.45, 111.98, 72.84, 71.20, 67.03, 62.98, 62.16, 60.84, 49.58, 49.24, 44.31, 42.94, 39.16, 27.72, 26.20, 25.68. LC-MS (ESI): calcd for $\text{C}_{40}\text{H}_{40}\text{ClFN}_6\text{O}_2$: 691.29581 $[\text{M}+\text{H}]^+$, found: 691.26 $[\text{M}+\text{H}]^+$, $R_t = 5.63$ min; HR-MS found 691.29659 $[\text{M}+\text{H}]^+$.

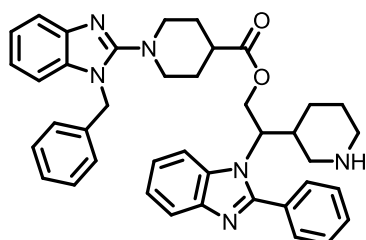


2-(2-Phenyl-1H-benzo[d]imidazol-1-yl)-2-(piperidin-4-yl)ethyl 1-(1-(thiophen-3-ylmethyl)-1H-benzo[d]imidazol-2-yl)piperidine-4-carboxylate (92) The product was synthesized according to General Procedure (D) starting from the protected piperidine (61 mg, 0.08 mmol) to afford the HCl-salt in quantitative yield. The residue was dissolved in methanol (500 μ L) and applied to a preparative C18-RP column eluting with a gradient (CH₃CN: H₂O 1:5 to 9:1 containing 0.1% acetic acid), to afford free piperidine **92** (33 mg, 0.005 mmol, 59%). ¹H NMR (600 MHz, DMSO-*d*₆) δ 7.84 (d, *J* = 6.0 Hz, 1H), 7.69 – 7.62 (m, 3H), 7.58 – 7.50 (m, 3H), 7.51 – 7.46 (m, 1H), 7.39 (t, *J* = 8.0 Hz, 1H), 7.26 – 7.17 (m, 4H), 7.08 – 6.99 (m, 2H), 6.92 – 6.87 (m, 1H), 5.15 (s, 2H), 4.89 – 4.77 (m, 1H), 4.54 (dd, *J* = 12.0, 3.5 Hz, 1H), 4.48 – 4.34 (m, 1H), 3.32 (d, *J* = 12.6 Hz, 1H), 3.24 (d, *J* = 12.5 Hz, 1H), 3.01 – 2.78 (m, 4H), 2.72 (d, *J* = 11.8 Hz, 1H), 2.45 – 2.36 (m, 1H), 2.26 – 2.18 (m, 1H), 1.80 – 1.76 (m, 1H), 1.64 – 1.38 (m, 4H), 1.14 – 1.05 (m, 1H), 0.86 – 0.70 (m, 2H). ¹³C NMR (151 MHz, DMSO-*d*₆) δ 174.30, 158.13, 155.48, 143.70, 141.96, 138.43, 135.64, 133.83, 131.19, 130.50, 130.37, 129.35, 127.87, 127.28, 123.22, 122.93, 122.78, 121.88, 121.47, 120.28, 117.96, 113.16, 110.36, 109.99, 63.22, 61.45, 50.12, 45.73, 45.62, 43.61, 36.18, 29.43, 27.81, 27.68. LC-MS (ESI): calcd for C₃₈H₄₀N₆O₂S: 645.30062 [M+H]⁺, found: 645.27 [M+H]⁺, R_t = 5.31 min; HR-MS found 645.30123 [M+H]⁺.



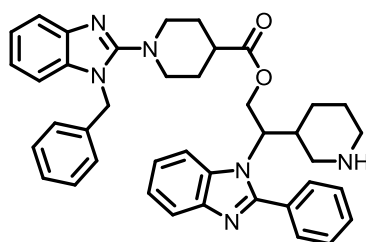
3-Methyl-2-(2-phenyl-1H-benzo[d]imidazol-1-yl)butyl 1-(1-benzyl-1H-benzo[d]imidazol-2-yl)piperidine-4-carboxylate (93) The product was synthesized by Carsten Schultz-Fademrecht, LDC Dortmund. ¹H NMR (400 MHz, CDCl₃) δ 7.80 (d, *J* = 7.8 Hz, 1H), 7.67 (m, 2H), 7.62 (t, *J* = 7.9 Hz, 1H), 7.54 (d, *J* = 7.6 Hz, 1H), 7.50 - 7.46 (m, 3H), 7.34 - 7.23 (m, 5H), 7.19 (t, *J* = 7.8 Hz, 1H), 7.14 (d, *J* = 7.4 Hz, 2H), 7.09 (t, *J* = 7.4 Hz, 1H), 7.02 (d, *J* = 8.0 Hz, 1H), 5.15 (s, 2H), 4.77 (m, 1H), 4.53 (dd, *J* = 3.8 Hz, *J* = 12.2 Hz, 1H), 4.39 (dt, *J* = 3.8 Hz, *J* =

10.2 Hz, 1H), 3.39 (d, $J = 12.2$ Hz, 1H), 3.32 (d, $J = 12.6$ Hz, 1H), 2.91 (m, 2H), 2.64 (m, 1H), 2.31 (m, 1H), 1.75 - 1.52 (m, 4H), 1.09 (d, $J = 6.6$ Hz, 3H), 0.68 (d, $J = 6.6$ Hz, 3H). LC-MS: 5min_B: $t_R = 2.88$ min, 10min_D: $t_R = 4.54$ min. MS (ES) $C_{38}H_{39}N_5O_2$ calcd: 597, found: 598 $[M+H]^+$. LC-MS: 5min_B: $R_t = 2.88$ min, 10min_D: $R_t = 4.54$ min. MS (ESI) $C_{38}H_{39}N_5O_2$ calcd: 597, found: 598 $[M+H]^+$. LC-MS (ESI, HR-MS): calcd for $C_{38}H_{39}N_5O_2$: 598.31765. $[M+H]^+$ found 598.31918 $[M+H]^+$.



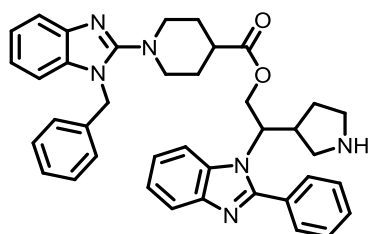
diastereoisomer 1

2-(2-Phenyl-1H-benzo[d]imidazol-1-yl)-2-(piperidin-3-yl)ethyl 1-(1-benzyl-1H-benzo[d]imidazol-2-yl)piperidine-4-carboxylate (diastereoisomer 1) (94) The product was synthesized by Carsten Schultz-Fademrecht, LDC Dortmund. 1H NMR (400 MHz, $CDCl_3$) δ 7.80 (d, $J = 7.9$ Hz, 1H), 7.68 (m, 2H), 7.62 (d, $J = 7.7$ Hz, 1H), 7.57 (d, $J = 6.7$ Hz, 1H), 7.49 (m, 3H), 7.29 (m, 5H), 7.18 (t, $J = 7.6$ Hz, 1H), 7.13 (d, $J = 7.1$ Hz, 2H), 7.09 (t, $J = 7.5$ Hz, 1H), 7.02 (d, $J = 7.9$ Hz, 1H), 5.15 (s, 2H), 4.79 (t, $J = 10.5$ Hz, 1H), 4.55 (t, $J = 10.5$ Hz, 1H), 4.49 (dd, $J = 3.9$ Hz, $J = 11.5$ Hz, 1H), 3.36 (dd, $J = 14.4$ Hz, $J = 14.0$ Hz, 2H), 3.27 (d, $J = 10.2$ Hz, 1H), 2.91 (m, 3H), 2.46 (m, 3H), 2.32 (m, 1H) 1.71 (m, 3H), 1.60 (t, $J = 12.9$ Hz, 1H), 1.44 (m, 1H), 1.28 (m, 2H), 0.86 (m, 1H). LC-MS: 5min_B: $R_t = 1.98$ min, 10min_D: $R_t = 3.33$ min. LC-MS (ESI) $C_{40}H_{42}N_6O_2$ calcd: 638, found: 639 $[M+H]^+$. LC-MS (ESI, HR-MS): calcd for $C_{40}H_{42}N_6O_2$: 639.34402. $[M+H]^+$ found 639.34605 $[M+H]^+$.



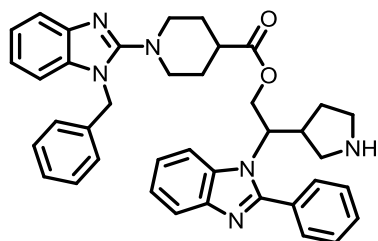
diastereoisomer 2

2-(2-Phenyl-1H-benzo[d]imidazol-1-yl)-2-(piperidin-3-yl)ethyl 1-(1-benzyl-1H-benzo[d]imidazol-2-yl)piperidine-4-carboxylate (diastereoisomer 2) (95) The product was synthesized by Carsten Schultz-Fademrecht, LDC Dortmund. ^1H NMR (400 MHz, CDCl_3) δ 7.79 (d, $J = 7.1$ Hz, 1H), 7.72 (m, 2H), 7.62 (d, $J = 7.7$ Hz, 1H), 7.58 (d, $J = 8.2$ Hz, 1H), 7.48 (m, 3H), 7.34 - 7.24 (m, 5H), 7.18 (dt, $J = 1.1$ Hz, $J = 7.7$ Hz, 1H), 7.13 (d, $J = 8.0$ Hz, 2H), 7.09 (dt, $J = 1.1$ Hz, $J = 7.3$ Hz, 1H), 7.02 (d, $J = 8.0$ Hz, 1H), 5.15 (s, 2H), 4.76 (t, $J = 10.4$ Hz, 1H), 4.58 (t, $J = 9.9$ Hz, 1H), 4.51 (dd, $J = 3.5$ Hz, $J = 11.6$ Hz, 1H), 3.39 (d, $J = 12.4$ Hz, 1H), 3.32 (d, $J = 12.3$ Hz, 1H), 2.91 (m, 3H), 2.50 (m, 3H), 2.30 (m, 1H), 2.15 (t, $J = 10.9$ Hz, 1H), 2.00 (m, 1H), 1.74 - 1.49 (m, 6H), 1.23 (m, 1H). LC-MS: 5min_B: $R_t = 1.98$ min, 10min_D: $R_t = 3.14$ min. MS (ESI) $\text{C}_{40}\text{H}_{42}\text{N}_6\text{O}_2$ calcd: 638, found: 639 $[\text{M}+\text{H}]^+$. LC-MS (ESI, HR-MS): calcd for $\text{C}_{40}\text{H}_{42}\text{N}_6\text{O}_2$: 639.34402 $[\text{M}+\text{H}]^+$ found 639.34598 $[\text{M}+\text{H}]^+$.



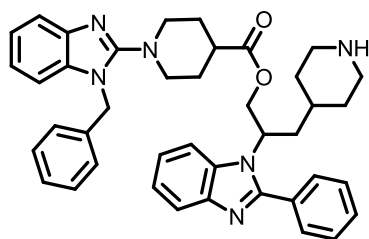
diastereoisomer 1

2-(2-Phenyl-1H-benzo[d]imidazol-1-yl)-2-(pyrrolidin-3-yl)ethyl 1-(1-benzyl-1H-benzo[d]imidazol-2-yl)piperidine-4-carboxylate (diastereoisomer 1) (96) The product was synthesized by Carsten Schultz-Fademrecht, LDC Dortmund. ^1H NMR (400 MHz, $\text{DMSO}-d_6$) δ 7.90 (dd, $J = 3.0$ Hz, $J = 6.3$ Hz, 1H), 7.73 (m, 2H), 7.67 (dd, $J = 2.7$ Hz, $J = 6.3$ Hz, 1H), 7.52 (m, 3H), 7.42 (d, $J = 7.5$ Hz, 1H), 7.34 - 7.34 (m, 5H), 7.13 (m, 3H), 7.07 (dt, $J = 1.2$ Hz, $J = 7.5$ Hz, 1H), 7.02 (dt, $J = 1.1$ Hz, $J = 7.6$ Hz, 1H), 5.22 (s, 2H), 4.79 (t, $J = 11.5$ Hz, 1H), 4.54 (dt, $J = 3.0$ Hz, $J = 9.7$ Hz, 1H), 4.46 (dd, $J = 4.0$ Hz, $J = 12.1$ Hz, 1H), 3.25 (m, 1H), 3.10 (m, 1H), 2.85 (m, 4H), 2.42 (m, 3H), 2.16 (t, $J = 9.5$ Hz, 1H), 1.99 (m, 1H), 1.63 - 1.41 (m, 5H). LC-MS: 5min_B: $t_R = 1.78$ min, 10min_D: $t_R = 2.86$ min. LC-MS (ES) $\text{C}_{39}\text{H}_{40}\text{N}_6\text{O}_2$ calcd: 624, found: 625 $[\text{M}+\text{H}]^+$. LC-MS (ESI, HR-MS): calcd for $\text{C}_{39}\text{H}_{40}\text{N}_6\text{O}_2$: 625.32855 $[\text{M}+\text{H}]^+$ found 625.33015 $[\text{M}+\text{H}]^+$.



diastereoisomer 2

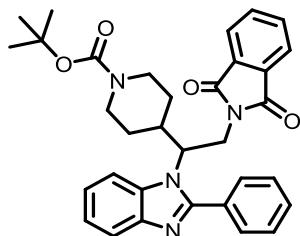
2-(2-Phenyl-1H-benzo[d]imidazol-1-yl)-2-(pyrrolidin-3-yl)ethyl 1-(1-benzyl-1H-benzo[d]imidazol-2-yl)piperidine-4-carboxylate (diastereoisomer 2) (97) The product was synthesized by Carsten Schultz-Fademrecht, LDC Dortmund. ^1H NMR (400 MHz, $\text{DMSO-}d_6$) δ 7.89 (m, 1H), 7.69 (m, 3H), 7.53 (m, 3H), 7.42 (d, $J = 8.1$ Hz, 1H), 7.34 - 7.23 (m, 5H), 7.13 (m, 3H), 7.07 (dt, $J = 1.2$ Hz, $J = 7.5$ Hz, 1H), 7.02 (dt, $J = 1.1$ Hz, $J = 7.5$ Hz, 1H), 5.22 (s, 2H), 4.82 (t, $J = 10.8$ Hz, 1H), 4.56 (t, $J = 10.8$ Hz, 1H), 4.40 (dd, $J = 3.4$ Hz, $J = 12.0$ Hz, 1H), 3.34 (d, $J = 13.1$ Hz, 1H), 3.27 (d, $J = 11.4$ Hz, 1H), 3.12 (m, 2H), 2.88 (q, $J = 12.0$ Hz, 2H), 2.67 (m, 2H), 2.43 (m, 1H), 1.67 - 1.43 (m, 4H), 1.27 (m, 2H), 1.03 (m, 1H). LC-MS:5min_B: $t_{\text{R}}=1.86\text{min}$, 10min_D: $t_{\text{R}}=3.03\text{min}$. LC-MS (ESI, HR-MS): calcd for $\text{C}_{39}\text{H}_{40}\text{N}_6\text{O}_2$: 625.32855. $[\text{M}+\text{H}]^+$ found 625.33000 $[\text{M}+\text{H}]^+$.



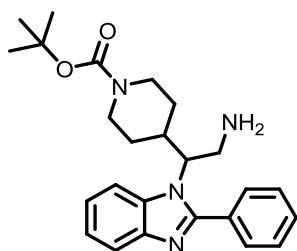
2-(2-Phenyl-1H-benzo[d]imidazol-1-yl)-3-(piperidin-4-yl)propyl 1-(1-benzyl-1H-benzo[d]imidazol-2-yl)piperidine-4-carboxylate (98) The product was synthesized by Carsten Schultz-Fademrecht, LDC Dortmund. ^1H NMR (400 MHz, CDCl_3) δ 7.82 (d, $J = 7.2$ Hz, 1H), 7.67 (m, 2H), 7.62 (d, $J = 8.0$ Hz, 1H), 7.54 - 7.46 (m, 4H), 7.34 - 7.25 (m, 5H), 7.18 (dt, $J = 1.3$ Hz, $J = 7.6$ Hz, 1H), 7.14 (d, $J = 8.2$ Hz, 2H), 7.09 (dt, $J = 1.1$ Hz, $J = 7.6$ Hz, 1H), 7.02 (d, $J = 7.9$ Hz, 1H), 5.16 (s, 2H), 4.91 (m, 1H), 4.80 (t, $J = 10.5$ Hz, 1H), 4.44 (dd, $J = 4.8$ Hz, $J = 11.4$ Hz, 1H), 3.41 (d, $J = 12.4$ Hz, 1H), 3.34 (d, $J = 12.6$ Hz, 1H), 2.92 (m, 4H), 2.36 (m, 3H), 2.18 (m, 2H), 1.83 - 1.58 (m, 5H), 1.34 (d, $J = 13.5$ Hz, 1H), 1.11 (m, 1H), 0.95 (m, 2H). LC-MS: 5min_B: $t_{\text{R}}=2.13\text{min}$, 10min_D: $t_{\text{R}}=3.17\text{min}$. MS (ESI) $\text{C}_{41}\text{H}_{44}\text{N}_6\text{O}_2$ calcd: 652,

found: 653 [M+H]⁺. LC-MS (ESI, HR-MS): calcd for C₄₁H₄₄N₆O₂: 653.35985 [M+H]⁺, found 653.36179 [M+H]⁺.

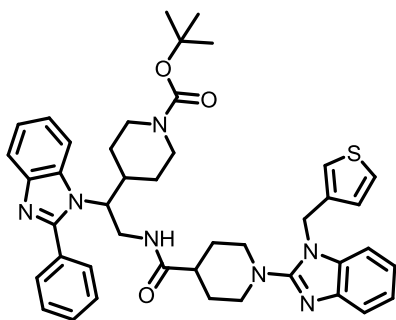
Synthesis of amide-linked *bis*-benzimidazoles



tert-Butyl 4-(2-(1,3-dioxoisindolin-2-yl)-1-(2-phenyl-1H-benzo[d]imidazol-1-yl)ethyl)piperidine-1-carboxylate (99) To a mixture of tert-butyl 4-(2-hydroxy-1-(2-phenyl-1H-benzo[d]imidazol-1-yl)ethyl)piperidine-1-carboxylate¹ (300 mg, 0.71 mmol), phthalimide (157 mg, 1.07 mmol), polymer-bound triphenylphosphine (474 mg, 3 mmol/g) and toluene (5 mL) at 0°C was added di-tert-butyl azodicarboxylate (327 mg, 1.42 mmol). After 10 min the reaction mixture was allowed to warm to room temperature and stirred for 16 h. Due to incomplete conversion phthalimide (300 mg, 0.71 mmol), polymer-bound triphenylphosphine (400 mg) and di-tert-butyl azodicarboxylate (330 mg, 1.44 mmol) were added to the reaction mixture at room temperature. The mixture was stirred for an additional 16 h and filtered. The polymer resin was washed with a mixture of DCM and ethyl acetate (50:50 vol%, 100 mL) and the combined filtrates were concentrated in vacuo. After purification by column chromatography (gradient cyclohexane : ethyl acetate 5:1 to 1:2) the desired compound was isolated (320 mg, 0.58 mmol, 82 %). ¹H NMR (400 MHz, CDCl₃) δ 7.87 – 7.74 (m, 1H), 7.73 – 7.59 (m, 5H), 7.41 – 7.29 (m, 3H), 7.24 – 7.06 (m, 4H), 4.53 – 4.43 (m, 1H), 4.41 – 4.31 (m, 1H), 4.24 (d, J = 13.0 Hz, 1H), 4.13 – 3.94 (m, 2H), 2.80 (t, J = 12.4 Hz, 1H), 2.65 – 2.39 (m, 2H), 2.08 (d, J = 13.0 Hz, 1H), 1.56 – 1.29 (m, 10H), 1.29 – 1.10 (m, 2H). ¹³C NMR (101 MHz, CDCl₃) δ 167.19, 155.21, 154.83, 143.82, 134.32, 133.99, 131.86, 130.11, 129.85, 129.71, 128.66, 123.59, 123.21, 122.92, 120.90, 111.92, 79.95, 60.92, 38.19, 37.84, 30.68, 29.07, 28.64, 27.12. LC-MS (ESI): calcd for C₃₃H₃₄N₄O₄: 551.26528 [M+H]⁺, found: 551.20 [M+H]⁺, Rt = 8.41 min; HR-MS found 551.26641 [M+H]⁺.

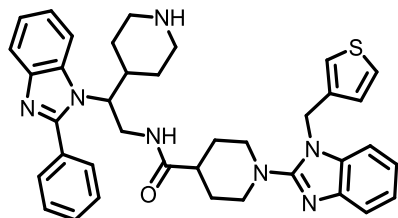


tert-Butyl 4-(2-amino-1-(2-phenyl-1H-benzo[d]imidazol-1-yl)ethyl)piperidine-1-carboxylate (100) To a solution of phthalimide **99** (300 mg, 0.54 mmol) in EtOH (3 mL) was added hydrazine hydrate (0.22 mL, 0.44 mmol). The reaction mixture was stirred at room temperature for 72 h. The reaction mixture was concentrated *in vacuo*, and co-evaporated with EtOH (3x 5 mL). The colorless residue was taken up in DCM (10 mL). To the resulting suspension was added sat. NaHCO₃ solution (10 mL). The aqueous layer was extracted with DCM (3x 15mL). The combined organic layers were dried over MgSO₄, filtered and concentrated *in vacuo* to afford the product (200 mg, 0.47 mmol, 87%). ¹H NMR (400 MHz, DMSO-*d*₆) δ 7.86 – 7.74 (m, 3H), 7.69 – 7.62 (m, 1H), 7.57 – 7.46 (m, 3H), 7.26 – 7.14 (m, 2H), 4.13 – 4.00 (m, 1H), 3.85 (d, *J* = 13.2 Hz, 1H), 3.70 – 3.51 (m, 1H), 3.51 – 3.37 (m, 1H), 3.14 (d, *J* = 10.1 Hz, 1H), 2.74 – 2.52 (m, 1H), 2.38 – 2.11 (m, 2H), 1.77 (d, *J* = 13.1 Hz, 1H), 1.28 (s, 9H), 0.96 – 0.78 (m, 1H), 0.64 – 0.41 (m, 2H). LC-MS (ESI): calcd for C₂₅H₃₂N₄O₂: 421.25980 [M+H]⁺, found: 421.16 [M+H]⁺; HR-MS found 421.25938 [M+H]⁺.

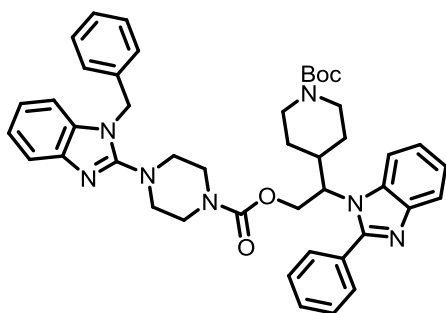


tert-Butyl 4-(1-(2-phenyl-1H-benzo[d]imidazol-1-yl)-2-(1-(1-(thiophen-3-ylmethyl)-1H-benzo[d]imidazol-2-yl)piperidine-4-carboxamido)ethyl)piperidine-1-carboxylate (101) To a mixture of acid **83** (122 mg, 0.36 mM), amine **100** (100 mg, 0.24 mM) in DMF (2 mL) at room temperature was added DIPEA (51 μL, 0.36 mM) and PyBOP (185 mg, 0.36 mmol). The reaction mixture was stirred at room temperature for 2 d and then concentrated *in vacuo*. The residue was dissolved in methanol (500 μL) and applied to a preparative C18-RP column eluting with a gradient (CH₃CN:H₂O 1:4 to 9:1 containing 0.1% TFA), to afford the product (119 mg, 0.16 mmol, 67%). ¹H NMR (400 MHz, CDCl₃) δ 7.74 (d, *J* = 7.7 Hz, 1H), 7.58 – 7.46 (m, 4H), 7.44 – 7.36 (m, 3H), 7.30 – 7.19 (m, 3H), 7.17 – 7.12 (m, 1H), 7.08 (dd, *J* = 3.9, 2.1 Hz, 2H), 6.97 – 6.94 (m, 1H), 6.91 (dd, *J* = 5.0, 1.2 Hz, 1H), 5.12 (s, 2H), 4.37 (td, *J* = 10.3, 3.5 Hz, 1H), 4.29 – 4.19 (m, 1H), 4.09 (t, *J* = 11.1 Hz, 1H), 3.98 – 3.76 (m, 1H), 3.72 – 3.57 (m, 1H), 3.37 (d, *J* = 12.3 Hz, 2H), 2.83 – 2.72 (m, 2H), 2.66 (t, *J* = 12.3 Hz, 1H), 2.40 (t, *J* = 11.2 Hz, 1H), 2.26 (d, *J* = 11.2 Hz, 1H), 2.12 – 2.02 (m, 2H), 2.01 – 1.91 (m, 1H), 1.79 – 1.63 (m, 3H), 1.56 – 1.47 (m, 1H), 1.38 (s, 9H), 1.33 – 1.19 (m, 2H). ¹³C NMR (101 MHz, CDCl₃) δ 175.14, 158.10, 155.72, 154.74, 143.65, 141.45, 137.57, 135.28, 133.31, 130.23, 130.20,

130.03, 129.02, 127.30, 126.22, 123.31, 123.10, 122.23, 121.84, 121.72, 120.71, 118.19, 111.91, 109.56, 79.86, 62.31, 50.62, 44.13, 42.72, 39.83, 38.14, 30.11, 28.88, 28.75, 28.59, 28.32. LC-MS (ESI): calcd for C₄₃H₄₉N₇O₃S: 744.36904 [M+H]⁺, found: 744.36824 [M+H]⁺; HR-MS found 744.36824 [M+H]⁺.

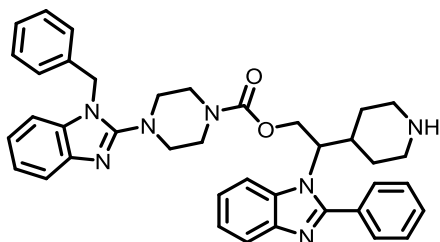


N-(2-(2-Phenyl-1H-benzo[d]imidazol-1-yl)-2-(piperidin-4-yl)ethyl)-1-(1-(thiophen-3-ylmethyl)-1H-benzo[d]imidazol-2-yl)piperidine-4-carboxamide (102) The product was synthesized according to General Procedure (D) starting from the protected piperidine **101** (61 mg, 0.13 mmol) to afford the HCl-salt in quantitative yield. The residue was dissolved in methanol (500 μ L) and applied to a preparative C18-RP column eluting with a gradient (CH₃CN: H₂O 1:5 to 9:1 containing 0.1% TFA), to afford the desired piperidine as a TFA salt (66 mg, 0.010 mmol, 59%). ¹H NMR (400 MHz, DMSO-*d*₆) δ 9.19 (s, 1H), 8.99 (s, 1H), 8.29 (t, *J* = 5.7 Hz, 1H), 8.15 (d, *J* = 7.9 Hz, 1H), 7.90 (d, *J* = 7.8 Hz, 1H), 7.77 (d, *J* = 7.5 Hz, 2H), 7.70 (t, *J* = 7.4 Hz, 1H), 7.64 (t, *J* = 7.5 Hz, 2H), 7.62 – 7.53 (m, 4H), 7.49 – 7.47 (m, 1H), 7.38 (t, *J* = 7.1 Hz, 1H), 7.36 – 7.32 (m, 1H), 7.31 – 7.27 (m, 1H), 7.08 – 7.04 (m, 1H), 5.39 (s, 2H), 4.19 (t, *J* = 8.8 Hz, 1H), 3.94 (dd, *J* = 11.7, 7.0 Hz, 1H), 3.77 (d, *J* = 9.6 Hz, 2H), 3.61 – 3.53 (m, 3H), 3.33 – 3.16 (m, 4H), 3.03 (dt, *J* = 12.3, 7.3 Hz, 2H), 2.90 – 2.61 (m, 4H), 2.28 (t, *J* = 10.8 Hz, 1H), 2.16 (d, *J* = 13.4 Hz, 1H), 1.76 – 1.71 (m, 2H), 1.71 – 1.62 (m, 1H), 1.62 – 1.45 (m, 3H), 1.44 – 1.29 (m, 3H), 1.16 – 1.09 (m, 1H). ¹³C NMR (151 MHz, DMSO-*d*₆) δ 174.60, 152.43, 136.25, 132.57, 131.05, 129.92, 128.50, 127.09, 125.08, 124.53, 123.57, 115.17, 112.92, 112.06, 67.69, 64.33, 49.49, 49.32, 46.14, 45.95, 43.20, 43.12, 39.11, 34.30, 28.61, 27.51, 26.84, 25.80, 25.64. LC-MS (ESI): calcd for C₃₈H₄₁N₇OS : 644.31661 [M+H]⁺, found: 644.32 [M+H]⁺, *R*_t = 5.30 min; HR-MS found 644.31661 [M+H]⁺.

Synthesis of carbamate-linked *bis*-benzimidazoles

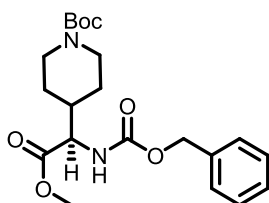
1-(2-(4-(1-Benzyl-1H-benzo[d]imidazol-2-yl)piperazine-1-carboxyloxy)-1-(tert-butoxycarbonyl)piperidin-4-yl)ethyl-2-phenyl-1H-benzo[d]imidazol-6-ylidium (105) To 4-nitrophenyl chloroformate (65 mg, 0.32 mmol) in THF (1 mL) was added pyridine (26 μ L, 0.32 mmol) and the mixture was stirred at room temperature for 30 min. The *tert*-butyl 4-(2-hydroxy-1-(2-phenyl-1H-benzo[d]imidazol-1-yl)ethyl)piperidine-1-carboxylate (90 mg, 0.21 mmol) was added and the reaction mixture was stirred at room temperature for 16 h. 4-Nitrophenyl chloroformate (65 mg, 0.32 mmol) and pyridine (26 μ L, 0.32 mmol) were added and stirring was continued for 16 h. The reaction mixture was concentrated *in vacuo*, the residue dissolved in DCM (10 mL) and extracted with a sat. NH_4Cl -solution (10 mL). The aqueous layer was reextracted with DCM (3 x 10 mL). The combined organic layers were dried over Na_2SO_4 , filtered and concentrated *in vacuo*. To a solution of HOBT (48 mg, 0.32 mmol) in DCM (3 mL) molecular sieves (4 Angstrom, 50 mg) were added and the mixture was stirred for 5 min. After 5 min 1-benzyl-2-(piperazin-1-yl)-1H-benzo[d]imidazole¹²⁵ (94 mg, 0.32 mmol) was added and the resulting mixture was stirred for 16 h. The reaction mixture was concentrated *in vacuo*, the residue dissolved in DCM (5 mL) and extracted with sat. NaHCO_3 . The aqueous layer was reextracted with DCM (3x 10 mL). The combined organic layers were dried over Na_2SO_4 , filtered and concentrated *in vacuo*. The residue was purified by flash chromatography (gradient cyclohexane: ethyl acetate 10:1 to 1:2.5) to afford the product (71 mg, 46%). ^1H NMR (400 MHz, CDCl_3) δ 7.81 (d, $J = 7.4$ Hz, 1H), 7.65 – 7.56 (m, 3H), 7.56 – 7.40 (m, 4H), 7.35 – 7.22 (m, 5H), 7.18 (t, $J = 7.6$ Hz, 1H), 7.14 – 7.06 (m, 3H), 7.02 (d, $J = 7.8$ Hz, 1H), 5.18 (s, 2H), 4.76 – 4.60 (m, 2H), 4.49 (t, $J = 11.5$ Hz, 1H), 4.19 – 4.05 (m, 1H), 3.98 – 3.76 (m, 1H), 3.55 – 2.95 (m, 6H), 2.77 – 2.59 (m, 1H), 2.53 – 2.30 (m, 2H), 1.89 (d, $J = 11.8$ Hz, 1H), 1.40 (s, 9H), 1.32 – 1.17 (m, 1H), 1.08 – 0.84 (m, 2H). ^{13}C NMR (101 MHz, CDCl_3) δ 157.39, 154.75, 154.59, 141.42, 136.21, 135.53, 130.59, 130.13, 130.00, 129.31, 128.95, 128.06, 126.19, 123.16, 122.89, 122.41, 122.08, 120.82, 118.49, 111.81, 109.68, 79.92, 64.24, 61.30, 50.40,

47.73, 43.56, 37.03, 30.24, 28.80, 28.60, 27.12. LC-MS (ESI): calcd for $C_{44}H_{49}N_7O_4$: 740.39188 $[M+H]^+$, found: 740.33 $[M+H]^+$, $R_t = 7.84$ min; HR-MS found 740.39234 $[M+H]^+$.



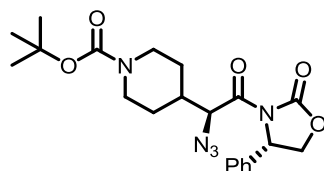
2-(2-Phenyl-1H-benzo[d]imidazol-1-yl)-2-(piperidin-4-yl)ethyl 4-(1-benzyl-1H-benzo[d]imidazol-2-yl)piperazine-1-carboxylate (106) The product was synthesized according to General Procedure (D) starting from the protected piperidine **105** (30 mg, 0.040 mmol) to afford the HCl-salt in quantitative yield. The residue was dissolved in methanol (500 μ L) and applied to a preparative C18-RP column eluting with a gradient (CH_3CN : H_2O 1:5 to 9:1 containing 0.1% TFA), to afford the product (17 mg, 0.026 mmol, 66%) as the TFA-salt. 1H NMR (400 MHz, $DMSO-d_6$) δ 7.87 – 7.79 (m, 1H), 7.71 – 7.63 (m, 1H), 7.63 – 7.55 (m, 2H), 7.56 – 7.46 (m, 3H), 7.43 (d, $J = 7.2$ Hz, 1H), 7.35 – 7.27 (m, 2H), 7.27 – 7.20 (m, 3H), 7.20 – 7.11 (m, 3H), 7.11 – 6.98 (m, 2H), 5.28 (s, 2H), 4.69 (t, $J = 10.8$ Hz, 1H), 4.58 (d, $J = 8.2$ Hz, 1H), 4.45 – 4.35 (m, 1H), 3.42 – 2.76 (m, 10H), 2.94 – 2.81 (m, 1H), 2.70 (d, $J = 13.6$ Hz, 1H), 2.45 – 2.33 (m, 2H), 2.18 (t, $J = 10.2$ Hz, 1H), 1.80 (d, $J = 10.9$ Hz, 1H), 1.07 (d, $J = 9.5$ Hz, 1H), 0.91 – 0.71 (m, 2H). ^{13}C NMR (101 MHz, $DMSO-d_6$) δ 157.01, 154.82, 153.80, 143.05, 141.12, 136.82, 135.03, 133.32, 130.53, 129.67, 128.68, 128.58, 127.39, 126.54, 122.49, 122.03, 121.34, 121.03, 119.62, 117.54, 112.47, 109.90, 72.16, 70.51, 63.46, 61.28, 60.19, 49.73, 46.71, 45.56, 45.44, 42.84, 35.86, 30.93, 29.32. LC-MS (ESI): calcd for $C_{39}H_{41}N_7O_2$: 640.33945 $[M+H]^+$, found: 640.29 $[M+H]^+$, $R_t = 5.62$ min; HR-MS found 640.33988 $[M+H]^+$.

Enantioselective synthesis of *bis*-benzimidazoles

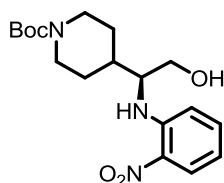


tert-butyl (R)-4-(1-(((benzyloxy)carbonyl)amino)-2-methoxy-2-oxoethyl)piperidine-1-carboxylate (113) The compound was synthesized in an analogous fashion to the literature method.⁹¹ 1H NMR (400 MHz, $CDCl_3$) δ 7.41 – 7.29 (m, 5H), 5.35 (d, $J = 9.0$ Hz, 1H), 5.09 (s,

2H), 4.40 – 4.30 (m, 1H), 4.20 – 4.02 (m, 2H), 3.73 (s, 3H), 2.74 – 2.56 (m, $J = 9.1$ Hz, 2H), 1.96 – 1.83 (m, 1H), 1.70 – 1.45 (m, 2H), 1.44 (s, 9H), 1.35 – 1.18 (m, 2H). ; $[\alpha]_D^{20}$: -22.0° (Lit -20.7° , $c=1.0$, CHCl_3); Chiral HPLC (isohexane:isopropylalcohol:TFA 9:1:0.1): R_t 11.0 min, 88% ee (Lit: 94%). LC-MS (ESI): calcd for $\text{C}_{21}\text{H}_{30}\text{N}_2\text{O}_6$: 407.21 $[\text{M}+\text{H}]^+$, found: 406.75 $[\text{M}+\text{H}]^+$, $R_t = 7.53$ min.

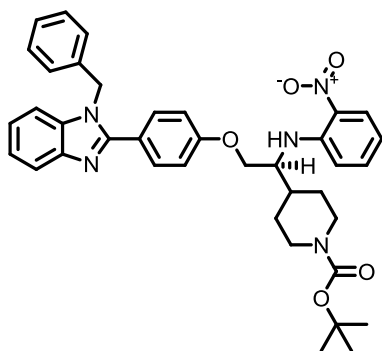


tert-Butyl 4-((S)-1-azido-2-oxo-2-((S)-2-oxo-4-phenyloxazolidin-3-yl)ethyl)piperidine-1-carboxylate (116) The product was synthesized according to literature methods.⁹⁰ ^1H NMR (400 MHz, CDCl_3) δ 7.45 – 7.27 (m, 5H), 5.45 (dd, $J = 8.7, 4.0$ Hz, 1H), 4.98 (d, $J = 7.8$ Hz, 1H), 4.75 (t, $J = 8.9$ Hz, 1H), 4.33 (dd, $J = 9.0, 4.0$ Hz, 1H), 4.23 – 4.06 (m, 2H), 2.74 – 2.59 (m, 2H), 2.11-1.97 (m, 1H), 1.84-1.74 (m, 1H), 1.53-1.63 (m, 1H), 1.45 (s, 9H), 1.41-1.32 (m, 2H). Analytical data are consistent with literature data.



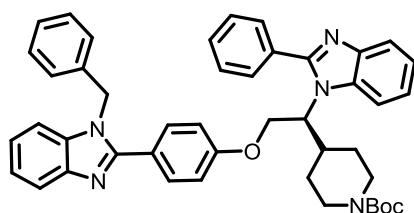
(S)-tert-Butyl 4-(2-hydroxy-1-(2-nitrophenylamino)ethyl)piperidine-1-carboxylate (107)
 Synthesis starting from azide **116**: To a solution of azide **116** (2.0 g, 4.7 mmol) in MeOH (5 mL) was added NaBH_4 (530 mg, 14.1 mmol) at room temperature. The reaction mixture was stirred at room temperature for 2 h and NaBH_4 (530 mg, 14.1 mmol) was added to the reaction mixture. After stirring for an additional 12 h sat. NH_4Cl -solution (20 mL) was added, followed by DCM (30 mL). The aqueous layer was extracted with DCM (3x 30 mL). The combined organic layers were dried (Na_2SO_4), filtered, evaporated to dryness and the residue was purified by flash chromatography (gradient cyclohexane : ethyl acetate 10:1 to 1:1). To a solution of the intermediate azido alcohol (1.0 g, 3.67 mmol) in degassed ethanol was added palladium on carbon (5%, 100 mg). The reaction vessel was evacuated and then refilled with argon three times. The reaction mixture was stirred under H_2 (1 atm) for 2 h at room temperature. The reaction vessel was then evacuated and refilled with argon, ethyl acetate (50 mL) was added and filtered over Celite. The filter cake was washed with ethanol and ethyl acetate (100 mL, respectively), evaporated to dryness and used without any further purification (LC-MS:ESI

244.89 [M+H]⁺). To a solution of the free amine in NMP (10 mL) was added 1-fluoro-2-nitrobenzene (0.66 mL, 6.14 mmol), and DIPEA (0.35 mL, 2 mmol). The reaction mixture was heated to 90°C for 8 h, cooled to room temperature and diluted with DCM (50 mL). To the reaction mixture was added a sat. of NH₄Cl solution (40 mL). The aqueous layer was extracted with DCM (2x 50 mL). The combined organic layers were dried over MgSO₄, filtered and then evaporated to dryness. The crude product was purified by column chromatography to yield the desired compound (1.35 g, 3.7 mmol, 45%). ¹H NMR (400 MHz, CDCl₃) δ 8.13 (d, *J* = 9.1 Hz, 1H), 8.09 (dd, *J* = 8.6, 1.5 Hz, 1H), 7.33 (dd, *J* = 8.4, 7.2 Hz, 1H), 6.85 (d, *J* = 8.8 Hz, 1H), 6.57 (dd, *J* = 8.4, 7.2 Hz, 1H), 4.19 – 3.97 (m, 2H), 3.77 (dd, *J* = 11.2, 4.2 Hz, 1H), 3.70 (dd, *J* = 11.1, 5.3 Hz, 1H), 3.59 – 3.48 (m, 1H), 2.61 (t, *J* = 12.3 Hz, 2H), 2.00–1.96 (m, 1H), 1.87 – 1.57 (m, 4H), 1.37 (s, 9H), 1.31 – 1.10 (m, 3H). ¹³C NMR (101 MHz, CDCl₃) δ 154.92, 145.89, 136.52, 132.42, 127.38, 115.81, 114.42, 79.82, 62.56, 58.73, 38.44, 29.21, 28.74, 28.64. LC-MS (ESI): calcd for C₁₈H₂₇N₃O₅: 388.18429 [M+Na]⁺, *R*_t = 9.41 min; HR-MS found 388.18459 [M+Na]⁺; [α]_D²⁰: -243.0° (c=1.6, DCM).

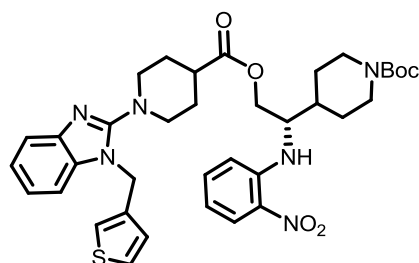


(S)-tert-Butyl 4-(2-(4-(1-benzyl-1H-benzo[d]imidazol-2-yl)phenoxy)-1-(2-nitrophenylamino)ethyl)piperidine-1-carboxylate ((S)-117) The product was synthesized according to Procedure C for the connection of two benzimidazoles via Mitsunobu reaction starting from alcohol (*S*)-**53** (30 mg, 0.10 mmol). The crude product was purified by automated flash chromatography using a gradient of cyclohexane: ethyl acetate 20:1 to 1:2 to yield the desired compound (45 mg, 0.07 mmol, 70%). ¹H NMR (400 MHz, CDCl₃) δ 8.36 (d, *J* = 9.1 Hz, 1H), 8.17 (dd, *J* = 8.6, 1.6 Hz, 1H), 7.83 (t, *J* = 7.3 Hz, 1H), 7.63 – 7.58 (m, 2H), 7.45 – 7.39 (m, 1H), 7.36 – 7.26 (m, 4H), 7.24 – 7.15 (m, 2H), 7.13 – 7.07 (m, 2H), 6.97 – 6.89 (m, 3H), 6.70 – 6.62 (m, 1H), 5.42 (s, 2H), 4.35 – 4.01 (m, 3H), 3.97 – 3.77 (m, 1H), 2.72 (t, *J* = 12.0 Hz, 2H), 2.10 – 1.99 (m, 1H), 1.90 (d, *J* = 12.6 Hz, 1H), 1.77 (d, *J* = 12.7 Hz, 1H), 1.49 – 1.21 (m, 12H). ¹³C NMR (101 MHz, CDCl₃) δ 159.86, 154.88, 154.08, 145.31, 143.28, 136.66, 136.51, 136.32, 132.56, 131.01, 129.29, 127.98, 127.45, 126.10, 123.34, 123.12, 122.87,

119.96, 115.91, 115.04, 114.10, 110.60, 79.84, 67.75, 56.27, 48.58, 38.80, 29.21, 28.70, 28.65. $[\alpha]_D^{20}$: -62.5° (c=1.5, DCM).

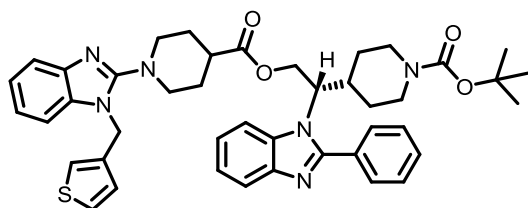


(S)-tert-Butyl 4-(2-(4-(1-benzyl-1H-benzo[d]imidazol-2-yl)phenoxy)-1-(2-phenyl-1H-benzo[d]imidazol-1-yl)ethyl)piperidine-1-carboxylate (S)-57 To a solution of **(S)-117** (40 mg, 0.066 mmol) in MeOH, H₂O and DMSO (8:2:1, 2 mL) was added benzaldehyde (18 μ L, 0.18 mmol) and sodium dithionite (23 mg, 0.14 mmol). The reaction mixture was heated to 65°C and after 0.5, 1, and 2 h sodium dithionite (3x 23 mg, 0.14 mmol) was added. After 6 h the reaction mixture was allowed to cool to room temperature. The reaction mixture was concentrated under reduced pressure and then extracted with DCM (3x 20 mL). The combined organic phases were dried (Na₂SO₄), filtered and concentrated to dryness. Purification by flash chromatography (gradient cyclohexane : ethyl acetate 5:1 to 1:5) afforded enantiomerically pure **(S)-89** (25 mg, 0.035mmol, 53%).



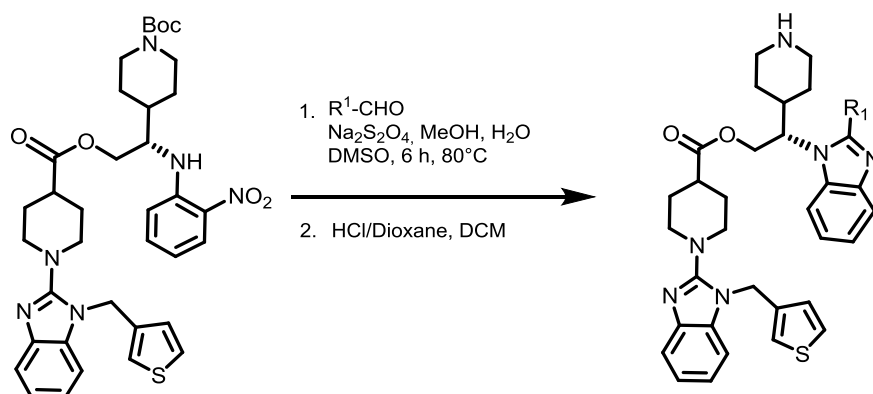
(S)-tert-Butyl 4-(1-(2-nitrophenylamino)-2-(1-(1-(thiophen-3-ylmethyl)-1H-benzo[d]imidazol-2-yl)piperidine-4-carboxyloxy)ethyl)piperidine-1-carboxylate ((S)-118) The product was synthesized according to Procedure E for the connection of two benzimidazoles via Mitsunobu reaction starting from alcohol (1.0 g, 2.74 mmol). The crude product was purified by automated flash chromatography using a gradient of cyclohexane: ethyl acetate 20:1 to 1:2 to yield the desired compound (1.33 g, 1.94 mmol, 71%). ¹H NMR (400 MHz, CDCl₃) δ 8.19 – 8.13 (m, 2H), 7.63 – 7.58 (m, 1H), 7.43 – 7.38 (m, 1H), 7.33 (dd, J = 5.0, 3.0 Hz, 1H), 7.22 – 7.16 (m, 1H), 7.13 – 7.10 (m, 2H), 7.04 – 6.99 (m, 1H), 6.97 – 6.89 (m, 2H), 6.64 (ddd, J = 8.1, 7.0, 1.1 Hz, 1H), 5.16 (s, 2H), 4.30 – 4.08 (m, 4H), 3.79 (td, J = 11.5, 5.5 Hz, 1H), 3.45 (d, J = 12.5 Hz, 2H), 2.96 (dd, J = 16.8, 7.0 Hz, 2H), 2.70 (t, J = 12.1 Hz,

2H), 2.47 (tt, $J = 11.2, 4.1$ Hz, 1H), 1.98 – 1.69 (m, 6H), 1.37 – 1.17 (m, 3H). ^{13}C NMR (101 MHz, CDCl_3) δ 174.55, 158.15, 154.85, 145.39, 141.69, 137.65, 136.53, 135.40, 132.60, 127.42, 127.32, 126.25, 122.20, 121.78, 121.74, 118.37, 116.08, 114.18, 109.52, 79.91, 64.16, 55.71, 50.60, 50.53, 44.17, 41.00, 38.96, 29.11, 28.65, 28.13. LC-MS (ESI): calcd for $\text{C}_{18}\text{H}_{27}\text{N}_3\text{O}_5$: 689.31158 $[\text{M}+\text{H}]^+$, found: 689.29 $[\text{M}+\text{H}]^+$, $R_t = 8.47$ min; HR-MS found 689.31133 $[\text{M}+\text{H}]^+$; $[\alpha]_D^{20}$: -50.0° ($c=1.8$, DCM).

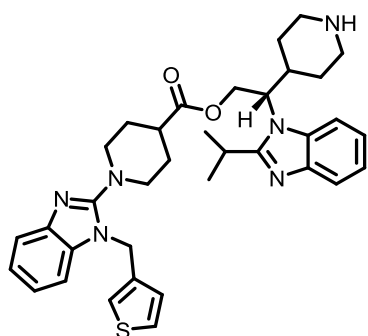


(*S*)-tert-Butyl 4-(1-(2-phenyl-1H-benzo[d]imidazol-1-yl)-2-(1-(1-(thiophen-3-ylmethyl)-1H-benzo[d]imidazol-2-yl)piperidine-4-carboxyloxy)ethyl)piperidine-1-carboxylate ((*S*)-89**)** To a solution of (*S*)-**118** (30 mg, 0.044 mmol) in MeOH, H_2O and DMSO (8:2:1, 3 mL) was added benzaldehyde (9 μL , 0.09 mmol) and sodium dithionite (23 mg, 0.14 mmol). The reaction mixture was heated to 65°C and after 0.5, 1, and 2 h sodium dithionite (3x 23 mg, 0.14 mmol) was added. After 5 h the reaction mixture was allowed to cool to room temperature. The reaction mixture was concentrated under reduced pressure and then extracted with DCM (3x 20 mL). The combined organic phases were dried (Na_2SO_4), filtered and concentrated to dryness. Purification by flash chromatography (gradient cyclohexane : ethyl acetate 5:1 to 1:5) afforded enantiomerically pure (*S*)-**89** (20 mg, 0.031 mmol, 61%).

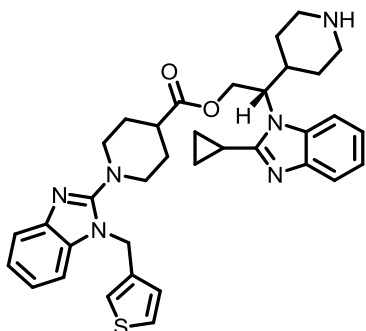
General procedure F for the cyclisation of nitro anilines to benzimidazoles



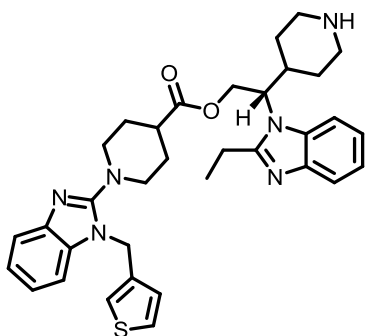
To a solution of (*S*)-**118** (20 mg, 0.029 mmol) in MeOH, H₂O and DMSO (8:2:1, 2 mL) was added the corresponding aldehyde (0.06 mmol) and sodium dithionite (12 mg, 0.007 mmol). The reaction mixture was heated to 65°C and after 0.5, 1, and 2 h sodium dithionite (3x 12 mg) was added. The reaction was followed by TLC and LC-MS and was allowed to cool to room temperature upon completion. The reaction mixture was then concentrated under reduced pressure and extracted with DCM (3x 20 mL). The combined organic phases were dried (Na₂SO₄), filtered and concentrated to dryness. Purification by automated flash chromatography (gradient cyclohexane : ethyl acetate 5:1 to 1:5) afforded the Boc-protected intermediates. The Boc protected intermediates were then deprotected with HCl/dioxane as described and purified by preparative C18-RP column eluting with a gradient (CH₃CN: H₂O 1:5 to 9:1 containing 0.1% TFA), to afford the desired piperidines as TFA salts.



(*S*)-2-(2-Isopropyl-1H-benzo[d]imidazol-1-yl)-2-(piperidin-4-yl)ethyl 1-(1-(thiophen-3-ylmethyl)-1H-benzo[d]imidazol-2-yl)piperidine-4-carboxylate ((*S*)-127) The compound was synthesized according to General procedure F. Yield (10 mg, 56 %) ¹H NMR (600 MHz, DMSO-*d*₆) δ 8.82 – 8.76 (m, 1H), 8.54 – 8.44 (m, 1H), 7.96 (d, *J* = 7.6 Hz, 1H), 7.70 (d, *J* = 7.4 Hz, 1H), 7.57 – 7.55 (m, 1H), 7.49 (d, *J* = 7.9 Hz, 1H), 7.44 – 7.31 (m, 4H), 7.31 – 7.22 (m, 2H), 7.02 – 6.97 (m, 1H), 5.30 (s, 2H), 4.87 – 4.73 (m, 2H), 4.57 – 4.54 (m, 1H), 3.60 – 3.52 (m, 2H), 3.47 (d, *J* = 13.1 Hz, 1H), 3.39 (d, *J* = 12.0 Hz, 1H), 3.22 – 3.07 (m, 3H), 2.95 – 2.84 (m, 1H), 2.82 – 2.64 (m, 2H), 2.09 (d, *J* = 13.3 Hz, 1H), 1.76 – 1.64 (m, 2H), 1.61 – 1.49 (m, 2H), 1.42 – 1.33 (m, 7H), 1.09 (d, *J* = 13.4 Hz, 1H). ¹³C NMR (151 MHz, DMSO-*d*₆) δ 173.71, 160.64, 159.34, 159.12, 158.90, 158.68, 153.72, 136.56, 133.15, 131.60, 128.35, 127.10, 124.54, 124.04, 123.40, 118.33, 117.34, 116.36, 114.02, 111.77, 62.69, 59.83, 49.11, 49.08, 45.57, 43.36, 43.31, 39.44, 33.55, 27.41, 27.38, 26.48, 26.01, 25.85, 21.91. LC-MS (ESI, HR-MS): calcd for C₃₅H₄₂N₆O₂S: 611.31627 [M+H]⁺, found 611.31707 [M+H]⁺. [α]_D²⁰ : 12.6° (c=0.6, DMSO).

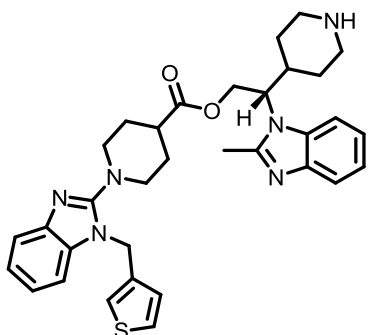


(S)-2-(2-Cyclopropyl-1H-benzo[d]imidazol-1-yl)-2-(piperidin-4-yl)ethyl 1-(1-(thiophen-3-ylmethyl)-1H-benzo[d]imidazol-2-yl)piperidine-4-carboxylate ((S)-128) The compound was synthesized according to General procedure F. Yield (10 mg, 57 %) ^1H NMR (600 MHz, DMSO- d_6) δ 8.73 – 8.64 (m, 1H), 8.44 – 8.32 (m, 1H), 7.97 – 7.89 (m, 1H), 7.63 – 7.58 (m, 1H), 7.58 – 7.55 (m, 1H), 7.48 (d, J = 7.9 Hz, 1H), 7.44 – 7.24 (m, 6H), 7.02 – 6.97 (m, 1H), 5.30 (s, 2H), 4.95 – 4.89 (m, 1H), 4.81 – 4.72 (m, 1H), 4.65 – 4.56 (m, 1H), 3.37 (d, J = 11.3 Hz, 1H), 3.24 – 3.09 (m, 3H), 2.96 – 2.82 (m, 1H), 2.82 – 2.64 (m, 2H), 2.59 – 2.47 (m, 4H), 2.41 – 2.33 (m, 1H), 2.11 (d, J = 13.0 Hz, 1H), 1.73 – 1.58 (m, 3H), 1.53 – 1.14 (m, 8H). ^{13}C NMR (151 MHz, DMSO- d_6) δ 173.72, 159.35, 159.13, 158.91, 158.69, 157.38, 153.26, 136.28, 132.83, 131.85, 131.28, 128.44, 127.04, 124.89, 124.53, 124.38, 123.44, 118.26, 116.95, 116.30, 113.60, 111.90, 62.47, 60.33, 49.03, 45.75, 43.25, 39.32, 33.38, 27.35, 26.39, 25.93, 10.30, 9.33, 7.66. LC-MS (ESI): calcd for $\text{C}_{35}\text{H}_{40}\text{N}_6\text{O}_2\text{S}$: 609.30062 $[\text{M}+\text{H}]^+$, found 609.30079 $[\text{M}+\text{H}]^+$. $[\alpha]_D^{20}$: 8.0° ($c=0.4$, DMSO).

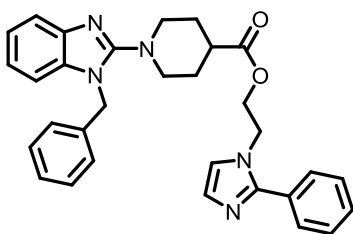


(S)-2-(2-Ethyl-1H-benzo[d]imidazol-1-yl)-2-(piperidin-4-yl)ethyl 1-(1-(thiophen-3-ylmethyl)-1H-benzo[d]imidazol-2-yl)piperidine-4-carboxylate ((S)-129) The compound was synthesized according to general procedure F. Yield (11 mg, 64 %) ^1H NMR (600 MHz, DMSO- d_6) δ 8.71 (d, J = 9.8 Hz, 1H), 8.40 (d, J = 10.3 Hz, 1H), 8.02 (d, J = 7.8 Hz, 1H), 7.72 (d, J = 7.4 Hz, 1H), 7.58 – 7.54 (m, 1H), 7.51 – 7.23 (m, 7H), 7.00 (d, J = 5.0 Hz, 1H), 5.31 (s, 2H), 4.79 – 4.71 (m, 2H), 4.61 – 4.51 (m, 1H), 3.23 – 3.02 (m, 5H), 2.95 – 2.82 (m, 1H), 2.83

– 2.67 (m, 2H), 2.56 – 2.49 (m, 1H), 2.08 (d, $J = 13.5$ Hz, 1H), 1.72 – 1.58 (m, 3H), 1.54 – 1.44 (m, 1H), 1.43 – 1.29 (m, 5H), 1.12 (d, $J = 13.6$ Hz, 1H). ^{13}C NMR (151 MHz, DMSO- d_6) δ 173.66, 159.39, 159.16, 158.94, 158.72, 157.08, 153.23, 136.29, 132.83, 131.22, 128.43, 127.03, 125.59, 125.36, 124.88, 124.37, 123.44, 116.42, 114.35, 113.56, 111.90, 62.53, 60.48, 49.02, 45.74, 43.26, 39.30, 33.30, 27.33, 26.25, 25.81, 20.22, 11.85. LC-MS (ESI, HR-MS): calcd for $\text{C}_{34}\text{H}_{40}\text{N}_6\text{O}_2\text{S}$: 597.30062 $[\text{M}+\text{H}]^+$, found 597.30139 $[\text{M}+\text{H}]^+$. $[\alpha]_D^{20}$: 15.0° (c=0.5, DMSO).

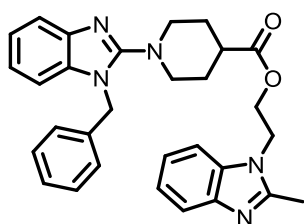


(S)-2-(2-Methyl-1H-benzo[d]imidazol-1-yl)-2-(piperidin-4-yl)ethyl 1-(1-(thiophen-3-ylmethyl)-1H-benzo[d]imidazol-2-yl)piperidine-4-carboxylate ((S)-130) The compound was synthesized according to General procedure F. Yield (4 mg, 24 %) ^1H NMR (600 MHz, DMSO- d_6) δ 8.74 – 8.56 (m, 1H), 8.39 – 8.21 (m, 1H), 8.03 (d, $J = 7.8$ Hz, 1H), 7.76 – 7.65 (m, 1H), 7.58 – 7.52 (m, 1H), 7.51 – 7.41 (m, 3H), 7.41 – 7.24 (m, 4H), 6.99 (d, $J = 4.9$ Hz, 1H), 5.31 (s, 2H), 4.75 – 4.68 (m, 2H), 4.61 – 4.54 (m, 1H), 2.92 – 2.84 (m, 2H), 2.81 – 2.69 (m, 5H), 2.58 – 2.51 (m, 1H), 2.08 (d, $J = 13.3$ Hz, 1H), 1.70 – 1.61 (m, 3H), 1.54 – 1.12 (m, 5H). LC-MS (ESI, HR-MS): calcd for $\text{C}_{33}\text{H}_{38}\text{N}_6\text{O}_2\text{S}$: 583.28487 $[\text{M}+\text{H}]^+$, found 583.28497 $[\text{M}+\text{H}]^+$. $[\alpha]_D^{20}$: 15.3° (c=0.5, DMSO).

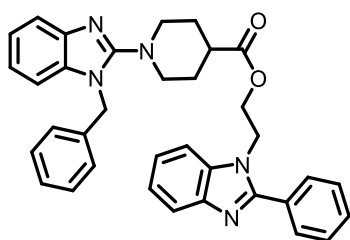


2-(2-Phenyl-1H-imidazol-1-yl)ethyl 1-(1-benzyl-1H-benzo[d]imidazol-2-yl)piperidine-4-carboxylate (131) The product was synthesized by Carsten Schultz-Fademrecht, LDC. ^1H

NMR (400MHz, CDCl₃) δ 7.64 (d, J = 8.0 Hz, 1H), 7.57 (dd, J = 1.4 Hz, J = 8.0 Hz, 2H), 7.47 - 7.38 (m, 3H), 7.37 - 7.25 (m, 3H), 7.23 - 7.13 (m, 4H), 7.10 (dt, J = 1.1 Hz, J = 7.2 Hz, 1H), 7.05 (d, J = 1.3 Hz, 1H), 7.03 (d, J = 7.9 Hz, 1H), 5.20 (s, 2H), 4.31 (s, 4H), 3.44 (dt, J = 12.8 Hz, J = 3.5 Hz, 2H), 2.97 (dt, J = 2.6 Hz, 12.0 Hz, 2H), 2.36 (m, 1H), 1.91 - 1.70 (m, 4H). LC-MS: 5min_A: R_t = 1.51min, 10min_C: R_t = 2.94min. LC-MS (ESI) C₃₁H₃₁N₅O₂ calcd: 505, found: 506 [M+H]⁺. LC-MS (ESI, HR-MS): calcd for C₃₁H₃₁N₅O₂: 506.25505 [M+H]⁺, found 506.25570 [M+H]⁺.

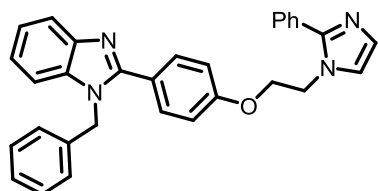


2-(2-Methyl-1H-benzo[d]imidazol-1-yl)ethyl 1-(1-benzyl-1H-benzo[d]imidazol-2-yl)piperidine-4-carboxylate (132) The product was synthesized by Carsten Schultz-Fademrecht, LDC Dortmund. ¹H NMR (400MHz, CDCl₃) δ 7.67 (m, 1H), 7.62 (d, J = 7.9 Hz, 1H), 7.34 - 7.27 (m, 3H), 7.23 - 7.18 (m, 3H), 7.17 - 7.13 (m, 3H), 7.10 (dt, J = 1.2 Hz, J = 7.6 Hz, 1H), 7.03 (d, J = 8.0 Hz, 1H), 5.17 (s, 2H), 4.40 (m, 4H), 3.40 (dt, J = 13.0 Hz, J = 3.3 Hz, 2H), 2.93 (dt, J = 2.6 Hz, J = 12.1 Hz, 2H), 2.64 (s, 3H), 2.37 (m, 1H), 1.84 - 1.62 (m, 4H). LC-MS: 5min_A: R_t = 1.52min, 10min_C: R_t = 2.94min. MS (ES) C₃₁H₃₁N₅O₂ calcd: 493, found: 494 [M+H]⁺. LC-MS (ESI, HR-MS): calcd for C₃₀H₃₁N₅O₂: 494.25505 [M+H]⁺, found 494.25563 [M+H]⁺.



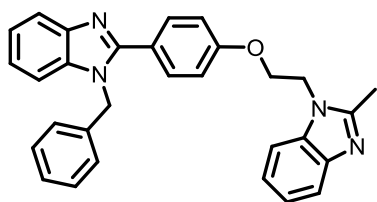
2-(2-Phenyl-1H-benzo[d]imidazol-1-yl)ethyl 1-(1-benzyl-1H-benzo[d]imidazol-2-yl)piperidine-4-carboxylate (133) The product was synthesized by Carsten Schultz-Fademrecht, LDC. ¹H NMR (400MHz, CDCl₃) δ 7.82 (m, 1H), 7.73 (dd, J = 1.6 Hz, J = 7.9 Hz, 2H), 7.63 (d, J = 7.9 Hz, 1H), 7.53 - 7.48 (m, 3H), 7.44 (m, 1H), 7.35 - 7.25 (m, 5H), 7.19 (dt, J = 1.0 Hz, J = 7.6 Hz, 1H), 7.14 (d, J = 7.0 Hz, 2H), 7.09 (dt, J = 0.8 Hz, J = 7.6 Hz, 1H), 7.02

(d, $J = 7.9$ Hz, 1H), 5.16 (s, 2H), 4.55 (t, $J = 5.6$ Hz, 2H), 4.35 (t, $J = 5.6$ Hz, 2H), 3.37 (dt, $J = 12.8$ Hz, $J = 3.1$ Hz, 2H), 2.88 (dt, $J = 2.8$ Hz, $J = 12.0$ Hz, 2H), 2.19 (m, 1H), 1.71 - 1.55 (m, 4H). LC-MS: 5min_A: $R_t = 1.72$ min, 10min_C: $R_t = 3.59$ min. MS (ES) $C_{35}H_{33}N_5O_2$ calcd: 555, found: 556 $[M+H]^+$. LC-MS (ESI, HR-MS): calcd for $C_{35}H_{33}N_5O_2$: 556.27070. $[M+H]^+$ found 556.27199 $[M+H]^+$.



1-Benzyl-2-(4-(2-(2-phenyl-1H-imidazol-1-yl)ethoxy)phenyl)-1H-benzo[d]imidazole (134)

The product was synthesized by Carsten Schultz-Fademrecht, LDC Dortmund. 1H NMR (400 MHz, $CDCl_3$) δ 7.85 (d, $J = 7.4$ Hz, 1H), 7.61 (m, 4H), 7.50 - 7.40 (m, 3H), 7.39 - 7.27 (m, 4H), 7.22 (dd, $J = 8.2$ Hz, 1.4 Hz, 2H), 7.17 (d, $J = 13.0$ Hz, 2H), 7.11 (d, $J = 6.5$ Hz, 2H), 6.88 (d, $J = 8.8$ Hz, 2H), 5.43 (s, 2H), 4.43 (t, $J = 5.4$ Hz, 2H), 4.24 (t, $J = 5.4$ Hz, 2H). LC-MS: 5min_A: $t_R = 1.57$ min, 10min_C: $R_t = 3.11$ min. LC-MS (ES) $C_{31}H_{26}N_4O$ calcd: 470, found: 471 $[M+H]^+$. LC-MS (ESI, HR-MS): calcd for $C_{31}H_{27}N_4O$: 471.21794 $[M+H]^+$, found 471.21850 $[M+H]^+$.

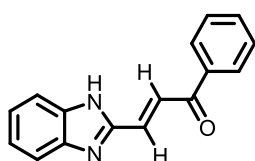


1-Benzyl-2-(4-(2-(2-methyl-1H-benzo[d]imidazol-1-yl)ethoxy)phenyl)-1H-

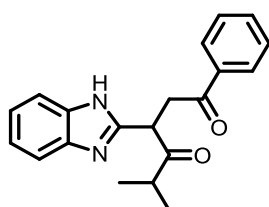
benzo[d]imidazole (135) The product was synthesized by Carsten Schultz-Fademrecht, LDC Dortmund. 1H NMR (400 MHz, $CDCl_3$) δ 7.84 (d, $J = 7.9$ Hz, 2H), 7.74 - 7.67 (m, 2H), 7.57 (d, $J = 8.8$ Hz, 2H), 7.40 - 7.15 (m, 7H), 7.07 (d, $J = 7.5$ Hz, 2H), 6.86 (d, $J = 8.8$ Hz, 2H), 5.38 (s, 2H), 4.54 (t, $J = 5.3$ Hz, 2H), 4.32 (t, $J = 5.3$ Hz, 2H), 2.72 (s, 3H). LC-MS: 5min_A: R_t

=1.57min, 10min_C: R_t =3.12min. MS (ES) $C_{30}H_{26}N_4O$ calcd: 458, found: 459 $[M+H]^+$. LC-MS (ESI, HR-MS): calcd for $C_{30}H_{26}N_4O$: 459.21794 $[M+H]^+$, found 459.21835 $[M+H]^+$.

Synthesis of benzimidazole-pyrrole hybrid compounds

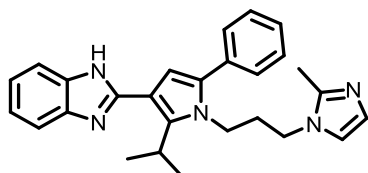


(E)-3-(1H-Benzo[d]imidazol-2-yl)-1-phenylprop-2-en-1-one (148) To a suspension of 2-formyl benzimidazole (500 mg, 3.42 mmol) in DMF (40 mL) was added (benzoylmethylene)triphenylphosphorane (1.3 g, 3.42 mmol). The reaction mixture was stirred overnight at 60°C. The solvent was removed *in vacuo* and the residue purified by automated flash chromatography (DCM:MeOH 100:1 to 10:1) to yield the desired product (612 mg, 72%). 1H NMR (400 MHz, $CDCl_3$) δ 8.17 (d, J = 15.6 Hz, 1H), 7.98 (d, J = 15.6 Hz, 1H), 7.89 – 7.82 (m, 2H), 7.71 – 7.62 (m, 2H), 7.54 – 7.47 (m, 1H), 7.38 – 7.25 (m, 4H). ^{13}C NMR (101 MHz, $cdCl_3$) δ 190.24, 148.82, 137.21, 133.85, 132.22, 129.00, 128.86, 127.01, 124.46. LC-MS (ESI): calcd for $C_{16}H_{12}N_2O$: 249.10224 $[M+H]^+$, HR-MS found: 249.10269 $[M+H]^+$.

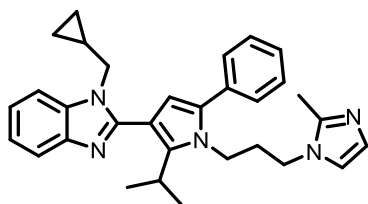


3-(1H-Benzo[d]imidazol-2-yl)-5-methyl-1-phenylhexane-1,4-dione (151) To a mixture of isobutyraldehyde (184 μ L, 2.0 mmol) and benzimidazole **90** (100 mg, 0.4 mmol) in ethanol (4 mL) was added triethylamine (40 μ L, 0.8 mmol) and then 3-Ethyl-5-(2-hydroxyethyl)-4-methylthiazolium bromide (101 mg, 0.40 mmol). The reaction mixture is heated in a closed system to 70°C and stirred overnight. The reaction mixture is allowed to cool to room temperature. To the reaction mixture is added DCM (15 mL) the reaction mixture is extracted with saturated ammonium chloride solution (5 mL). The organic phase is extracted with brine (5 mL), dried over magnesium sulfate, filtered and evaporated to dryness. The crude product is purified by automated flash chromatography (cyclohexane: EtOAc 100:1 to 1:1) to yield the desired product (58 mg, 45%). 1H NMR (400 MHz, DMSO- d_6) δ 12.53 (s, 1H), 8.07

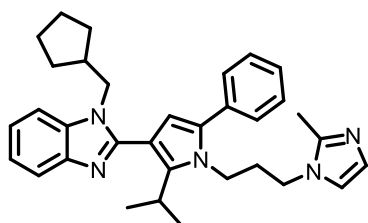
– 7.94 (m, 2H), 7.71 – 7.39 (m, 5H), 7.21 – 7.04 (m, 2H), 4.88 (dd, $J = 9.4, 4.5$ Hz, 1H), 4.13 – 3.95 (m, 1H), 3.53 (dd, $J = 18.2, 4.6$ Hz, 1H), 2.90 (hept, $J = 6.9$ Hz, 1H), 1.14 (d, $J = 6.9$ Hz, 3H), 0.86 (d, $J = 6.9$ Hz, 3H). ^{13}C NMR (101 MHz, DMSO- d_6) δ 209.83, 197.96, 151.88, 136.81, 134.12, 129.46, 128.65, 122.80, 46.61, 39.47, 39.38, 19.53, 18.61. LC-MS (ESI): calcd for $\text{C}_{20}\text{H}_{20}\text{N}_2\text{O}_5$: 321.15975 $[\text{M}+\text{H}]^+$, HR-MS found: 321.16019 $[\text{M}+\text{H}]^+$.



(3-(2-Methyl-1H-imidazol-1-yl)propyl)-5-phenyl-1H-pyrrol-3-yl)-1H-benzo[d]imidazole (153) To a mixture of diketone **151** (60 mg, 0.19 mmol) and 1-(3-Aminopropyl)-2-methyl-1H-imidazole (**152**) (57 mg, 0.41 mmol) in toluene (1 mL) was added acetic acid (106 μL , 1.87 mmol). The reaction mixture is heated in a closed microwave vial to 100°C for 3 h. The reaction mixture was cooled to RT and extracted with NaHCO_3 (10 mL). The aqueous phase is extracted with DCM (2x 10 mL), the combined organic phases were dried over MgSO_4 , filtered and evaporated to dryness. The crude product was dissolved in EtOAc (1 mL), and cyclohexane was added (1 mL). The mixture was heated at 60°C for 10 min, the mixture allowed then to cool to room temperature and the colorless solid was collected by filtration (69 mg, 87%). ^1H NMR (400 MHz, DMSO- d_6) δ 12.10 (s, 1H), 7.59 – 7.50 (m, 1H), 7.47 – 7.32 (m, 6H), 7.13 – 7.04 (m, 2H), 6.88 (d, $J = 1.2$ Hz, 1H), 6.66 (d, $J = 1.2$ Hz, 1H), 6.63 (s, 1H), 4.10 – 3.97 (m, 2H), 3.97 – 3.83 (m, 1H), 3.77 (t, $J = 6.7$ Hz, 2H), 2.09 (s, 3H), 1.87 – 1.76 (m, 2H), 1.41 (d, $J = 7.1$ Hz, 6H). ^{13}C NMR (101 MHz, DMSO- d_6) δ 150.67, 144.80, 144.10, 140.41, 134.73, 133.60, 133.33, 129.38, 129.25, 127.99, 127.01, 121.84, 121.43, 120.15, 118.63, 111.10, 110.99, 109.99, 43.05, 42.37, 32.65, 25.82, 21.62, 13.05. LC-MS (ESI): calcd for $\text{C}_{27}\text{H}_{29}\text{N}_5$: 424.24957 $[\text{M}+\text{H}]^+$, found: 424.28 $[\text{M}+\text{H}]^+$, $R_t = 4.67$ min. HR-MS found: 424.24905 $[\text{M}+\text{H}]^+$,

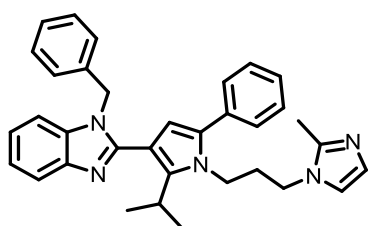


1-(Cyclopropylmethyl)-2-(2-isopropyl-1-(3-(2-methyl-1H-imidazol-1-yl)propyl)-5-phenyl-1H-pyrrol-3-yl)-1H-benzo[d]imidazole (154) To a suspension of benzimidazole **153** (20 mg, 0.05 mmol) in MeCN (1 mL) was added caesiumcarbonate (18 mg, 0.06 mmol) and (iodomethyl)cyclopropane (13 mg, 0.07 mmol). The reaction mixture was stirred at room temperature for 6 hours. The reaction temperature was then raised to 50°C and stirring was continued at this temperature for an additional 18 hours. The reaction mixture was cooled to RT diluted with DCM (10 mL) and extracted with NaHCO₃ (10 mL). The aqueous phase was extracted with DCM twice (2x 10 mL), the combined organic phases were dried over MgSO₄, filtered and evaporated to dryness. The crude was purified by automated flash chromatography (DCM: MeOH 100 :1 to 10:1 with 0.1% triethylamine) to yield the final product (11 mg, 48%). ¹H NMR (400 MHz, DMSO-d₆) δ 7.63 – 7.59 (m, 2H), 7.44 – 7.34 (m, 5H), 7.25 – 7.15 (m, 2H), 6.92 – 6.88 (m, 1H), 6.69 – 6.67 (m, 1H), 6.28 (s, 1H), 4.09 (d, *J* = 6.8 Hz, 2H), 4.08 – 3.99 (m, 2H), 3.77 (t, *J* = 6.9 Hz, 2H), 3.21 – 3.09 (m, 1H), 2.12 (s, 3H), 1.91 – 1.82 (m, 2H), 1.17 (d, *J* = 7.0 Hz, 6H), 1.12 – 1.06 (m, 1H), 0.45 – 0.38 (m, 2H), 0.29 – 0.23 (m, 2H). ¹³C NMR (101 MHz, DMSO-d₆) δ 151.33, 144.06, 143.33, 140.32, 135.75, 133.56, 133.05, 129.37, 129.31, 127.89, 127.03, 122.28, 121.85, 120.07, 119.30, 111.21, 110.85, 109.85, 48.58, 43.04, 41.88, 32.76, 26.34, 22.79, 13.03, 11.92, 4.61. LC-MS (ESI): calcd for C₃₁H₃₅N₅: 478.29652 [M+H]⁺, HR-MS found 478.29638[M+H]⁺.

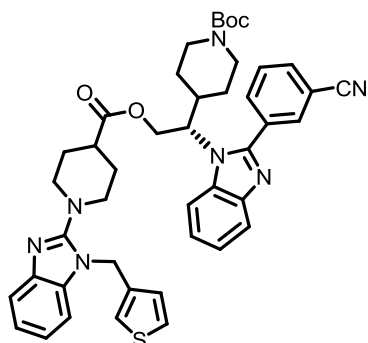


1-(Cyclopentylmethyl)-2-(2-isopropyl-1-(3-(2-methyl-1H-imidazol-1-yl)propyl)-5-phenyl-1H-pyrrol-3-yl)-1H-benzo[d]imidazole (155) To a suspension of benzimidazole **153** (20 mg, 0.05 mmol) in MeCN (1 mL) was added caesiumcarbonate (18 mg, 0.06 mmol) and (iodomethyl)cyclopentane (13 mg, 0.06 mmol). The reaction mixture was stirred at 50°C for 5 days. The reaction mixture was allowed to cool to room temperature and caesiumcarbonate (18 mg, 0.06 mmol) and (iodomethyl)cyclopentane (13 mg, 0.06 mmol) were added again. The reaction mixture was stirred at 50°C overnight. The reaction mixture was cooled to RT, diluted with DCM (10 mL) and extracted with NaHCO₃ (10 mL). The aqueous phase was extracted with DCM (2x 10 mL), the combined organic phases were dried over MgSO₄, filtered and evaporated to dryness. The crude product was dissolved in methanol and purified by reverse

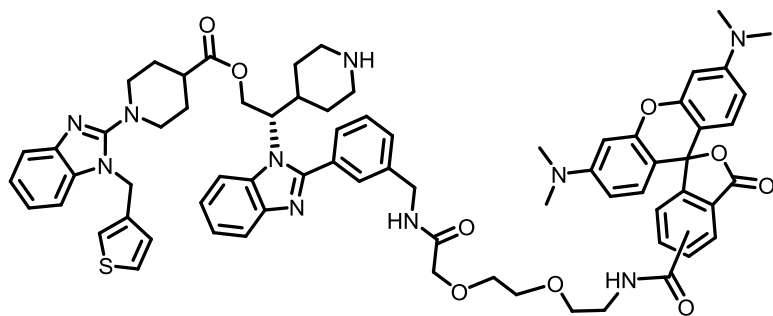
phase chromatography (CH₃CN: H₂O 1:5 to 9:1 containing 0.1% TFA) and obtained as a TFA salt (5.5 mg, 23%). ¹H NMR (600 MHz, DMSO-d₆) δ 7.99 (d, *J* = 6.7 Hz, 1H), 7.81 (d, *J* = 7.2 Hz, 1H), 7.57 – 7.51 (m, 2H), 7.47 (d, *J* = 2.0 Hz, 1H), 7.44 – 7.33 (m, 6H), 6.48 (s, 1H), 4.30 (d, *J* = 7.7 Hz, 2H), 4.11 – 4.04 (m, 2H), 4.02 (t, *J* = 6.7 Hz, 2H), 3.28 – 3.17 (m, 1H), 2.41 – 2.35 (m, 1H), 2.33 (s, 3H), 1.89 – 1.82 (m, 2H), 1.56 – 1.46 (m, 4H), 1.45 – 1.39 (m, 2H), 1.20 – 1.16 (m, 8H). ¹³C NMR (151 MHz, DMSO-d₆) δ 144.46, 141.55, 134.68, 132.60, 129.49, 129.44, 128.68, 122.47, 118.83, 111.15, 49.77, 44.67, 41.89, 31.02, 30.37, 26.45, 24.72, 22.54, 10.62. LC-MS (ESI): calcd for C₃₃H₃₉N₅: 506.32782 [M+H]⁺, found: 506.38 [M+H]⁺, R_t = 5.49 min, HR-MS found 506.32798 [M+H]⁺.



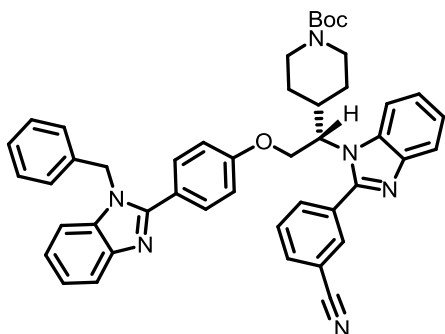
1-Benzyl-2-(2-isopropyl-1-(3-(2-methyl-1H-imidazol-1-yl)propyl)-5-phenyl-1H-pyrrol-3-yl)-1H-benzo[d]imidazole (156) To a suspension of benzimidazole **153** (30 mg, 0.06 mmol) in acetonitrile (1 mL) was added caesium carbonate (18 mg, 0.06 mmol). After half an hour benzylbromide (7 μL, 0.06 mmol) was added to the reaction mixture. The reaction mixture was stirred at RT for 2 days. Methanol was added and directly applied to reverse phase chromatography (CH₃CN: H₂O 1:5 to 9:1 containing 0.1% TFA) yielding the desired product (16 mg, 45%). ¹H NMR (600 MHz, DMSO-d₆) δ 7.82 – 7.75 (m, 2H), 7.51 – 7.43 (m, 3H), 7.40 – 7.32 (m, 6H), 7.30 – 7.23 (m, 3H), 7.10 – 7.06 (m, 2H), 6.39 (s, 1H), 5.59 (s, 2H), 4.01 (t, *J* = 6.8 Hz, 4H), 3.15 – 3.10 (m, 1H), 2.33 (s, 3H), 1.88 – 1.79 (m, 2H), 1.04 (d, *J* = 7.0 Hz, 6H). LC-MS (ESI): calcd for C₃₄H₃₅N₅: 514.29652 [M+H]⁺, HR-MS found: 514.29644 [M+H]⁺.

Synthesis of labeled *bis*-benzimidazoles

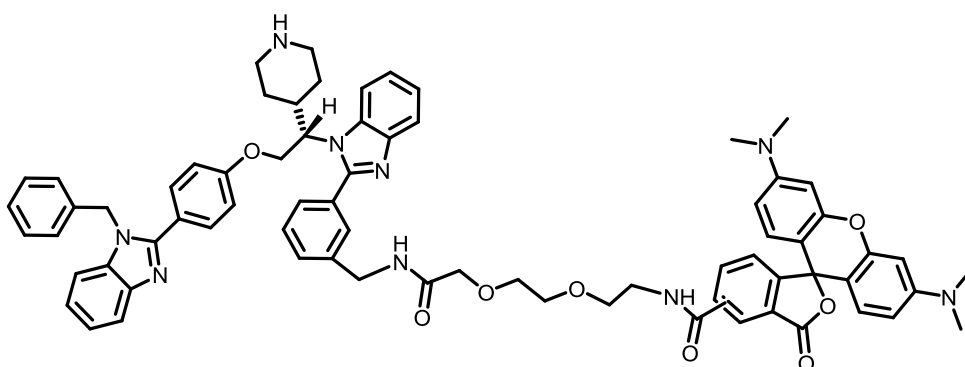
(S)-tert-Butyl 4-(1-(2-(3-cyanophenyl)-1H-benzo[d]imidazol-1-yl)-2-(1-(1-(thiophen-3-ylmethyl)-1H-benzo[d]imidazol-2-yl)piperidine-4-carboxyloxy)ethyl)piperidine-1-carboxylate ((S)-136) To a solution of (100 mg, 0.15 mmol) in MeOH, H₂O and DMSO (8:2:1, 5 mL) was added 3-cyano benzaldehyde (43 mg, 0.33 mmol) and sodium dithionite (81 mg, 0.46 mmol). The reaction mixture was heated to 65°C and after 0.5, 1, and 2 h sodium dithionite (3x 81 mg, 0.46 mmol) was added. After 5 h the reaction mixture was allowed to cool to room temperature. The reaction mixture was concentrated under reduced pressure and then extracted with DCM (3x 50 mL). The combined organic phases were dried (Na₂SO₄), filtered and concentrated to dryness. Purification by flash chromatography (gradient cyclohexane : ethyl acetate 5:1 to 1:5) afforded **(S)-136** (74 mg, 0.010 mmol, 64%). ¹H NMR (400 MHz, CDCl₃) δ 8.06 – 7.95 (m, 2H), 7.87 (dd, *J* = 12.8, 5.8 Hz, 2H), 7.74 (t, *J* = 7.4 Hz, 2H), 7.60 (d, *J* = 5.1 Hz, 1H), 7.46 – 7.27 (m, 5H), 7.17 (d, *J* = 7.9 Hz, 1H), 7.08 (d, *J* = 1.4 Hz, 1H), 6.93 (d, *J* = 5.0 Hz, 1H), 5.20 (s, 2H), 5.04 – 4.91 (m, 1H), 4.62 (dd, *J* = 11.9, 3.8 Hz, 1H), 4.38 (t, *J* = 7.9 Hz, 1H), 4.17 (d, *J* = 13.3 Hz, 1H), 4.00 – 3.83 (m, 1H), 3.77 – 3.56 (m, 2H), 3.42 – 3.22 (m, 2H), 2.70 (t, *J* = 12.3 Hz, 1H), 2.62 – 2.34 (m, 3H), 2.00 – 1.79 (m, 3H), 1.79 – 1.53 (m, 2H), 1.40 (s, 9H), 1.24 (t, *J* = 10.1 Hz, 1H), 0.96 – 0.67 (m, 2H). ¹³C NMR (101 MHz, CDCl₃) δ 173.09, 161.89, 161.53, 154.66, 153.12, 152.33, 141.54, 134.45, 134.10, 133.52, 132.74, 132.02, 130.82, 130.63, 130.54, 128.67, 125.59, 125.53, 124.92, 124.74, 124.36, 122.56, 120.44, 118.01, 117.93, 115.05, 113.60, 112.28, 110.59, 80.21, 63.52, 61.71, 49.35, 46.05, 39.68, 37.35, 29.93, 28.83, 28.57, 27.50. LC-MS (ESI): calcd for C₁₈H₂₇N₃O₅: 689.31158 [M+H]⁺, found: 689.29 [M+H]⁺, R_t = 8.47 min; HR-MS found 689.31133 [M+H]⁺.



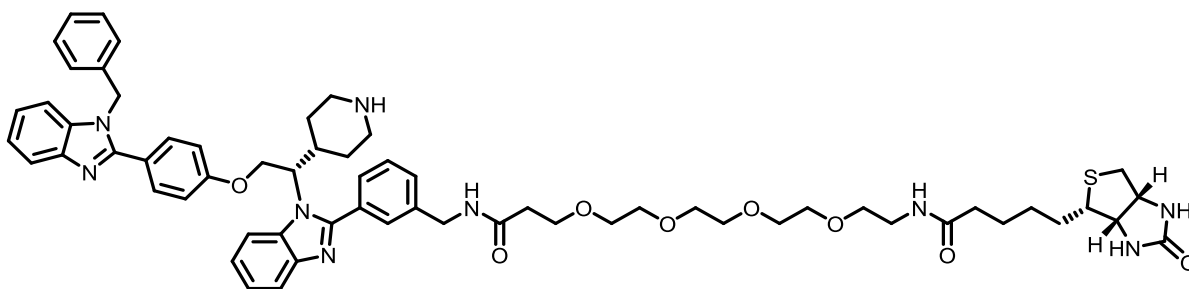
2-(3-(3,12-dioxo-5,8-dioxa-2,11-diazatridecyl)phenyl)-1H-*enzo*[d]imidazol-1-yl)-2-(piperidin-4-yl)ethyl 1-(1-(thiophen-3-ylmethyl)-1H-benzo[d]imidazol-2-yl)piperidine-4-carboxylate = TAMRA-(S)-92. Raney Nickel (Aldrich, W.R. Grace and Co. Raney[®]2800, slurry, in H₂O, 40 mg) was added to an argon filled flask containing ammonia in ethanol (2.0 M, 1 mL). After 5 minutes of stirring the liquid was removed via syringe. The flask was evacuated and flushed with argon. Ammonia in ethanol (2.0 M, 4 mL) was then added, followed by compound (**S**) (15 mg, 19 μmol). The solution was purged with argon for 2 minutes and kept under an atmosphere of hydrogen (1 atm, balloon). The resulting reaction mixture was stirred at room temperature for 3 h to afford the free amine (LC-MS: 6.36 min retention time, [M+H]⁺ 774.36). The reaction mixture was filtered over a pad of Celite, the filter cake was washed with EtOH (30 mL) and ethylacetate (20 ml) and the filtrate was concentrated under reduced pressure. To the crude amine in DMF (1 mL) was added PyBOP (12 mg, 23 μmol) and TAMRA-PEG-COOH (13 mg, 23 μmol). The reaction mixture was stirred at room temperature overnight. The reaction mixture was concentrated under reduced pressure. To the residue was added HCl in dioxane (4 M) and the mixture was stirred for 2 h at room temperature. The reaction mixture was concentrated under reduced pressure, the residue was dissolved in methanol and purified by reverse phase chromatography to yield TAMRA-(S)-92 (7 mg, 6 μmol, 29%). ¹H NMR (400 MHz, DMSO-*d*₆) δ 8.95 (t, *J* = 5.5 Hz, 1H), 8.63 (s, 1H), 8.54 – 8.46 (m, 1H), 8.46 – 8.38 (m, 1H), 8.30 – 8.23 (m, *J* = 8.1 Hz, 1H), 8.11 – 7.98 (m, 1H), 7.84 (d, *J* = 7.6 Hz, 1H), 7.67 – 7.60 (m, 2H), 7.58 – 7.39 (m, 6H), 7.35 – 7.22 (m, 4H), 7.22 – 7.11 (m, 2H), 7.06 – 6.87 (m, 6H), 5.23 (s, 2H), 4.89 (s, 1H), 4.56-4.38 (m, *J* = 45.4, 9.5 Hz, 3H), 3.97 (s, 2H), 3.08 – 2.90 (m, 3H), 2.88 – 2.76 (m, 1H), 2.75 – 2.61 (m, 1H) 2.08 – 1.91 (m, 2H), 1.71 – 1.27 (m, 7H), 1.27 – 1.13 (m, 2H), 1.15 – 0.91 (m, 3H). LC-MS (ESI): found: 1231.58 [M+H]⁺, R_t = 5.76 min; HR-MS calcd for C₇₀H₇₄N₁₀O₉S: 411.18597 [M+3H]³⁺, found 411.18576 [M+3H]³⁺.



(S)-3-(1-(2-(4-(1-benzyl-1H-benzo[d]imidazol-2-yl)phenoxy)-1-(piperidin-4-yl)ethyl)-1H-benzo[d]imidazol-2-yl)benzonitrile ((S)-169) The desired product was synthesized according to the procedure for (S)-136 starting from (S)-117 (15 mg, 60%). ¹H NMR (400 MHz, CDCl₃) δ 8.09 (s, 1H), 7.98 (d, *J* = 7.7 Hz, 1H), 7.80 – 7.71 (m, 3H), 7.63 – 7.51 (m, 4H), 7.31 – 7.20 (m, 6H), 7.18 – 7.10 (m, 2H), 7.03 – 6.97 (m, 2H), 6.85 (d, *J* = 8.8 Hz, 2H), 5.33 (s, 2H), 4.72 (t, *J* = 9.2 Hz, 1H), 4.49 – 4.34 (m, 2H), 4.17 – 4.02 (m, 1H), 3.92 – 3.72 (m, 1H), 2.64 (t, *J* = 12.5 Hz, 1H), 2.56 – 2.31 (m, 2H), 1.85 (d, *J* = 12.9 Hz, 1H), 1.33 (s, 9H), 1.26 – 1.11 (m, 1H), 0.86 – 0.74 (m, 2H). LC-MS (ESI): calcd for C₄₆H₄₅N₆O₃ 729.25 [M+H]⁺, found: 729.31 [M+H]⁺.

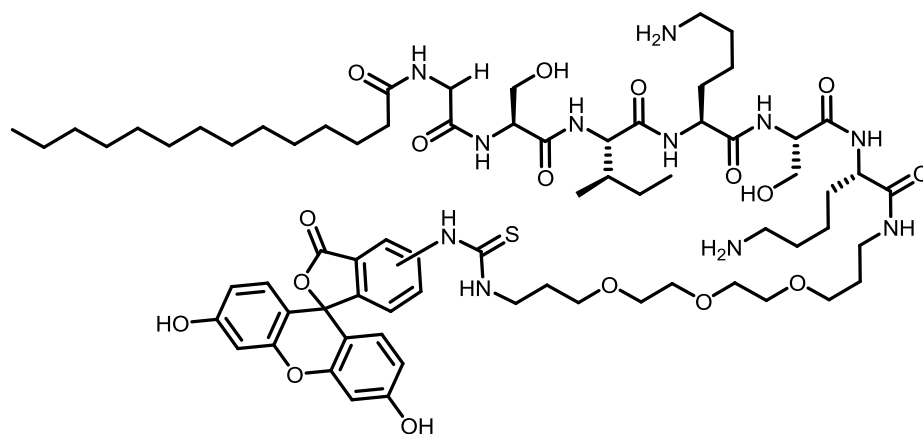


(S)-N-(2-(2-(2-(3-(1-(2-(4-(1-benzyl-1H-benzo[d]imidazol-2-yl)phenoxy)-1-(piperidin-4-yl)ethyl)-1H-benzo[d]imidazol-2-yl)benzylamino)-2-oxoethoxy)ethoxy)ethyl)-3',6'-bis(dimethylamino)-3-oxo-3H-spiro[isobenzofuran-1,9'-xanthene]-5-carboxamide (S)-137 (TAMRA-Deltarasin) The desired product was synthesized according to the procedure for TAMRA-(S)-92 starting from (S)-169 (5 mg, 20%). ¹H NMR (400 MHz, DMSO) δ 8.94 (t, *J* = 5.5 Hz, 1H), 8.70 – 8.58 (m, 2H), 8.40 (t, *J* = 6.2 Hz, 1H), 8.24 (dd, *J* = 8.0, 1.7 Hz, 1H), 8.19 – 8.02 (m, 1H), 7.95 (d, *J* = 7.0 Hz, 1H), 7.78 – 7.57 (m, 6H), 7.57 – 7.41 (m, 4H), 7.41 – 7.19 (m, 6H), 7.15 – 6.87 (m, 9H), 5.55 (s, 2H), 4.86 (t, *J* = 9.6 Hz, 1H), 4.67 – 4.48 (m, 2H), 4.43 (d, *J* = 6.0 Hz, 2H), 3.94 (s, 2H), 2.79 – 2.63 (m, 2H), 2.10 (d, *J* = 12.5 Hz, 1H), 1.50 – 1.34 (m, 1H), 1.11 – 0.87 (m, 2H). LC-MS (ESI): calcd for C₇₂H₇₁N₉O₈: 1190.54 [M+H]⁺, found: 1190.1 [M+H]⁺.

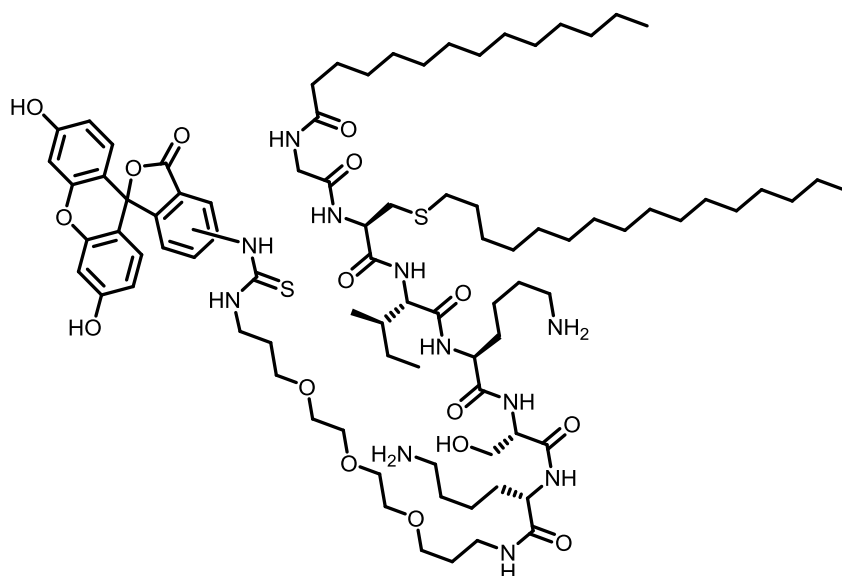


N-(3-(1-((R)-2-(4-(1-Benzyl-1H-benzo[d]imidazol-2-yl)phenoxy)-1-(piperidin-4-yl)ethyl)-1H-benzo[d]imidazol-2-yl)benzyl)-1-(5-((3a*S*,4*S*,6a*R*)-2-oxohexahydro-1H-thieno[3,4-*d*]imidazol-4-yl)pentanamido)-3,6,9,12-tetraoxapentadecan-15-amide (170) To the hydrogenated product of (*S*)-**169** (65 mg, 0.09 mmol) was added Biotin-PEG-COOH (44 mg, 0.09 mmol), DIPEA (79 μ L, 0.44 mmol) and HATU (34 mg, 0.09 mmol). The reaction mixture was stirred at room temperature for 18 h. Water (2 mL) was added to the reaction mixture, the precipitate was collected and washed with water (2x 4 mL). The solid was dissolved in DCM (1 mL), HCl/dioxane (1 mL, 4 M) was added and the reaction mixture was stirred at room temperature for 3 h. The solvent is removed in vacuo, redissolved in MeOH and purified by reverse phase chromatography to yield the desired compound as an TFA salt (48 mg, 45%). ^1H NMR (400 MHz, DMSO- d_6) δ 8.64 – 8.53 (m, 1H), 8.49 (t, $J = 5.8$ Hz, 1H), 8.17 – 8.02 (m, 1H), 7.97 (d, $J = 7.6$ Hz, 1H), 7.84 – 7.73 (m, 2H), 7.71 – 7.63 (m, 4H), 7.60 – 7.49 (m, 2H), 7.49 – 7.42 (m, 1H), 7.41 – 7.25 (m, 6H), 7.17 – 7.10 (m, 2H), 7.08 – 7.01 (m, 2H), 6.47 – 6.23 (m, 2H), 5.59 (s, 2H), 4.87 (t, $J = 9.7$ Hz, 1H), 4.64 (d, $J = 7.8$ Hz, 1H), 4.59 – 4.50 (m, 1H), 4.46 – 4.33 (m, 2H), 4.31 – 4.25 (m, 1H), 4.10 – 4.07 (m, 1H), 3.59 (t, $J = 6.3$ Hz, 2H), 3.48 – 3.26 (m, 16H), 3.18 – 3.11 (m, 2H), 3.09 – 3.01 (m, 2H), 2.94 – 2.63 (m, 5H), 2.38 (t, $J = 6.2$ Hz, 2H), 2.10 (d, $J = 13.0$ Hz, 1H), 2.04 (t, $J = 7.5$ Hz, 2H), 1.64 – 1.53 (m, 1H), 1.51 – 1.37 (m, 4H), 1.33 – 1.19 (m, 2H), 1.11 – 0.92 (m, 2H). LC-MS (ESI): calcd for $\text{C}_{62}\text{H}_{75}\text{N}_9\text{O}_8\text{S}$: 1106.55321 $[\text{M}+\text{H}]^+$, found: 1106.44 $[\text{M}+\text{H}]^+$, HR-MS found 1106.55238 $[\text{M}+\text{H}]^+$.

Synthesis of lipidated *N*-terminal Lyn peptide



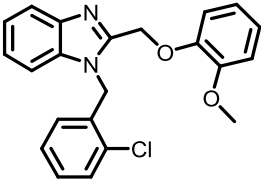
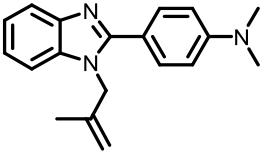
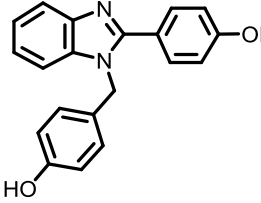
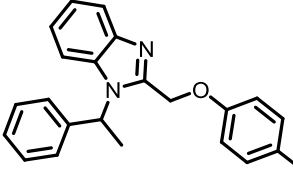
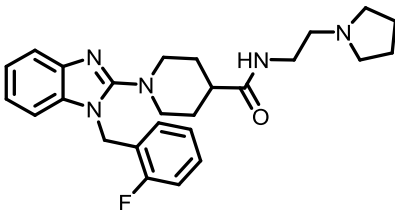
Mono lipidated *N*-terminal Lyn peptide 179 (Fmoc)-Boc-Lys-Allyl was synthesized and immobilized as previously described.⁴⁰ *N*-terminal elongation was achieved by cycles of *N*-deprotection and peptide bond formation using Fmoc-(Trt)-SerOH, Fmoc-(Mtt)-Lys-OH, Fmoc-Ile-OH, Fmoc-Gly-OH and myristic acid. Deprotection was achieved using 5 mL of 20% piperidine and 2% DBU in DMF twice for 10 minutes. Subsequently the resin was washed 5 times with DMF. All amino acids were coupled twice employing 4 eq of amino acid, 4 eq of HCTU and 8 eq of DIPEA in 5 ml DMF. Double couplings were carried out at 60°C for 15 minutes each cycle. The *C*-terminal allyl group was deprotected with 0.05 eq Pd(PPh₃)₄ and 10 eq of PhSiH₃ in THF for 2 hours. The allyl deprotected building block was coupled Fmoc-PEG-NH₂ (1eq) using PyBop (2 eq) and NMM (2eq), deprotected and treated with 2 eq FITC. Cleavage from the solid support and side chain deprotection was performed by treating the resin with 15 mL of 5 % TFA in dry DCM containing 2 % TES for 1 hour. The solvent was evaporated and redissolved in MeOH. The resulting solution was filtered, and the filtrate purified by preparative HPLC using a C18 column (Yield 8%).¹H NMR (400 MHz, dmsO) δ 10.11 (s, 2H), 9.97 (s, 1H), 8.22 (s, 1H), 8.19 – 8.11 (m, 2H), 8.05 (t, *J* = 5.6 Hz, 2H), 8.00 – 7.85 (m, 3H), 7.81 (d, *J* = 8.2 Hz, 1H), 7.78 – 7.56 (m, 9H), 7.16 (d, *J* = 8.3 Hz, 1H), 6.66 (d, *J* = 2.2 Hz, 2H), 6.63 – 6.51 (m, 4H), 5.17 (s, 1H) 4.44 – 4.31 (m, 1H), 4.30 – 4.18 (m, 2H), 4.12 (t, *J* = 7.6 Hz, 2H), 3.73 – 3.46 (m, 17H), 3.09 – 3.02 (m, 2H), 2.83 – 2.62 (m, 5H), 2.10 (t, *J* = 7.5 Hz, 2H), 1.85 – 1.36 (m, 18H), 1.33 – 1.20 (m, 20H), 1.13 – 0.98 (m, 1H), 0.91 – 0.74 (m, 9H). LC-MS (ESI): calcd for C₇₁H₁₀₉N₁₁O₁₇S: 1420.77 [M+H]⁺, found 1421.57 [M+H]⁺, R_t = 6.76 min.

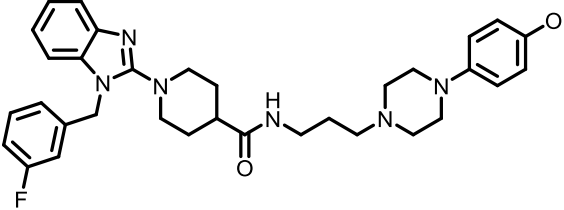
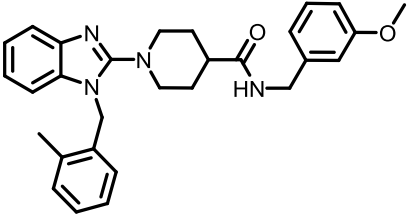
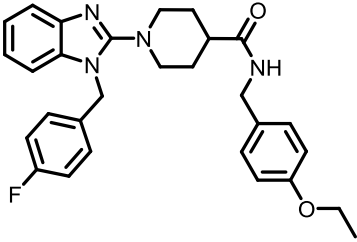
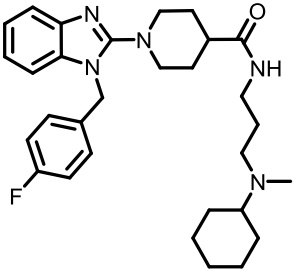
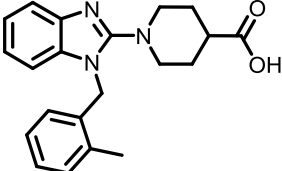


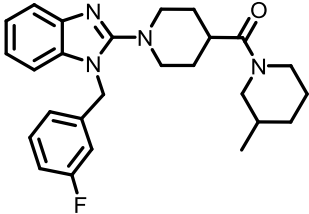
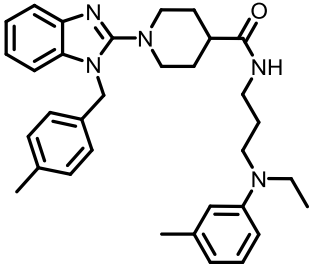
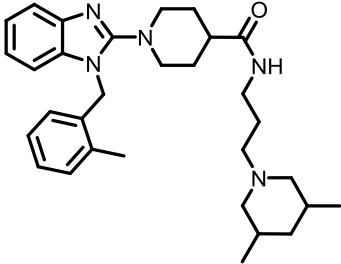
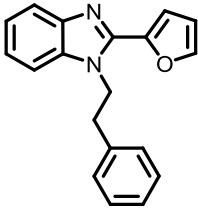
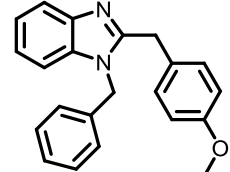
Double lipidated N-terminal Lyn 180 The peptide was synthesized in an analogous fashion to the mono lipidated peptide **179**. The racemization-prone hexadecylated cysteine¹²⁶ building block was coupled twice at room temperature for 5 h. (Yield 4%). ¹H NMR (400 MHz, dmsO) δ 10.11 (s, 2H), 10.03 – 9.90 (m, 1H), 8.22 (s, 1H), 8.19 – 8.09 (m, 2H), 8.09 – 8.02 (m, 2H), 8.02 – 7.93 (m, 4H), 7.89 (d, $J = 8.1$ Hz, 1H), 7.84 – 7.58 (m, 10H), 7.16 (d, $J = 8.4$ Hz, 1H), 6.66 (d, $J = 2.2$ Hz, 2H), 6.63 – 6.46 (m, 4H), 5.18 (s, 1H), 4.50 – 4.41 (m, 1H), 4.29 – 4.17 (m, 2H), 4.17 – 4.05 (m, 2H), 3.74 – 3.39 (m, 15H), 3.13 – 3.02 (m, 3H), 2.81 – 2.58 (m, 6H), 2.10 (t, $J = 7.5$ Hz, 2H), 1.87 – 1.36 (m, 18H), 1.36 – 1.12 (m, 60H), 0.87 – 0.74 (m, 13H). LC-MS (ESI): calc for C₈₇H₁₄₁N₁₁O₁₆S₂ 1661.00 found: 1661.70 [M+H]⁺, R_t = 7.36 min.

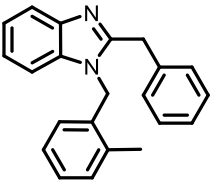
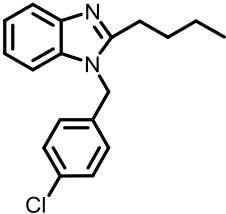
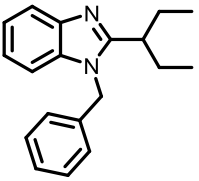
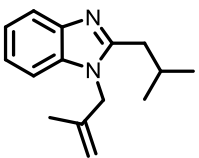
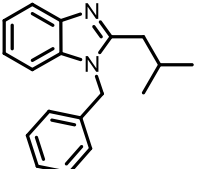
7 APPENDIX

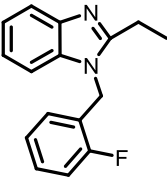
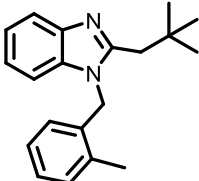
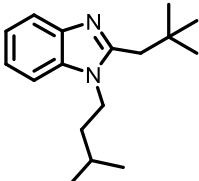
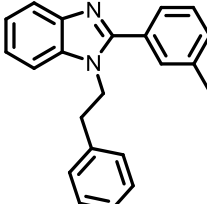
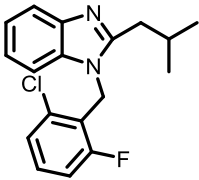
$K_{D,app}$ values determined by Alpha technology (COMAS).

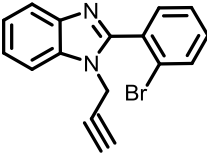
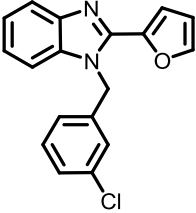
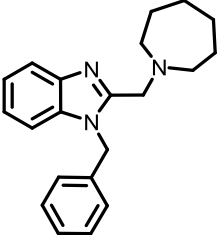
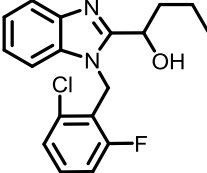
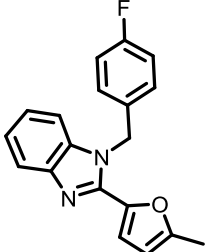
Compound	K_D / nM
	280
	560
	90
	540
	310

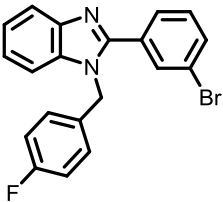
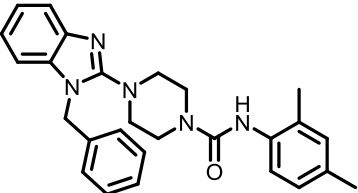
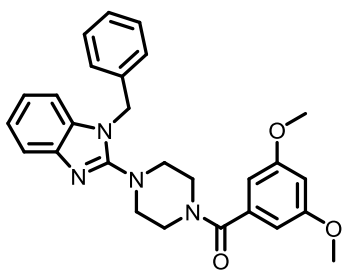
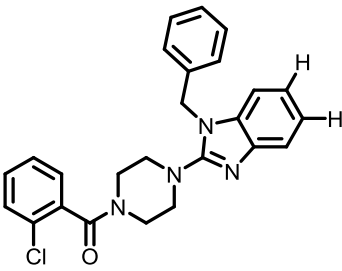
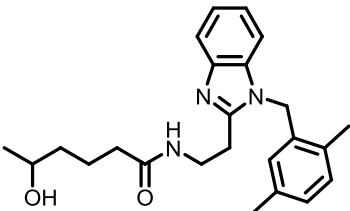
Compound	K_D / nM
	530
	110
	100
	520
	2580

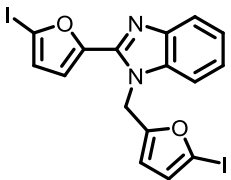
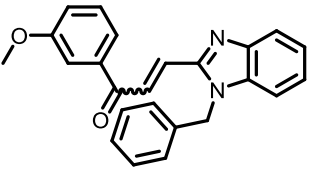
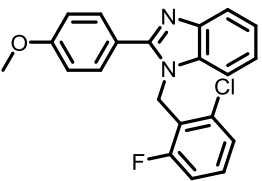
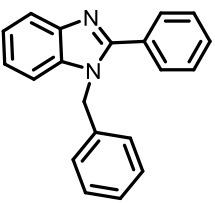
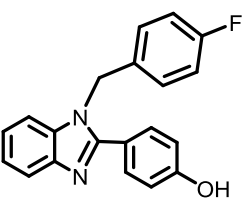
Compound	K_D / nM
	1100
	3570
	140
	710
	580

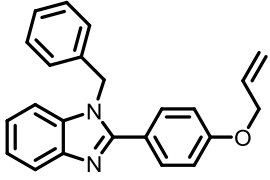
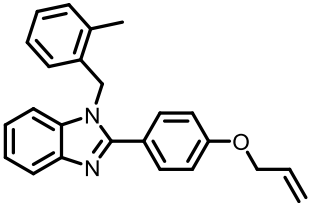
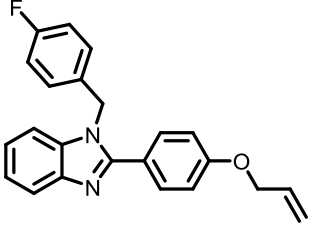
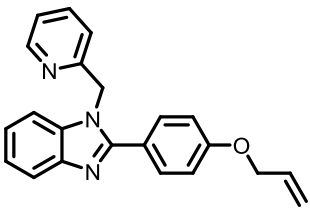
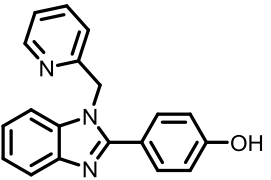
Compound	K_D / nM
	1980
	600
	1430
	620
	210

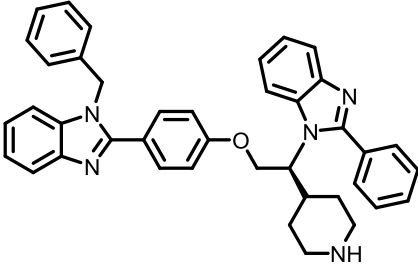
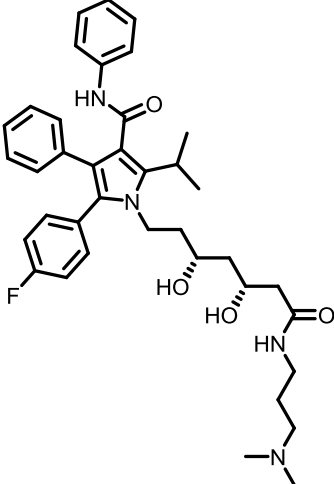
Compound	K_D / nM
	500
	80
	180
	1880
	70

Compound	K_D / nM
	9170
	960
	110
	440
	210

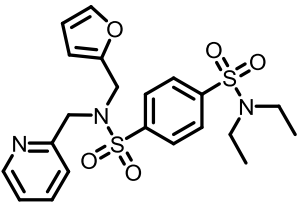
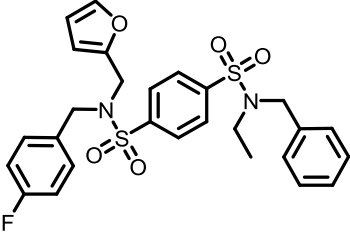
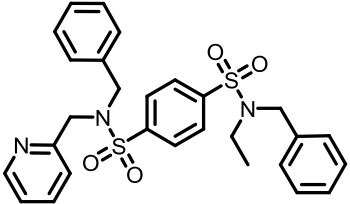
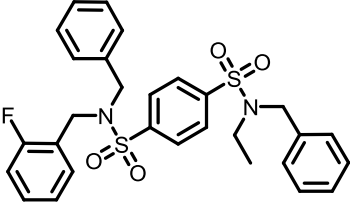
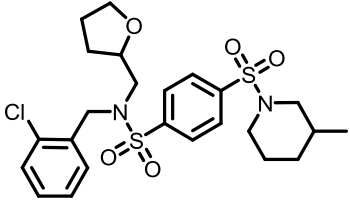
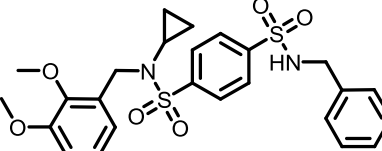
Compound	K_D / nM
	1020
	670
	190
	580
	>10000

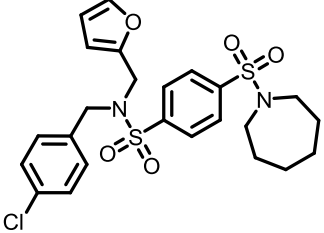
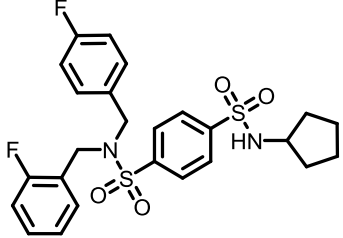
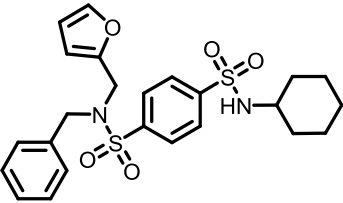
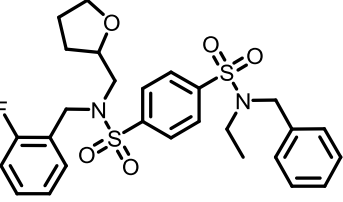
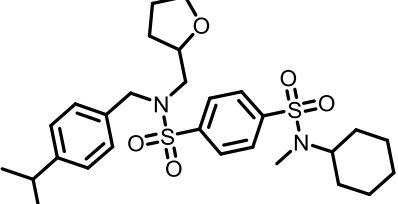
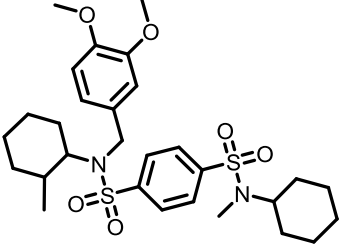
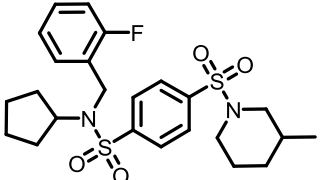
Compound	K_D / nM
	100
	1385
	810
	280
	190

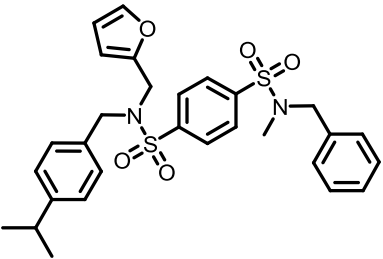
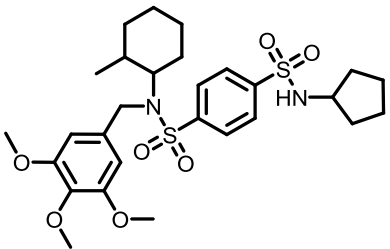
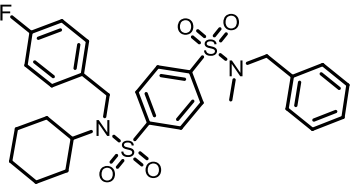
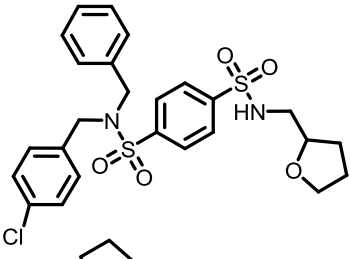
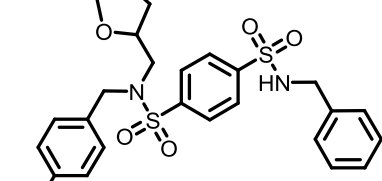
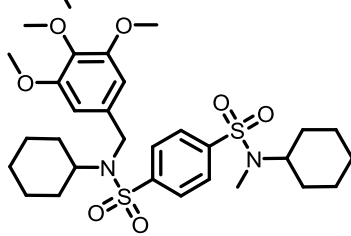
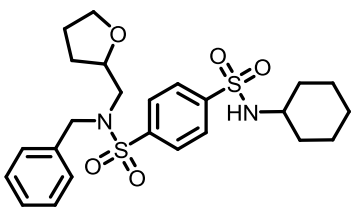
Compound	K_D / nM
	2960
	1000
	750
	>10000
	2270

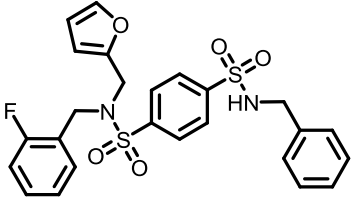
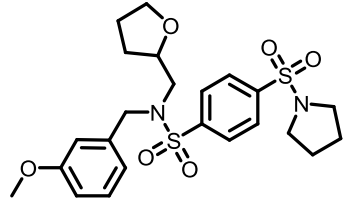
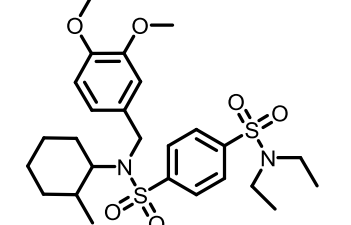
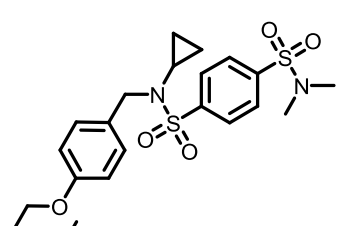
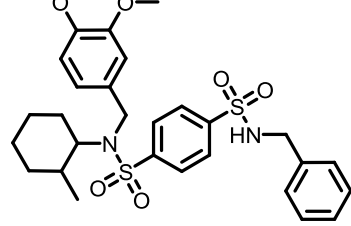
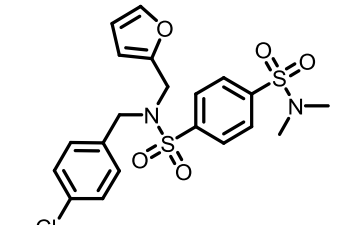
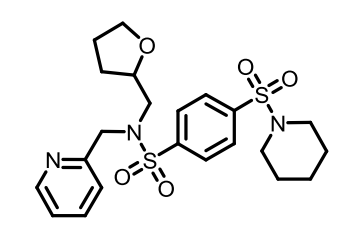
Compound	K_D / nM
	70
	70

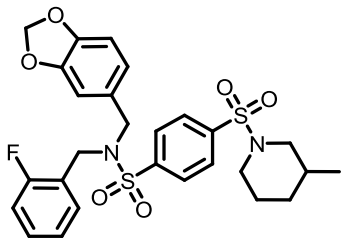
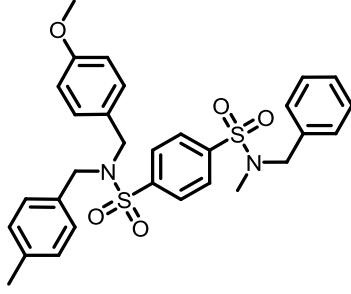
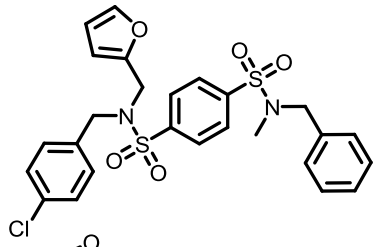
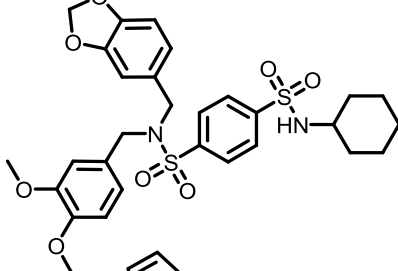
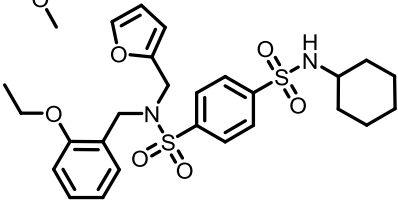
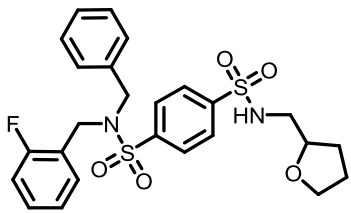
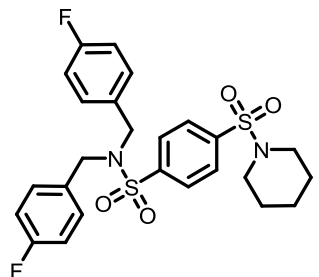
K_D values of sulfonamides in nM, determined by means of fluorescence polarization assays (average of triplicate determination)

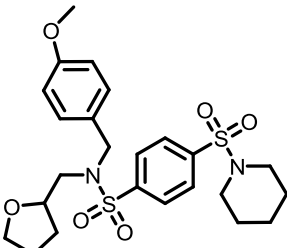
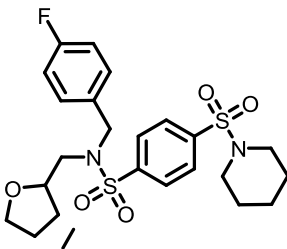
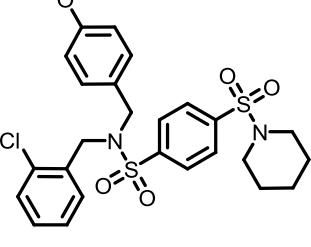
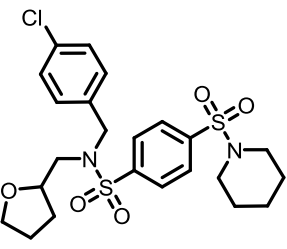
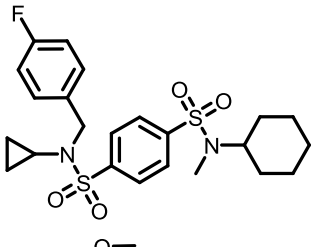
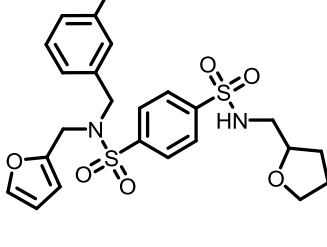
Compound	K _D / nM
	267
	31
	<5
	5
	373
	575

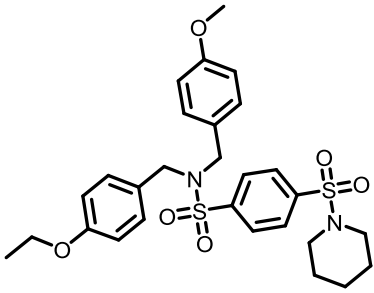
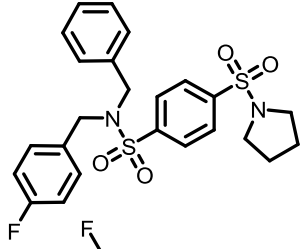
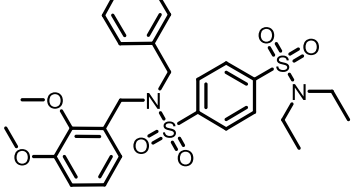
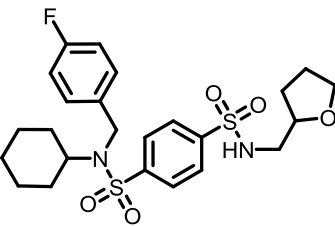
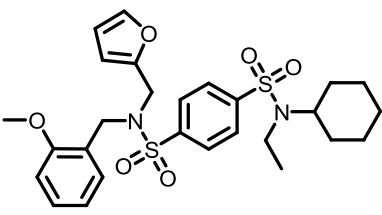
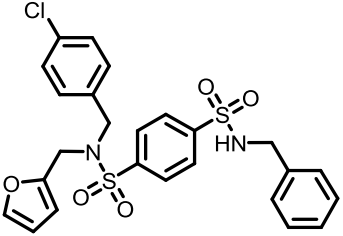
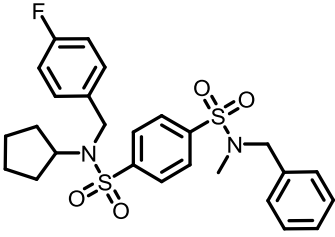
Compound	K_D / nM
	633
	175
	79
	<5
	22
	135
	63

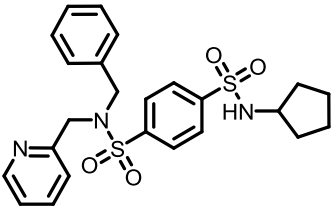
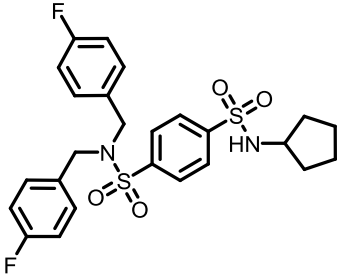
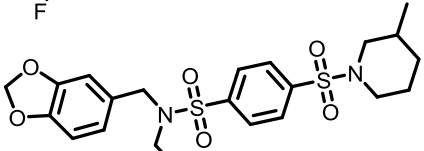
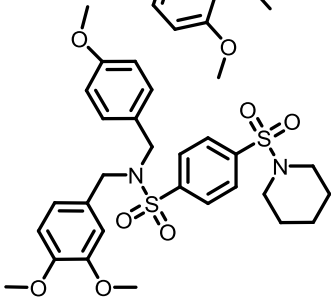
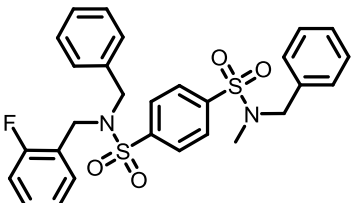
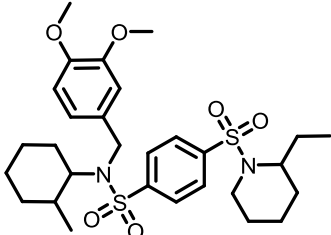
Compound	K_D / nM
	714
	109
	10
	862
	6
	463
	8

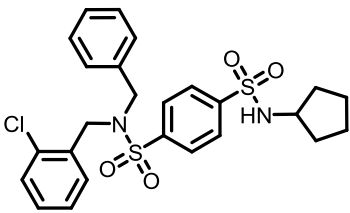
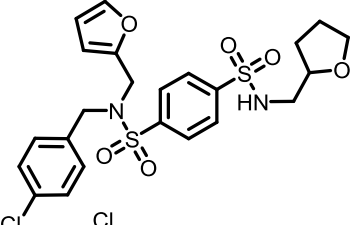
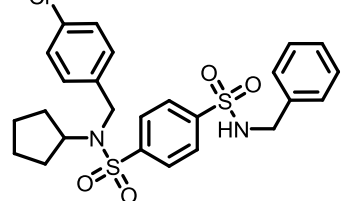
Compound	K_D / nM
	1941
	440
	29
	394
	280
	2889
	256

Compound	K_D / nM
	439
	1950
	1186
	341
	854
	939
	1213

Compound	K_D / nM
	99
	47
	270
	87
	6
	388

Compound	K_D / nM
	2950
	1243
	888
	8
	152
	58
	<5

Compound	K_D / nM
	273
	1080
	2086
	1785
	225
	6

Compound	K_D / nM
	270
	84
	<5

8 ZUSAMMENFASSUNG

Ras-Proteine sind molekulare Schalter, die in gesunden Zellen Wachstum und Teilung regulieren. Mutationen in *Ras*-Genen können zu einem dauerhaft angeschalteten Zustand führen und im ungünstigsten Fall zur Entstehung von Tumoren durch permanentes Zellwachstum beitragen. Da fast jeder dritte Tumor eine Mutation in einem der Ras-Proteine aufweist, befinden sich diese Proteine seit Jahren im Fokus der Wirkstoffentwicklung. Von herausragendem Interesse ist dabei die besonders aggressive K-Ras Isoform. Die Lokalisation von K-Ras in der Zelle ist eng mit der biologischen Schalterfunktion verknüpft, da K-Ras nur an der Plasmamembran aktiv die Signaltransduktion beeinflussen kann.

Das Transport-Protein PDE δ reguliert die zelluläre Lokalisation von K-Ras und damit die K-Ras abhängige Signaltransduktion. Im Gegensatz zu K-Ras selbst weist PDE δ eine große hydrophobe Bindungstasche auf, die es erlaubt mittels kleinen synthetischen Molekülen die Signaltransduktion von Ras zu beeinflussen. Wichtigstes Ziel dieser Arbeit war deshalb die Identifikation und Optimierung von Inhibitoren der K-Ras-PDE δ -Wechselwirkung.

Identifikation und Optimierung von Benzimidazole basierten K-Ras-PDE δ Inhibitoren

Für die biochemische Hochdurchsatztestung von Inhibitoren wurde ein C-terminales K-Ras-Peptid synthetisiert und PDE δ heterolog in *E. Coli* produziert. Eine 40000 Moleküle umfassende Substanzbibliothek wurde dann mittels Alpha screen bezüglich ihrer Wirkung auf die K-Ras-PDE δ -Interaktion untersucht. Dabei wurde das Benzimidazolfragment **10** identifiziert als nanomolarer Inhibitor der K-Ras-PDE δ -Interaktion identifiziert (Abbildung 1, a). Durch Kokristallisation des Benzimidazolfragments mit PDE δ und isothermaler Titrationskalorimetrie (ITC) konnte die Bindung von zwei Benzimidazol-Fragmenten **10** an das Protein nachgewiesen werden (Abbildung 1, b). In ITC-Messungen wurde dabei eine stark Enthalpie getriebene Interaktion der Benzimidazole mit PDE δ festgestellt, welche sich auf die Ausbildung von zwei Wasserstoffbrücken zu jedem der Benzimidazolfragmente (Arg61 und Tyr149, Abbildung 1, b) zurückführen lässt. Um die Affinität und damit auch die Spezifität der Benzimidazol-Liganden zu verbessern, wurden die zwei Fragmente des Benzimidazoles **10** miteinander verknüpft. Die besten Phenylether-verbrückten *bis*-Benzimidazole wiesen K_D Werte bis zu 16 nM auf und zeigten damit eine deutliche bessere Affinität als das Fragment **10**. In der Kristallstruktur des *bis*-Benzimidazols **55** mit PDE δ (Abbildung 1, c) zeigt die Allylgruppe in Richtung der Carbonylfunktion des Rückgratamids von Cys56. Deshalb wurden in der Folge Moleküle zu

synthetisiert, welche eine weitere Wasserstoffbrücke zur Carbonylgruppe von Cys56 ausbilden können. Dazu wurde die verbrückende Phenylether-Einheit durch einen flexibleren Piperidyl-Ester ersetzt (Abbildung 1, a, rechts) und die Allylgruppe durch ein Piperidin substituiert.

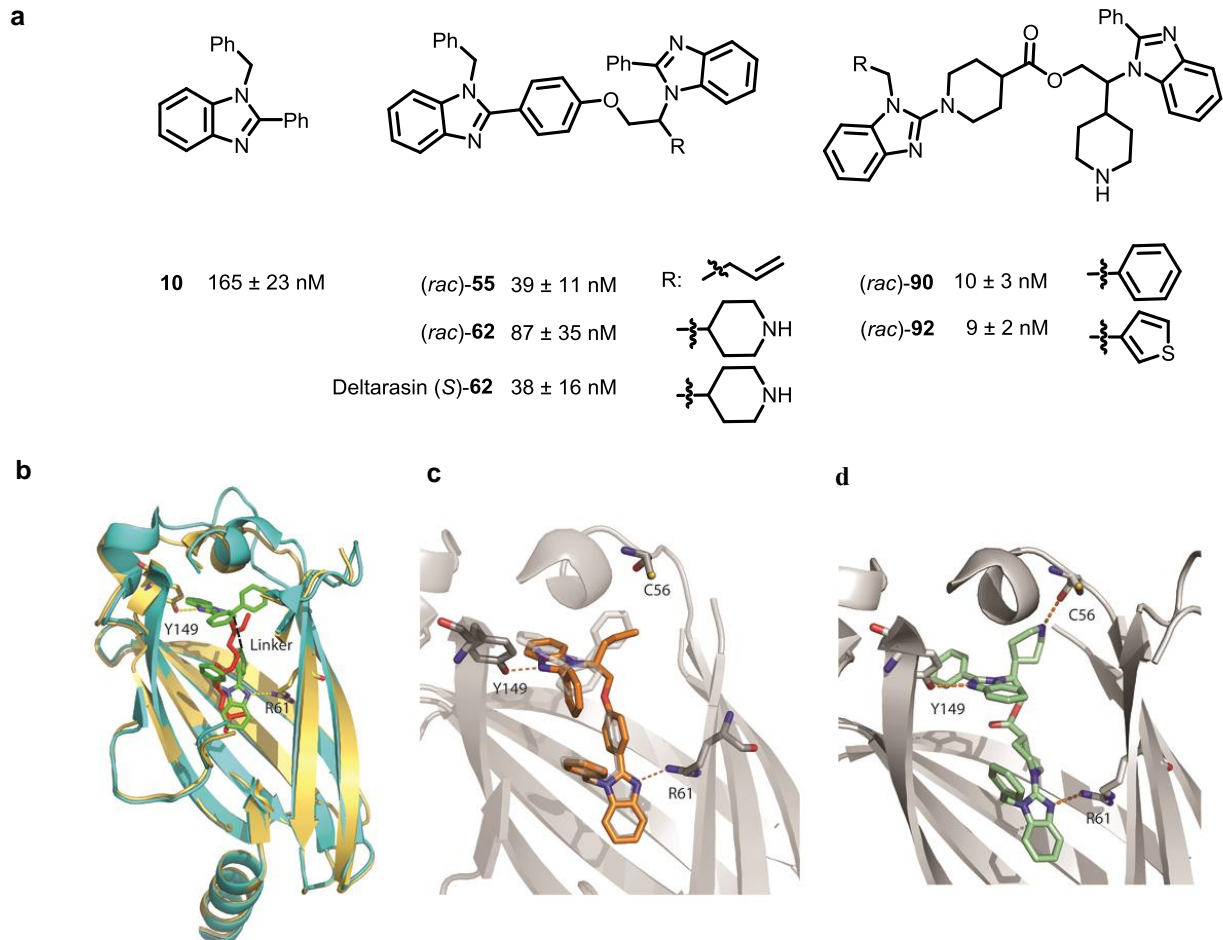


Abbildung 1 Strukturen und Bindungsaffinitäten der synthetisierten Benzimidazole bestimmt durch Verdrängungstirationen von Fluorescein-Atorvastatin.⁷⁹ a) Strukturen der Benzimidazol-basierten Inhibitoren; b) Kokristallstruktur von Benzimidazolfragment **10** mit PDE δ (gelb). Überlagert ist die Struktur der vorher bestimmten Kristallstruktur von farnesyliertem Rheb-Peptid mit PDE δ (cyan). Das Benzimidazolfragment **10** (grün) und die Farnesylgruppe (rot) sind als Stäbchenmodell dargestellt. Wasserstoffbrückenbindungen zwischen den zwei Benzimidazolfragmenten **10** und dem Protein sind hervorgehoben; c) Struktur von *(rac)*-**55** (orange) im Komplex mit PDE δ . Überlagert sind die zwei Benzimidazolfragmente **10** (schwach graue Stäbchen); d) Die Kokristallstruktur von (*S*)-**90** und PDE δ bestätigt die erwartete Wasserstoffbrücke zwischen der Piperidingruppe und dem Rückgratcarbonyl von Cys56. Die Kokristallstrukturen wurden von Dr. Shehab Ismail gelöst.

Die Ester-verbrückten *bis*-Benzimidazole **90** und **92** wiesen dabei verbesserte Affinitäten auf. Die durch Computermodellierung vorhergesagte Wasserstoffbrücke zu Cys56 konnte durch eine Kokristallstruktur verifiziert werden (Abbildung 1, d). Direkte Titrations der fluoreszenzmarkierten Moleküle TAMRA-(*S*)-**62**-Deltarasin und TAMRA-(*S*)-**92** mit

PDE δ bestätigten die hohe Affinität der *bis*-Benzimidazole (K_D -Werte 5-7 nM). Hingegen konnte keine Interaktion mit den Lipid-bindenden Proteinen UNC119a/HRG4, UNC119b and Galectin 1/3 beobachtet werden, was auf eine sehr gute Selektivität der *bis*-Benzimidazole hindeutet. Durch zeitaufgelöste Fluoreszenzanisotropie-Messungen konnte die Kinetik der Interaktion zwischen fluoreszenzmarkierten *bis*-Benzimidazolen und PDE δ untersucht werden. Dabei wurden für den TAMRA-(*S*)-**92**-PDE δ -Komplex Dissoziations-Halbwertszeiten im Stundenbereich gemessen. Mittels Oberflächenplasmonenresonanz (SPR) konnten sowohl die sehr langsame Dissoziation der *bis*-Benzimidazol-PDE δ -Komplexe als auch die sehr niedrigen K_D -Werte verifiziert werden. Für den nicht fluoreszenzmarkierten Ester (*S*)-**90** konnte dabei aus kinetischen Messdaten eine Affinität von 77 pM berechnet werden.

Inhibitoren der K-Ras-PDE δ -Wechselwirkung hemmen die onkogene Ras-Signaltransduktion

Da die sehr potenten Esterverbindungen jedoch potentiell empfindlich gegenüber Hydrolasen sind, wurde in zellulären Experimente nur mit Ether-verknüpften *bis*-Benzimidazolen gearbeitet. Das gut lösliche *bis*-Benzimidazole (*S*)-**62** Deltarasin wurde deshalb bezüglich seines Effekts auf PDE δ in Zellen untersucht. Sowohl für immobilisiertes als auch für freies Deltarasin konnte die Interaktion mit PDE δ in Zellysaten mittels Western Blot nachgewiesen werden. Björn Papke konnte zeigen, dass Deltarasin auch die Wechselwirkung zwischen K-Ras und PDE δ in lebenden Zellen inhibitiert. Darüberhinaus hemmt Deltarasin die Erk-Phosphorylierung und stoppt selektiv das Wachstum von Ras-abhängigen Zelllinien, sowohl *in cellulo* als auch *in vivo* im Maus-Xenograft-Modell.

Optimierung und Identifikation neuer Substanzklassen von PDE δ Inhibitoren

Durch weitere strukturbasierte Optimierung konnte das Molekulargewicht und die Hydrophobizität der *bis*-Benzimidazole gesenkt werden, wobei die Affinität für das PDE δ erhalten blieb. In einem weiteren Ansatz konnte der literaturbekannte PDE δ -Inhibitor Atorvastatin rational modifiziert werden und die Affinität um fast zwei Größenordnungen verbessert werden. Durch Hochdurchsatztestung identifizierte *bis*-Sulfonamide wurden durch eine kommerziell erhältliche Bibliothek von 56 Derivaten ergänzt. Diese Verbindungen zeigten sehr hohe Affinitäten im niedrig nanomolaren Bereich.

Allosterische Verdrängung von PDE δ Inhibitoren durch Arl2/3.

Obwohl Deltarasin und andere Inhibitoren eine nanomolare Potenz in biochemischen Assays aufwiesen, konnten keine Inhibitoren mit nanomolarer Aktivität in zellulären Testsystemen identifiziert werden. Dies deutet auf einen Chemotyp-unabhängigen Mechanismus hin, der die Wirkung der Inhibitoren blockiert. Die GTPasen Arl2/3 regulieren die K-Ras-PDE δ Interaktion allosterisch durch Bildung eines transienten ternären Komplexes. Die allosterische Regulation wurde deshalb im Rahmen dieser Arbeit auch für die hoch affinen Sonden TAMRA-(S)-**62**-Deltarasin und TAMRA-(S)-**92** untersucht. Dabei konnte festgestellt werden, dass sowohl Arl2 als auch Arl3 das fluoreszenzmarkierte (S)-**62** Deltarasin aus der Bindungstasche verdrängen, während der stärker bindende Ester TAMRA-(S)-**92** nur von Arl3 aus der Bindungstasche entfernt werden konnte. Interessanterweise zeigte sich in zeitaufgelösten Verdrängungsexperimenten, dass Arl3 eine sehr viel höhere Affinität gegenüber PDE δ aufweist als Arl2. Diese Messdaten deuten auf zwei unterschiedliche Funktionen von Arl2 und Arl3 in der Zelle hin. Demnach kontrolliert Arl2 die Lokalisation von relativ schwach bindenden, prenylierten GTPasen wie Ras im Zytoplasma. Arl3 hingegen lokalisiert hauptsächlich im primären Cilium, wo es hochaffine Binder wie die Inositol-Phosphatase INPP5E aus der Farnesylbindungstasche von PDE δ verdrängt.

Prenylspezifität der Bindung von Proteinen an PDE δ

PDE δ transportiert farnesylierte Proteine wie K-Ras in der Zelle. Die Interaktion mit geranylgeranylierten Proteinen hingegen wird in der Literatur kontrovers diskutiert. Gerade im Hinblick auf mögliche Nebenwirkungen von Inhibitoren der K-Ras-PDE δ -Wechselwirkung ist die Prenylspezifität jedoch von entscheidender Bedeutung. Im Rahmen dieser Arbeit wurde erstmals eine Peptidsequenz untersucht, welche sowohl geranylgeranyliert als auch farnesyliert vorlag. Dabei konnte eine leichte Präferenz (Faktor 2.5) von PDE δ für farnesylierte Peptide abgeleitet werden. Die gemessene Selektivität liegt weit unterhalb der Literaturwerte, die einen dramatischen Affinitätsunterschied (mindestens Faktor 100) zwischen geranylgeranylierten und farnesylierten Peptiden suggerieren.

Rationales Design von UNC119a/b Inhibitoren

UNC119a und UNC119b sind myristoyl-bindende Proteine, die eine hohe Sequenzidentität mit PDE δ aufweisen. Die Lipidbindungstasche befindet sich jedoch auf der anderen Seite der β -Fass-Struktur der Proteine. Basierend auf der literaturbekannten Kokristallstruktur von UNC119a mit dem *N*-Terminus von Transducin- α wurde versucht rationale Inhibitoren *in silico* zu entwerfen. In vorherigen ITC Messungen konnte die Lipidabhängigkeit der Interaktion zwischen *N*-terminalen Transducin- α -Peptiden und UNC119a gezeigt werden. Eine Analyse der Kokristallstruktur von UNC119a/Transducin- α zeigte darüberhinaus die Interaktion von Ser218 (UNC119a) mit der Carbonylfunktion des *N*-terminalen Amids von Transducin- α . Deshalb wurden lipidierte Moleküle mit starken Wasserstoffbrückenakzeptoren bezüglich ihrer Bindung an UNC119a und UNC119b untersucht. Dabei wurde festgestellt, dass das lipidierte, β -Lacton Palmostatin B an UNC119a mit einer mikromolaren Affinität bindet.

In einem weiteren Ansatz wurde die helikale Sekundärstruktur des *N*-Terminus von Transducin- α im Komplex mit UNC119a/b für das Design von stabilen Peptidmakrozyklen ausgenutzt. Dabei wurde der myristoylierte *N*-Terminus von Transducin- α durch lipidierte Peptidmakrozyklen ersetzt. Die Peptidmakrozyklen zeigten dabei Affinitäten für UNC119a/b im niedrig nanomolaren Bereich und sind deshalb sehr gut zur Untersuchung des Transports von myristoylierten Proteinen im Zytoplasma und im primären Cilium geeignet.

9 LIST OF ABBREVIATIONS

Alpha	amplified luminescent proximity homogeneous assay
Arl	Arf-like
Arf	ADP ribosylation factors
Arg	arginine
aq	aqueous
au	arbitrary units
Bn	benzyl
Boc	<i>tert</i> -butyl carboxycarbonyl
δ	chemical shift in ppm (NMR)
Cbz	carboxylbenzyl
Cps	counts per second
Cpd	compound
Cys	cysteine
Da	dalton
DIPEA	diisopropyl ethyl amine
DCM	dichloromethane
DMAP	4-dimethylaminopyridine
DMF	<i>N, N</i> -dimethylformamide
DMSO	dimethylsulfoxide
<i>ee</i>	enantiomeric excess
eq	equivalents
ESI	electro spray ionization
Et	ethyl
EtOH	ethanol

LIST OF ABBREVIATIONS

EtOAc	ethyl acetate
FACS	fluorescence-activated cell sorting
Far	farnesyl
FITC	fluorescein isothiocyanate
FLIM	fluorescence lifetime imaging
FP	fluorescence polarization
FRET	Förster resonance energy transfer
g	gram
GppNHp	5'-guanylyl imidodiphosphate
GDP	guanosine diphosphate
Gli	transcription factor identified in <u>Glioblastoma</u>
GTP	guanosine triphosphate
GTPase	guanosine triphosphatase
h	hour
HCTU	O-(1H-6-Chlorobenzotriazole-1-yl)-1,1,3,3-tetramethyluronium hexafluorophosphate
His	histidine
HPLC	high performance liquid chromatography
HR-MS	high resolution mass spectrometry
Hz	hertz
ITC	isothermal titration calorimetry
J	coupling constant
KD	thermodynamic equilibrium constant
kcal	kilocalorie
L	liter

LIST OF ABBREVIATIONS

m	multiplet
MDCK	Madin-Darby canine kidney
Me	methyl
MeCN	acetonitrile
MeOH	methanol
MORM	mental retardation, truncal obesity, retinal dystrophy and micropenis
Mtt	4-methyl trityl
m/z	mass to charge ratio
n-BuLi	<i>n</i> -butyl lithium
nd	not determined
NMM	N-methyl morpholine
NMP	N-methyl pyrrolidone
OD	optical density (absorbance)
P	power
PAMPA	parallel artificial membrane permeability assay
PDAC	pancreatic ductal adenocarcinoma
PDE δ	non catalytic δ -subunit of phosphodiesterase 6, prenyl binding protein PrBP/ δ
PEG	polyethylene glycol
PMSF	phenylmethanesulfonylfluoride
Ph	phenyl
PM	plasma membrane
RMSD	root square mean deviation
Ras	rat sarcoma (protein)
Rheb	ras homologue enriched in brain
RhoGDI	ras homologue guanosine diphosphate dissociation inhibitor

LIST OF ABBREVIATIONS

RT	room temperature
RTCA	real time cell analysis
s	singlet
si-RNA	small interfering ribonucleic acid
SPR	surface plasmon resonance
T _m	protein melting point
TAMRA	tetramethylrhodamine
TES	triethylsilane
TFA	trifluoroacetic acid
THF	tetrahydrofuran
TMAD	N,N,N',N'-tetramethylazodicarboxamide
UNC	uncoordinated (protein)
Ser	serine
Tyr	tyrosine

10 REFERENCES

- (1) Brunsveld, L.; Kuhlmann, J.; Alexandrov, K.; Wittinghofer, A.; Goody, R. S.; Waldmann, H. *Angew Chem Int Ed Engl* **2006**, *45*, 6622.
- (2) Ahearn, I. M.; Haigis, K.; Bar-Sagi, D.; Philips, M. R. *Nat Rev Mol Cell Biol* **2012**, *13*, 39.
- (3) Prior, I. A.; Hancock, J. F. *Semin Cell Dev Biol* **2012**, *23*, 145.
- (4) Wittinghofer, A.; Waldmann, H. *Angew Chem Int Ed Engl* **2000**, *39*, 4192.
- (5) Berndt, N.; Hamilton, A. D.; Sebt, S. M. *Nat Rev Cancer* **2011**, *11*, 775.
- (6) Konstantinopoulos, P. A.; Karamouzis, M. V.; Papavassiliou, A. G. *Nat Rev Drug Discov* **2007**, *6*, 541.
- (7) Maurer, T.; Garrenton, L. S.; Oh, A.; Pitts, K.; Anderson, D. J.; Skelton, N. J.; Fauber, B. P.; Pan, B.; Malek, S.; Stokoe, D.; Ludlam, M. J.; Bowman, K. K.; Wu, J.; Giannetti, A. M.; Starovasnik, M. A.; Mellman, I.; Jackson, P. K.; Rudolph, J.; Wang, W.; Fang, G. *Proc Natl Acad Sci U S A* **2012**, *109*, 5299.
- (8) Sun, Q.; Burke, J. P.; Phan, J.; Burns, M. C.; Olejniczak, E. T.; Waterson, A. G.; Lee, T.; Rossanese, O. W.; Fesik, S. W. *Angew Chem Int Ed Engl* **2012**, *51*, 6140.
- (9) Lim, S. M.; Westover, K. D.; Ficarro, S. B.; Harrison, R. A.; Choi, H. G.; Pacold, M. E.; Carrasco, M.; Hunter, J.; Kim, N. D.; Xie, T.; Sim, T.; Jänne, P. A.; Meyerson, M.; Marto, J. A.; Engen, J. R.; Gray, N. S. *Angew Chem Int Ed Engl* **2014**, *53*, 199.
- (10) Ostrem, J. M.; Peters, U.; Sos, M. L.; Wells, J. A.; Shokat, K. M. *Nature* **2013**, *503*, 548.
- (11) Rocks, O.; Peyker, A.; Kahms, M.; Verveer, P. J.; Koerner, C.; Lumbierres, M.; Kuhlmann, J.; Waldmann, H.; Wittinghofer, A.; Bastiaens, P. I. *Science* **2005**, *307*, 1746.
- (12) Stephen, A. G.; Esposito, D.; Bagni, R. K.; McCormick, F. *Cancer Cell* **2014**, *25*, 272.
- (13) Schmick, M.; Vartak, N.; Papke, B.; Kovacevic, M.; Truxius, D. C.; Rossmannek, L.; Bastiaens, P. I. *Cell* **2014**, *157*, 459.

- (14) Rocks, O.; Gerauer, M.; Vartak, N.; Koch, S.; Huang, Z. P.; Pechlivanis, M.; Kuhlmann, J.; Brunsveld, L.; Chandra, A.; Ellinger, B.; Waldmann, H.; Bastiaens, P. I. *Cell* **2010**, *141*, 458.
- (15) Rocks, O.; Peyker, A.; Bastiaens, P. I. *Curr Opin Cell Biol* **2006**, *18*, 351.
- (16) To, M. D.; Wong, C. E.; Karnezis, A. N.; Del Rosario, R.; Di Lauro, R.; Balmain, A. *Nat Genet* **2008**, *40*, 1240.
- (17) Spiegel, S.; Cromm, P.; Zimmermann, G.; Grossmann, T.; Waldmann H., *Nat Chem Biol* **2014**, *in press*.
- (18) Chandra, A.; Grecco, H. E.; Pisupati, V.; Perera, D.; Cassidy, L.; Skoulidis, F.; Ismail, S. A.; Hedberg, C.; Hanzal-Bayer, M.; Venkitaraman, A. R.; Wittinghofer, A.; Bastiaens, P. I. *Nat Cell Biol* **2012**, *14*, 148.
- (19) Dekker, F. J.; Rocks, O.; Vartak, N.; Menninger, S.; Hedberg, C.; Balamurugan, R.; Wetzel, S.; Renner, S.; Gerauer, M.; Schölermann, B.; Rusch, M.; Kramer, J. W.; Rauh, D.; Coates, G. W.; Brunsveld, L.; Bastiaens, P. I.; Waldmann, H. *Nat Chem Biol* **2010**, *6*, 449.
- (20) Holstein, S. A.; Hohl, R. J. *Curr Opin Pharmacol* **2012**, *12*, 704.
- (21) Whyte, D. B.; Kirschmeier, P.; Hockenberry, T. N.; Nunez-Oliva, I.; James, L.; Catino, J. J.; Bishop, W. R.; Pai, J. K. *J Biol Chem* **1997**, *272*, 14459.
- (22) Lobell, R. B.; Liu, D.; Buser, C. A.; Davide, J. P.; DePuy, E.; Hamilton, K.; Koblan, K. S.; Lee, Y.; Mosser, S.; Motzel, S. L.; Abbruzzese, J. L.; Fuchs, C. S.; Rowinsky, E. K.; Rubin, E. H.; Sharma, S.; Deutsch, P. J.; Mazina, K. E.; Morrison, B. W.; Wildonger, L.; Yao, S. L.; Kohl, N. E. *Mol Cancer Ther* **2002**, *1*, 747.
- (23) Wang, Y.; Kaiser, C. E.; Frett, B.; Li, H. Y. *J Med Chem* **2013**, *56*, 5219.
- (24) Laheru, D.; Shah, P.; Rajeshkumar, N. V.; McAllister, F.; Taylor, G.; Goldsweig, H.; Le, D. T.; Donehower, R.; Jimeno, A.; Linden, S.; Zhao, M.; Song, D.; Rudek, M. A.; Hidalgo, M. *Investigational new drugs* **2012**, *30*, 2391.
- (25) Levy, R.; Grafi-Cohen, M.; Kraiem, Z.; Kloog, Y. *Mol Cancer Ther* **2010**, *9*, 2208.

-
- (26) Riely, G. J.; Johnson, M. L.; Medina, C.; Rizvi, N. A.; Miller, V. A.; Kris, M. G.; Pietanza, M. C.; Azzoli, C. G.; Krug, L. M.; Pao, W.; Ginsberg, M. S. *Journal of thoracic oncology : official publication of the International Association for the Study of Lung Cancer* **2011**, *6*, 1435.
- (27) Cho, K. J.; Park, J. H.; Piggott, A. M.; Salim, A. A.; Gorfe, A. A.; Parton, R. G.; Capon, R. J.; Lacey, E.; Hancock, J. F. *J Biol Chem* **2012**, *287*, 43573.
- (28) van der Hoeven, D.; Cho, K. J.; Ma, X.; Chigurupati, S.; Parton, R. G.; Hancock, J. F. *Mol Cell Biol* **2013**, *33*, 237.
- (29) Li, N.; Florio, S. K.; Pettenati, M. J.; Rao, P. N.; Beavo, J. A.; Baehr, W. *Genomics* **1998**, *49*, 76.
- (30) Zhang, H.; Constantine, R.; Frederick, J. M.; Baehr, W. *Vision Res* **2012**, *75*, 19.
- (31) Zhang, H.; Liu, X. H.; Zhang, K.; Chen, C. K.; Frederick, J. M.; Prestwich, G. D.; Baehr, W. *J Biol Chem* **2004**, *279*, 407.
- (32) Constantine, R.; Zhang, H.; Gerstner, C. D.; Frederick, J. M.; Baehr, W. *Vision Res* **2012**, *75*, 26.
- (33) DerMardirossian, C.; Bokoch, G. M. *Trends Cell Biol* **2005**, *15*, 356.
- (34) Gopalakrishna, K. N.; Doddapuneni, K.; Boyd, K. K.; Masuho, I.; Martemyanov, K. A.; Artemyev, N. O. *J Biol Chem* **2011**, *286*, 28954.
- (35) Gorska, M. M.; Alam, R. *Curr Allergy Asthma Rep* **2012**, *12*, 396.
- (36) Gorska, M. M.; Alam, R. *Blood* **2012**, *119*, 1399.
- (37) Zhang, H.; Li, S.; Doan, T.; Rieke, F.; Detwiler, P. B.; Frederick, J. M.; Baehr, W. *Proc Natl Acad Sci U S A* **2007**, *104*, 8857.
- (38) Nancy, V.; Callebaut, I.; El Marjou, A.; de Gunzburg, J. *J Biol Chem* **2002**, *277*, 15076.
- (39) Nikolova, S.; Guenther, A.; Savai, R.; Weissmann, N.; Ghofrani, H. A.; Konigshoff, M.; Eickelberg, O.; Klepetko, W.; Voswinckel, R.; Seeger, W.; Grimminger, F.; Schermuly, R. T.; Pullamsetti, S. S. *Respir Res* **2010**, *11*, 146.

- (40) Chen, Y. X.; Koch, S.; Uhlenbrock, K.; Weise, K.; Das, D.; Gremer, L.; Brunsveld, L.; Wittinghofer, A.; Winter, R.; Triola, G.; Waldmann, H. *Angew Chem Int Ed Engl* **2010**, *49*, 6090.
- (41) Hanzal-Bayer, M.; Renault, L.; Roversi, P.; Wittinghofer, A.; Hillig, R. C. *EMBO J* **2002**, *21*, 2095.
- (42) Hanzal-Bayer, M.; Linari, M.; Wittinghofer, A. *J Mol Biol* **2005**, *350*, 1074.
- (43) Hillig, R. C.; Hanzal-Bayer, M.; Linari, M.; Becker, J.; Wittinghofer, A.; Renault, L. *Structure* **2000**, *8*, 1239.
- (44) Ismail, S. A.; Chen, Y. X.; Rusinova, A.; Chandra, A.; Bierbaum, M.; Gremer, L.; Triola, G.; Waldmann, H.; Bastiaens, P. I.; Wittinghofer, A. *Nat Chem Biol* **2011**, *7*, 942.
- (45) Goody, R. S.; Rak, A.; Alexandrov, K. *Cell Mol Life Sci* **2005**, *62*, 1657.
- (46) Zhang, H.; Frederick, J. M.; Baehr, W. *Adv Exp Med Biol* **2006**, *572*, 485.
- (47) Wätzlich, D.; Vetter, I.; Gotthardt, K.; Miertzschke, M.; Chen, Y. X.; Wittinghofer, A.; Ismail, S. *EMBO Rep* **2013**, *14*, 465.
- (48) Linari, M.; Ueffing, M.; Manson, F.; Wright, A.; Meitinger, T.; Becker, J. *Proc Natl Acad Sci U S A* **1999**, *96*, 1315.
- (49) Yuan, S.; Sun, Z. *Annu Rev Genet* **2013**.
- (50) Hakim, S.; Bertucci, M. C.; Conduit, S. E.; Vuong, D. L.; Mitchell, C. A. *Curr Top Microbiol Immunol* **2012**, *362*, 247.
- (51) Hampshire, D. J.; Ayub, M.; Springell, K.; Roberts, E.; Jafri, H.; Rashid, Y.; Bond, J.; Riley, J. H.; Woods, C. G. *Eur J Hum Genet* **2006**, *14*, 543.
- (52) Jacoby, M.; Cox, J. J.; Gayral, S.; Hampshire, D. J.; Ayub, M.; Blockmans, M.; Pernot, E.; Kisseleva, M. V.; Compère, P.; Schiffmann, S. N.; Gergely, F.; Riley, J. H.; Pérez-Morga, D.; Woods, C. G.; Schurmans, S. *Nat Genet* **2009**, *41*, 1027.
- (53) Nag, C.; Ghosh, M.; Das, K.; Ghosh, T. *Ann Med Health Sci Res* **2013**, *3*, 291.

- (54) Humbert, M. C.; Weihbrecht, K.; Searby, C. C.; Li, Y.; Pope, R. M.; Sheffield, V. C.; Seo, S. *Proc Natl Acad Sci U S A* **2012**, *109*, 19691.
- (55) Miertzschke, M.; Koerner, C.; Spoerner, M.; Wittinghofer, A. *Biochem J* **2013**.
- (56) Thomas, S.; Wright, K. J.; Le Corre, S.; Micalizzi, A.; Romani, M.; Abhyankar, A.; Saada, J.; Perrault, I.; Amiel, J.; Litzler, J.; Filhol, E.; Elkhartoufi, N.; Kwong, M.; Casanova, J. L.; Boddaert, N.; Baehr, W.; Lyonnet, S.; Munnich, A.; Burglen, L.; Chassaing, N.; Encha-Ravazi, F.; Vekemans, M.; Gleeson, J. G.; Valente, E. M.; Jackson, P. K.; Drummond, I. A.; Saunier, S.; Attié-Bitach, T. *Hum Mutat* **2013**.
- (57) Briscoe, J.; Thérond, P. P. *Nat Rev Mol Cell Biol* **2013**, *14*, 416.
- (58) Ji, Z.; Mei, F. C.; Xie, J.; Cheng, X. *J Biol Chem* **2007**, *282*, 14048.
- (59) Morris, J. P.; Wang, S. C.; Hebrok, M. *Nat Rev Cancer* **2010**, *10*, 683.
- (60) Pyrrole compounds and uses thereof, US patent, US 7323490 B2.
- (61) Chidley, C.; Haruki, H.; Pedersen, M. G.; Muller, E.; Johnsson, K. *Nat Chem Biol* **2011**, *7*, 375.
- (62) Dadvar, P.; O'Flaherty, M.; Scholten, A.; Rumpel, K.; Heck, A. J. *Mol Biosyst* **2009**, *5*, 472.
- (63) Dadvar, P.; Kovanich, D.; Folkers, G. E.; Rumpel, K.; Raijmakers, R.; Heck, A. J. *Chembiochem* **2009**, *10*, 2654.
- (64) Raijmakers, R.; Dadvar, P.; Pelletier, S.; Gouw, J.; Rumpel, K.; Heck, A. J. *ChemMedChem* **2010**, *5*, 1927.
- (65) Gottlieb, D.; Grunwald, C.; Nowak, C.; Kuhlmann, J.; Waldmann, H. *Chem Commun (Camb)* **2006**, 260.
- (66) Zhang, J. H.; Chung, T. D.; Oldenburg, K. R. *J Biomol Screen* **1999**, *4*, 67.
- (67) Abad-Zapatero, C.; Metz, J. T. *Drug Discov Today* **2005**, *10*, 464.

-
- (68) Ladbury, J. E.; Doyle, M. L. *Biocalorimetry 2*; Wiley: Chichester, 2004.
- (69) Ladbury, J. E.; Klebe, G.; Freire, E. *Nat Rev Drug Discov* **2010**, *9*, 23.
- (70) Ladbury, J. E. *Biochem Soc Trans* **2010**, *38*, 888.
- (71) Leavitt, S.; Freire, E. *Curr Opin Struct Biol* **2001**, *11*, 560.
- (72) Velazquez-Campoy, A.; Freire, E. *Nat Protoc* **2006**, *1*, 186.
- (73) Kawasaki, Y.; Freire, E. *Drug Discov Today* **2011**, *16*, 985.
- (74) Freyer, M. W.; Lewis, E. A. *Methods Cell Biol* **2008**, *84*, 79.
- (75) Huang, X.; Aulabaugh, A. *Methods Mol Biol* **2009**, *565*, 127.
- (76) Lea, W. A.; Simeonov, A. *Expert Opin Drug Discov* **2011**, *6*, 17.
- (77) Li, Y.; Xie, W.; Fang, G. *Anal Bioanal Chem* **2008**, *390*, 2049.
- (78) Wang, Z. X. *FEBS Lett* **1995**, *360*, 111.
- (79) Zimmermann, G.; Papke, B.; Ismail, S.; Vartak, N.; Chandra, A.; Hoffmann, M.; Hahn, S. A.; Triola, G.; Wittinghofer, A.; Bastiaens, P. I.; Waldmann, H. *Nature* **2013**, *497*, 638.
- (80) Tempest, P.; Ma, V.; Thomas, S.; Hua, Z.; Kelly, M. G.; Hulme, C. *Tetrahedron Letters* **2001**, *42*, 4959.
- (81) Tsunoda, T.; Uemoto, K.; Nagino, C.; Kawamura, M.; Kaku, H.; Itô, S. *Tetrahedron Letters* **1999**, *40*, 7355.
- (82) Brandts, J. F.; Lin, L. N. *Biochemistry* **1990**, *29*, 6927.
- (83) Mayhood, T. W.; Windsor, W. T. *Anal Biochem* **2005**, *345*, 187.
- (84) Fedorov, O.; Niesen, F. H.; Knapp, S. *Methods Mol Biol* **2012**, *795*, 109.
- (85) Niesen, F. H.; Berglund, H.; Vedadi, M. *Nat Protoc* **2007**, *2*, 2212.
- (86) Suladze, S.; Ismail, S.; Winter, R. *J Phys Chem B* **2014**.

- (87) Celej, M. S.; Montich, G. G.; Fidelio, G. D. *Protein science : a publication of the Protein Society* **2003**, *12*, 1496.
- (88) Meyer, E. A.; Castellano, R. K.; Diederich, F. *Angew Chem Int Ed Engl* **2003**, *42*, 1210.
- (89) Salonen, L. M.; Ellermann, M.; Diederich, F. *Angew Chem Int Ed Engl* **2011**, *50*, 4808.
- (90) Monovich, L. G.; Tommasi, R. A.; Fujimoto, R. A.; Blancuzzi, V.; Clark, K.; Cornell, W. D.; Doti, R.; Doughty, J.; Fang, J.; Farley, D.; Fitt, J.; Ganu, V.; Goldberg, R.; Goldstein, R.; Lavoie, S.; Kulathila, R.; Macchia, W.; Parker, D. T.; Melton, R.; O'Byrne, E.; Pastor, G.; Pellas, T.; Quadros, E.; Reel, N.; Roland, D. M.; Sakane, Y.; Singh, H.; Skiles, J.; Somers, J.; Toscano, K.; Wigg, A.; Zhou, S.; Zhu, L.; Shieh, W. C.; Xue, S.; McQuire, L. W. *J Med Chem* **2009**, *52*, 3523.
- (91) Shieh, W.-C.; Xue, S.; Reel, N.; Wu, R.; Fitt, J.; Repič, O. *Tetrahedron: Asymmetry* **2001**, *12*, 2421.
- (92) Alimardanov, A.; Nikitenko, A.; Connolly, T. J.; Feigelson, G.; Chan, A. W.; Ding, Z.; Ghosh, M.; Shi, X.; Ren, J.; Hansen, E.; Farr, R.; MacEwan, M.; Tadayon, S.; Springer, D. M.; Kreft, A. F.; Ho, D. M.; Potoski, J. R. *Organic Process Research & Development* **2009**, *13*, 1161.
- (93) Connolly, T. J.; Hansen, E. C.; MacEwan, M. F. *Organic Process Research & Development* **2010**, *14*, 466.
- (94) Stanley, L. M.; Hartwig, J. F. *J Am Chem Soc* **2009**, *131*, 8971.
- (95) Sigurskjold, B. W. *Anal Biochem* **2000**, *277*, 260.
- (96) Shalom-Feuerstein, R.; Levy, R.; Makovski, V.; Raz, A.; Kloog, Y. *Biochim Biophys Acta* **2008**, *1783*, 985.
- (97) Shalom-Feuerstein, R.; Plowman, S. J.; Rotblat, B.; Ariotti, N.; Tian, T.; Hancock, J. F.; Kloog, Y. *Cancer Res* **2008**, *68*, 6608.
- (98) Douglass, E. F.; Miller, C. J.; Sparer, G.; Shapiro, H.; Spiegel, D. A. *Journal of the American Chemical Society* **2013**, *135*, 6092.

-
- (99) http://www.urmc.rochester.edu/hts/_source/alphascreenpracticalguide.pdf , 23.05.2014
- (100) Copeland, R. A.; Pompliano, D. L.; Meek, T. D. *Nat Rev Drug Discov* **2006**, *5*, 730.
- (101) Ciulli, A. *Methods Mol Biol* **2013**, *1008*, 357.
- (102) Frostell, A.; Vinterbäck, L.; Sjöbom, H. *Methods Mol Biol* **2013**, *1008*, 139.
- (103) Holdgate, G.; Geschwindner, S.; Breeze, A.; Davies, G.; Colclough, N.; Temesi, D.; Ward, L. *Methods Mol Biol* **2013**, *1008*, 327.
- (104) Personal Communication, Prof. Wittinghofer.
- (105) Personal Communication, Eyad Fansa and Biaffin GmbH.
- (106) Ismail, S. A.; Chen, Y. X.; Miertzschke, M.; Vetter, I. R.; Koerner, C.; Wittinghofer, A. *EMBO J* **2012**, *31*, 4085.
- (107) Wright, K. J.; Baye, L. M.; Olivier-Mason, A.; Mukhopadhyay, S.; Sang, L.; Kwong, M.; Wang, W.; Pretorius, P. R.; Sheffield, V. C.; Sengupta, P.; Slusarski, D. C.; Jackson, P. K. *Genes Dev* **2011**, *25*, 2347.
- (108) Ziegler, S.; Pries, V.; Hedberg, C.; Waldmann, H. *Angew Chem Int Ed Engl* **2013**, *52*, 2744.
- (109) Singh, A.; Greninger, P.; Rhodes, D.; Koopman, L.; Violette, S.; Bardeesy, N.; Settleman, J. *Cancer Cell* **2009**, *15*, 489.
- (110) Lai, C. K.; Gupta, N.; Wen, X.; Rangell, L.; Chih, B.; Peterson, A. S.; Bazan, J. F.; Li, L.; Scales, S. J. *Molecular biology of the cell* **2011**, *22*, 1104.
- (111) Jacoby, M.; Cox, J. J.; Gayral, S.; Hampshire, D. J.; Ayub, M.; Blockmans, M.; Pernot, E.; Kisseleva, M. V.; Compere, P.; Schiffmann, S. N.; Gergely, F.; Riley, J. H.; Perez-Morga, D.; Woods, C. G.; Schurmans, S. *Nat Genet* **2009**, *41*, 1027.
- (112) Zhang, H.; Hosier, S.; Terew, J. M.; Zhang, K.; Cote, R. H.; Baehr, W. *Methods Enzymol* **2005**, *403*, 42.

- (113) Tnimov, Z.; Guo, Z.; Gambin, Y.; Nguyen, U. T.; Wu, Y. W.; Abankwa, D.; Stigter, A.; Collins, B. M.; Waldmann, H.; Goody, R. S.; Alexandrov, K. *J Biol Chem* **2012**, *287*, 26549.
- (114) Simon, S. M., T. *Peptide-Lipid Interactions*; Academic Press: San Diego, California, 2002; Vol. 52.
- (115) Zhang, H.; Constantine, R.; Vorobiev, S.; Chen, Y.; Seetharaman, J.; Huang, Y. J.; Xiao, R.; Montelione, G. T.; Gerstner, C. D.; Davis, M. W.; Inana, G.; Whitby, F. G.; Jorgensen, E. M.; Hill, C. P.; Tong, L.; Baehr, W. *Nat Neurosci* **2011**, *14*, 874.
- (116) Lee, Y.; Chung, S.; Baek, I. K.; Lee, T. H.; Paik, S. Y.; Lee, J. *Cell Cycle* **2013**, *12*, 1303.
- (117) Karan, S.; Zhang, H.; Li, S.; Frederick, J. M.; Baehr, W. *Vision Res* **2008**, *48*, 442.
- (118) Sinha, S.; Majumder, A.; Belcastro, M.; Sokolov, M.; Artemyev, N. O. *Cell Signal* **2013**, *25*, 341.
- (119) Hedberg, C.; Dekker, F. J.; Rusch, M.; Renner, S.; Wetzel, S.; Vartak, N.; Gerding-Reimers, C.; Bon, R. S.; Bastiaens, P. I.; Waldmann, H. *Angew Chem Int Ed Engl* **2011**, *50*, 9832.
- (120) Rusch, M.; Zimmermann, T. J.; Bürger, M.; Dekker, F. J.; Görmer, K.; Triola, G.; Brockmeyer, A.; Janning, P.; Böttcher, T.; Sieber, S. A.; Vetter, I. R.; Hedberg, C.; Waldmann, H. *Angew Chem Int Ed Engl* **2011**, *50*, 9838.
- (121) Spiegel, J.; Cromm, P. M.; Itzen, A.; Goody, R. S.; Grossmann, T. N.; Waldmann, H. *Angew Chem Int Ed Engl* **2014**, *53*, 2498.
- (122) Roehrl, M. H.; Wang, J. Y.; Wagner, G. *Biochemistry* **2004**, *43*, 16056.
- (123) Alexandrov, K.; Scheidig, A. J.; Goody, R. S. *Methods Enzymol* **2001**, *329*, 14.
- (124) Arosio, D.; Manzoni, L.; Araldi, E. M.; Scolastico, C. *Bioconjug Chem* **2011**, *22*, 664.
- (125) Orjales, A.; Mosquera, R.; Labeaga, L.; Rodes, R. *J Med Chem* **1997**, *40*, 586.
- (126) Triola, G.; Brunsveld, L.; Waldmann, H. *J Org Chem* **2008**, *73*, 3646.

11 ACKNOWLEDGEMENTS (DANKSAGUNG)

Herrn Prof. Dr. Herbert Waldmann möchte ich herzlich für die interessante und herausfordernde Themenstellung und die stete Unterstützung während der Anfertigung dieser Arbeit danken. Darüberhinaus gilt Herrn Waldmann mein Dank für die ausgezeichneten Arbeitsbedingungen in der Abteilung, die gewährte wissenschaftliche Freiheit, das nette Arbeitsumfeld und fortwährende wissenschaftliche Diskussionen.

Herrn Prof. Dr. Daniel Rauh danke ich für die Übernahme des Zweitgutachtens. Dr. Gemma Triola danke ich herzlichst für ihre wissenschaftlichen Denkanstöße und die stets freundliche Unterstützung. Meinen Kollaborationspartnern Björn Papke, Shehab Ismail, Philipp Kuchler und Carsten Schultz-Fademrecht möchte ich für die produktive Zusammenarbeit danken. Dem gesamten Arbeitskreis Waldmann danke ich für die kollegiale, freundschaftliche Zusammenarbeit und die angenehme Arbeitsatmosphäre. Dabei möchte ich besonders meinen vormaligen und aktuellen Labor- und Bürokollegen danken. Für gemeinsame Unternehmungen auch außerhalb des Instituts möchte ich an dieser Stelle Philipp Kuchler, Melanie Schwalfenberg, Peter Schröder, Anja Richter, Hannah Schuster, Kathrin Wittstein, Jochen Spiegel, Philipp Cromm und Kirsten Tschalpalda danken. Dem Fonds der Chemischen Industrie danke ich für die finanzielle Unterstützung im Rahmen eines Kekulé-Stipendiums.

Meinen Eltern danke ich für die uneingeschränkte Unterstützung während der Promotion und des Studiums. Schließlich möchte ich mich ganz besonders bei Aljona bedanken. Ohne deine Geduld und Unterstützung wäre diese Arbeit nicht möglich gewesen.

EIDESSTATTLICHE ERKLÄRUNG

Hiermit versichere ich an Eides statt, dass ich die vorliegende Arbeit selbstständig und nur mit den angegebenen Hilfsmitteln angefertigt habe.

Dortmund, den 23.5. 2014

Gunther Zimmermann

CURRICULUM VITAE

EDUCATION AND QUALIFICATIONS

3/2010 – present	Doctoral studies at Max Planck Institute, Dortmund with Prof. Herbert Waldmann
1/2009 – 9/2009	Practical work towards chemistry diploma with Prof. Eric Meggers, University of Marburg, Medicinal Chemistry
9/2007 – 3/2008	Research stay in Cambridge, UK with Prof. Steven Ley, Organic Chemistry
9/2004 – 9/2009	Undergraduate studies, University of Marburg, final grades: Vordiplom: 1.1, Diplom: 1.1
9/2001 – 6/2002	Exchange student, Rochester, USA
6/1995 – 6/2004	High school education, Christian-Wirth-Schule, Usingen, final grade: 1.3

SCHOLARSHIPS

Scholarship of Studienstiftung des deutschen Volkes (11/2004 – 9/2009),

Kekulé Scholarship (Fonds der Chemischen Industrie e.V.) (8/2010 – 8/2012)

PUBLICATIONS

Weise, K.; Kapoor, S.; Werkmüller, A.; Möbitz, S.; Zimmermann, G.; Triola, G.; Waldmann, H.; Winter, R., Dissociation of the K-Ras4B/PDE δ complex upon contact with lipid membranes. *J Am Chem Soc* **2012**, *134* (28), 11503-10.

Zimmermann, G.*; Papke, B.*; Ismail, S.*; Vartak, N.; Chandra, A.; Hoffmann, M.; Hahn, S. A.; Triola, G.; Wittinghofer, A.; Bastiaens, P. I.; Waldmann, H., Small molecule inhibition of the K-Ras4B/PDE δ interaction impairs oncogenic K-Ras signaling. *Nature* **2013**, 497 (7451), 638-42.

Spiegel, S.; Cromm, P.; Zimmermann, G.; Grossmann, T.; Waldmann H., Small molecule modulation of Ras Signaling - The Holy Grail in Anti-Cancer Drug Discovery. *Nature Chemical biology* (review), accepted.

Zimmermann, G.; Schultz-Fademrecht C.; Kuechler, P; Murarka, S.; Ismail, S.; Triola G.; Nussbaumer P.; Wittinghofer A.; Waldmann H., Structure-guided design and kinetic analysis of highly potent benzimidazole inhibitors targeting the prenyl binding site of PDE *J Med Chem*, accepted.

PATENTS

Bastiaens, P. I.; Papke, B.; Ismail, S.; Triola, G.; Vartak, N.; Waldmann, H. Wittinghofer, A.; Zimmermann G. PCT / EP 2013 / 067047.